# Analysis of the Concerted Functions of Major Cathepsin Proteases and their Role in Neurodegenerative Diseases

Dissertation

In fulfilment of the requirement for the degree

„Doctor rerum naturalium (Dr. rer. nat)“

of the Faculty of Mathematics and Natural Sciences

at the Christian-Albrechts-University of Kiel

submitted by

Lisa Gallwitz

Kiel, May 2023

| | |
|---|---|
| Referee: | Prof. Dr. Paul Saftig |
| Co-Referee: | Prof. Dr. Eric Beitz |
| Date of thesis defense: | 24.07.2023 |
| Approved for publication: | 24.07.2023 |

# Index

1 Introduction ..... 1
1.1 Proteolysis ..... 1
1.2 The Biological function of proteolysis ..... 1
1.2.1 Post-translational proteolytic processing ..... 2
1.2.2 Protein degradation ..... 3
1.3 Lysosomal proteases ..... 8
1.3.1 The cysteine-type proteases CTSB and CTSL ..... 10
1.3.2 The aspartic-type protease CTSD ..... 12
1.4 Proteolysis malfunctions in diseases ..... 13
1.4.1 Lysosomal storage disorders (LSDs) ..... 13
1.4.2 Alzheimer's disease (AD) ..... 15
2 Objectives ..... 20
3 Material and Methods ..... 22
3.1 Material ..... 22
3.1.1 Chemicals and Buffers ..... 22
3.1.2 Ready-made reagents and kits ..... 22
3.1.3 Cell culture medium and additives ..... 22
3.1.4 Primary antibodies ..... 23
3.1.5 Secondary antibodies ..... 24
3.1.6 Oligonucleotides ..... 25
3.1.7 Single guide RNAs for CRISPR/Cas9 ..... 25
3.1.8 Bacteria ..... 25
3.1.9 Cell lines ..... 26
3.1.10 Mouse strains ..... 26
3.1.11 Plasmids ..... 27

3.1.12 Frequently used buffers and aqueous solutions ..... 27
3.2 Methods ..... 29
3.2.1 Molecular Biological Methods ..... 29
3.2.2 Cell biological methods ..... 30
3.2.3 Protein biochemical methods ..... 35
3.2.4 Histological methods ..... 43
3.2.5 Animal Experiments ..... 45
3.2.6 Computer Software and Statistical Analysis Techniques ..... 48
4 Results ..... 49
4.1 Basal analysis of the expression and activity of CTSs in HeLa and SH-SY5Y cells ..... 49
4.2 Generation and validation of CTS-deficient SH-SY5Y cell lines using the CRISPR/Cas9 technique ..... 53
4.3 SH-SY5Y CTSBDL-triple deficient cells are characterized by enlarged and increased numbers of lysosomes ..... 56
4.4 Combined CTSBDL-deficiency in SH-SY5Y cells causes mild effects on the autophagic flux ..... 62
4.5 SH-SY5Y CTSBDL-deficient cells have impaired proteolysis of endocytosed proteins ..... 69
4.6 Consequences for the cellular proteome after a CTSBDL-deficiency in SH-SY5Y cells ..... 71
4.7 Amyloid-β, derived from the Amyloid Precursor Protein, is a known substrate of Cathepsin D ..... 76
4.7.1 Recombinant human pro-CTSD gets self-activated under acidic pH conditions ..... 77
4.7.2 Human Aβ1-42 is a substrate of human CTSD ..... 78
4.8 Intracranial dosing of rhpro-CTSD in a CLN10 mouse model does not affect the expression of mouse Aβ species ..... 79

4.8.1 After intracranial injection rhpro-CTSD is endocytosed and activated in neurons and microglia of CTSD-deficient mice ..... 80

4.8.2 Intracranial dosing of CTSD-deficient mice with rhpro-CTSD does not alter their APP and Aβ metabolites ..... 81

4.9 Inhibition of CTSD in HEK APP overexpressing cells leads to an increase of intracellular Aβ1-42 ..... 85

4.9.1 Rhpro-CTSD becomes activated within HEK cells ..... 85

4.9.2 Inhibition of CTSD in HEK APPswe cells increases intracellular Aβ1-42 ..... 86

4.10 Analysis of rhpro-CTSD uptake and Aβ clearance in an Alzheimer's disease mouse model ..... 89

4.10.1 Aβ1-42 accumulation in brains of two-months old 5xFAD mice ..... 89

4.10.2 Effect of intracranial rhpro-CTSD application on the APP and Aβ metabolism in one-month old 5xFAD mice ..... 91

4.10.3 Effect of rhpro-CTSD application on the APP and Aβ metabolism in two-month old 5xFAD mice ..... 93

4.10.4 Effect of rhpro-CTSD on the APP and Aβ metabolism in three-month old 5xFAD mice ..... 94

4.10.5 Plaque morphology and neuroinflammation are not affected after rhpro-CTSD treatment in 5xFAD mice ..... 96

5 Discussion ..... 101

5.1 Cathepsins are differently expressed in SH-SY5Y and HeLa cells ..... 101

5.2 Cathepsin-deficiencies differently influence the lysosomal phenotype and accumulation of autofluorescent storage material ..... 101

5.3 CTSBDL-triple deficiency leads to mild impairment of the autophagic flux 104

5.4 CTSB, CTSD and CTSL can partially compensate for each other sharing the same substrates ..... 108

5.5 CTSB, CTSD and CTSL are involved in APP degradation ..... 109

5.6 Recombinant human Cathepsin D cleaves recombinant Aβ1-42 in vitro .. 111

5.7 Intracranial dosing of rhpro-CTSD to CTSD-deficient mice did not alter the amount of Aβ-species ..... 112

5.8 Rhpro-CTSD treatment does not alter the processing of APP in HEK cells ..... 114

5.9 Intracranial injection of rhpro-CTSD does not alter the APP processing in 5xFAD mice ..... 115

5.10 Aβ levels are surprisingly elevated in the CSF of 5xFAD mice after rhpro-CTSD dosing ..... 118

5.11 Amyloid-β-containing plaque load and neuroinflammation are not altered after rhpro-CTSD dosing to 5xFAD mice ..... 119

6 Outlook ..... 121

7 Summary ..... 123

8 Zusammenfassung ..... 125

9 References ..... 127

10 Appendix ..... 158

10.1 Supplement Figure ..... 158

10.2 List of Abbreviations ..... 159

10.3 List of Figures ..... 162

10.4 List of Tables ..... 165

11 Declaration ..... 167

12 Publications and scientific participations ..... 169

13 Acknowledgements ..... 171

# 1 Introduction

## 1.1 Proteolysis

The concept of protein turnover, a continuous synthesis and degradation of proteins by proteolysis, was originally proposed by Rudolf Schoenheimer in 1943 (Schoenheimer 1943). First, Schoenheimer's revolutionary finding was neglected but Christian de Duve's discovery of the lysosome in the late 1950s brought proteolysis back in focus (Bond 2019; Duve et al. 1955). Lysosomes were identified as degrading organelles containing hydrolyzing enzymes. However, how proteins and peptides reached these compartments remained an essential question in the field. Blocking lysosomal proteolysis did not significantly prevent the intracellular breakdown of all proteins (Poole et al. 1978). This suggested that a proteolytic system apart from the lysosome existed. In 1978, Hershko and Ciechanover discovered the ATP-dependent proteolysis factor (APF-1) which was later identified as ubiquitin (Ciechanover et al. 1980). The ubiquitin-proteasome system was classified as a proteolytic degradation machinery in the following years (Wolf and Menssen 2018). A significant role for proteolysis in cellular protein quality control has been discovered in recent years. This essential process occurs in all living cells and regulates several functions including the regulation of protein function and the removal of damaged or unnecessary proteins (Berg et al. 2018). Subsequently, dysregulation in the proteolysis can cause various diseases like cancer, inflammation, and neurological disorders (Bhagwat et al. 2018). The hydrolysis of peptide bonds is catalyzed by proteases as it usually is an extremely slow process and the lifetimes of proteins and peptides range from a few minutes to weeks (Voet and Voet op. 2011; Chepyala et al. 2021; Hammond et al. 2022; Eden et al. 2011). In humans, there are 641 genes encoding for proteases which account for 3% of the overall human genome (Bond 2019).

## 1.2 The Biological function of proteolysis

To maintain protein homeostasis eukaryotic cells have established a range of pathways to control the protein conformation, concentration, and subcellular localization (López-Otín and Bond 2008). Among them, there is a huge set of complex processes regulating protein synthesis, folding, translocation, and clearance (López-Otín and Bond 2008). Proteolysis is one of the fundamental processes that increases

the variety of the available proteins encoded by the genome and is involved in the regulation of the cellular metabolism (López-Otín and Bond 2008). The breakdown of proteins into smaller polypeptides is an often underappreciated post-translational modification (PTM) which is irreversible yet also requiring to be strictly controlled (Rogers and Overall 2013; Bhagwat et al. 2018; López-Otín and Bond 2008). Regulated proteolytic processing plays a key role in cellular functions like protein quality control, cell cycle and cell division, apoptosis, and modulation of metabolic pathways (Ciechanover 2005). Almost all proteins are subject to proteolysis as they eventually get co- and post-translationally hydrolyzed or degraded.

### 1.2.1 Post-translational proteolytic processing

Post-translational modifications (PTMs) extend the complexity and functional diversity of proteins. These processes may involve the removal of amino(N)-terminal methionine to determine the half-life of proteins or the cleavage of signal peptides or pro-peptides for translocation, activation or inactivation of certain proteins (Dissmeyer et al. 2017; Murcha et al. 2012; Dalbey et al. 2017).

Proteins destined for a certain cellular location contain a cleavable N-terminal signal sequence (Dalbey et al. 2017). Signal peptides of newly synthesized proteins are recognized and bound by the signal recognition particle (SRP) immediately after leaving the ribosome (Berg et al. 2018). By binding to the SRP-receptor at the membrane of the endoplasmic reticulum (ER) the ribosome-SRP-complex is transferred to the translocon which translocates the newly synthesized protein with its signal peptide to the ER lumen (Berg et al. 2018). A signal peptidase residing within the ER cleaves off the signal sequence inducing the protein folding into its quaternary structure within the ER lumen (Berg et al. 2018).

Proteases are often synthesized as inactive forms called preproteins or zymogens. By expressing proteases in their inactive conformation, but available for a fast activation cells can adjust their metabolism rapidly. On the other hand, a premature activation can lead to fatal consequences as a variety of proteases are determined for specific organelles only. To convert pre-proteins or zymogens into active and mature proteases they need to get (auto)proteolytically processed (Raju 2019; López-Otín and Bond 2008). Usually, inactive precursor proteins are composed of additional polypeptide

chains that upon cleavage ensure maturation and correct folding of the proteases into their active form (Müller-Esterl 2018).

### 1.2.2 Protein degradation

Proteolysis plays an important role in the disposal of proteins. In general, proteins can be hydrolyzed by the proteasome or lysosomal enzymes. In eukaryotes, these two major pathways are independent but inter-connected processes (Zhao et al. 2022). The proteasome is fundamentally responsible for the degradation of short-lived and soluble misfolded proteins by the ubiquitin-proteasome system (UPS). Lysosomes degrade long-lived proteins, insoluble aggregates, macromolecular compounds, entire organelles and intracellular pathogens via endocytosis, phagocytosis or macroautophagy pathways (Zhao et al. 2022; Dikic 2017).

#### 1.2.2.1 The ubiquitin-proteasomal system (UPS)

Damaged and unfolded proteins are degraded by proteasomes, which are part of the ubiquitin-proteasome system (UPS). The UPS includes a number of ubiquitin ligases and de-ubiquitinating enzymes (DUBs) (Majumder and Baumeister 2019). The substrate is polyubiquitinated through repeated actions of three ubiquitinated enzymes Ub ligase (E3), Ub conjugating enzyme (E2), and Ub activating enzyme (E1) (Ravid and Hochstrasser 2008). Proteins labeled with ubiquitin are then targeted to the proteasome complex (Molineaux 2012). The proteasome consists of two subunits: two terminal regulatory particles (19S proteasome) bound to both ends of the catalytic core particle (20S proteasome) (Tanaka 2009). The 19S compartment recognizes ubiquitylated proteins and assists in their unfolding and translocation into the core of the 20S particle (Tanaka 2009). The 20S proteasome consists of three subunits which are associated with caspase-like, trypsin-like, and chymotrypsin-like activities (Tanaka 2009). Utilizing these subunits the proteasome can cleave peptide bonds respectively at the C-terminal side of acidic, basic and hydrophobic amino acid residues (Tanaka 2009).

#### 1.2.2.2 The lysosomal pathway

In recent years, the function of lysosomes have moved from being the simple “garbage bags” of the cells to more fundamental organelles involved in secretion, signaling, and energy metabolism (Duve et al. 1955; Settembre et al. 2013; Bouhamdani et al. 2021).

Lysosomes are cellular organelles with an acidic lumen (pH 4.5-5), limited by a single-lipid bilayer membrane (Ohkuma and Poole 1978; Settembre et al. 2013). To maintain the acidic pH the vacuolar ATPase (v-ATPase) is located within the lysosomal membrane and translocates protons from the cytosol to the lysosomal lumen (Forgac 1999). The low pH ensures optimal conditions for more than 60 different types of hydrolases residing in the lysosomal lumen (Saftig and Klumperman 2009; Rudnik and Damme 2021). The lysosomal membrane harbors more than 50 transmembrane proteins which are often highly glycosylated (Rudnik and Damme 2021; Saftig and Klumperman 2009; Xu and Ren 2015; Eskelinen et al. 2003). The most abundant ones are lysosomal integral membrane proteins (LIMPs) and lysosomal associated membrane proteins (LAMPs). They play a pivotal role in preventing lysosomal hydrolases from destroying other membrane proteins and the lysosome membrane by forming a glycocalyx with their large, carbohydrate-rich luminal domains, which cover the entire inner membrane (Wilke et al. 2012; Fukuda 1991). Additionally, transiently associated cytosolic proteins are recruited to the lysosomal membrane to interact with lysosomal membrane proteins and lipids to mediate cell responses or aid the organelle’s movement throughout the cell via the cytoskeleton (Cabukusta and Neefjes 2018). Cargo destined for degradation via the lysosomal pathway is transported to the lysosomes by endocytosis and phagocytosis, and autophagy (Xu and Ren 2015) (Figure 1).

##### 1.2.2.2.1 Endocytosis

Endocytosis (Figure 1) is a cellular process to internalize extracellular molecules from the plasma membrane (Sigismund et al. 2021). The cargo consists of fluids, nutrients or parts of the plasma membrane and is distributed throughout the cell in vesicles called endosomes (Kaksonen and Roux 2018). Endocytosis is necessary for nutrient uptake, extracellular sensing, homeostasis of the plasma membrane and maintaining the surface area and tension of the cell (Thottacherry et al. 2019). The process can be divided in two major types: clathrin-mediated and clathrin-independent endocytosis

(Thottacherry et al. 2019; Casamento and Boucrot 2020). The best studied endocytic pathway is clathrin-mediated endocytosis. It is initiated by the clustering of cargo at the plasma membrane followed by assembly of clathrin. Clathrin forms a pit around the cargo followed by the plasma membrane shaping into an invagination (Thottacherry et al. 2019; Kaksonen and Roux 2018). Finally, an early endosome is separated from the plasma membrane by vesicle scission by dynamin, a large GTPase (Kaksonen and Roux 2018).

These vesicles mature or fuse with early endosomes while it is decided whether the cargo is recycled to the plasma membrane or is designated for degradation. The Endosomal sorting complex required for transport (ESCRT) sorts membrane proteins marked by ubiquitination into intraluminal vesicles, which form late endosomes or multivesicular bodies (Henne et al. 2013).

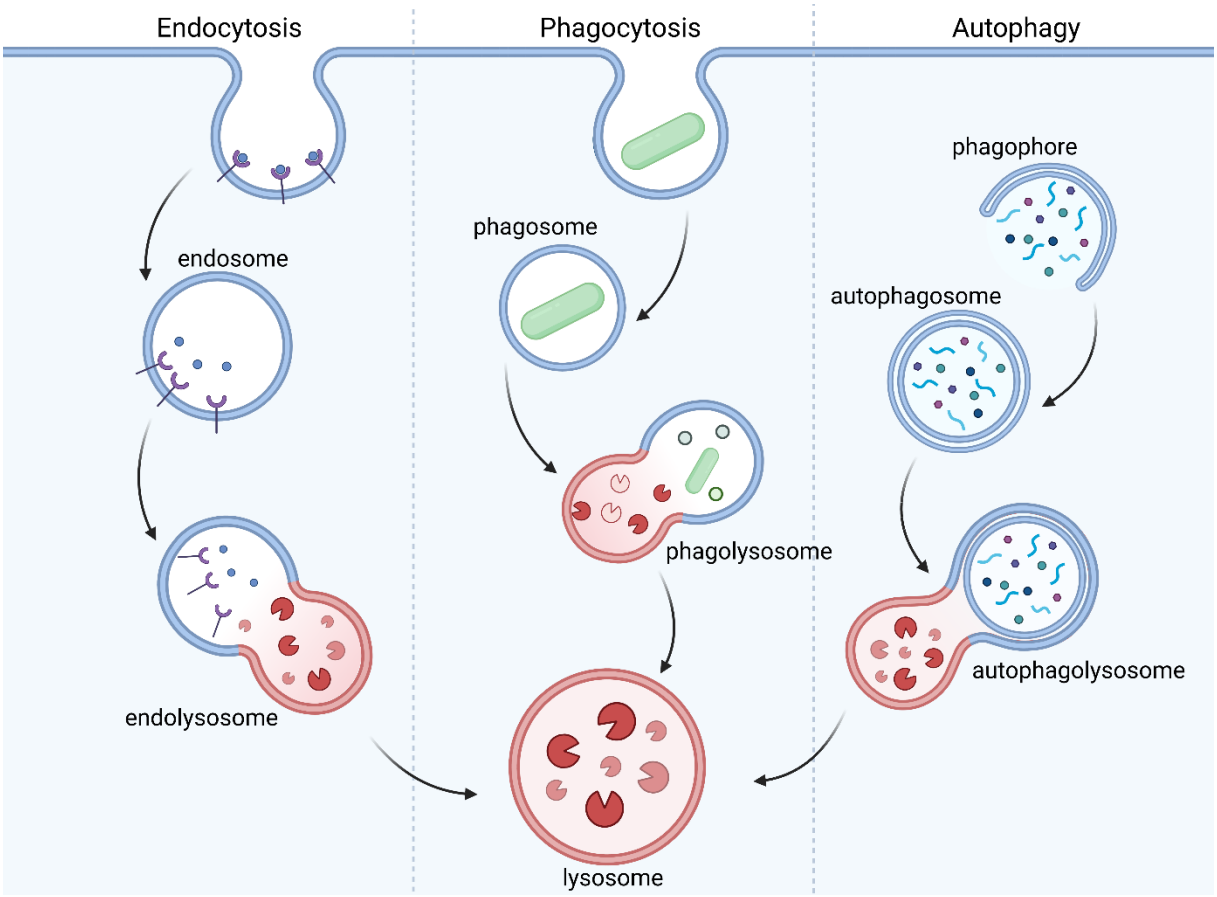


**Figure 1: Schematic overview of endocytosis, phagocytosis and autophagy.** Cargo destined for degradation is transported to lysosomes via three major pathways. Endocytosis and phagocytosis enclose extracellular material like receptors or pathogens into endosomes or phagosomes. Intracellular material like misfolded or aggregated proteins are engulfed into autophagosomes. All vesicles fuse with lysosomes where lysosomal proteases degrade the protein cargo.

#### 1.2.2.2.2 Phagocytosis

Phagocytosis (Figure 1) is responsible for taking up particles larger than 0.5 µm, pathogens or apoptotic cells (Uribe-Querol and Rosales 2020). Various receptors at the cell's plasma membrane are able to recognize and bind pathogens (Brubaker et al. 2015). The cargo is enclosed into vesicles derived from plasma membrane called phagosomes (Vernon and Tang 2013). Phagosomes fuse with lysosomes to form phagolysosomes, in which the engulfed pathogens are inactivated and degraded by lysosomal proteases (Uribe-Querol and Rosales 2020).

#### 1.2.2.2.3 Autophagy

The intracellular bulk degradation system is called macroautophagy (hereafter called autophagy, [Figure 2]) (Settembre et al. 2013; Myerowitz et al. 2021). Cytoplasmic components like damaged, dysfunctional, aged or long-lived proteins as well as organelles (e.g. mitochondria) are enwrapped in double-membrane vesicles called autophagosomes that later fuse with lysosomes to be degraded or recycled (Tanida et al. 2005; Lopez et al. 2018; Kobayashi 2015). Autophagy plays a pivotal role in maintaining cell homeostasis as it protects cells from damaged proteins but also provides nutrients like amino acids or free fatty acids under starvation conditions (Lopez et al. 2018; Kobayashi 2015). Defects in this pathway can have critical effects on the cell's metabolism and survival and is often associated with diseases like cancer or neurodegenerative disorders and aging (Tanida et al. 2005). The process is induced by intracellular or extracellular signals and starts with the formation of a phagophore. For instance, one signal can be the inactivation of the mammalian target of rapamycin complex 1 (mTORC1) caused by a lack of nutrients (Kobayashi 2015). Upon autophagy induction the Unc-51 like autophagy activating kinase (ULK1)-complex (ULK1, Atg13, FIP200, Atg101) is activated and translocated to the ER. The ULK1-complex activates the phosphoinositide 3-kinases (PI3K)-complex leading to the assembly and elongation of the autophagosome membrane and sequestration of labeled intracellular components recognized by adaptor proteins (Kobayashi 2015; Kageyama et al. 2021).

Two ubiquitin-conjugation systems are involved in the elongation process. One protein, microtubule-associated proteins 1A/1B light chain 3B (MAP1LC3A/LC3), is part of one of these systems and becomes cleaved into LC3-I followed by a covalent attachment

of a phosphatidylethanolamine (PE) molecule to form LC3-II (Kageyama et al. 2021). LC3-II is recruited to the phagophore membrane assisted by a complex of Atg5, Atg12 and Atg16 (Kageyama et al. 2021). The determination of cytosolic LC3-I and membrane-bound lipidated LC3-II by immunostainings or -blots is frequently used to analyze autophagy activation or the autophagic flux (Elbialy 2021; Klionsky et al. 2016). Another autophagy marker is sequestosome 1 (SQSTM1/p62) which can directly interact with LC3 and ubiquitinated cargo engulfed by the phagophore (Bjørkøy et al. 2009; Schläfli et al. 2016). When autophagy is active, p62 is constantly degraded and serves as a surrogate for autophagic degradation (Schläfli et al. 2016; Klionsky et al. 2016).

To complete the maturation the nutrient-sensitive regulator Atg9 is essential (Zavodszky et al. 2013). Only matured autophagosomes or endosomes can fuse with lysosomes promoted by membrane trafficking small Ras-like GTPase Rab proteins and a soluble NSF attachment protein receptor (SNARE) complex (Ao et al. 2014; Mizushima 2014). Autolysosomes are formed and after degradation of the autophagosomal membrane by a so far unidentified mammalian lipase the lysosomal hydrolases gain access to the autophagic substrates (Yim and Mizushima 2020). The final step of autophagy is the autophagic lysosome reformation (ALR) resulting in the restoration of lysosomes from autolysosomes (Yim and Mizushima 2020). ALR is initiated after reactivation of mTORC1 caused by a negative feedback loop resulting from the restoration of amino acid levels released from the autolysosomes (Mizushima and Komatsu 2011; Yim and Mizushima 2020).

Tubules are formed depending on an optimal balance between PI3P and PI4P and are severed by the GTPase Dynamin 2 (Yim and Mizushima 2020). After acidification, the newly formed lysosomes become able to activate lysosomal hydrolases and fuse again with late endosomes.

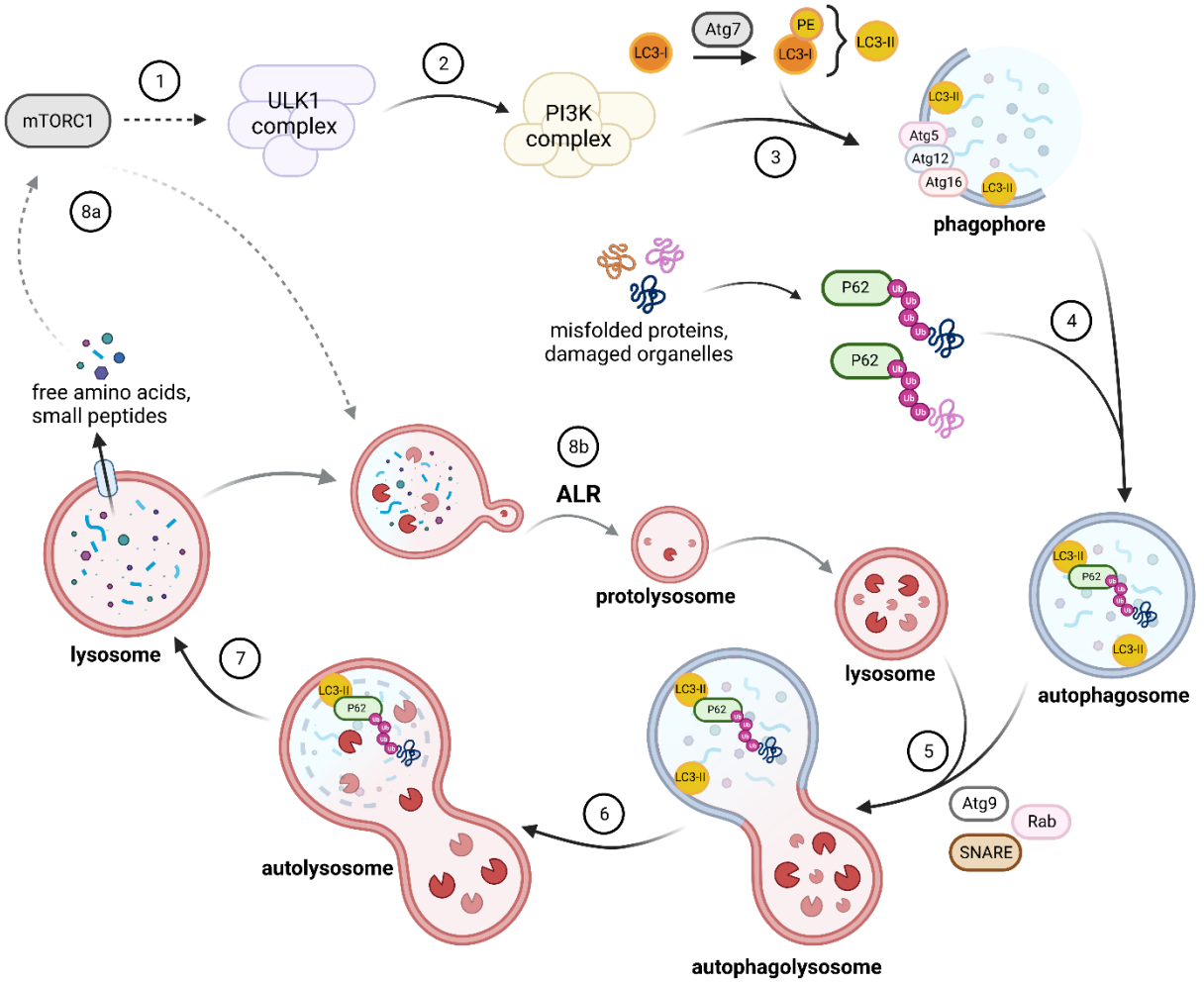


**Figure 2: Macroautophagy pathway.** (1) Starvation can inactivate mTORC1 which in turn activates the Unc-51 like autophagy activating kinase (ULK1)-complex followed by (2) activation of Phosphoinositide 3-kinases (PI3K)-complex. (3) LC3-I gets lipidated to form LC3-II by covalent binding to a phosphatidylethanolamine (PE) molecule with the help of Atg9. Atg5, Atg12 and Atg16 assist to form a phagophore and LC3-II is recruited to its membrane. (4) Cargo destined for degradation is ubiquitinated. P62 can bind to the ubiquitinated proteins and to LC3-II residing in the phagophore's membrane. The phagophore closes. (5) Maturated autophagosomes can fuse with lysosomes with the help of Rab proteins, Atg9, and a soluble NSF attachment protein receptor (SNARE) complex. (6) The vesicle acidifies and lysosomal hydrolases are able to (7) degrade the cargo, p62 and LC3-II. (8a) Amino acids and small peptides are released from the lysosome. A negative feedback loop can activate mTORC1 to inactivate the autophagic pathway and (8b) to initiate the autophagic lysosome reformation (ALR).

## 1.3 Lysosomal proteases

Extra- and intracellular material destined for degradation is transported to lysosomes by endocytosis, phagocytosis and autophagy (Figure 1). Lysosomes contain more than 60 different acidic hydrolytic enzymes including phosphatases (e.g. lysosomal acid phosphatase 2), glycolytic enzymes (e.g. β-galactosidase, β-glucuronidase, β-hexosaminidase), and proteolytic enzymes (e.g. cathepsins, legumain) (Ishidoh and Kominami 2002; Ashtari et al. 2016).

The most abundant hydrolases residing in the lysosome belong to the family of cathepsins (CTSs) (Turk et al. 2012; Yadati et al. 2020). CTSs are differently distributed throughout cell types and tissues and can be assigned into three subgroups: aspartic-, cysteine- and serine-type CTSs depending on their catalytic mechanism (Stoka et al. 2016; Patel et al. 2018). In humans, there are 15 different CTSs present in the lysosome which act as important regulators in physiological functions like digestion, autophagy, innate immunity, proliferation, or apoptosis (Turk et al. 2012; Patel et al. 2018). Mostly synthesized in the ER as inactive pre-pro-enzymes, CTSs are subjected to several proteolytic cleavage events (Figure 3) to become fully active and matured enrooted to the lysosome (Stoka et al. 2016). The N-terminal signal peptide is cleaved off in the lumen of the ER. The pro-enzyme becomes N-glycosylated to form a zymogen (Guay et al. 2000; Stoka et al. 2016). The pro-peptide supports the correct folding of the zymogen and targets it to the endosomes and lysosomes in a mannose-6-phosphate-dependent or -independent matter (Figura and Hasilik 1986). The pro-peptide is removed from the zymogen which in turn is released into its active mature form either autocatalytically or with the help of another protease (Ménard et al. 1998; Caglic et al. 2007; Turk et al. 2012). This last step is further supported by the low pH within the late endosome and lysosome (Turk et al. 1993; Turk et al. 2012; Stoka et al. 2016). The pH serves as an activity regulator of CTSs since a neutral pH (cytoplasm, endosomes) keeps the enzyme mainly in an inactive state while an acidic pH as present in lysosomes activates the enzymes (Stoka et al. 2016).

The cysteine proteases CTSB and CTSL and the aspartic protease CTSD are the most abundant lysosomal hydrolases and are often linked to autophagy as well as lysosomal or neurodegenerative diseases (Hook et al. 2011; Marques et al. 2020; Iwama et al. 2021; Prieto Huarcaya et al. 2022). They also interact and regulate each other as CTSB and CTSL assist in the maturation process of CTSD while CTSD is able to proteolytically cleave CTSL (Turk et al. 1999; Laurent-Matha et al. 2006; Zheng et al. 2008).

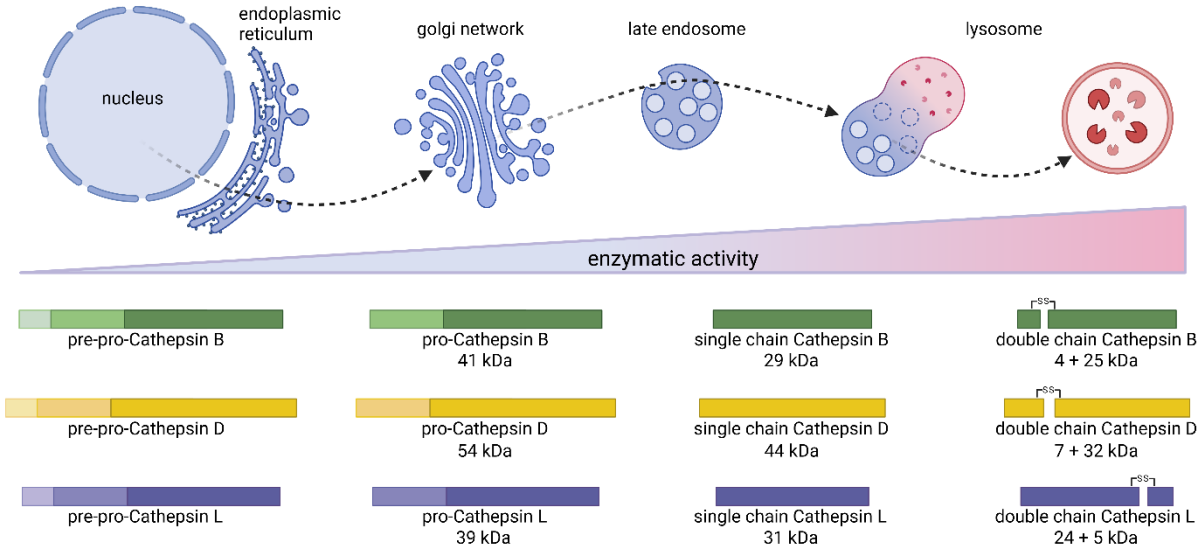


**Figure 3: Maturation process of Cathepsin B, Cathepsin D and Cathepsin L.** CTSB, D and L are synthesized as pre-pro-peptides. Upon maturation they are transported through the endoplasmic reticulum where the signal peptide is cleaved off. The pro-peptides are transported to the Golgi network and further processed to single chain peptides in the late endosomes. After transport to the lysosomes the mature double chain forms represent active proteases.

### 1.3.1 The cysteine-type proteases CTSB and CTSL

The cysteine proteases CTSB and CTSL are ubiquitously expressed in human tissues indicating a contribution to normal protein degradation and turnover (Turk et al. 2012). In humans, CTSB is mainly expressed in the thyroid, uterus and spleen while CTSL is mainly found in the placenta, liver, and adipose tissue (Uhlén et al. 2015). Both CTSB and CTSL are endopeptidases while CTSB also presents peptidyl-dipeptidasen activity (Brix et al. 2008; Yoon et al. 2022). The optimal pH for both CTSB and CTSL is found within the lysosomes (Turk et al. 2012). However, there is also evidence that cysteine CTSs have specific intra- and extracellular functions and that these enzymes are also active proteases under neutral pH conditions (Vasiljeva et al. 2007; Yoon et al. 2022). There have been several approaches to identify their individual roles and substrate specificities as they show redundant functions and a high similarity in their substrate recognition pattern (Poreba et al. 2018; Poreba et al. 2019). Both CTSB and CTSL share a conserved S1 pocket favoring basic amino acids like arginine and lysine for the P1 position (Puzer et al. 2004; Poreba et al. 2018; Poreba et al. 2019; Schmitz et al. 2019). Both enzymes recognize valine as the most suitable residue at position P2 (Turk et al. 2012; Poreba et al. 2018; Poreba et al. 2019). These similarities indicate redundant functions for CTSB and CTSL. However, Table 1 provides an overview of prioritized amino acids for positions P2-P4 demonstrating different preferences and

individual target specificities for the cleavage pattern of CTSB and CTSL (Turk et al. 2012; Poreba et al. 2018; Poreba et al. 2019; Schmitz et al. 2019). Only a few known substrates of either CTSB or CTSL are known including the Amyloid Precursor Protein (APP) for CTSB or collagen and elastine for CTSL (Brix et al. 2008; Kitamoto et al. 2007).

| position | P4 | P3 | P2 | P1 | P1' | P2' | P3' | P4' |
|---|---|---|---|---|---|---|---|---|
| **CTSB** | Arg<br>His | Ile<br>Leu<br>Lys | Val<br>Tyr | Arg<br>Lys | Ala | | | |
| **CTSL** | His<br>Lys | Arg<br>Lys | Val<br>Phe<br>Tyr | Arg<br>Lys | | | | |

**Table 1: Favorable amino acids for P4-P1' positions of CTSB and CTSL (Turk et al. 2012; Poreba et al. 2018; Poreba et al. 2019)**

CTSB-deficient mice do not show an obvious phenotype and they are fertile and viable (Deussing et al. 1998). These mice have a high resistance towards tumor necrosis factor-α-mediated hepatocyte apoptosis and show a reduction of trypsinogen activation in the pancreas (Deussing et al. 1998; Halangk et al. 2000). A knockout of CTSL in mice leads to a reduced hair growth and hair loss but the overall lifespan or fertility is not affected when compared to wildtype mice (Roth et al. 2000). Interestingly, a double-deficiency in CTSB and CTSL leads to a severe phenotype in mice (Felbor et al. 2002). These mice suffer from high apoptosis of neurons within the brain resulting in severe neurodegeneration accompanied by accumulation of lysosomal bodies (Felbor et al. 2002; Stahl et al. 2007). The double-deficiency in CTSB and CTSL also alters the autophagic flux (Koike 2000). Despite, both CTSB and CTSL being ubiquitously expressed throughout cell types and tissues, severe damages are found mainly within the brain. Therefore, CTSB and CTSL appear to be necessary for the development and homeostasis of the central nervous system (CNS) (Felbor et al. 2002). These findings indicate compensation effects or redundant functions of CTSB and CTSL as only the double deficiency leads to severe malfunction within the brain

and a strongly reduced lifespan of about 4 weeks (Felbor et al. 2002; Di Spiezio et al. 2021).

The neurodegeneration seen in CTSB and CTSL-double deficient mice is comparable to another lysosomal storage disease (LSD) found in mice and humans called Neuronal Lipofuscinosis 10 (CLN10) caused by a deficiency in CTSD (Koike 2000).

### 1.3.2 The aspartic-type protease CTSD

CTSD is an aspartic protease which constitutes about 10% of the total soluble lysosomal proteins with concentrations measured in the liver lysosomes from up to 0.7 mM making it the most abundant lysosomal hydrolase (Dean and Barrett 1976). The enzyme is distributed in almost all cell types and tissues but is mainly found within the brain, lung, and gall bladder (Uhlén et al. 2015). CTSD is an endopeptidase stable at an acidic pH and found in lysosomes (Morris 1978; Mijanovic et al. 2021). CTSD is known to cleave substrates between Phe-Phe bonds (Pimenta et al. 2001; Sun et al. 2013). In addition, other amino acids like tyrosine, leucine, and methionine are favored at the P1 position (Pimenta et al. 2001). In Table 2 the amino acids preferred for P3 to P1' by CTSD are listed.

| position | P4 | P3 | P2 | P1 | P1' | P2' | P3' | P4' |
|---|---|---|---|---|---|---|---|---|
| CTSD | | Leu | | Phe | Phe | | | |
| | | Val | Lys | Tyr | Tyr | | | |
| | | Glu | Ser | Leu | Phe | | | |
| | | Pro | | Met | Met | | | |

**Table 2: Favorable amino acids for P3-P1' positions of CTSD (Pimenta et al. 2001; Sun et al. 2013)**

CTSD has important functions in the brain and in the clearance of proteins produced by neurons e.g. APP, α-synuclein or huntingtin (Vidoni et al. 2016). Subsequentially, mutations of the CTSD gene affecting its maturation, activity, and localization are linked to the development of severe neurodegenerative disorders such as Alzheimer's disease (AD) or CLN10 (Koike 2000; Suire et al. 2020). Neurons depend on the proteolytic activity of CTSD to maintain neuronal cell homeostasis by degrading unfolded or aggregated proteins reaching the lysosome via autophagy or endocytosis (Vidoni et al. 2016). In mice, a CTSD-deficiency leads to a severe phenotype

characterized by seizures, neurodegeneration and early death after approximately three weeks (Saftig et al. 1995). Additionally, the lack of CTSD causes an impairment in the autophagic flux resulting in the accumulation of storage material including lipofuscin and saposins (Marques et al. 2020).

There have been approaches to analyze if other CTSs like CTSB or CTSL can clear those accumulated material or repair the autophagic impairments (Di Spiezio et al. 2021). Evidences suggest that lysosomal CTSs act in concert and might function in a hierarchical and redundant manner. However, there is no intensive knowledge of how lysosomal protein storage is degraded and which enzymes or CTSs hydrolyzes the respective substrates first. It is speculated that certain substrates have to be cleaved by specific enzymes first in order to be further degraded by other hydrolases.

## 1.4 Proteolysis malfunctions in diseases

Proteolysis plays a major role in maintaining cell homeostasis. Abnormalities in the transport, maturation or activation of enzymes relying on proteolytic modifications can cause severe consequences for the cell's metabolism, organ function, and the overall status of human health (Raju 2019). Deficiencies or malfunctions of lysosomal hydrolases are associated with many diseases. Autoimmune diseases like rheumatoid arthritis are caused by pathological release of lysosomal hydrolases into the extracellular space (Cuda et al. 2016). Once released active hydrolases digest proteins in the tissues resulting in chronic inflammation (Cuda et al. 2016). Lysosomal storage disorders (LSD) and neurodegenerative diseases like CLN10 , Alzheimer's disease (AD), and Parkinson's disease (PD) are associated with malfunctions in lysosomal hydrolases and autophagy (Raju 2019; Suire et al. 2020; Prieto Huarcaya et al. 2022).

### 1.4.1 Lysosomal storage disorders (LSDs)

Accumulation of non-degraded substrates within lysosomes due to malfunctioning hydrolases is the cause of a group of inherited metabolic disorders or lysosomal storage disorders (LSDs) (Sun 2018; Platt et al. 2018). LSDs comprise about 70 monogenic disorders of lysosomal metabolism originating from mutations in genes encoding lysosomal proteases, integral membrane proteins, transporters, enzyme modifiers, and activators (Platt et al. 2018). Many LSDs are pediatric

neurodegenerative disorders as lysosomal hydrolases play a key role in the development of the CNS. Pulmonary and heart problems, skeletal abnormalities, dementia, deafness, blindness, and movement problems are exemplary clinical symptoms of LSDs (Marques and Saftig 2019).

With a worldwide incidence ranging from 1:12,500 to 1:100,000 patients, Neuronal Ceroid Lipofuscinosis (CLN) is the most common neurodegenerative disorder in childhood (Vesa et al. 2002; Schulz et al. 2013; Trivedi et al. 2020). CLN is a family of LSDs characterized by the accumulation of lipofuscin and symptoms including dementia, motor decline, epilepsy, and visual failures (Dyken and Wisniewski 1995; Schulz et al. 2013). The classification of CLN is based on the age of onset and genetic mutation (Schulz et al. 2013; Platt et al. 2018). In the past years, enzyme replacement therapy has been proven to efficiently treat many LSDs and selected CLN (Marques and Saftig 2019).

#### 1.4.1.1 Ceroid Lipofuscinosis 10 (CLN10)

With an onset before or around birth CLN10 is the earliest and most severe form of CLN caused by a deficiency in CTSD (Marques and Saftig 2019). CLN10 leads to microcephaly, neonatal epilepsy, later on to ataxia, visual loss, cognitive decline, and eventually to early death (Fritchie et al. 2009; Platt et al. 2018). Pathomorphological characteristics are damage and loss of neurons in the retina and brain, neuroinflammation, and accumulation of autofluorescent ceroid lipofuscin (Marques et al. 2020). Autophagic markers including LC3 and p62 are accumulating indicating impairment in the autophagic pathway (Marques et al. 2020).

A possible and promising treatment might be enzyme replacement therapy (ERT) where the missing enzyme is infused to patients (Marques and Saftig 2019; Kohlschütter et al. 2019). However, the beneficial effects of ERT in LSDs or CLN are limited. For instance, the therapeutic enzyme cannot cross the blood-brain barrier (BBB) to reach the central nervous system (CNS), which is affected by two-thirds of all LSDs (Marques and Saftig 2019). On note, intracerebroventricular infusion of the recombinant human proenzyme Tripeptidyl peptidase 1 (TPP1) (Cerliponase alfa, Brineura™) in CLN2 patients was approved in 2017 (Markham 2017). Patients that receive this treatment once a week profit from reduced lysosomal storage material resulting in improved motor and language functions (Kohlschütter et al. 2019).

Recently, intracerebroventricular injection of recombinant-pro-CTSD to a CLN10 mouse model could increase the lifespan and reduce pathophysiological and -morphological symptoms of these mice indicating beneficial treatment of the disease (Marques et al. 2020; Prieto Huarcaya et al. 2022).

### 1.4.2 Alzheimer's disease (AD)

Alzheimer's disease is the most common form of dementia with 50 million patients worldwide (Knopman et al. 2021). This neurodegenerative disorder shows symptoms like short-term memory deficits, impairment in communication, and reduction in mental agility (Knopman et al. 2021). Other behavioral and cognitive disturbances like dementia, anxiety, apathy, psychosis, or aggression can also occur (Golde 2022).

The most important non-genetic risk factor is age but also genetic risk factors can cause the outbreak of symptoms since AD has strong heritable components (Tanzi 2012; Dourlen et al. 2019), although the heritability of AD is only 5% (Tanzi 2012). Dominant mutation in *Amyloid Precursor Protein* (*APP*), *Presenilin 1* (*PS1*), and *PS2* or *Apolipoprotein E* (*APOE)* contribute to almost all dominantly inherited AD cases (Haass et al. 2012). Interestingly, also protective mutants like the Islandic mutation in APP (A673T) exist (Jonsson et al. 2012).

There are two main hypotheses addressing the critical molecules that could be causal to the initiation and progression of AD: the Amyloid hypothesis and the Tau hypothesis (Knopman et al. 2021; Golde 2022). In the past decades, research has mainly focused on the Amyloid cascade hypothesis but therapeutics addressing Tau and ApoE just entered early stages of development as well (Long and Holtzman 2019). Amyloid-β (Aβ) is a small peptide derived from APP. Aβ was first described in 1984 and found to be the main constituent of neuritic plaques (Wong et al. 1985; Masters et al. 1985). Aβ emerges only during the amyloidogenic pathway as APP can be cleaved in mainly two different pathways (Figure 4) (Knopman et al. 2021).

Many pharmacological approaches are being suggested but only two classes of therapeutics are available for AD patients at present (Weller and Budson 2018; Knopman et al. 2021). There are three cholinesterase inhibitors recommended for the treatment of severe AD and one NMDA (N-methyl-D-aspartic acid) receptor antagonist for moderate-to-severe AD patients (Weller and Budson 2018). Current research also focuses on treatments targeting Tau and Aβ directly (Weller and Budson 2018). Aβ

might be cleared after being targeted with an antibody to improve removal from the brain. To reduce the Aβ plaque burden, there are approaches to inhibit APP degrading enzymes to prevent Aβ production and accumulation (Weller and Budson 2018). Although Aβ and Tau alterations have a significant influence in the induction of neurotoxicity and neuronal death, another hypothesis has been proposed recently (López-Ornelas et al. 2022). The disruption of the BBB followed by the activation of the innate immune system might have a strong potential in the onset and progression of AD (Zlokovic 2011). Accumulation of various molecules as consequence can, among other things, suppress capillary blood flow, promote neurotoxicity and memory impairment or increase neuronal injuries (Zlokovic 2011). There are approaches to enhance BBB integrity by different delivery strategies of growth factors like Vascular endothelial growth factor (VEGF) or Insulin-like growth factor 2 (IGF2) to reduce the Aβ burden within the brain (Zlokovic 2011).

#### 1.4.2.1 APP processing

APP is transported through the secretory pathway from the Trans-Golgi network (TGN) to the plasma membrane (Capell et al. 2000). From there, over 50% of APP can be reinternalized to the endosomes dependent on the Low-density Lipoprotein Receptor (LDL-R) (Capell et al. 2000). Only small amounts of APP are transported back to the plasma membrane while the majority is transported to the lysosomes (Zhang and Song 2013; Wang et al. 2017). APP is first cleaved by the β-secretase (BACE1), that is mainly located in the TGN and endosomes but also at the plasma membrane (Vassar et al. 1999; Whyte et al. 2020). BACE1 cleaves APP at its N-terminal part resulting in a soluble fragment (sAPPβ) and the membrane bound C-terminal fragment (CTF) called C99 (Kumar-Singh 2008). The APP-C99-fragment can be further processed by the γ-secretase complex (Thinakaran and Koo 2008; Holtzman et al. 2011; Whyte et al. 2020). The APP intracellular domain (AICD) and Aβ are the results after cleavage by the γ-secretase (Knopman et al. 2021). The AICD is released into the cytosol and supposed to be transported to the nucleus where it may function as a transcription factor (Müller et al. 2008; Konietzko 2012). Aβ can be secreted as monomer into the extracellular space or is degraded by endocytosis after fusion of endosomes with lysosomes (Kumar-Singh 2008). Due to its sequence and its hydrophobicity Aβ is prone to form aggregates in dependence of its concentration (Knopman et al. 2021).

Aβ also exist in different lengths depending on the processing protease (Andrew et al. 2016). In addition to α-, β- and γ-secretases other APP processing proteases are known. For example, η-secretase processing creates sAPPη and Aηα fragments (Willem et al. 2015). Meprin β releases shorter forms of Aβ starting from position 2 forming Aβ2-x fragments (Becker-Pauly and Pietrzik 2016).

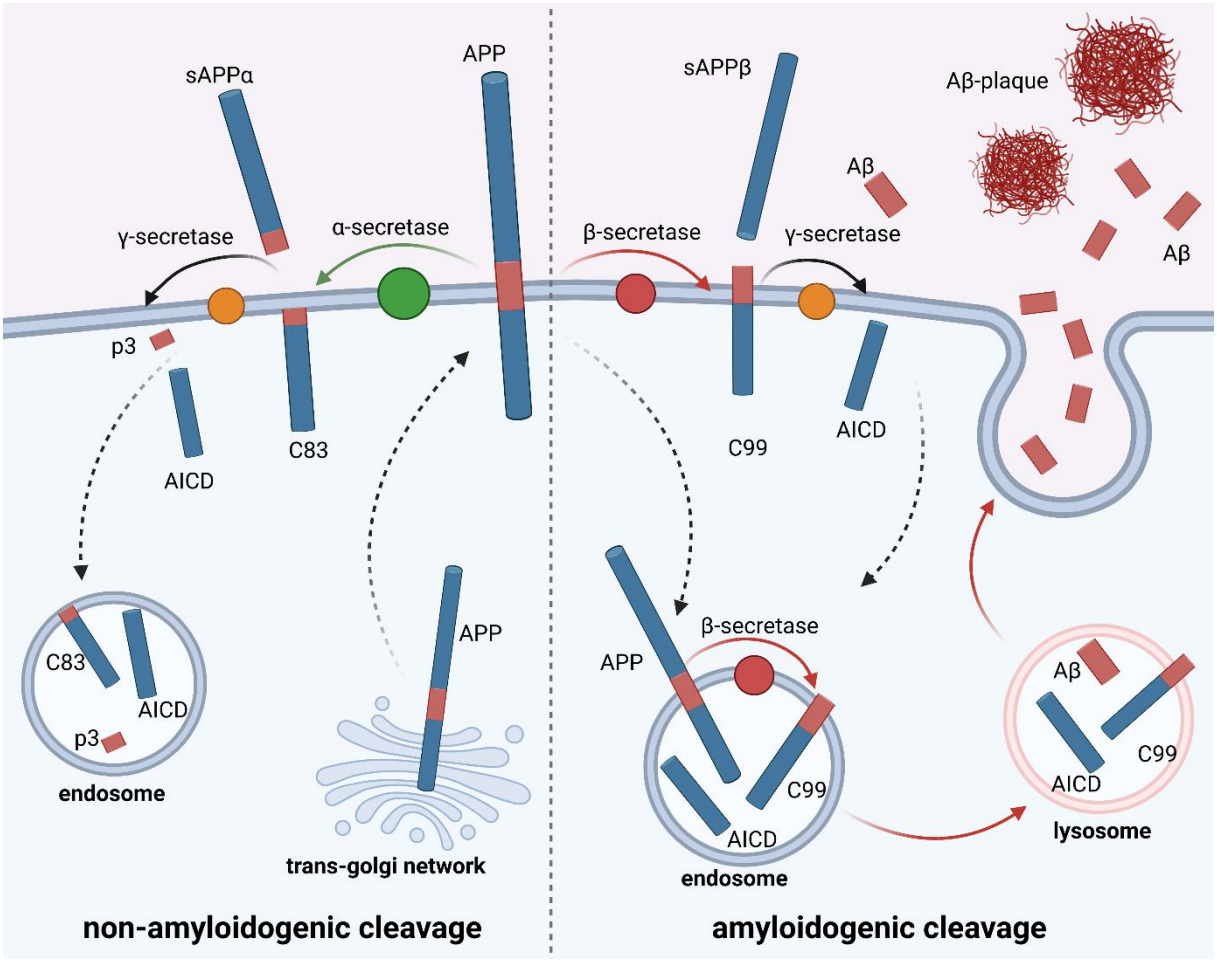


**Figure 4: Major cleavage events on the Amyloid Precursor Protein (APP).** APP is transported from the Golgi network to the plasma membrane. Over 50% of the protein is internalized to endosomes. APP can be proteolytically processed via two different pathways. The non-amyloidogenic pathway (left) is initiated by cleavage of the α-secretase (ADAM10) at the plasma membrane to form the soluble APPα (sAPPα) and the membrane bound C-terminal APP-C83. APP-C83 can be further cleaved by the γ-secretase complex into the p3 peptide and the APP intracellular domain (AICD). The amyloidogenic pathway (right) begins with cleavage of APP by the β-secretase (BACE1) at the plasma membrane or at the endosome. sAPPβ and the APP-C99 fragment are formed. The γ-secretase complex cleaves APP-C99 into AICD and Aβ. Aβ is released into the extracellular space after cleavage of sAPPβ at the plasma membrane or after exocytosis. Due to its hydrophobicity, Aβ is prone to form aggregates – the Aβ-plaques.

The other pathway how APP can be processed is the non-amyloidogenic pathway where no Aβ is released. Here, the α-secretase ADAM10 generates the soluble sAPPα and the membrane-bound C-terminal fragment APP-C83 at the plasma membrane (Jorissen et al. 2010; Haass and Willem 2019). The APP-C83-fragment is further processed by the γ-secretase resulting in a soluble p3 fragment and the AICD (Haass

and Willem 2019). P3 is released into the extracellular space and is believed to exert neurotoxic characteristics (Müller et al. 2008; Nhan et al. 2015).

#### 1.4.2.2 Consequences of the production of Aβ

A pathological hallmark of AD are Amyloid plaques derived from fibrils forms by Aβ peptides (Brown et al. 2020). Aβ is constantly produced within the brain.

It is believed that the etiology of AD is linked to a malfunction in the clearance of Aβ from the brain (Wang et al. 2021). However, the influence of Aβ accumulation on the development of AD is poorly understood. The main studies focus on Aβ1-40 and Aβ1-42, however Aβ peptides can differ in length with N- or C-terminally truncated species (Nhan et al. 2015; Gireud-Goss et al. 2021). Aβ1-40 is believed to be less toxic than Aβ1-42 and makes up 90% of the total Aβ (Kumar et al. 2018; Sharda et al. 2021). The highly toxic Aβ1-42 accounts for the other 10% and forms fibrils which can aggregate to form Aβ plaques (Seeman and Seeman 2011; Nhan et al. 2015; Sharda et al. 2021). There is evidence that accumulation of soluble Aβ oligomers is the earliest pathogenic event, rather than the fibrils (Bilousova et al. 2016). However, the exact properties of these small oligomers still remain unclear (Wang et al. 2021). An accumulation of Aβ disrupts synaptic function including an induction of neurotoxicity and loss of neurons (Gireud-Goss et al. 2021). Aβ plaques can alter the form of neurons, increase their distance and disrupt their communication within hippocampus and cortex (Selkoe and Hardy 2016). Additionally, it triggers neuroinflammation and hyperactivates microglia and astroglia (Heneka et al. 2015; Gireud-Goss et al. 2021). Besides its neurotoxic properties Aβ can also serve as a transcriptional factor, cholesterol transport regulator or antimicrobial agent (Nhan et al. 2015).

There are several pathways how Aβ is cleared from the brain under basal conditions. One way is through the BBB via LRP1 assisted by ApoE (Shibata et al. 2000; Zlokovic 2005; Storck et al. 2016). This pathway accounts for 50% of the transport of Aβ from the brain (Tanzi et al. 2004). As the transport through the BBB gets less efficient with age or in AD, the second major way to eliminate Aβ is the transport through interstitial fluid to the cerebrospinal fluid (CSF) followed by drainage into the blood (Kumar-Singh 2008; Parodi-Rullán et al. 2020). Aβ can also be enzymatically degraded either extracellularly or intracellularly (Wang et al. 2021). Enzymes secreted by cells like

neprilysin degrade extracellularly while endocytosed Aβ can be degraded within lysosomes by lysosomal hydrolases (Whyte et al. 2020; Wang et al. 2021).

#### 1.4.2.3 Involvement of CTSD in the APP metabolism

As the endo-lysosomal pathway is involved in the degradation of Aβ it is not surprising that this pathway is molecularly linked to the pathogenesis of AD (Whyte et al. 2020). Alterations in the expression and activity of lysosomal proteases have been reported. There is an increase in β-galactosidase and β-hexosaminidase (Magini et al. 2015) while glucocerebrosidase levels and activity are decreased (Choi et al. 2015). The main lysosomal protease within the brain, CTSD, is also linked to AD as there are studies showing lower enzymatic activity in an AD mouse model (Torres et al. 2012) and increased Aβ levels in CTSD-deficient mice (Suire et al. 2020). Early studies have already identified CTSD as Aβ degrading enzyme (Hamazaki 1996; McDermott and Gibson 1996) and a recent study identified CTSD as the main lysosomal hydrolyzing enzyme for intracellular Aβ1-42 (Suire et al. 2020). Suire and colleagues could also show inhibitory effects of Aβ1-42 on CTSD indicating a possible mechanistic link between Aβ and CTSD in AD (Suire et al. 2020). Increased Aβ deposits in CTSD-deficient mice and the inhibitory effects of Aβ on CTSD suggests that significant quantities of Aβ are transported and degraded by CTSD in the lysosome. However, it is not clear if boosted lysosomal CTSD activity may have an influence on a better clearance of Aβ.

# 2 Objectives

Cathepsins (CTSs) play a unique role within lysosomal protein degradation and recycling. They have a broad substrate specificity, overlapping cleavage patterns and act in concert. Previous studies revealed also special physiological functions of some CTSs in CTS-knockout mice. A CTSD-deficiency led to a severe phenotype with mice dying at young age. However, a lack of CTSB or CTSL in mice did not lead to serious abnormalities but a combined knockout of CTSB and CTSL shares similar pathophysiological features with CTSD-deficient mice. It might be that some CTSs are able to compensate for the loss of another CTS and obviously share redundant functions. However, there is a lack of knowledge of their individual substrates, site-specific cleavage, or possible hierarchical cleavage pattern.

The aim of this present work was to further investigate on the redundant but also site-specific function of CTSB, CTSD and CTSL in the human neuroblastoma cell line SH-SY5Y. First, various CTS-deficient cell lines were generated with the CRISPR/Cas9 technique. Resulting cells were initially characterized in regards of phenotypic and morphological differences of their lysosomes to address pathophysiological consequences. CTS-deficiencies in mice and humans can lead to abnormal autophagy and are often associated with the accumulation of lysosomal storage material. Therefore, the different SH-SY5Y CTS-knockout cell lines were analyzed for lysosomal aggregates by immunofluorescence and electron microscopy. Changes in their autophagic flux were addressed after starvation assays were conducted and evaluated by immunoblot and -fluorescence. In addition, proteolysis of endocytosed albumin, a common substrate of CTSB, CTSD and CTSL, was examined to gain initial knowledge about the impact on broad lysosomal proteolysis after a loss of three major lysosomal CTSs.

To further study the differences in protein abundance after all three major CTSs have been depleted, proteomic analysis was performed. Significantly upregulated protein expression identified by proteomics was further investigated and validated by immunoblot. Re-transfection of single or combined CTSs was used to support the specificity of the proteomic analysis and get an insight into the possible hierarchical cleavage order of the analyzed CTSs.

Another topic of this thesis focused on the special role of Cathepsin D as the main lysosomal hydrolase within the brain and its association with Alzheimer's disease (AD). The pathophysiological cleavage of the Amyloid precursor protein (APP) leads to abnormal amounts of Amyloid-β (Aβ) which is prone to form amyloid plaques in AD patients. In the past years, CTSD has been identified as the principal enzyme cleaving intracellular Aβ. To investigate the influence of CTSD on Aβ, HEK APPswe cells were treated with human recombinant pro-CTSD (rhpro-CTSD). CTSD-deficient and 5xFAD (an AD mouse model) mice were intracerebroventricularly injected with rhpro-CTSD at young age to examine whether the Aβ burden was reduced or delayed in older mice. The effects of rhpro-CTSD on APP, Aβ and neuroinflammation in HEK APPswe cells and CTSD-KO and 5xFAD (an AD mouse model) mouse brains were analyzed by immunoblot, ELISA and immunofluorescence.

# 3 Material and Methods

## 3.1 Material

### 3.1.1 Chemicals and Buffers

All chemicals were purchased with the purity grade “pro analysis” (p.a.) from Sigma-Aldrich, Carl Roth, AppliChem or Merck, unless stated otherwise.

### 3.1.2 Ready-made reagents and kits

| | |
|---|---|
| AmyloGlo RTD | Biosensis |
| Complete Protease Inhibitor Cocktail | Roche |
| ECL Advance™ Western Blotting Detection Kit | GE Healthcare |
| ELISA Human Amyloid-beta (1-40) | IBL International GmbH |
| ELISA Human Amyloid-beta (1-42) | IBL International GmbH |
| ELISA Mouse/Rat Amyloid-beta (1-40) | IBL International GmbH |
| ELISA Mouse/Rat Amyloid-beta (1-42) | IBL International GmbH |
| FastRuler Low Range DNA Ladder | Thermo Fisher Scientific |
| GeneJET PCR Purification Kit | Thermo Fisher Scientific |
| GeneRuler 100bp Plus DNA Ladder | Thermo Fisher Scientific |
| GeneRuler 1kb DNA Ladder | Thermo Fisher Scientific |
| High Pure PCR Product Purification Kit | Roche |
| Loading Dye | Thermo Fisher Scientific |
| MES Buffer | Thermo Fisher Scientific |
| NeonTM Transfection-Kit | Thermo Fisher Scientific |
| NuPAGE Gel 4-12% Bis-Tris | Thermo Fisher Scientific |
| PageRuler Plus Prestained Protein Ladder | Thermo Fisher Scientific |
| Pierce™ BCA Protein Assay Kit | Thermo Fisher Scientific |
| PureYield™ Plasmid Midiprep System | Promega |

### 3.1.3 Cell culture medium and additives

| | |
|---|---|
| Bafilomycin A1b | Sigma-Aldrich |
| BMV-109 | (Verdoes et al. 2013) |
| BSA-Alexa 647 | Thermo Fisher Scientific |
| CTSD&E substrate | EnzoLife Science |
| Dulbecco’s modified eagle medium (DMEM) | Life Technologies |

| | |
|---|---|
| E64D | EnzoLife Science |
| Earle’s Balanced Salt Solution (EBSS) | Sigma-Aldrich |
| Fetal bovine serum (FBS) | Biochrom |
| G418 | Invivo Gen |
| Human Amyloid β 1-42 | EnzoLife Science |
| Leupeptin | EnzoLife Science |
| MEM amino acids 50x | Life Technologies |
| MEM Non-essential amino acids 100x | Life Technologies |
| Penicillin-Streptomycin (P/S) | Life Technologies |
| Pepstatin A | EnzoLife Science |
| Recombinant human pro-CTSD (rhpro-CTSD) | Self-made (Marques et al. 2020) |
| Trypsin/Ethylenediaminetetraacetic acid (EDTA) | Sigma-Aldrich |

### 3.1.4 Primary antibodies

| **Antibody** | **Host** | **Dilutions** | | **Supplier/source** |
|---|---|---|---|---|
| | | **IF** | **WB** | |
| APP C-terminal (A8717) | rabbit | | 1:1000 | Sigma-Aldrich |
| APP N-terminal (22C11) | mouse | | 1:2000 | Sigma-Aldrich |
| Cathepsin B (AF953) | goat | | 1:1000 | R&D Systems |
| Cathepsin D (AF1014) | goat | 1:300 | 1:1000 | R&D Systems |
| Cathepsin L (AF952) | goat | | 1:1000 | R&D Systems |
| Cathepsin Z (AF934) | goat | | 1:1000 | R&D Systems |
| GAPDH (sc-25778) | rabbit | | 1:5000 | Santa Cruz Biotechnology |
| GFAP (G3893) | mouse | 1:2000 | | Sigma-Aldrich |
| Iba1 (GTX100042) | rabbit | 1:750 | | GeneTex |
| ITGA2 (AF1740) | sheep | | 1:1000 | Thermo Fisher Scientific |
| LC3 (PM036) | rabbit | 1:100 | 1:1000 | MBL |
| LAMP1 (1D4B) | rat | 1:300-1:750 | | DSHB |
| LAMP1 (H4A3) | mouse | 1:250 | 1:1000 | DSHB |
| LIMP2 (L2T2) | rabbit | 1:300 | | Pineda Antibody Service (Zunke et al., 2016) |
| MAP2 (4542) | rabbit | 1:750 | | Cell Signaling Technology |
| P62 (BHL-PW-9860) | rabbit | | 1:1000 | EnzoLife Science |

| | | | | |
|---|---|---|---|---|
| sAPPα/Amyloid-β human (6E10) | mouse | 1:300 | 1:1000 | BioLegend |
| sAPPα mouse (39153) | rabbit | | 1:1000 | BioLegend |
| sAPPβ human (18957) | rabbit | | 1:1000 | IBL-America |
| sAPPβ mouse (39138) | rabbit | | 1:1000 | BioLegend |
| sAPPβ Swe (6A1) | mouse | | 1:1000 | IBL International GmbH |
| Tubulin (E7) | mouse | | 1:2000 | DSHB |
| β-Actin (A2066) | rabbit | | 1:2000 | Sigma-Aldrich |
| β-Amyloid Antibody Sampler Kit (85314) | | | | Cell Signaling Technology |
| Aβ 1-37 (D2A6H) | mouse | | 1:1000 | |
| Aβ 1-40 (D8Q71) | mouse | | 1:1000 | |
| Aβ 1-42 (D3E10) | mouse | | 1:1000 | |

**Table 3: List of primary antibodies.** Dilution factors are presented for either immunofluorescence stainings (IF) or immunoblots (WB)

### 3.1.5 Secondary antibodies

| Antibody | Coupled to | Host | Dilution | Reference |
|---|---|---|---|---|
| Anti-goat | HRP | Rabbit | 1:10000 | Dianova |
| Anti-mouse | HRP | Goat | 1:10000 | Dianova |
| Anti-rabbit | HRP | Goat | 1:10000 | Dianova |
| Anti-sheep | HRP | Donkey | 1:10000 | Dianova |
| Anti-mouse | Alexa Fluor 488 | Donkey | 1:500 | Cell Signalling Technology |
| Anti-mouse | Alexa Fluor 594 | Donkey | 1:500 | Cell Signalling Technology |
| Anti-mouse | Alexa Fluor 647 | Donkey | 1:500 | Cell Signalling Technology |
| Anti-rabbit | Alexa Fluor 488 | Donkey | 1:500 | Cell Signalling Technology |
| Anti-rabbit | Alexa Fluor 594 | Donkey | 1:500 | Cell Signalling Technology |
| Anti-rat | Alexa Fluor 488 | Donkey | 1:500 | Cell Signalling Technology |

**Table 4: List of secondary antibodies used for immunoblots (coupled to horseradish peroxidase - HRP) or immunofluorescence stainings (coupled to Alexa fluor dyes).**

### 3.1.6 Oligonucleotides

| Primer name | Sequence 5‘-3‘ | Annealing Temperature |
|---|---|---|
| gCTSBfw | ATTCTGTCCACTCCCACCCT | 70.5 °C |
| gCTSBrv | CACTCCACCTAATCCTCGCC | |
| gCTSD40+41fw | TTGCCATTCACTGACTTGGG | 67.3 °C |
| gCTSD40+41rv | AGAAAGGAGTGTGGCTGAGC | |
| gCTSL88fw | AATGGCGTGGATTATGAGCA | 67.3 °C |
| gCTSL88rv | TCCTGGGCTTACGGTTTTGA | |
| 5xFAD 1644 | AATAGAGAACGGCAGGAGCA | 60 °C |
| 5xFAD 1645 | GCCATGAGGGCACTAATCAT | |
| 5xFAD 7338 | CTAGGCCACAGAATTGAAAGATCT | |
| 5xFAD 7339 | GTAGGTGGAAATTCTAGCATCATCC | |
| CD53 exon1 | AGACTAACAGGCCTGTTCCC | 58°C |
| CD53 exon2 | TCAGCTGTAGTTGCTCACATG | |
| neo-Kiel3 | GTTGTCACTGAAGCGGGAAGGGACTGGCTG | |
| neo-Kiel4 | GCGAACAGTTCGGCTGGCGCGAGCCCCTGA | |

**Table 5: List of primers to genotype CRISPR/Cas9-modified cells (indicated with ‘g’), 5xFAD and CTSD-deficient mice.**

### 3.1.7 Single guide RNAs for CRISPR/Cas9

| Gene of interest | Single guide RNA sequence |
|---|---|
| Cathepsin B | UGCAGGCAGCUUCAGGUCCU |
| Cathepsin D | UGGACGUGAACUUGUGCAGC |
| Cathepsin L | GAUGAUUGAACUGCACAAUC |

**Table 6: List of single guide RNAs used to modify cells by CRISPR/Cas9**

### 3.1.8 Bacteria

The amplification of plasmids was performed using *Escherichia Coli* XL1-blue (Agilent Technologies).

Genotype:

*recA1 endA1 gyrA96 thi-1 hsdR17 supE44 relA1 lac [F’ proAB laclqZΔM15 Tn10(Tetr)]*

### 3.1.9 Cell lines

| Cell line | Description | Origin/supplier |
|---|---|---|
| SH-SY5Y | Human neuroblastoma cells | (Biedler et al. 1978) |
| SH-SY5Y CTSB KO | CRISPR/Cas9-mediated knockout of CTSB in SH-SY5Y WT cells | This work |
| SH-SY5Y CTSD KO | CRISPR/Cas9-mediated knockout of CTSD in SH-SY5Y WT cells | This work |
| SH-SY5Y CTSL KO | CRISPR/Cas9-mediated knockout of CTSL in SH-SY5Y WT cells | This work |
| SH-SY5Y CTSBDL KO | CRISPR/Cas9-mediated knockout of CTSB, CTSD and CTSL in SH-SY5Y WT cells | This work |
| HeLa | Human cervix carcinoma cells (Henrietta Lacks) | DMSZ, established cell line |
| HEK293 | Human embryonic kidney cells | DKFZ, Heidelberg, Germany |
| HEK293 hAPP | HEK293 cells overexpressing human APP695 | (Haass et al. 1993) |
| HEK293 APPswe | HEK293 cells overexpressing Swedish mutant human APP695-swe | (Citron et al. 1992) |

**Table 7: List of cell lines.**

### 3.1.10 Mouse strains

| Mouse strain | Mutation | Source | reference |
|---|---|---|---|
| 5xFAD | APP Swedish (KM670/671NL)<br>APP Florida (I716V)<br>APP London (V717I)<br>PSEN1 (M146L)<br>PSEN1 (L286V) | Commercially available from the Jackson Laboratory | (Oakley et al. 2006) |
| CTSD -/- | *CTSD* deletion | | (Saftig et al. 1995) |
| C57BL/6NCrl | Control mice | Commercially available from the Jackson Laboratory | |

**Table 8: List of mouse strains and their mutations.**

### 3.1.11 Plasmids

| Plasmid | Insert | Reference/supplier |
|---|---|---|
| pcDNA3.1-Hygro(+) | - | (Huang, Morielli, and Peralta 1993) |
| pcDNA3.1-Hygro(+) | CTSB | Addgene (kindly provided by M. Saudenova) |
| pcDNA3.1-Hygro(+) | CTSD | C.Cappel |
| pcDNA3.1-Hygro(+) | CTSL-Myc | C.Cappel |
| pEGFP-C1 | mRFP-EGFP tandem fluorescent-tagged LC3 | (Kimura et al. 2007) |

**Table 9: List of plasmids used for transfection.**

### 3.1.12 Frequently used buffers and aqueous solutions

| | |
|---|---|
| **10x SDS running buffer** | 15% Glycine<br>250 mM Tris/HCl<br>1% SDS |
| **50x Tris-acetate-EDTA (TAE) buffer** | 2 mM Tris/HCl<br>5% (v/v) acidic acid<br>50 mM EDTA<br>pH 8.0 |
| **5x Laemmli buffer** | 60 mM Tris-Cl pH 6.8<br>2% SDS<br>10% glycerol<br>5% β-mercaptoethanol<br>0.01% bromophenol blue |
| **$CaCl_2$-solution** | 0.1 M $CaCl_2$ x $2H_2O$<br>5 mM Tris<br>5 mM $MgCl_2$ x 6H2O<br>pH 7.0 |
| **DEA lysis buffer for brains** | 50 mM NaCl<br>0.2% (w/v) diethyl amine<br>1x Protease Inhibitor<br>pH 10 |
| **Harsh stripping buffer** | 62.5 mM Tris/HCl pH 6.8<br>2% (w/v) SDS<br>0.83% (v/v) β-mercaptoethanol |
| **Lysogeny broth (LB) agar** | 1.5% (w/v) agar-agar<br>in LB medium |
| **Lysogeny broth (LB) medium** | 1% (w/v) Tryptone/Peptone<br>0.5% (w/v) yeast extract<br>1% (w/v) NaCl<br>pH 7.0 |
| **Mild stripping buffer** | 100 mM Glycin<br>20 mM Magnesium acetate<br>50 mM KCl<br>pH 2.2 |

| | |
|---|---|
| **Mounting medium** | 1x PBS pH 7.4<br>17% (w/v) Mowiol 4-88<br>33% (v/v) Glycerol<br>20 mg/ml 1,4-diaza-bicyclo-2,2,2-octane (DABCO) |
| **Phosphate buffer (0.1 M)** | 77.4 mM $Na_2HPO_4$<br>22.6 mM $NaH_2PO_4$<br>pH 7.4 |
| **Phosphate-buffered saline (PBS) (10x)** | 100 mM $Na_2HPO_4$<br>18 mM $KH_2PO_4$<br>1.37 M NaCl<br>27 mM KCl<br>pH 6.8 |
| **Ponceau S solution** | 5% acetic acid<br>Ponceau S |
| **RIPA lysis buffer for brains** | 20 mM Tris-HCl pH 7.5<br>150 mM NaCl<br>1 mM $Na_2EDTA$<br>1% (v/v) NP-40<br>1% (w/v) sodium deoxycholate<br>2.5 mM sodium pyrophosphate<br>1x Complete |
| **RIPA lysis buffer for cells** | 50 mM Tris-HCl pH 7.4<br>150 mM NaCl<br>1% NP-40<br>0.5% sodium deoxycholate<br>0.01% SDS<br>1x Complete |
| **RIPA lysis buffer modified for proteomic analysis** | 50 mM Tris-HCl pH 8.0<br>150 mM NaCl<br>5 mM EDTA pH 8.0<br>1% Triton X-100<br>0.5% sodium deoxycholate<br>0.1% SDS<br>1x Complete |
| **Separating gel buffer:** | 1.5 M Tris/HCl pH 8.8<br>0.4 % (w/v) SDS |
| **Stacking gel buffer:** | 0.5 M Tris/HCl pH 6.8<br>0.4% (w/v) SDS |
| **Transfer buffer** | 100 mM Glycine<br>25 mM Tris/HCl<br>10% methanol |
| **Tris-buffered saline (TBS)** | 13,7 mM NaCl<br>0,27 mM KCl<br>2,5 mM Tris/HCl<br>pH 7.4 |

**Table 10: List of buffers and aqueous solutions.**

## 3.2 Methods

### 3.2.1 Molecular Biological Methods

#### 3.2.1.1 Generation of chemically competent *Escherichia coli*

To generate chemically competent *Escherichia coli* (*E.coli*) an overnight start culture was prepared by adding an aliquot of *E.coli* XL1-blue cells (3.1.8) to 5 ml of LB medium (Table 10) and 5 µl tetracycline. The next day 50 ml LB medium containing 50 µl tetracycline was inoculated with the start culture until it reached an $OD_{600}$ of 0.4-0.6. The culture was stored on ice for 20 min and centrifuged at 5000 g for 10 min at 4 °C. The resulting pellet was resuspended in 20 ml ice cold TBS (Table 10) and centrifuged again. Afterwards the pellet was resuspended in 20 ml ice cold $CaCl_2$ solution and stored on ice up to 60 min followed by another centrifugation step. The final resulting pellet was resuspended in 2 ml ice cold $CaCl_2$ solution and stored on ice for 1 h. 500 µl 86% glycerin was added. The mixture was vortexed and 50 µl aliquots were quick-frozen in liquid nitrogen and stored at -80 °C.

#### 3.2.1.2 Transformation and purification of chemically competent *E.coli*

An aliquot of 50 µl chemically competent *E.coli* XL1-blue (3.1.8) was incubated with 150 ng of desired plasmid on ice for 30 to 60 min followed by a heat shock at 42 °C for 40 s. The cells were stored on ice for 5 min and were shaken with 300 µl LB medium at 37 °C for 1 h. 100 µl of this solution was plated on a LB-plate with respective antibiotics according to the resistance encoded in the plasmid and incubated at 37 °C overnight. Plates were stored at 4 °C. To amplify the desired plasmid, a single colony was picked and transferred to 300 ml LB medium with 100 µg/ml ampicillin and incubated overnight at 37 °C and the DNA was isolated by the PureYield Plasmid Midiprep System (Promega) according to the manufacturer's protocol.

#### 3.2.1.3 Measuring DNA concentration

The concentration of DNA at 260 nm was determined using a Synergy HT microplate reader (Biotek). The sample concentration was calculated using an OD of 1 at 260 nm, which corresponds to a concentration of 50 g/ml (DNA). Adsorption at 280 nm was also measured to ensure sample purity. For a clean sample, the A260/A280 ratio should be between 1.8 and 2.

### 3.2.1.4 Polymerase Chain Reaction (PCR)

The polymerase chain reaction (PCR) was used to amplify DNA fragments. The following pipetting scheme and cycling program (Table 11) was used. The annealing temperature indicated with an “X” is dependent on the primer (Table 5) used for the PCR.

| | µl |
|---|---|
| Forward Primer | 1.25 |
| Reverse Primer | 1.25 |
| 10x DreamTaq Puffer | 5 |
| dNTP 2 mM | 5 |
| DreamTaq 5U | 0.5 |
| Template | 1 |
| add $H_20$ | 50 |

| Step | t | T (°C) | |
|---|---|---|---|
| Initial denaturation | 3 min | 95 | |
| Denaturation | 10 s | 95 | 35 x |
| Annealing | 45 s | X | |
| Elongation | 30 s | 72 | |
| Final elongation | 10 | 72 | |
| End | ∞ | 10 | |

**Table 11: PCR pipetting scheme and cycling program.**

### 3.2.1.5 Agarose gel electrophoresis

For the genotyping of mice and sequencing of the CRISPR/Cas9-edited cell lines, PCR samples were analyzed using agarose gel electrophoresis. A 1.5% agarose gel in 1x TAE buffer (Table 10) containing ethidium bromide to intercalate into the DNA samples was prepared. DNA samples were prepared for gel electrophoresis by adding 6x loading dye (Thermo Fisher Scientific) and loaded on the agarose gel. By applying an electric field (120 V, 30 min) DNA fragments migrate through the gel matrix according to their size. Using UV-light the signals can be visualized and the product size can be determined by using GeneRuler 1 kb DNA Ladder (Thermo Fisher Scientific).

## 3.2.2 Cell biological methods

### 3.2.2.1 Cultivation of mammalian cell lines

Mammalian cell lines were kept in the cell culture incubator with 5% $CO_2$ at 37 °C. All cell lines were maintained in Dulbecco’s modified Eagle Medium (DMEM) containing 4.5 g/L of D-Glucose and L-glutamine (Thermo Fisher Scientific) and were supplemented with 10% (v/v) fetal bovine serum (FBS) and 1% Penicillin/Streptomycin (P/S). HEK hAPP and APPswe cells were additionally treated with 200 µg/ml G418. Cells were handled under sterile conditions under a

laminar flow clean bench and after reaching a confluency of 80-100%, cells were split up into a new cell culture dish twice per week. Therefore, old media was removed, cells were washed in sterile PBS and detached using Trypsin/EDTA. Detached cells were resuspended in fresh media and transferred to a new cell culture dish. The splitting ratio depended on the cell growth of the respective cell line (HEK cells: 1:20, HeLa cells: 1:10 and SH-SY5Y cells: 1:3-1:5).

#### 3.2.2.2 Cryopreservation and thawing of mammalian cell lines

Preservation of especially CRISPR/Cas9-mediated cell lines was done at the earliest passage number (P=2-4) as possible. For this, cells were grown to 80-100% confluency, washed in PBS and detached from the plate with trypsin/EDTA at 37 °C. Detached cells were then resuspended in medium and centrifuges at 300 g for 10 min at RT. The cell pellet was resuspended in FBS containing 10% DMSO and subsequently frozen at -80 °C for at least 24 h and stored in liquid nitrogen for long-time storage.

To thaw and re-cultivate cells, they were incubated in a water bath at 37 °C for 5 min and mixed with 10 ml pre-warmed fresh cultivation medium on a sterile cell culture dish. The next day, the medium was changed to remove the DMSO from the cells. Cells were cultivated at least one week before any experiment was conducted on them.

#### 3.2.2.3 Transient transfection of mammalian cell lines

Cells were seeded on a cell culture plate (1-1.5x$10^6$ cells for a 6 cm dish) with a cover slip if needed for a following experiment one day prior transfection. The next day, 1-3 µg of the desired plasmid was incubated with Turbofect in 300 µl DMEM for 15 min at RT. Then the solution was added to the cells and after 5-8 h the medium was changed. Cells were grown for 48 h until further usage.

#### 3.2.2.4 Generation of CRISPR/Cas9 knockout cell lines

To modify double-stranded DNA (dsDNA) to precisely delete gene sequences the CRISPR/Cas9-technology is broadly used. A single guide RNA (sgRNA) composed of a short CRISPR RNA (crRNA) and a trans-activating crRNA (tracrRNA) can bind the

Cas9 enzyme (Adli 2018). The crRNA is the complement to the target sequence and guides the CRISPR/Cas9 complex to the DNA locus thus creating breaks within the dsDNA (Jinek et al. 2012). DNA double-strand breaks are repaired by non-homologous DNA end joining (NHEJ) (Chang et al. 2017). NHEJ can create diverse DNA sequences with base pair deletions, inserts but also without loss of nucleotides (Chang et al. 2017).

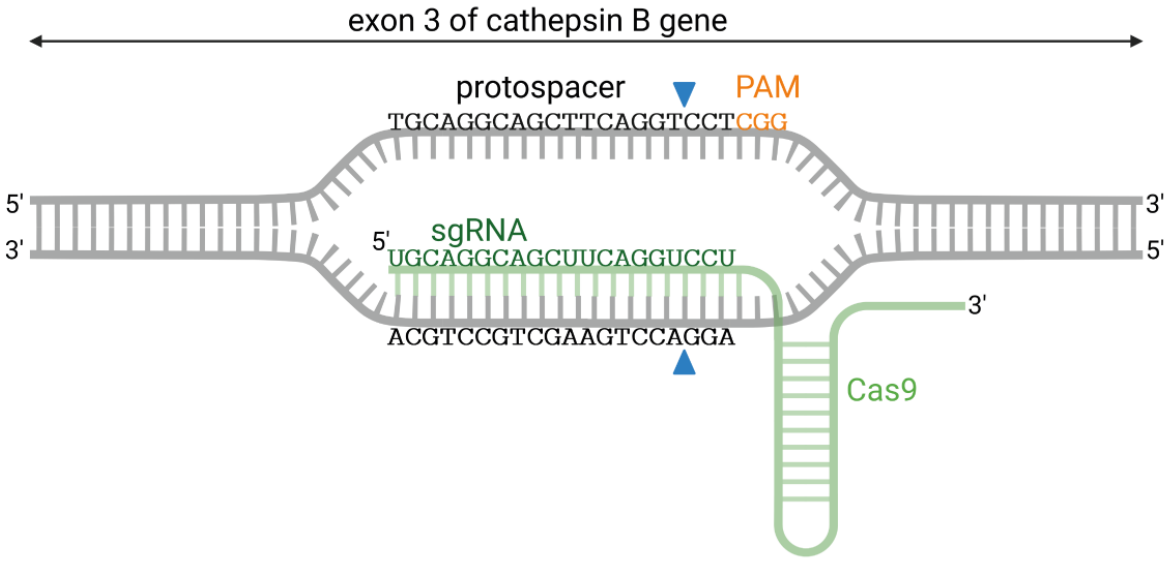


**Figure 5: Schematic overview of the CRISPR gene editing strategy.** The scheme shows the binding of the Cas9-guided sgRNA-sequence (green) to the matching genomic DNA in the exon 4 of the human CTSB gene. The protospacer adjacent motif (PAM)-sequence (orange) followed by the protospacer sequence targets the Cas9 nuclease to bind to the gene region of interest to cleave the targeted DNA region (blue arrow).

To generate different SH-SY5Y CTS-deficient cell lines by CRISPR/Cas9-mediation the Neon™ Transfection System (Thermo Fisher Scientific) was used. A mixture containing SH-SY5Y cells, single guide RNAs (sgRNA) (Table 7) and Cas9 was prepared as listed in Table 12. Cell were counted and the respective amount resuspended in Buffer R provided by the company. Next, sgRNA and Cas9 was added from a pre-mixture to the cells (Table 12). By using the electroporation pipet tips 10 µl of the cell/sgRNA/Cas9 mixture was transferred to the electroporation device according to the manufacturer's indications. The program recommended for SH-SY5Y cells provided by the company was used to deliver the sgRNA and Cas9 into the cells. Cell were plated in DMEM containing 20% FBS. The next day medium was exchanged. Cells were separated into single cells into 96-well-plates after they reached a confluency of 80-100%. To expand the cells from mixed clone to single clones they

were kept in DMEM containing 20% FBS and 1% P/S. Single clones were expanded for cryopreservation (3.2.2.2), sequencing and western blot analysis (3.2.3.5).

| | 6 cm dish | 10 cm dish |
|---|---|---|
| Cas9 62 µM (Synthego)<br>sgRNA 100 µM (Synthego)<br>$H_2O$ | 1 µl<br>each sgRNA 1.25 µl<br>add 6.25 µl | 1 µl<br>each sgRNA 1.25 µl<br>add 6.25 µl |
| | → 2.5 µl per 25 µl cells | → 5 µl per 50 µl cells |
| cells | $1.4x10^6$ in 25 µl | $2.8x10^6$ in 50 µl |
| electroporation | 2 times 10 µl | 4 times 10 µl |

**Table 12: Preparation of cell, sgRNA and Cas9 mixture for CRISPR/Cas9-mediated genome editing**

To generate SH-SY5Y CTSBDL-deficient cell lines, a confirmed CTSB-deficient clone (SH-SY5Y CTSB KO #3) was used to simultaneously introduce the sgRNAs for CTSD and CTSL. For analysis of the targeting efficacy of the transfection, genomic DNA of the single clones was isolated using DirectPCR® Lysis Reagent Tail (Peqlab) and proteinase K at 55 °C overnight. To inactivate proteinase K the mixture was kept at 85 °C for 45 min.

The DNA was used as a template for a genotyping PCR (3.2.1.4) amplifying the sequence close by the binding position of the sgRNA (primers are listed in Table 5). The annealing temperature of each sequencing primer pair used for the genotyping PCR was determined by a temperature gradient PCR using DNA of SH-SY5Y WT cells as template. The final annealing temperatures can be found in Table 5. The resulting PCR product was purified using the GeneJET PCR Purification Kit (Thermo Fisher Scientific) and sent for sequencing to Eurofins Genomic GmbH according to their sample requirements. Subsequently, the DNA sequences of the modified SH-SY5Y cell lines were compared to the SH-SY5Y WT ones. They were analyzed in regards to base pair inserts or deletions (indels) with the Interference of CRISPR edits (ICE) tool offered by Synthego. In addition, the Knockout was confirmed by immunoblot analysis (3.2.3.5) using antibodies directed against the respective cathepsin.

### 3.2.2.5 Autophagic flux assay

To determine the autophagic flux, SH-SY5Y WT and CTSBDL-deficient cells were seeded on cell culture plates ($3x10^5$ in 6 cm plates, $1.5x10^6$ in 10 cm plates). The next day, cells were washed in PBS three times to remove leftover FBS. Cells were incubated with EBSS (Thermo Fisher Scientific), 1x essential amino acids (Thermo

Fisher Scientific), 1x non-essential amino acids (Thermo Fisher Scientific) and 10% FBS either with or without 500 nM Bafilomycin A1 (Sigma) or EBSS only with or without 500 nM Bafilomycin A1. These cell culture additives are listed in 3.1.3. After 3 h of incubation cells were washed in ice cold PBS and harvested using cell scrapers. Protein lysates were prepared (3.2.3.1) by adding 20 mM NaF, 4 mM glycerol 2-phosphate and 4 mM $NaVO_3$ additionally to the RIPA lysis buffer (3.2.3.1).

For analysis by IF (3.2.4.1) cells were seeded on coverslips and transiently transfected (3.2.2.3) with mRFP-GFP fluorescence-tagged LC3 (Table 9) and used for subsequent starvation assay as described above.

### 3.2.2.6 Activity based probe

To analyze the activity of the different HeLa and SH-SY5Y cell lines the pan-reactive cysteine quenched activity-based-probe (qABP) BMV-109 (kindly provided by M. Bogyo) was used (Figure 6).

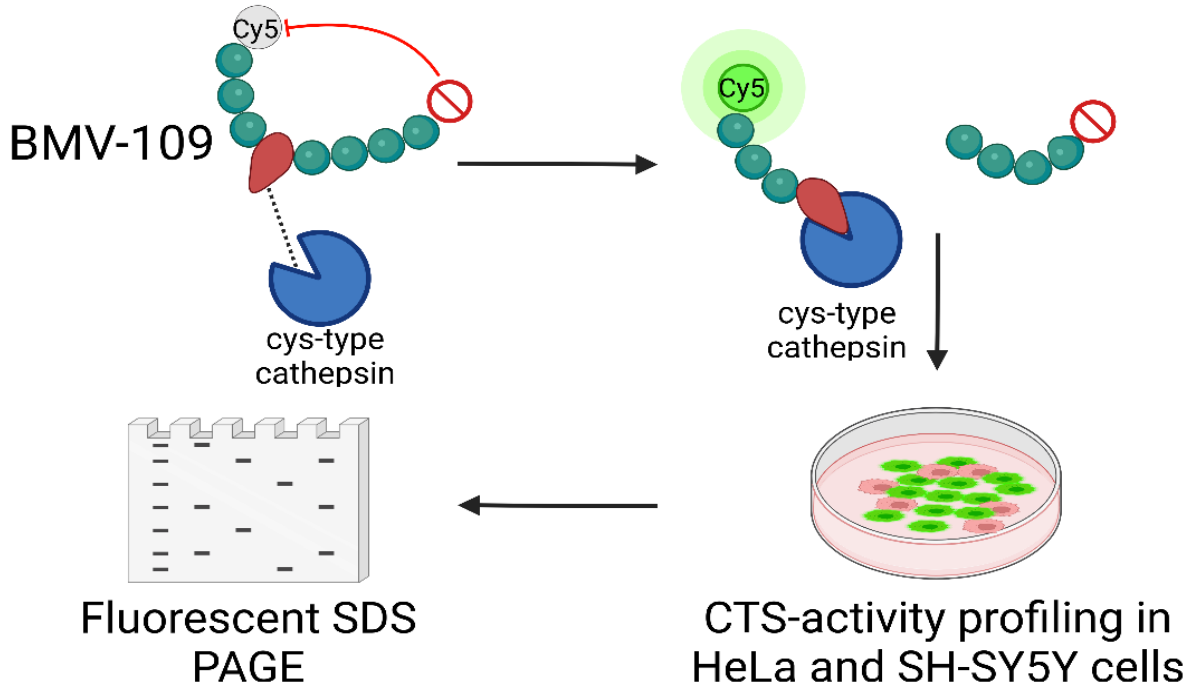


**Figure 6: Active Cysteine-type cathepsins can bind and cleave the pan-reactive cysteine quenched activity-based-probe (qABP) BMV-109**. BMV-109 is a qABP consisting of the fluorophore Cy5, the amino reactive quencher QSY™21 (red Ø) and a phenoxymethyl ketone reactive group (red) that reacts with the active site of cysteine-type cathepsins. Once the qABP is bound to the active site of the enzyme, the quencher is cleaved off and the active enzyme is bound to the fluorophore Cy5. Cells are able to take up BMV-109 by endocytosis and once it reached lysosomes the active cysteine-type cathepsins are bound to the fluorescing probe. Cell lysates of these samples can be analysed by a fluorescent SDS-PAGE. BMV-109 Cy5-signal can be detected at 635 nm. Scheme adapted from (Verdoes et al. 2013).

Once an active cathepsin binds to the qABP it cleaves off the quencher and the active site of the enzyme is then bound to the fluorescing probe. Therefore, $1.5x10^6$ SH-SY5Y cells were seeded in 6 cm plates 24 h prior the assay was applied. Cells were washed in PBS. Cells were incubated with 50 µM E64D, 20 µM Leupeptin and 10 µg/ml Pepstatin A or 500 nM Bafilomycin A1 in DMEM (3.1.3) only as controls (if needed) for 15 min prior application of 100 nM BMV-109 for another 2 h. Cells were harvested and lysed (3.2.3.1) while the samples were kept in the dark to prevent bleaching. SDS-PAGE was performed on a 15% polyacrylamide gel (3.2.3.4) in the dark. Using the Amersham™ Typhoon™ Biomolecular Imager (GE Healthcare) the in-gel Cy5-fluorescence signal was detected. Coomassie blue staining (GelCode™ Blue Stain Reagent, Thermo Fisher Scientific) was used as loading control.

#### 3.2.2.7 Endocytosis and processing of BSA-Alexa 647

Bovine serum albumin (BSA) is a broad substrate for proteases and a known substrate of CTSD. Therefore, it can be used to examine endocytosis, its intracellular processing and analysis of enzymatic activity of proteins hydrolyzing BSA.

$1.5x10^6$ SH-SY5Y WT and CTSBDL-deficient cells were seeded on 6 cm cell culture plates 24 h prior the assay was conducted. Cells were washed in PBS and 15 µg/ml BSA-Alexa 647 in DMEM containing 1% FBS and 1% P/S was added to the cells. Two types of experiments were performed using this method. First, cells were incubated with BSA-Alexa 647 for 1, 3, 5, 6, 8, 12, 14 and 16 h and harvested afterwards (3.2.3.1). Second, cells were incubated with BSA-Alexa 647 for 2 h, then washed with PBS and incubated for another 10, 20, 30 min, 1 h and 2 h in DMEM containing 1% FBS and 1% P/S (pulse-chase experiment). Cells were harvested and lysed (3.2.3.1) under protection of light. A fluorescent SDS-PAGE was used to analyze the samples (3.2.3.4). The in-gel fluorescence signal of BSA-Alexa 647 was detected using the Amersham™ Typhoon™ Biomolecular Imager (GE Healthcare).

### 3.2.3 Protein biochemical methods

#### 3.2.3.1 Preparation of cell lysates and protein extraction

To harvest cells, they were washed in ice cold PBS three times. By using cell scarpers, cells were collected in 1 ml ice cold PBS and centrifuged at 600 g for 10 min. To lyse

the cells, the cell pellet was resuspended in RIPA (Table 10) containing 1x Complete and incubated on ice for at least 1 h. Afterwards, the solution was centrifuged at 16.000 g for 10 min at 4 °C. The supernatant containing the protein lysates was collected in a new tube for protein concentration determination (3.2.3.3) and stored at -20 °C until further usage.

### 3.2.3.2 Preparation of murine tissue homogenates

Mouse brain lysates were generated by DEA extraction for soluble proteins followed by RIPA extraction for membrane and cytosolic proteins and FA extraction for insoluble proteins. Tissue was first homogenized with 3-4 porcelain beads (PeqLab) in DEA lysis buffer (Table 10) with 1x Complete with a Precellys® 24 homogenizer (Bertin) at 6500 g for 30 s at 4 °C. The supernatant was cleared by ultracentrifugation at 130.000 g for 1 h at 4 °C. The supernatant contains soluble proteins (=DEA fraction) while the resulting pellet was further resuspended in RIPA lysis buffer (Table 10) and homogenized by Precellys ® 24 homogenizer (Bertin) at 6500 g for 30 s at 4 °C. After centrifugation at 5000 g for 10 min at 4 °C the supernatant was ultra-centrifuged again at 130.000 rpm for 1 h at 4 °C. The resulting supernatant contains the membrane bound proteins (=RIPA fraction). The remained pellet contains insoluble proteins which gets resuspended in 70% formic acid and is again ultra-centrifuged at 130.000 rpm for 1 h at 4 °C. The resulting supernatant contains insoluble proteins (=FA fraction). The The pH of the DEA fraction was adjusted to pH 6.8 with 0.5 M Tris buffer. The FA fraction was diluted 1:20 with 1 M Tris buffer pH 9.5. Protein concentration was determined as described (3.2.3.3).

### 3.2.3.3 Determination of protein concentration

To determine the protein concentration of cell or mouse brain lysates, the Pierce BCA Assay kit (Thermo Fisher Scientific) was used according to the manufacturer's instructions. Samples were diluted 1:10 with respective lysis buffer and incubated in 100 µl of the assay mixture for 30 min at 37 °C. In addition to lysates, a BSA calibration series with known concentrations ranging from 0 to 2 mg/ml was analyzed to create a protein concentration curve. The absorbance at 562 nm was measured using a Synergy HT (BioTek) microplate reader.

### 3.2.3.4 SDS polyacrylamide electrophoresis (SDS-PAGE, fluorescent SDS-PAGE)

The analysis of the compositions of proteins of cell or tissue lysates can be performed by separating them by discontinuous sodium dodecyl sulphate polyacrylamide gel electrophoresis (SDS-PAGE). SDS polyacrylamide gels were prepared as shown in Table 13.

| | Separating gel | | | Stacking gel |
|---|---|---|---|---|
| | **10%** | **12.5%** | **15%** | **5.25%** |
| Separating/Stacking buffer | 2.6 ml | 2.6 ml | 2.6 ml | 1.35 ml |
| 30% (w/v) Acrylamide/bisacrylamide Rotiphorese Gel 30 (37, 5:1) | 3.3 ml | 4.2 ml | 5.0 ml | 1.75 ml |
| $H_2O$ | 4.0 ml | 3.1 ml | 2.3 ml | 6.85 ml |
| 10% (w/v) ammonium persulfate (APS) | 60 µl | 60 µl | 60 µl | 60 µl |
| Tetramethyletylenediamine (TEMED) | 30 µl | 30 µl | 30 µl | 30 µl |

**Table 13: Content of different percentage of SDS-gels**

Protein samples were prepared with a defined concentration in 5x Laemmli buffer (Table 10) by boiling them at 95 °C for 5 min. Proteins get coated with SDS proportional to their molecular weight resulting in a uniform negative charge. The secondary and tertiary protein structure gets disrupted and by adding β-mercaptoethanol disulfide-bonds are reduced. By loading equal amounts of samples on an SDS-gel, proteins are separated according to their molecular weight by applying an electric field. Either, self-made SDS-gels with concentration from 10-15% (Table 13) were prepared in advance or ready-made 4-12% Bis-Tris gels were used. Self-made gels were used with 1x running buffer (Table 10), ready-made gels used with MES buffer (3.1.2). A constant voltage of 80-100 V was applied. To determine the size of detected proteins the PageRuler Plus (Thermo Fisher Scientific) was used as molecular weight marker.

To detect in-gel fluorescence signals (3.2.2.6; 3.2.2.7) the SDS-PAGE was protected from light by covering the chambers with aluminum foil while protein separation. In-gel fluorescence was detected with the Amersham Typhoon Biomolecular Imager.

### 3.2.3.5 Western blot, immunodetection and re-probing of membranes

Protein samples separated by SDS-PAGE (3.2.3.4) were transferred onto a nitrocellulose membrane (GE Healthcare) using either a semi-dry system at 65 A per blot for 2 h or tank blot transfer at 250 mA for 2 h at 4 °C.

For semi-dry transfer, the SDS-gel was placed on a nitrocellulose membrane embedded by two pieces of Whatman® Blotting paper equilibrated in 1x transfer buffer (Table 10) at the bottom and on top in a semi-dry transfer chamber (Figure 7).

For tank-blot transfer, the Whatman® Blotting paper, SDS-gel and nitrocellulose membrane was put in a tank completely filled up with 1x transfer buffer (Table 10).

After transfer, the membrane was blocked in 5% milk in TBS-T for 30 min followed by incubation with the first antibody at 4 °C overnight. The following day, the membranes were washed in TBS-T three times each 15 min at RT. Second antibodies conjugated to horseradish peroxidase (HRP) were incubated for 1 h at RT in blocking solution. Detection of proteins was done using the ECL Advance™ Western Blotting Detection Kit (GE Healthcare) supplemented with 0.11% (w/v) p-coumaric acid in DMSO and 0.025% (w/v) in 0.1 M Tris/HCl pH 8.6. 300 µl of the detection solution was carefully pipetted on each membrane.

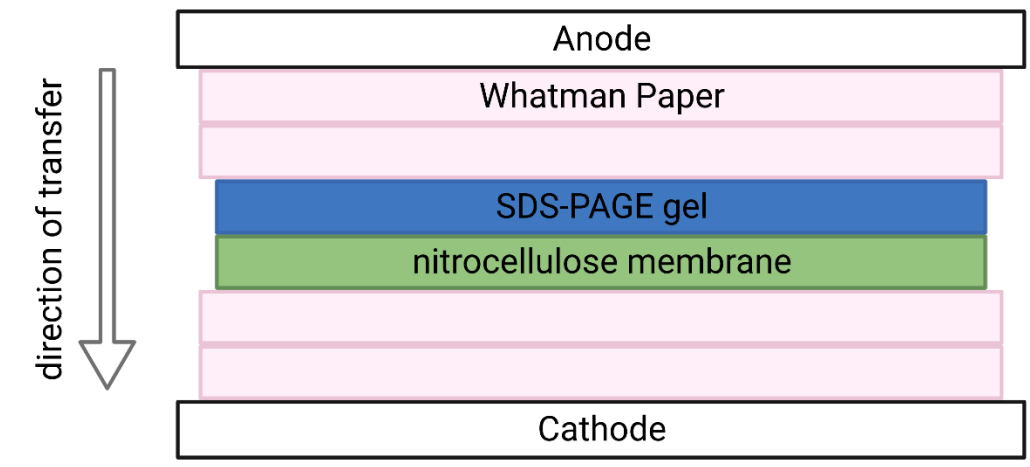


**Figure 7: Scheme for protein transfer from SDS-gel to a nitrocellulose membrane used for western blotting.**

To re-probe membranes with additional first antibodies, membranes were either stripped by using mild stripping buffer for 30 min at RT or harsh stripping buffer for 30 min at 95 °C (Table 10). Membranes were washed in TBS-T at RT and newly incubated with antibodies overnight.

Signals were detected with the AmershamTM Imager 680. Quantification of the signals was done with the ImageJ software.

### 3.2.3.6 Enzyme-linked immunosorbent assay (ELISA)

To quantify mouse and human Aβ1-40 and Aβ1-42 from CTSD-deficient and 5xFAD mice, the DEA, RIPA, FA fractions (3.2.3.2), CSF and plasma samples were analyzed by using the Enzyme-linked immunosorbent assay (ELISA) Kits purchased from IBL International GmbH (3.1.2). 96-well plates pre-coated with respective antibody detecting mouse or human Aβ1-40 or Aβ1-42. The samples are added in pre-tested dilutions. DEA and RIPA samples were diluted 1:100 and FA and CSF were diluted 1:500 in EIA buffer provided by the manufacturer. Samples are incubated on the plate overnight and any Aβ1-40 or Aβ1-42 within the samples binds to the capture antibody pre-coated on the plate. After washing, an enzyme-linked second antibody binds to the captured Aβ1-40 or Aβ1-42. The chromogen Tetra Methyl Benzidine (TMB) serves as an electron donor for the peroxidase coupled to the secondary antibody. Upon oxidation by peroxidase TMB form a blue water-soluble solution. By adding an acidic stop solution, the blue color is converted to yellow due to the acidic pH. The absorbance at 450 nm is measured. The intensity of the color is proportional to the quantities of Aβ. By using a standard curve of known concentrations, the amount of respective protein could be calculated.

### 3.2.3.7 Meso Scale Discovery (MSD) Assay

An electrochemiluminescence-based assay was developed (neo-epitope specific Aβ34 and the sulfo-tagged 6E10 (binds to the N-terminus of human Aβ) or the sulfo-tagged 4G8 for rodent samples (binds to the mid domain of Aβ) using the ELISA Conversion Kit from MSD (USA). High-bind or custom-printed 4-plex plates (using mab34, 4G8 (Biolegend) for pan-Aβ assay, G2-10 for 1-plex Aβ40 assay, and MSD's validated mouse monoclonal anti-Aβ38, anti-Aβ40, and anti-Aβ42 antibodies) were blocked (MSD 5% Blocker A in PBS) for 1 h at 22 °C and washed three times with PBS-Tween (PBS-T) for 1 min at 22 °C, loaded with SULFO-TAG TM 6E10 or 4G8 detection antibody (diluted to 1× in MSD Diluent 100) and sample or peptide calibrator (in MSD Diluent 35 or cell culture medium), and incubated for 16 h at 4 °C with shaking

at 600 rpm. After three washing steps with PBS-T for 1 min at 22 °C, 150 µL 2× MSD read buffer was added per well. All plates were read using an MSD QuickPlex SQ 120 Imager and data analyzed using MSD Workbench® software. Standard curves were fitted using a non-linear four-parameter logistic fit. This assay was conducted by I. Ulku from McGill University Montreal in Canada.

#### 3.2.3.8 Proteome Analysis

SH-SY5Y WT and both SH-SY5Y CTSBDL-deficient clones were seeded 24 h after cell pellet collection. Cells were washed in ice cold PBS and harvested with a cell scraper. A modified RIPA lysis buffer (Table 10) was used to lyse the cells for 30 min on ice. The supernatant was collected after centrifugation at 16.000 rpm for 10 min at 4°C. 10 µl were used to determine protein concentration (3.2.3.3), the rest was frozen in liquid nitrogen. Samples were sent for proteome analysis to S. Lichtenthaler from DZNE in Munich:

Per sample 25 µg protein was subjected to the filter aided sample preparation protocol (FASP) (Wiśniewski et al. 2009) using Vivacon spin filters with a 30 kDa cut-off (Sartorius). Protein were reduced with 20 mM DTT followed by alkylation of cysteine residues with 50 mM iodoacetamide (Sigma Aldrich). Next, proteins were washed with 8 M urea (Sigma Aldrich) and digested first with 0.5 µg LysC (Promega) for 16 h at 37 °C and second with 0.25 µg trypsin (Promega) for 4 h at 37 °C. Generated peptides were eluted by centrifugation and acidified with 8 % (v/v) formic acid to pH<3. Proteolytic peptides were desalted by stop and go extraction (STAGE) with self-packed C18 tips (Empore) and dried by vacuum centrifugation (Rappsilber et al. 2003). Peptides were dissolved in 20 µl 0.1 % formic acid (FA) and protein concentration was determined by nanodrop photometer at 280 nm.

Peptides were analyzed for label-free protein quantification (LFQ) on an Easy nLC 1200 nanoHPLC (Thermo Scientific) which was coupled online to a Nanospray Flex Ion Source (Thermo Sientific) equipped with a PRSO-V1 column oven (Sonation) to a Q-Exactive HF mass spectrometer (Thermo Scientific). 1.3 µg of peptides was separated on in-house packed C18 columns (30 cm x 75 µm ID, ReproSil-Pur 120 C18-AQ, 1.9 µm, Dr. Maisch GmbH) using a binary gradient of water (A) and acetonitrile (B) supplemented with 0.1% FA (0 min, 2% B; 3:30 min, 5% B; 137:30 min, 25% B; 168:30 min, 35% B; 182:30 min, 60% B) at 50°C column temperature.

Data dependent acquisition (DDA) was used for LFQ. Full MS scans were acquired at a resolution of 120,000 (m/z range: 300-1400; automatic gain control (AGC) target: 3E+6). The 15 most intense peptide ions per full MS scan were selected for peptide fragmentation (resolution: 15,000; isolation width: 1.6 m/z; AGC target: 1E+5; normalized collision energy (NCE): 26%). A dynamic exclusion of 120 s was used for peptide fragmentation.

The MS raw data was analyzed with the software Maxquant, version 1.6.15.0 (maxquant.org, Max-Planck Institute Munich) (Cox et al. 2014). The MS data was searched against a reviewed canonical fasta database of Homo sapiens from UniProt (download: 2020-01-16, 20617 entries). Trypsin was defined as a protease. Two missed cleavages were allowed for the database search. The option first search was used to recalibrate the peptide masses within a window of 20 ppm. For the main search peptide and peptide fragment mass tolerances were set to 4.5 and 20 ppm, respectively. Carbamidomethylation of cysteine was defined as static modification. Acetylation of the protein N-terminal as well as oxidation of methionine were set as variable modifications. The false discovery rate for both peptides and proteins was adjusted to less than 1%. The “match between runs” option was enabled with a matching window of 1 min. LFQ of proteins required at least one ratio count of unique peptides. The protein LFQ reports of Maxquant were further processed in Perseus version 1.6.14 (Tyanova et al. 2016). The protein LFQ intensities were log2 transformed and log2 fold changes were calculated between cathepsin KO clones and respective WT controls. An unpaired Student’s t-test with two-tailed distribution was applied to evaluate the significance of proteins with changed abundance. Additionally, a permutation based false discovery rate (FDR) estimation (threshold: FDR = 5%) was used to perform multiple hypothesis correction for each comparison (Tusher et al. 2001).

#### 3.2.3.9 Cathepsin D Activity Assay

To measure CTSD activity in cells, lysates were prepared in RIPA lysis buffer without protease inhibitors to keep protease activity. 100 µl activity buffer (50 mM sodium acetate (pH 5.5), 0.1 M NaCl, 1 mM EDTA, and 0.2% Triton X-100) containing 10 µM of CTSD substrate (3.1.3) was either incubated with 5 µl sample, 0.75 µl of 0.2 mg/ml pre-activated rhpro-CTSD with or without Pepstatin A (PepA) as controls were

incubated at 37 °C. The AMC (7-Amino-4-Methylcoumarin)-fluorescence was measured every 15 min for 120 min using a Synergy™ HT Multi-Detection microplate reader (exc: 360 nm; em: 440 nm, band pass 40). To quantify the CTSD activity, the protein concentration of the samples was determined (3.2.3.3) and used to measure the activity per µg protein per sample.

#### 3.2.3.10 Liquid chromatography-mass spectrometry (LC-MS)

To analyze the Aβ1-42 cleavage fragments generated by self-made rhpro-CTSD, samples were sent for LC-MS to A. Tholey (Institute for Experimental Medicine, University Kiel). First, rhpro-CTSD was activated in 50 mM sodium acetate, 50 mM NaCl at pH 4.5 for 2 h at 37 ◦C. 2 µg pre-activated rhCTSD was incubated with 100 µM human Aβ1-42 (Enzo) in presence with or without Pepstatin A at 37 °C. Samples were collected after 0, 15, 30 and 60 min, frozen at -20 °C and analyzed via LC-MS. Aliquots of the samples were diluted 1:100 in LC loading buffer (3% acetonitrile (ACN) and 0.1% trifluoroacetic acid in water), and transferred to glass autosampler vials. LC-MS analysis was performed on a Dionex U3000 nanoRSLC UHPLC (Thermofisher, Dreieich, Germany) equipped with an Acclaim PepMap100 column (2 µm particle size, 75 µm x 500 mm) and µ-precolumn (300 µm x 5 mm) coupled online to a Q Exactive HF mass spectrometer (Thermofisher, Bremen, Germany). The eluents used were; eluent A: 0.05% formic acid (FA), eluent B: 80% CAN + 0.05% FA. The separation was performed over a programmed 40-min run. Chromatographic conditions were: 4% B for 3 min followed by a linear gradient from 4% to 50% B over 10 min, a 2-min increase to 90% B, and 10 min at 90% B. Following this, an inter-run equilibration of the column was achieved by 15 min at 4% B. A constant flow rate of 300 nl/min was used and 1 µl of sample was injected per run. Acquisition of data was performed on the Orbitrap Q Exactive HF mass spectrometer utilizing HCD fragmentation at a normalized collision energy of 27. A full scan MS acquisition was performed (resolution 60,000) with subsequent data dependent MS/MS (resolution 15,000) of the top 10 most intense ions; dynamic exclusion was enabled (2 s duration). Database searches were performed in Proteome Discoverer (Ver. 2.2.0.388) using the SequestHT search algorithm and combined database that included the Aβ1–42 peptide, CTSD, and the cRAP list of commonly occurring laboratory contaminants. Small database search criteria were employed in which a

fixed PSM was used and only peptides assigned as high confidence (Maximum delta Cn:0.5).

### 3.2.4 Histological methods

#### 3.2.4.1 Indirect immunofluorescence staining of cells

Cells were grown on coverslips for at least 24 h, washed in ice cold PBS and fixed in 4% paraformaldehyde (PFA) for 20 min, permeabilized with PBS and 0.2% saponin for 5 min and quenched with PBS, 0.2% saponin and 0.12% glycine for 10 min at RT. Blocking solution (PBS, 0.2% saponin, 10% FBS) was added for 1 h and then cells were incubated in the first antibody (Table 3) diluted in blocking solution overnight at 4°C. To detect proteins of interest, cells were incubated with fluorescence-tagged secondary antibodies (Table 4) in blocking solution for at least 2 h at RT. Cells were washed in PBS and 0.2% saponin (3-4 times) followed by two washing steps with water and mounted on slides with DABCO/Mowiol containing 1µl/ml DAPI. Slides were stored in the dark at 4 °C until further analysis. Imaging was performed with the Keyence fluorescence microscope BZ-X 800 (Keyence).

#### 3.2.4.2 Electron microscopy of fixed cells

SH-SY5Y WT and SH-SY5Y CTSBDL cells were seeded 24 h prior fixation. Cells were washed in PBS and fixated in double-strength fixative (4% PFA, 2% glutaraldehyde (GA) in PBS) for 15 min. Double-strength fixative was discarded and replaced to simple fixative (4% PFA and 1% GA in PBS). Cells were harvested using a cell scraper and centrifuged at 300 g for 10 min. The supernatant was discarded and the pellet was washed in fresh fixative. Resulting pellets were shipped in fixative to M. Schweitzer (UKE, Hamburg). Cells were washed in PBS for three times and centrifuged at 1000 g for 5 min each time. Resulting pellets were rinsed in 0.1 M sodium cacodylate buffer (pH 7.2–7.4) and embedded in 2% agarose and osmicated using 1% osmium tetroxide in cacodylate buffer. Cells were dehydrated using ascending ethyl alcohol concentration steps and rinsed in propylene oxide for two times. Infiltration of the embedding medium was performed by immersing the samples in a 1:1 mixture of propylene oxide and Epon and finally in neat Epon and polymerized at 60 °C. Semithin sections (0.5 µm) from the SHSY5Y WT and CTSBDL-deficient cells were prepared

for light microscopy mounted on glass slides and stained for 1 min with 1% Toluidine blue. Ultrathin sections (60nm) were examined in an EM902 (Zeiss, Germany). Pictures were taken with a MegaViewIII digital camera (A. Tröndle, Moorenweis, Germany).

#### 3.2.4.3 Preparation of semi-thin cryosections

Mice were perfused with 0.1 M PB (Table 10) and their brains fixed in 4% PFA for 4 h at RT followed by incubation in 0.1 M PB overnight at 4 °C. Brains were then immersed in 30% sucrose in 0.1 M PB and stored at 4 °C until sections were cut. For this, brains were cut sagittally into 35 µm thick sections using the Leica SM 2000R sliding microtome (Leica Microsystems) with dry-ice cooling. Sections were stored in 0.1 M PB containing 0.02% (w/v) sodium azide until immunofluorescence staining (3.2.4.4) was performed.

#### 3.2.4.4 Immunofluorescence staining of semi-thin cryo-sections

Semi-thin brain sections (3.2.4.3) were washed three times with 0.1 M PB at RT followed by permeabilization for 30 min in 0.5% Triton X-100 in 0.1 M PB at RT. After the permeabilization solution was removed, the slices were blocked for 3h in 4% goat serum, 0.5% Triton X-100 in 0.1 M PB at RT. After this, the brain sections were incubated in a wet chamber with first antibody in blocking solution overnight at 4 °C. The next day, the slices were washed three times using 0.25% Triton X-100 in 0.1 M PB at RT, followed by incubation with secondary antibody for 3 h at RT in a wet chamber protected from light. Sections were washed three times each 20 min in 0.1 M PB followed by incubation with DAPI in 0.1 M PB for 10 min and three washings steps in 0.1 M PB for a total of 10 min. After that, the brain slices were mounted in Mowiol/DABCO on slides and stored at 4 °C. Images were taken on the Zeiss laser scanning microscope 980 with Airyscan 2 (Zeiss).

To stain Aβ plaques exclusively, AmyloGlo staining (3.1.2) was performed. Brain sections were dried at 55 °C on a gelatin-coated slide, transferred into a 70% ethanol solution for 5 min, washed in water. Slices were incubated for 10 min with the AmyloGlo staining solution provided by the manufacturer. Slides were briefly rinsed in 0,9% saline

solution and mounted in Mowiol/DABCO on slides. Imaging was performed with the Keyence fluorescence microscope BZ-X 800 (Keyence).

### 3.2.5 Animal Experiments

#### 3.2.5.1 Animal housing

In agreement with the German animal welfare law all animal handling and care were performed according to the guidelines of the Christian-Albrechts-University of Kiel. The Ministry of Energy, Agriculture, the Environment and Rural Areas Schleswig-Holstein approved animal experiments under the reference number V242–40536/2016 (81-6/16). All mice were housed in individually ventilated cage (IVC) under a 12 h light/12 h dark cycle with free access to food (pellets by Sniff Spezialdiäten, V1534) and water. Mice cages were maintained in a room with a temperature between 19 and 22°C and humidity of 45-60%.

#### 3.2.5.2 DNA isolation from tissue and Polymerase Chain Reaction (PCR) for genotyping

5xFAD and CTSD-deficient mice were genotyped by using PCR and analyzed by agarose gel electrophoresis (3.2.1.5). Tail and ear mark biopsies were digested with DirectPCR® Lysis Reagent Tail (Peqlab) containing 0.3 mg/ml Proteinase K at 55 °C overnight. To inactivate Proteinase K the samples were incubated at 85 °C for 45 min. The DNA lysates were used as template for genotyping PCRs.

To genotype the CTSD-deficient mice, two different PCRs were used. The CD53 primer pair binds exon 4 in *CTSD* resulting in a 200 bp band for wildtype mice while a 1400 bp band refers to the *CTSD* mutants harboring a neomycin cassette (Saftig et al. 1995). Additionally, a PCR using primers binding to the neomycin cassette (neo) were used. A wildtype mouse does not show any signal, while mice harboring the *CTSD* mutation and neomycin cassette display a 280 bp band. The different genotypes are then distinguished as followed: wildtype: CD53-PCR: 200 bp, neo-PCR: no band; heterozygous: CD53-PCR: 200bp and 1400 bp, neo-PCR: 280 bp and knockout: CD53-PCR: 1400bp, neo-PCR: 280 bp (Saftig et al. 1995). The CTSD-deficient mouse genotyping PCRs were conducted under the following conditions:

| Premix 1 | µl |
|---|---|
| CD53 exon1 10 µM | 1.0 |
| CD53 exon2 10 µM | 1.0 |
| 10x DreamTaq Puffer | 5.0 |
| dNTP 2 mM | 5.0 |
| DMSO | 2.5 |
| DreamTaq 5U | 0.5 |
| Template | 2.0 |
| add $H_20$ | 50 |

| Premix 2 | µl |
|---|---|
| neo-Kiel3 10 µM | 1.0 |
| neo-Kiel4 10 µM | 1.0 |
| 10x DreamTaq Puffer | 5.0 |
| dNTP 2 mM | 5.0 |
| DMSO | 2.5 |
| DreamTaq 5U | 0.5 |
| Template | 2.0 |
| add $H_20$ | 50 |

| Step | t (min) | T (°C) | |
|---|---|---|---|
| Initial denaturation | 5 | 95 | |
| Denaturation | 0.25 | 96 | 30 x |
| Annealing | 0.5 | 58 | |
| Elongation | 2 | 72 | |
| Final elongation | 3 | 72 | |
| End | ∞ | 10 | |

**Table 14: Genotyping PCR pipetting scheme for CTSD-deficient mice and the PCR program for both premixes 1 and 2**

To genotype 5xFAD mice, two primer pairs are used. The primer pair 1644 and 1645 binds do PSEN1 to identify the mutation PSEN1 (M146L). Mice harboring the *PSEN1* mutation show a band at 608bp within the agarose gel. The other primer pair (7338 and 7339) serves as an internal control to confirm the PCR worked indicated by a 324bp band within the agarose gel (Genotyping Protocol 23050, The Jackson Laboratory). The 5xFAD mouse genotyping PCR was conducted under the following conditions:

| | µl |
|---|---|
| Primer 1644 | 3.3 |
| Primer 1645 | 3.3 |
| Primer 7338 | 2.5 |
| Primer 7339 | 2.5 |
| 10x DreamTaq Puffer | 5 |
| dNTP 10 mM | 1 |
| DreamTaq 5U | 0.33 |
| Template | 3 |
| add $H_20$ | 50 |

| Step | t (min) | T (°C) | |
|---|---|---|---|
| Initial denaturation | 3 | 94 | |
| Denaturation | 0.5 | 94 | 35 x |
| Annealing | 1 | 60 | |
| Elongation | 1 | 72 | |
| Final elongation | 2 | 72 | |
| End | ∞ | 10 | |

**Table 15: Genotyping PCR pipetting scheme for 5xFAD mice and the PCR program**

#### 3.2.5.3 Intracerebroventricular injection of mice

Intracerebroventricular (ICV) injections with 10 µl of 10 µg/µl rhpro-CTSD were performed at P1 and P20 for both CTSD-deficient and 5xFAD (Marques et al. 2019). The PBS or rhpro-CTSD was injected in the cauda putamen with a microsyringe (30G) using a spacing devise with an injection depth of 1.15 mm over a period of 3 min. Injections in pups at P1 were done in the right hemisphere, while P20 injections were done in the left hemisphere. Mice at P20 were anaesthetized using isoflurane (2% in oxygenized air) while bedded at 37 °C on a heated mat. Mice were monitored after intracranial injections.

#### 3.2.5.4 CSF collection

Collection of cerebrospinal fluid (CSF) was performed to determine Aβ concentration by ELISA (3.2.3.6). Mice were anaesthetized (3.2.5.5). The skin of the neck was cut. The CSF was collected from the cisterna magna compartment using a glass capillary. The collected CSF was snap-frozen in liquid nitrogen until usage for ELISA.

#### 3.2.5.5 Mouse anesthesia

Mice were anaesthetized by intraperitoneal injection of 10 µl of 10 mg/ml Ketamine (Bremer Pharma GmbH, 26,706) and 6 mg/ml Rompun® (Bayer, KPOCCNU) in 0.1 M PB per grams body weight.

#### 3.2.5.6 Perfusion of mice

For transcardial perfusions, mice were anaesthetized (3.2.5.5). Perfusion was performed through the left heart ventricle with 30 ml of 0.1 M PB. Brains were collected, the right hemisphere was fixed with 4% PFA for immunohistochemistry and the left hemisphere was snap-frozen in liquid nitrogen for biochemical analysis.

### 3.2.6 Computer Software and Statistical Analysis Techniques

#### 3.2.6.1 Statistical Analysis

The detection of signal intensities in immunoblot was performed with the software ImageJ. Statistical analysis was done with GraphPad Prism 8.

#### 3.2.6.2 Measurement of lysosomal diameter

Imaging of lysosomes from SH-SY5Y CTSBDL-deficient and WT cells was done by using the confocal laser scanning microscope LSM980 Airyscan2 (Zeiss) under equal settings per experiment. Digital images were processed and adjusted equally by ZEN software (Zeiss) or ImageJ. Lysosomal size was determined by using the Line-Tool in Zen software to determine the diameter in biological triplicates.

#### 3.2.6.3 GFAP and Iba1 Analysis

The astroglia marker GFAP was used to determine the area of astrocytes in hippocampus and cortex of 5xFAD mouse brains. For this the area of the signals was determined using ImageJ.

The microglia ramification analysis of immunostainings from 5xFAD was done using the Sholl Analysis plugin in ImageJ. The signal of the microglia marker Iba1 was analyzed. The following setting for the Sholl Analysis plugin were used: start radius: 4.4 µm, step size: 3.3 µm, end radius: 34.9 µm. For each brain sample two slides were analyzed in the hippocampal region (CA1, CA3 and dentate gyrus) and cortex.

#### 3.2.6.4 Overview images of immunoblots and immunostainings, graphs and illustrations

Immunoblots and immunostainings were compiled by using Adobe Illustrator 2020. Adjustment of contrast and brightness of immunostainings was performed with ZEN Software provided by Zeiss. Graphs were created with GraphPad Prism 8. Illustrations were designed with BioRender.

# 4 Results

Lysosomal hydrolases are capable to degrade various macromolecules entering the compartment by endocytosis, phagocytosis or autophagy. The main peptide hydrolyzing hydrolases are cathepsins (CTSs) which are acid proteases classified by their structure and catalytic mechanisms. They are in most cases ubiquitously expressed, however there is not much known about their substrate spectrum, the usage of certain peptide bonds, the sequence of proteolytic processing by different CTSs and the potential overlapping use of substrate proteins. The aim of this study is to approach these questions. The important role of CTSs in the regulation of cell proteostasis and their possible compensatory enzymatic activity towards lysosomal substrates should be evaluated in human neuroblastoma SH-SY5Y cells since neurological symptoms or neurodegeneration are a major hallmark for lysosome-mediated diseases.

## 4.1 Basal analysis of the expression and activity of CTSs in HeLa and SH-SY5Y cells

RNA Sequencing Data retrieved from the Human Protein Atlas demonstrate that 14 out of 15 cathepsins are expressed in HeLa and SH-SY5Y cells (Karlsson et al. 2021).The highest expressed cathepsins in HeLa cells are CTSA, CTSC, CTSD, CTSL and CTSZ. In SH-SY5Y cells the CTSs with the highest expression are CTSA, CTSB, CTSC, CTSD and CTSL. No expression of CTSG is found in both cell types (Figure 8). CTSA and CTSC belong to the group of exopeptidases that hydrolyze peptide bonds of proteins and peptides from their C-terminal or N-terminal ends resulting in single amino acids, dipeptides or tripeptides (Galjart et al. 1991; McGuire et al. 1992). The endopeptidases CTSB, CTSD and CTSL cleave their substrates within their peptide backbone resulting in smaller peptides (Towatari and Katunuma 1983; Ketterer et al. 2020; Yoon et al. 2022). Studies suggested that lysosomal hydrolysis is initiated by endopeptidases (Huang and Tappel 1971; Goettlich-Riemann et al. 1971). The most highly expressed CTSB, CTSD and CTSL became the CTSs of choice to be further investigated in SH-SY5Y cells.

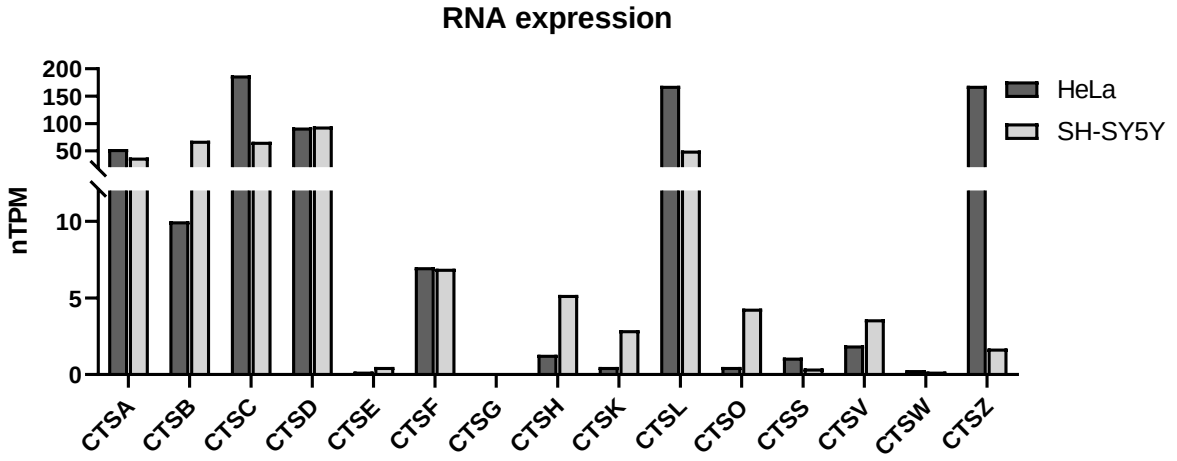


**Figure 8: Normalized transcript expression values of cathepsins in HeLa and SH-SY5Y cells.** RNA sequencing data from HeLa and SH-SY5Y cells show normalized transcripts per million (nTPM) for 15 human cathepsins provided by the Human Protein Atlas (data available from v21.0.proteinatlas.org). Whereas CTSE, CTSF, CTSG, CTSH, CTSK, CTSO, CTSS, CTSV and CTSW have no or only very low expression levels below 10 nTPM, CTSA, CTSB, CTSC, CTSD, CTSF, CTSL and CTSZ show high expression from 10 nTPM to 169 nTPM in HeLa cells. In SH-SY5Y cells CTSE, CTSF, CTSG, CTSH, CTSK, CTSO, CTSS, CTSV, CTSW and CTSZ are either not or very low expressed with less than 10 nTPM. In SH-SY5Y cells the highest RNA expression levels are shown in CTSA, CTB, CTSC, CTSD and CTSL.

Immunoblot analysis using available antibodies directed against CTSB, CTSD, CTSL and CTSZ were used to detect the endogenous protein expression and processing in SH-SY5Y and HeLa cells (Figure 9A). The antibodies against CTSB, CTSD, CTSL and CTSZ recognized the different processed CTS species in their pro- and mature forms. The predicted and detected sizes for CTSB are 41 kDa (pro-form), 29 kDa (single chain form) and 25 kDa (mature form) (Ishidoh and Kominami 2002). The antibody against CTSD confirmed the predicted sizes of 54 kDa (pro-form), 44 kDa (single chain form) and 34 kDa (mature form) (Ishidoh and Kominami 2002). While the maturation of CTSD is dependent on other cysteine proteases, the presence of the mature form indicates a delivery of the enzyme to the lysosome (Gieselmann et al. 1985; Ishidoh and Kominami 2002). The signals for CTSL in the immunoblot showed the 31 kDa single chain form and the 24 kDa mature form (Ishidoh and Kominami 2002). Mature CTSZ was detected at the expected size of 34 kDa only in HeLa cells. All cathepsin signals (pro-, single-chain and mature form) were included in the quantification and normalized to the internal loading control glyceraldehyde 3-phosphate dehydrogenase (GAPDH) (Figure 9B). In accordance with the RNA expression levels of CTSZ, its protein expression was highly abundant in HeLa but it is not present in SH-SY5Y cells. CTSB and CTSD were the highest expressed endopeptidases followed by CTSL in SH-SY5Y cells which also confirmed the RNA expression data. In HeLa cells the protein

expression of CTSL seemed to be the highest but one has to consider that the antibody against CTSZ only detects its mature form and therefore it appeared lower expressed when compared to the RNA expression data.

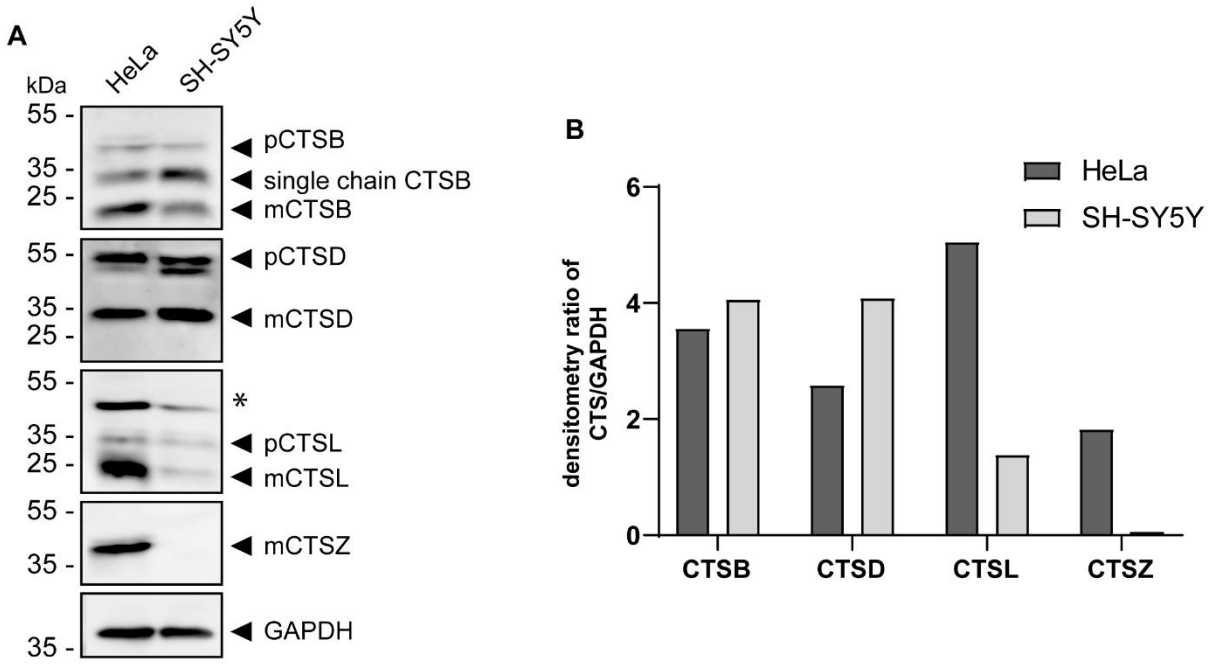


**Figure 9: Cell-type specific expression of Cathepsin B, D, L and Z in HeLa and SH-SY5Y cells. (A)** Comparative immunoblot analysis of endogenous CTSB, CTS D, CTSL and CTSZ expression in HeLa and SH-SY5Y WT cells. **(B)** Expression analysis of protein levels of CTSs in HeLa and SH-SY5Y cells. The signal intensities of all detected bands with respective CTS-antibodies was normalized to the housekeeping loading control glyceraldehyde 3-phosphate dehydrogenase (GAPDH). * indicates non-specific-binding of the antibody, p – pro, m – mature; kDa: kilodalton.

CTSs are post-translationally regulated and their abundance does often not correlate with proteolytic activity which is related to their biological relevance. Therefore, their enzymatic activity has also been addressed within this study. Using the activity-based probe (ABP) BMV-109 the endogenous enzymatic activity of cysteine-type proteases like CTSB, CTSL and CTSZ could be determined (Schleyer and Cui 2021). ABPs are chemical probes that contain a reactive group which covalently binds to the active-site of an enzyme. BMV-109 is an improved quenched fluorescent ABP containing a quencher (sulfo-QSY21) which quenches the bound fluorophore dye Cy5 (Verdoes et al. 2013). Once BMV-109 is covalently bound to a cysteine-type protease the quencher is removed and the fluorescence of the Cy5 dye can be measured at an excitation wavelength of 635 nm (Figure 10A).

Using this set up, HeLa and SH-SY5Y WT cells were analyzed after a 15 min pre-incubation with either 50 µM E64D, 20 µM Leupeptin and 10 µg/ml Pepstatin A (PepA) or 500 nM Bafilomycin A1 followed by another 2 h of incubation with BMV-109. Cells

were lysed and the Cy5-signal was analyzed using in gel fluorescent analysis after SDS-PAGE (3.2.3.4). Figure 10B shows the fluorescent SDS-PAGE with respective Cy5-signals for active cysteine-type proteases after excitation at 635 nm. Coomassie blue staining was used as a loading control. HeLa and SH-SY5Y WT cells both showed different signals and signal intensities for active cysteine-type proteases supporting the diverse expressions of CTSs. While the cysteine-protease inhibitor E64D successfully led to a complete loss of Cy5-signal in both HeLa and SH-SY5Y WT cells, the combination of Leupeptin and PepA or treatment with Bafilomycin A1 only reduced the intensity of some bands indicating that there were either other active cysteine-proteases or the inhibitor did not completely inhibit the respective lysosomal proteases and there are still some enzymes active at neutral pH.

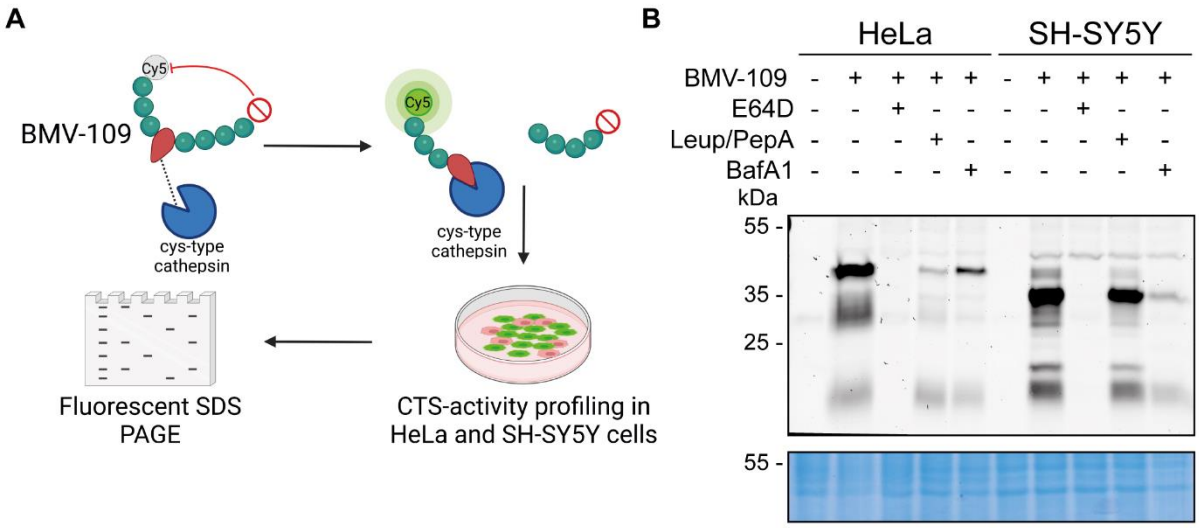


**Figure 10: Schematic mechanism of fluorescent cysteine-protease activity-based probe BMV-109 assay and its application in HeLa and SH-SY5Y WT cells using different lysosomal protease inhibitors. (A)** The quenched cysteine-protease activity-based probe (ABP) BMV-109 contains a fluorophore-quencher pair. Once the ABP binds covalently to the active-site cysteine the quenching group is released and the protease is irreversibly labeled resulting in emission of fluorescence that can be detected via fluorescent SDS-PAGE. **(B)** Fluorescent SDS PAGE and its Coomassie staining as loading control of BMV-109-labeled HeLa and SH-SY5Y WT cells treated with 50 µM E64D, 20 µM Leupeptin (Leup) and 10 µg/ml Pepstatin A (PepA), or 500 nM Bafilomycin A1 (BafA1) for 2 h. Cy5 signal was detected at excitation at 635 nm. kDa: kilodalton.

To also address the enzymatic activity of the aspartyl-protease CTSD, an independent assay was performed in both HeLa and SH-SY5Y WT cells. To this end, a quenched fluorogenic CTSD substrate was incubated with cell lysates and pre-activated CTSD with the inhibitor PepA as control (3.2.3.9). Figure 11 reveals the intensity of the released fluorescence signal over time after active CTSD cleaved the substrate. Pre-activated CTSD with PepA did not show any fluorescent signal indicating a successful inhibition of the CTSD activity. However, HeLa and SH-SY5Y WT without PepA

showed an increase in the fluorescent intensity over time. While in the SH-SY5Y cells a plateau after 60 min could be detected, the HeLa cells presented a higher CTSD activity since the plateau was not yet reached after 90 min.

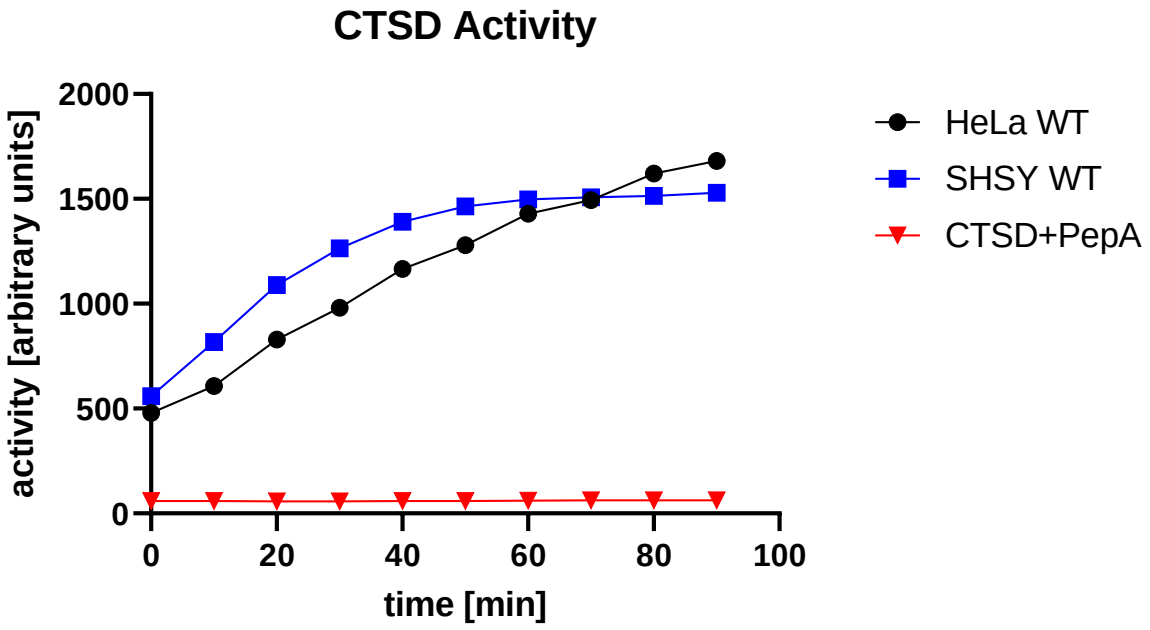


**Figure 11: CTSD-activity in HeLa and SH-SY5Y WT cells.** The graph shows the measured CTSD-activity per µg protein over time. By cleaving a quenched CTSD-substrate the fluorescence intensity can be measured at after excitation at 360 nm. CTSD-activity is shown for HeLa and SH-SY5Y WT cells, pre-activated rh-CTSD co-incubated with Pepstatin A (PepA).

Taken together the highest expressed endopeptidases CTSB, CTSD and CTSL were all abundantly found in SH-SY5Y WT cells and in HeLa WT cells which additionally express CTSZ. RNA and protein expression as well as the activity of these CTSs are cell type specific suggesting a different interplay, interaction or function of these CTSs for each cell type. To analyze their probably redundant function and to obtain an insight into their peptide usage and protein degradation patterns, SH-SY5Y cells were chosen for a more detailed analysis.

## 4.2 Generation and validation of CTS-deficient SH-SY5Y cell lines using the CRISPR/Cas9 technique

A classic way to study and to better understand the function of genes and proteins of interest, is to deplete the respective protein in commonly used model organisms and analyze the resulting phenotypic and biochemical consequences. Since 2012, the CRISPR (clustered regularly interspaced short palindromic repeats) gene editing which

is based on the CRISPR-Cas9 antiviral defense mechanism of bacteria, became a common and powerful methodology to manipulate gene and protein expression in cell lines (Jinek et al. 2012). For the investigations of the functions of CTSs within the lysosomal network and their usage of peptides and proteins several stable SH-SY5Y knockout (KO) cell lines were created using CRISPR-Cas9-mediated gene editing.

First, a single guide RNA (sgRNA) targeting CTSB was introduced into SH-SY5Y WT cells as described in 3.2.2.4. The resulting mixed clone was first analyzed by immunoblot (3.2.3.5) to evaluate the editing efficiency and to decide on how many single clones have to be further analyzed (Figure 12). For CTSB the editing efficiency was already high at the mixed clone level as immunoblot analysis revealed almost no detectable signal for CTSB. Cells were separated into single cells and grown to confluency (3.2.2.4). DNA was isolated and analyzed by PCR targeting the sequence close by the binding position of the sgRNA. The individual PCR product was sequenced. The Interference of CRISPR Edits (ICE) tool offered by Synthego (Conant et al. 2022) was used to analyze the single clones in regard to detect inserts or deletions compared to the WT cells (data not shown). The CTSB KO clone #3 has a one base pair (bp) deletion and the other CTSB KO clone #6 has an insert of one bp (data not shown). Thus, resulting in altered protein sequences with an earlier stop codon (Figure 13)

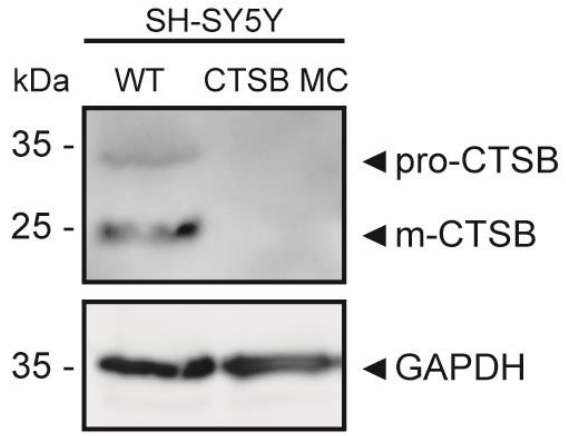


**Figure 12: Analysis of the SH-SY5Y CTSB mixed clone.** Western Blot analysis showing the SH-SY5Y WT vs. the CRISPR/Cas9-edited SH-SY5Y CTSB mixed clone (MC). GAPDH was used as loading control. kDa: kilodalton

Next, the single clones for CTSD and CTSL were generated in the same way as described above and analyzed by PCR using PCR primers covering the respective edited sgRNA binding position (3.1.7; 3.2.1.4). Both sgRNA targeting CTSD and CTSL bind within the respective exon 2. For each CTSD and CTSL KO two single clones were chosen to be used for further analysis. The two CTSD KO clones had a one and two bp deletion (CTSD #10 and #36). For the CTSL KO clones one of them had a one

bp deletion (CTSL #6) on one allele and a one bp insertion in the other allele while the other clone (CTSL #11) had a four bp deletion on one allele and a one bp insertion on the other allele. The resulting and altered protein sequences are shown in Figure 13.

The last step was the generation of a triple CTS-deficient SH-SY5Y cell line lacking CTSB, CTSD and CTSL. To reach this goal the CTSB KO clone #3 was chosen and both sgRNAs targeting CTSD and CTSL were introduced at the same time using the CRISPR/Cas9-gene editing strategy (3.1.7; 3.2.2.4). Two CTSBDL-triple KO clones were generated this way. One of them had a one bp deletion of eight bp in CTSD and an insert of 265 bp for CTSL (CTSBDL #4). The other clone had a deletion of one bp in CTSD and on one allele a four bp deletion and the other allele a one bp insertion (CTSBDL #9) in CTSL. The resulting protein sequences are shown in Figure 13.


**Figure 13: Protein sequences of edited CTS-deficient SH-SY5Y cell lines.** Protein sequences for CTSB, CTSD and CTSL of SH-SY5Y WT and CTSB KO clones 3 and 6, CTSD KO clones 10 and 36 and CTSBDL KO clones 4 and 9. The altered amino acids compared to the WT sequence are highlighted in red and stop codons are shown as [-]. Both CTSBDL KO clones (#4 and #9) derived from CTSB KO clone #3 and therefore share the same sequence for CTSB.

The next step was to investigate whether the insertions or deletions led to a loss of protein expression and activity. To analyze this, lysates of the clones were prepared (3.2.3.1) and studied by immunoblot analysis (3.2.3.4; 3.2.3.5). The immunoblot in Figure 14A shows the loss of all forms of CTSB, CTSD and CTSL in the single and the triple clones indicating a successful KO of the respective CTSs. To also confirm the loss of their protease activity, the cysteine-protease activity-based probe BMV-109 was applied on one clone of each CTS KO (Figure 14B). The fluorescent SDS-PAGE shows different Cy5-signal patterns of cysteine proteases in the SH-SY5Y WT cells and each

of the CTS-deficient clones. According to the work of Verdoes et al. the fluorescence signals were assigned to the mature forms of CTSB and CTSL (Verdoes et al. 2013). In the SH-SY5Y CTSB KO a loss of a prominent band at 30 kDa which has been referred to be CTSB was observed. The CTSL-deficient clone showed a loss of a signal at approximately 25 kDa which has been assigned as CTSL. Both CTSB- and CTSL-signals were absent in the CTSBDL-deficient cell line while there were still two other fluorescent bands observable.

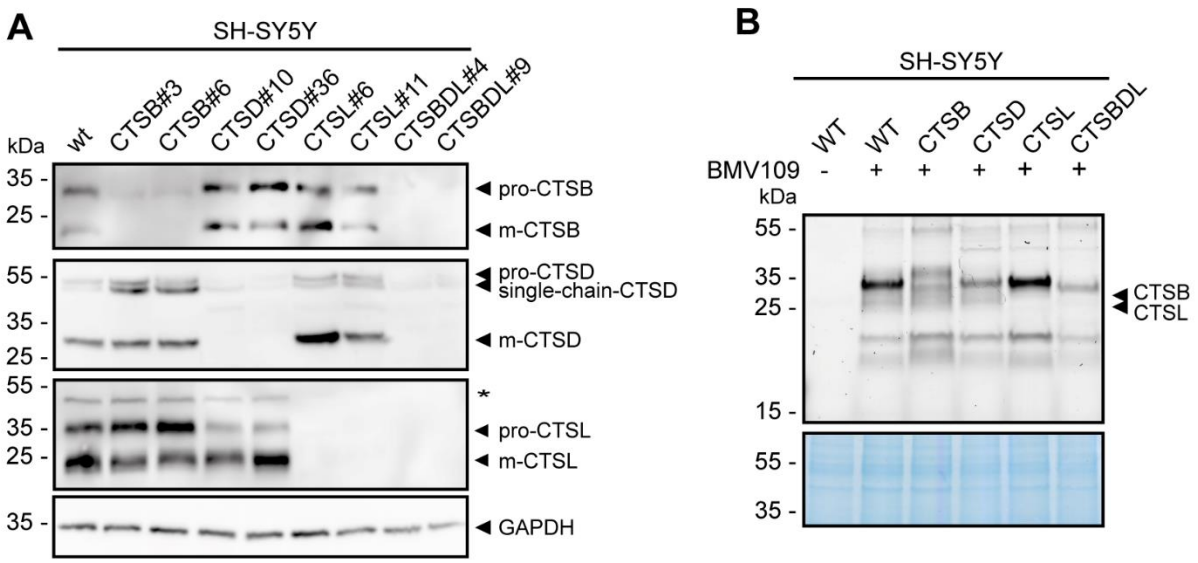


**Figure 14: Immunoblot analysis and activity determination using the cysteine-protease activity-based probe BMV-109 of SH-SY5Y CTS-deficient cell lines. (A)** Protein lysates analyzed via immunoblot show a successful generation of two SH-SY5Y CTSB, CTSD, CTSL and CTSBDL clones each. GAPDH was used as loading control. **(B)** Application of BMV-109 on SH-SY5Y WT, CTSB, CTSD, CTSL and CTSBDL KO clones. The fluorescent SDS-PAGE of protein lysates shows Cy5-signal of cysteine-proteases. The Cy5-signal was measured at excitation of 635 nm. Coomassie staining served as loading control. kDa: kilodalton

In summary, the generation of eight CTS-deficient clones using CRISPR/Cas9-edtiting was successful on both DNA and protein expression levels. It could also be shown that the respective cysteine-type CTS KO reveals a loss of cysteine protease activity and therefore providing a novel cellular model to further investigate the possible redundant function of CTSB, CTSD and CTSL within the lysosomal protease network.

## 4.3 SH-SY5Y CTSBDL-triple deficient cells are characterized by enlarged and increased numbers of lysosomes

The generation of several independent CTS-deficient cell lines presents an exciting tool to study the resulting effects in lysosomes, i.e. the analysis of the lysosomal

functions of degradation, involvement of CTSs in autophagy and recycling of macromolecules, proteins and peptides. First, it was aimed to understand the consequences of a loss of different lysosomal CTSs on the lysosomes themselves. To analyze if lysosome morphology is changed when the major CTSs are missing, SH-SY5Y WT, CTSB-, CTSD-, CTSL- and CTSBDL-deficient cell lines were analyzed by immunofluorescence staining using an established antibody directed against human LAMP1, an abundant lysosomal membrane protein (Figure 15). Comparing the lysosomal phenotypes of the CTS-deficient cell lines with WT control cells revealed that the single KO of CTSB and CTSL did not lead to obvious phenotypic changes in regard to the size, distribution or number of lysosomes. Interestingly, in the SH-SY5Y cells the CTSD KO showed a trend towards an increase in the size of lysosomes. More importantly, CTSBDL-triple KO cells were characterized by a significant expansion of the lysosomal size and number (Figure 15A).

To validate these findings the lysosomal diameter of all CTS-deficient cell lines was measured (3.2.6.2) and the results are presented in Figure 15B. The mean lysosomal diameter of the SH-SY5Y WT cells was 0.25 µm. The lysosome size of the two clones of CTSB KO (clone #3: 0.22 µm and clone #6: 0.31 µm) and CTSL KO (clone #6: 0.22 µm and clone #11: 0.22 µm) did not show changes when compared to the WT lysosome's size. The CTSD KO clones showed mildly increased lysosomal diameters of 1.2- to 1.3-fold (clone #10: 0.34 µm and clone #36: 0.29 µm). The most striking observation was that the combined loss of CTSB, CTSD and CTSL led to a significant increase in the diameter of the lysosomes. CTSBDL clone #4 showed a mean diameter of 0.72 µm and clone #9 showed a diameter of 0.67 µm which is 2.7- to 2.9-times the size of the WT lysosomes. Interestingly, there were also some lysosomes with a diameter up to 1.7 µm. which is 6.8-times the size of the mean lysosomal size of the SH-SY5Y WT cells.

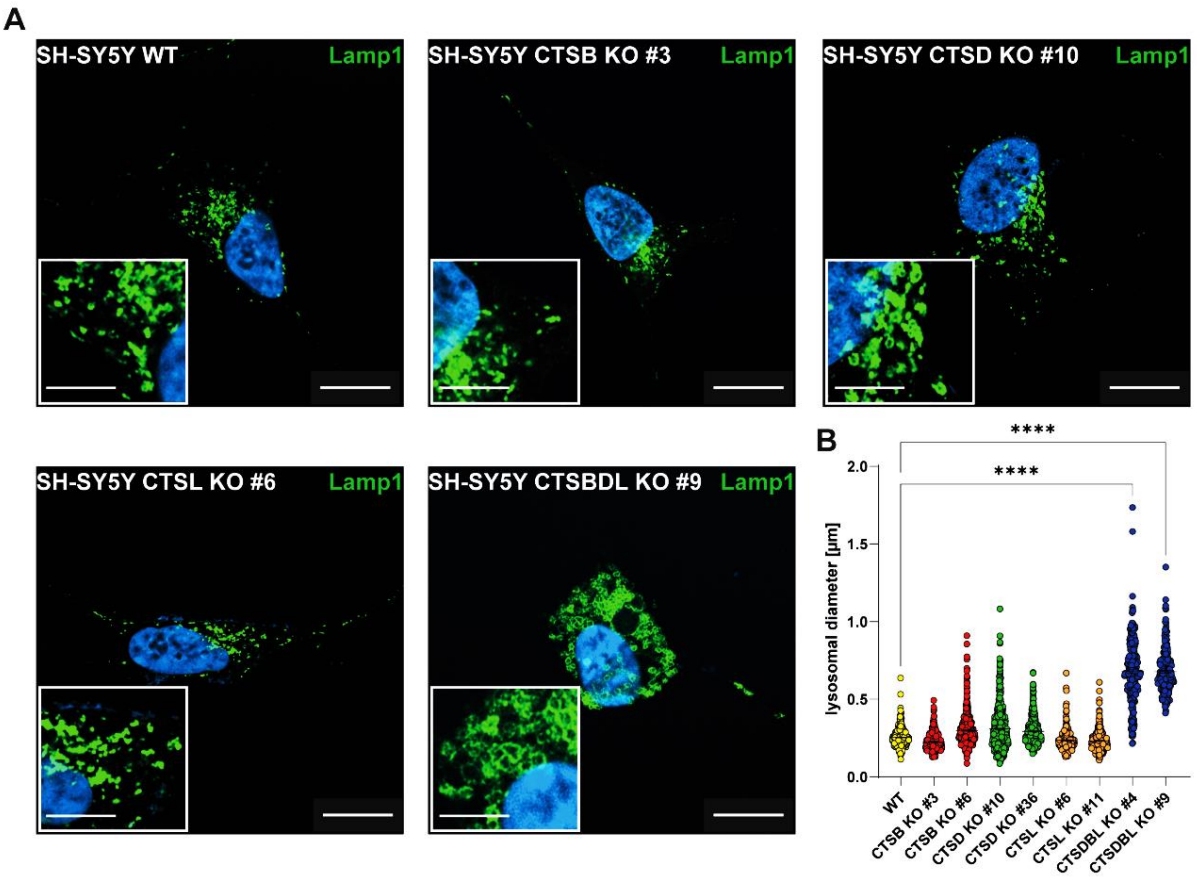


**Figure 15: CTSBDL-deficiency in SH-SY5Y leads to enlarged lysosomes. (A)** Respective immunostainings of endogenous lysosomal LAMP1 in SH-SY5Y WT and one of each CTSB, CTSD, CTSL single KO and CTSBDL-triple KO cells reveals differences in the size of lysosomes in the CTSBDL-deficient mutant compared to control SH-SY5Y WT cells. Cell were fixed in 4 % PFA. Nuclei are stained with DAPI. Scale bar: 10 µm, insert: 5 µm **(B)** Analysis of the lysosomal size of SH-SY5Y WT, CTSB KO #3 and #6, CTSD KO #10 and #36, CTSL KO #6 and #11, CTSBDL KO #4 and #9. The graph depicts the lysosomal diameter in µm derived from immunostainings of Lamp-1-positive vesicles from three individually stained experiment data sets. Data represent the mean ± SEM, one-way ANOVA with a Bonferroni's multiple comparison test. **** p<0.0001.

The lysosomal size between both clones of SH-SY5Y CTSB, CTSD and CTSL single KO and CTSBDL-triple KO was equal which excludes clonal effects. Consequently, the following experiments were conducted using SH-SY5Y CTSB clone #3, CTSD clone #10, CTSL clone #6 and CTSBDL clone #9 referred to as SH-SY5Y CTSB, CTSD, CTSL and CTSBDL KO, respectively.

In addition to the phenotypic changes in the lysosomal morphology of SH-SY5Y CTSBDL-deficient cell lines the LAMP1 protein expression was biochemically analyzed (Figure 16). In four independent experiments immunoblot analysis of cell lysates revealed a significant 3.27-fold increase of LAMP1 protein expression in the SH-SY5Y CTSBDL KO cells when compared to the SH-SY5Y WT expression (p=0.0026). SH-SY5Y CTSB, CTSD and CTSL single KO did not significantly express more LAMP1 compared to WT cells.

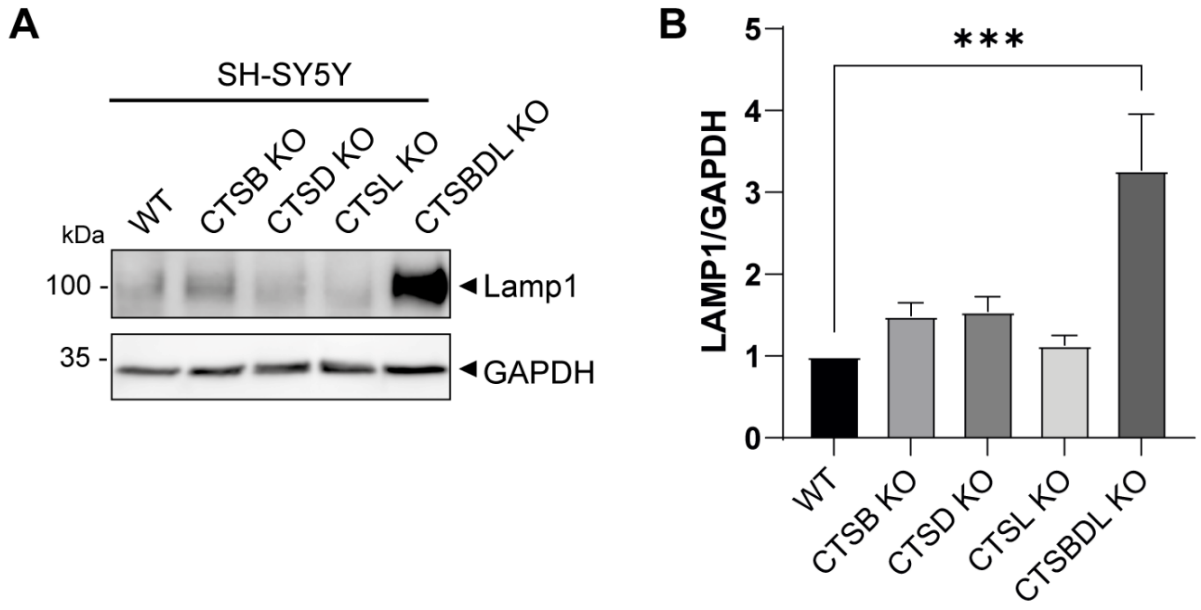


**Figure 16: LAMP1 protein expression is increased in the SH-SY5Y CTSBDL-deficient cells. (A)** Endogenous LAMP1 expression detected by immunoblot analysis of lysates from SH-SY5Y WT, CTSB, CTSD, CTSL and CTSBDL KO cells. GAPDH was used as a loading control. **(B)** Quantification of LAMP1 expression levels normalized to GAPDH with WT set as one from four individual experiments. Data represent the mean + SEM, one-way ANOVA with a Bonferroni's multiple comparison test with SH-SY5Y WT used as reference. *** $p<0.001$. kDa: kilodalton

Enlarged lysosomes are often a key feature in lysosomal storage disorders (LSD) where accumulated material remains undegraded within these organelles (Marques et al. 2020). The next aim was to address if the enlarged lysosomes of the SH-SY5Y CTSBDL-deficient cells were similarly filled with undigested cargo. Therefore, SH-SY5Y WT and CTSBDL-deficient cells were grown, fixed in PFA and sent for transmission electron microscopy (TEM) (3.2.4.2). In TEM images the lysosomal structures appeared as defined round organelles filled with electron dense and dark structures. As shown in Figure 17 SH-SY5Y CTSBDL-triple KO cells had expanded electron-dense vesicles indicated as lysosomes (L) with a more structured contour when compared to lysosomes in the SH-SY5Y WT cells. This could be specified as undigested lysosomal storage material. In addition, the TEM images also confirmed the enlargement of lysosomes as seen in immunostainings applying the LAMP1 antibody staining (Figure 15).

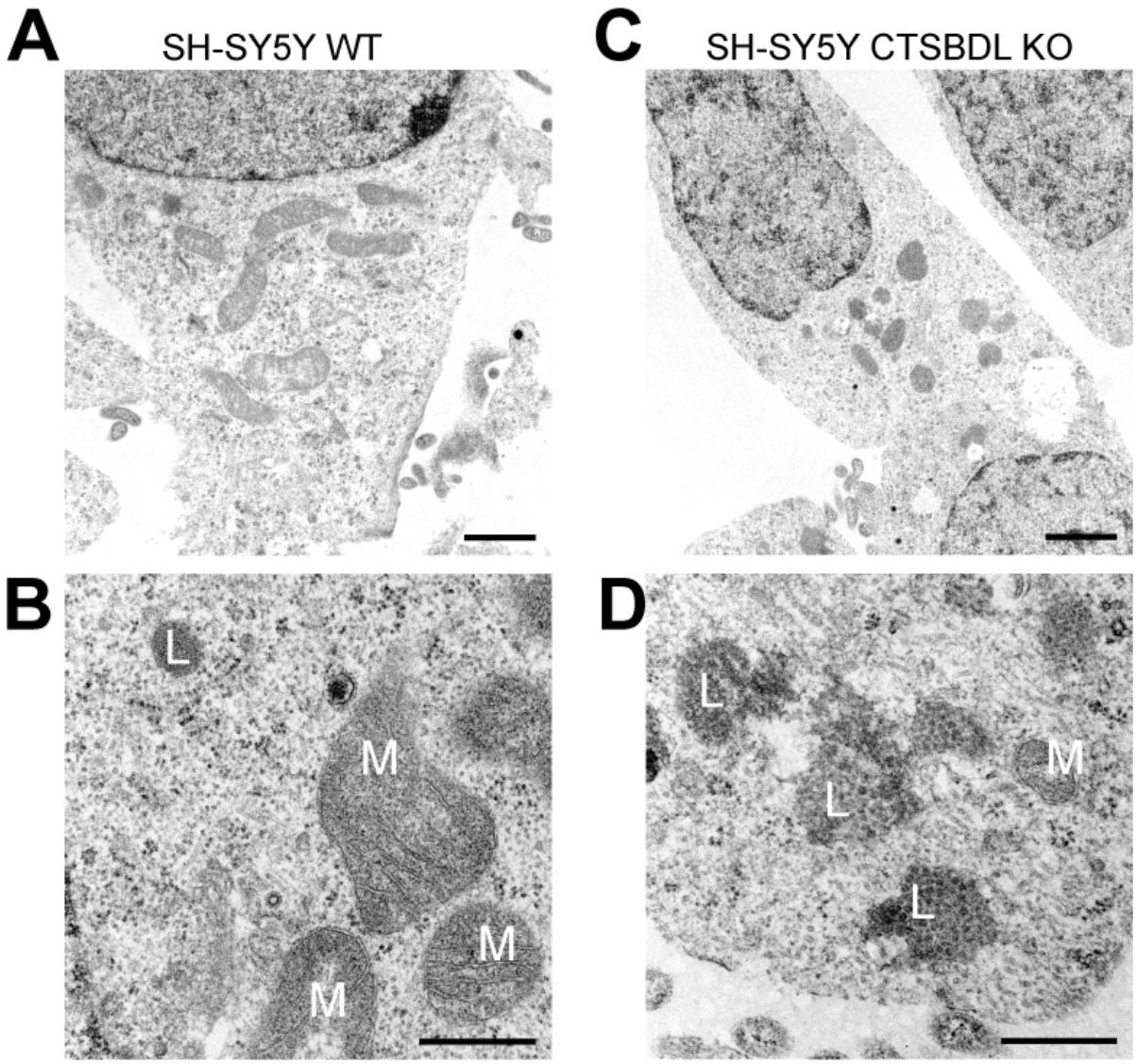


**Figure 17: Enlarged lysosomes of CTSBDL-deficient SH-SY5Y cells are filled with electron-dense storage material.** Transmission electron microscopy images of (A,B) SH-SY5Y WT and (C,D) CTSBDL-deficient cells fixed with 4 % PFA and 2 % glutaraldehyde in 0.1 M PB, pH 7.4. A CTSBDL-deficiency in SH SY5Y cells leads to enlarged lysosomal vesicles that are filled with electron dense storage material. Scale bar: (A,C): 1 µm, (B,D): 0.5 µm. L: lysosome, M: mitochondria. Images were taken and processed by Dr. M. Schweizer from the UKE, Hamburg.

Enlarged lysosomes in LSDs can be filled with undigested lipofuscin, a highly oxidized cross-linked aggregated protein and lipid mixture which also accumulates while aging (Jung et al. 2007). The fluorescence emission spectrum of lipofuscin ranges from 570 nm to 605 nm (Jung et al. 2007). Therefore, immunostainings of SH-SY5Y CTS-deficient cell lines stained with LAMP1 were prepared and the samples were investigated for autofluorescence at an emission wavelength of 594 nm by immunofluorescence microscopy (Figure 18).

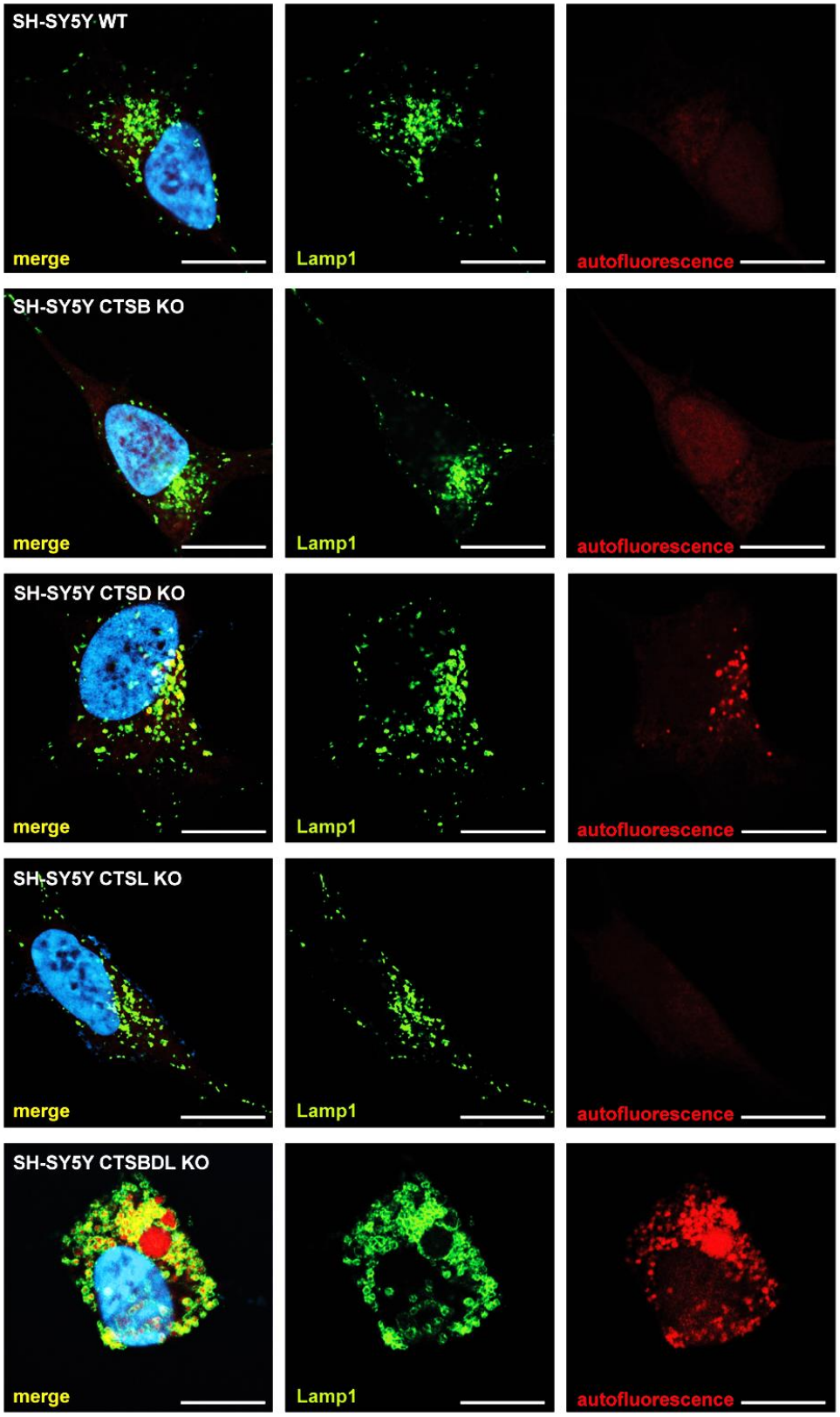


**Figure 18: Lipofuscin accumulates within lysosomes of the SH-SY5Y CTSD- and CTSBDL-deficient cells.** Immunostainings of SH-SY5Y WT and CTSB, CTSD and CTSL single KO and CTSBDL-triple KO cells fixed in 4 % and stained with the antibody binding to the lysosomal membrane protein LAMP1 (green). Stainings were analyzed at the excitation wavelength of 594 nm to detect auto-fluorescent signals of lipofuscin. While no auto-fluorescent signal was observed in SH-SY5Y WT, CTSB KO and CTSL KO cells SH-SY5Y CTSD KO and CTSBDL KO cells reveal autofluorescence of lipofuscin within the lysosomes. Nuclei staining was performed with DAPI. Scale bar: 10 µm

Images of SH-SY5Y WT did not show autofluorescent signal at 594 nm and the single KO of CTSB or CTSL also did not lead to an accumulation of lipofuscin as revealed by fluorescence emission. This result is in accordance to the unchanged size in lysosomes (Figure 15) indicating that there is possibly no accumulation of lysosomal storage material. SH-SY5Y CTSD-deficient cells confirmed an increased size of lysosomes when compared to SH-SY5Y WT cells (Figure 15). Interestingly, immunostainings showed autofluorescence signals in some LAMP1-positive vesicles supporting the hypothesis that an increase in lysosomal size caused by the loss of CTSD comes along with an accumulation of undigested lipofuscin. The most striking effect could be seen in the SH-SY5Y CTSBDL-triple KO cell line. Here, almost all lysosomes were enlarged and filled with lipofuscin fluorescing at 594 nm. These data confirm the findings derived from TEM images (Figure 17) where SH-SY5Y CTSBDL-deficient cells show enlarged lysosomes filled with electron dense material that probably also includes lipofuscin.

As lysosomal CTS activity loss, enlarged lysosomes, undigested cargo and accumulation of lipofuscin are markers for an impairment of the lysosomal function the next step was to investigate whether the autophagy system was affected by the loss of the major CTSs in SH-SY5Y cells.

## 4.4 Combined CTSBDL-deficiency in SH-SY5Y cells causes mild effects on the autophagic flux

Macromolecules destined for degradation are delivered to the lysosomes by endocytosis, phagocytosis or autophagy pathways. In particular autophagy plays an essential role mainly under starvation or nutrient-poor conditions to recover critical nutrients and energy for the cellular survival (Myerowitz et al. 2021; Settembre et al. 2013). It is a multistep process starting with the formation of a phagophore later forming the autophagosome which then fuses with lysosomes to degrade the residing macromolecules by lysosomal proteases for recycling of single amino acids or small peptides (Settembre et al. 2013; Klionsky et al. 2016). The microtubule-associated protein 1A/1B light chain 3B (MAP1LC3B, short: LC3) is a marker for autophagosomes and widely used to investigate autophagy (Klionsky et al. 2016).

To analyze endogenous LC3 in the SH-SY5Y WT, CTSB-, CTSD-, CTSL-single KO and CTSBDL-triple KO cells, the cells were grown on cover slips, fixated in 4 % PFA and stained with antibodies directed against the lysosomal integral membrane protein 2 (LIMP2) and LC3 (3.1.4; 3.2.4.1). In Figure 19 the fluorescence microscopy images are presented. SH-SY5Y WT cells expressed LIMP2 and showed that some of these lysosomal vesicles colocalize with LC3. There are two forms of LC3 present in cells, the cytosolic LC3-I and the membrane bound LC3-II (Kabeya et al. 2004). LC3-I can be conjugated to phosphatidylethanolamine to form LC3-II which is tightly bound to the membrane of autophagosomes and serves as a marker for autophagy induction and also impairment (Mizushima and Yoshimori 2007).

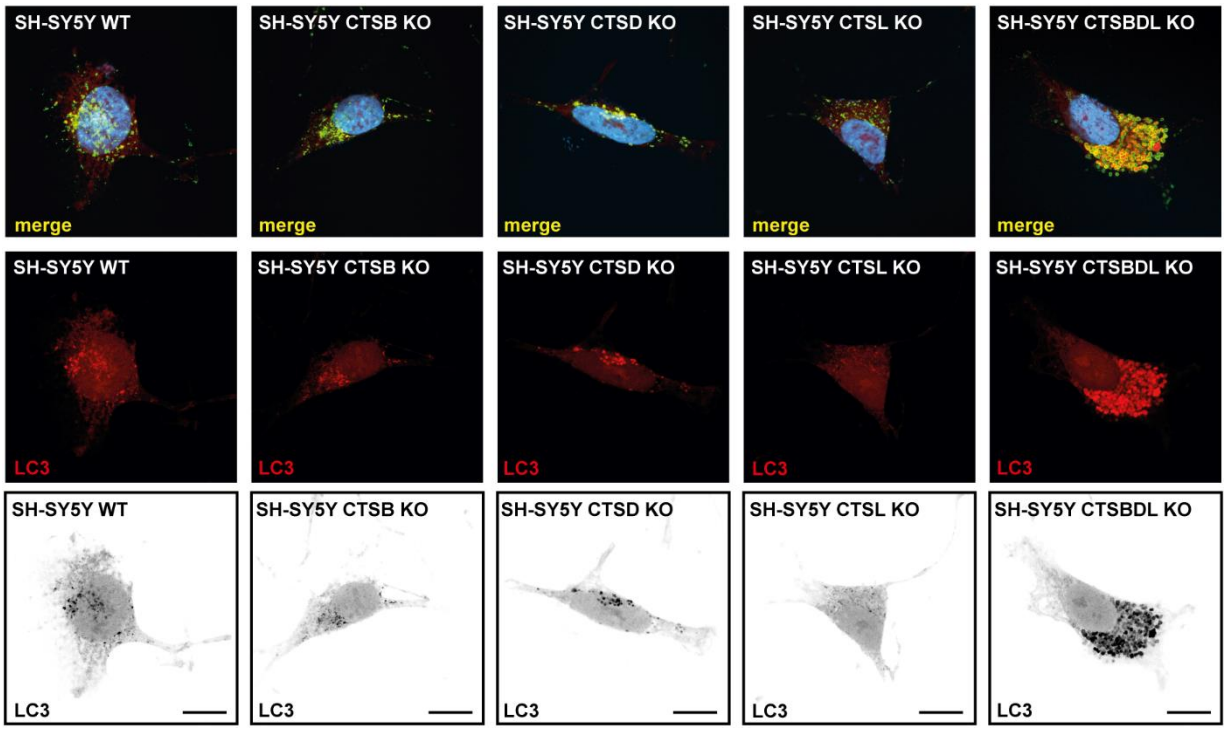


**Figure 19: LC3 accumulates in SH-SY5Y CTSBDL-deficient lysosomes.** SH-SY5Y WT, CTSB KO, CTSD KO, CTSL KO and CTSBDL KO cells were fixed with 4 % PFA and stained with antibodies directed against LIMP2 (green, only seen in merged images) and the microtubule-associated protein 1A/1B light chain 3B (MAP1LC3B/LC3) (red, black). Respective images show SH-SY5Y WT and CTSB and CTSL single KO with low expression of LC3. SH-SY5Y CTSD KO cells reveal some and CTBDL KO cells reveal a high accumulation of LC3 within lysosomes Scale bar: 10 µm

A CTSB, CTSD or CTSL KO in SH-SY5Y cells did not lead to a change in LC3 distribution. In contrast, a CTSBDL-triple deficiency in SH-SY5Y cells caused a strong fluorescence signal of LC3 indicating an altered autophagic flux. Interestingly, in all investigated SH-SY5Y cell lines the LC3 signal could be detected in the cytosol, which can be referred to as LC3-I. Only some LIMP2-positive vesicles of SH-SY5Y WT, CTSB and CTSD KO contained LC3 puncta assigned as membrane bound LC3-II.

Lysosomal LIMP2 signal in the SH-SY5Y CTSBDL-deficient cells almost completely colocalized with LC3-II puncta (Figure 19).

To support the LC3-microscopy analysis lysates of SH-SY5Y WT, CTSB, CTSD, CTSL and CTSBDL KO cells were prepared (3.2.3.1) and investigated by immunoblot (3.2.3.4; 3.2.3.5). Four individual experiments were conducted. Figure 20 displays the biochemical analysis by a respective immunoblot and its quantification. SH-SY5Y WT cells mainly expressed LC3-I which appeared at the predicted size of 18 kDa but only little amounts of LC3-II which was predicted at 16 kDa (Deretic 2008). A single KO of CTSB, CTSD or CTSL in the SH-SY5Y cells did not alter the LC3-II protein levels. However, a combined KO of CTSB, CTSD and CTSL in SH-SY5Y cells revealed significant upregulation of LC3-II protein expression by 2.56-fold (p=0.0053). These data were in line with the upregulation of expression of LC3 seen in immunostainings from SH-SY5Y CTSBDL-deficient cells when compared to the WT cells and give reason to further investigate the affected autophagy within these cell lines.

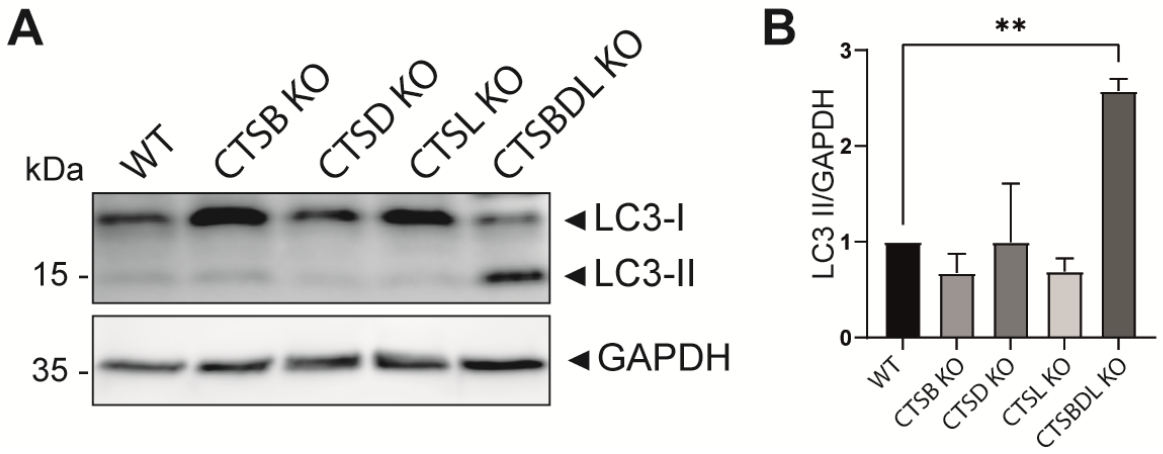


**Figure 20: The autophagosomal marker LC3-II is increased in SH-SY5Y CTSBDL-deficient cells. (A)** Immunoblot of lysates derived from SH-SY5Y WT, CTSB, CTSD and CTSL single KO and CTSBDL-triple KO cells. Under endogenous conditions and with full nutrient supply LC3-II accumulates in the SH-SY5Y CTSBDL-deficient cell line. GAPDH was used as a loading control. **(B)** Quantification of four individual experimental sets of lysates from SH-SY5Y WT, CTSB, CTSD, CTSL and CTSBDL KO cells. LC3-II protein levels were normalized to GAPDH with WT set as one. Data represent the mean + SEM, one-way ANOVA with a Bonferroni's multiple comparison test with SH-SY5Y WT used as reference. ** p<0.01. kDa: kilodalton.

To measure the degradation activity of the possible altered autophagy pathway, the autophagic flux was analyzed by quantifying LC3-II expression under different conditions by immunoblot. The autophagic flux was addressed by analyzing the degradation of autophagosomal marker LC3-II by lysosomal hydrolases. The elevated protein levels of LC3-II in the SH-SY5Y CTSBDL-deficient cells under endogenous conditions could be caused by either an increase in the formation of autophagosomes

(induction of autophagy) or by a blockage in the fusion of autophagosomes with lysosomes (blockage of autophagy) or by both processes. To investigate this question an autophagic flux assay (3.2.2.5) was conducted on the SH-SY5Y WT and CTSBDL-deficient cells. Cells were either grown under non-starvation (including essential and non-essential amino acids) or starvation conditions with or without the lysosomal inhibitor Bafilomycin A1 (BafA1) for 3 h (Klionsky et al. 2016). BafA1 targets the vacuolar ATPase (v-ATPase) thus preventing protons to passage into the lysosomal lumen causing inhibition of acidification of the organelle resulting in an inhibition of lysosomal proteases (Whitton et al. 2018). It also blocks the fusion of autophagosomes with lysosomes by a yet unknown mechanism (Mauvezin et al. 2015). Starvation conditions were used to determine the LC3-II protein accumulation within autophagosomes as autophagy is induced. By adding BafA1 to these conditions the contribution of lysosomal degradation of LC3-II can be revealed (Tanida et al. 2005).

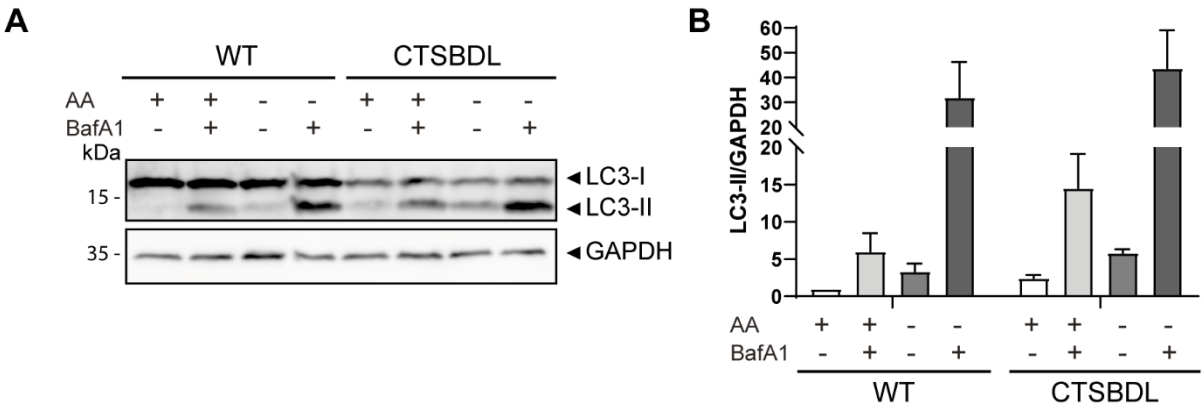


**Figure 21: Lysosomal degradation of LC3-II during autophagy is mildly impaired in the SH-SY5Y CTSBDL-deficient cell line. (A)** Respective immunoblot of an autophagy assay of SH-SY5Y WT and CTSBDL KO cells. Cells were grown in EBSS in nutrient-rich conditions with amino acids (AA) with (+) or without (-) the lysosomal inhibitor Bafilomycin A1 (BafA1, 500 nM) or in EBSS under starvation conditions without AA with or without BafA1 for 3 h. An antibody against the autophagosomal marker LC3 (detecting cytosolic LC3-I and membrane-bound LC3-II) was used. Glycerinaldehyd-3-phosphate (GAPDH) was used as a loading control. **(B)** Quantification of a set of three individual autophagy assays of SH-SY5Y WT and CTSBDL KO cells with LC3-II normalization to GAPDH with WT set as one. Data represent the mean + SEM. kDa: kilodalton.

Figure 21 shows the results of the autophagic flux assay. Three independent experiments were analyzed and quantified. The data revealed that under nutrient-rich conditions the LC3-II expression in SH-SY5Y CTSBDL-deficient cells was 2.44-fold higher compared to WT cells which was in line with the data from Figure 20. BafA1 treatment led to an accumulation of LC3-II in both cell types. In SH-SY5Y CTSBDL-deficient cells there was a 2.4-fold higher expression of LC3-II compared to WT cells. Under starvation conditions there was 1.75 times more LC3-II in the SH-SY5Y

CTSBDL-deficient cells compared to WT cells. By adding BafA1 the autophagic flux was further inhibited leading to a maximal accumulation of LC3-II in both cell types.

In summary, there was more LC3-II in all of the conditions in the SH-SY5Y CTSBDL-deficient cells when compared to the WT cells. The most interesting part was, that the possible autophagic flux impairment in the SH-SY5Y CTSBDL-deficient cells indicated by accumulation of LC3-II under nutrient-rich conditions (Figure 20, Figure 21) reflects only a mild impairment of autophagy as LC3-II expression can be further increased by either starving the cells, adding BafA1 or both. While starvation induced autophagy in both SH-SY5Y WT and CTBDL-deficient cells as indicated by an increase of LC3-II, the effect on a disturbed autophagic flux could be maximized by adding BafA1 leading to even higher levels of LC3-II. Under starvation conditions, SH-SY5Y WT cells only represented 10.43 % impairment of the maximum autophagic flux (≙ 100 %) while SH-SY5Y CTSBDL cells showed 13.33 % impairment of the maximum autophagic flux. These results also explain that under endogenous conditions the fusion of autophagosomes with lysosomes is still functioning in the SH-SY5Y CTSBDL-deficient cells as LC3-II can further increase after BafA1 treatment.

In addition to the biochemical analysis of LC3-II by immunoblot, a fluorescence assay to monitor the autophagic flux using a tandem mRFP-EGFP-tagged LC3 (Kimura et al. 2007) was conducted on SH-SY5Y WT and CTSBDL-deficient cells. A schematic overview on how the effects on the cells transfected with tandem mRFP-EGFP-LC3 reporter construct are analyzed is shown in Figure 22. Due to different properties of RFP and EGFP under acidic conditions the tandem fluorescent-tagged LC3 can be used to distinguish autophagosomes from autolysosomes (Kimura et al. 2007). Autophagosomes are formed under neutral pH conditions as LC3 gets lipidated at the vesicle membrane. Autophagosomes are characterized by red RFP and green EGFP fluorescent signals resulting in yellow vesicles in confocal laser scanning microscopy (LSM). Under acidic pH conditions as found in autolysosomes EGFP is quenched and only a red RFP fluorescence signal is observed. Therefore, autolysosomes appear as red vesicles. While LC3 gets lipidated under high autophagic flux conditions the yellow appearing cytoplasmic staining faints. By using this method, the question if LC3-II in the SH-SY5Y CTSBDL-deficient cells accumulates due to increased autophagosome formation or due to an inhibition in the fusion of autophagosomes with lysosomes can be addressed.

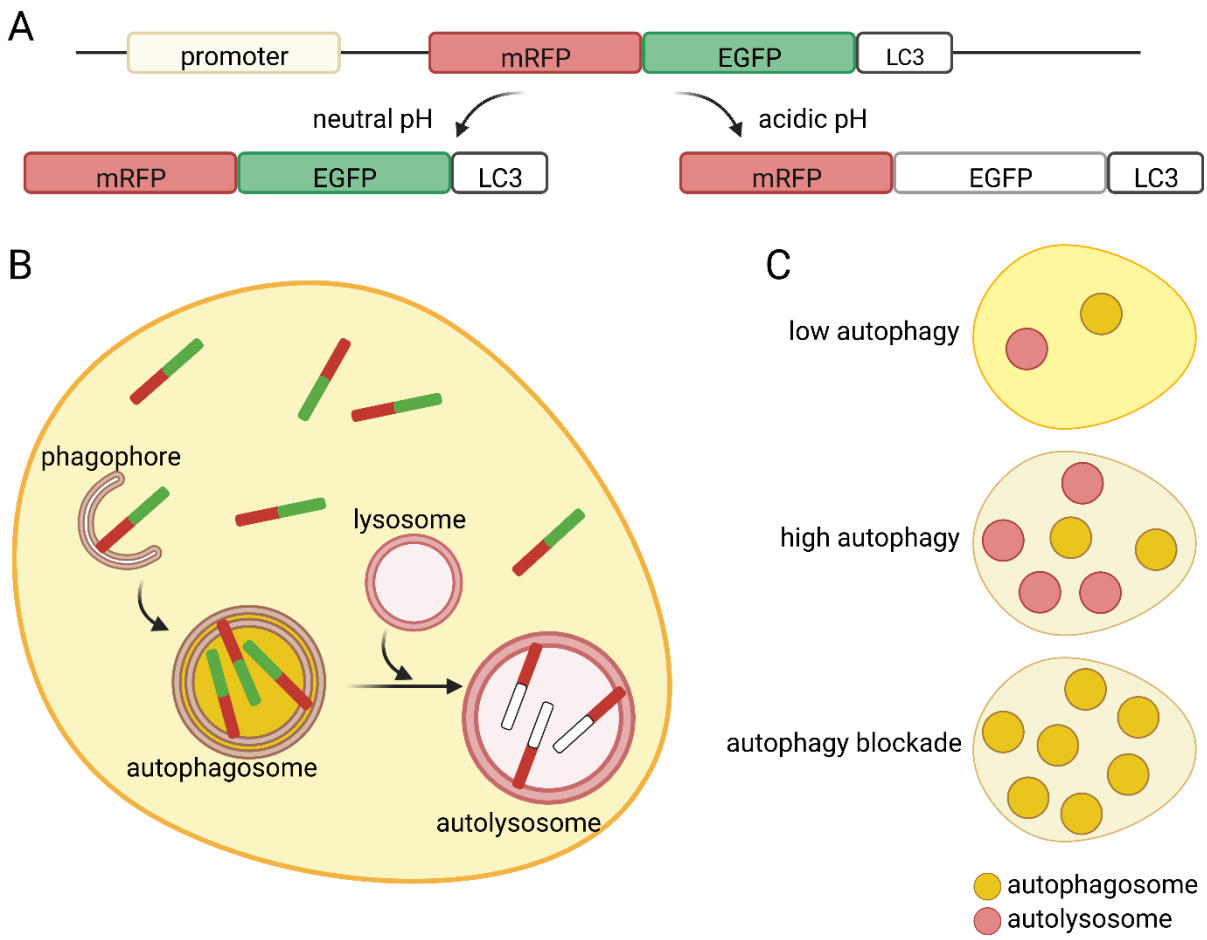


**Figure 22: Schematic overview to monitor the autophagic flux using the tandem mRFP-EGFP-LC3 reporter construct. (A)** Illustration of the mRFP-EGFP-LC3 reporter construct and how the protein reacts under different pH conditions. Acidic pH leads to the quenching of the EGFP signal so that only red RFP signal is observed while under neutral pH conditions both RFP and EGFP fluorescence signals can be monitored resulting in a yellow overlay signal in microscopy. **(B)** Representation of mRFP-EGFP-LC3 during autophagosome and autolysosome maturation. The tandem construct remains within the cytoplasm which appears light yellow. Lipidated LC3 (LC3-II) is recruited to the membrane of the phagophore and autophagosome. As the pH is neutral these vesicles are observed with a yellow color (red RFP and green EGFP fluorescence signal). Eventually, autophagosomes fuse with lysosomes to form autolysosomes. The tandem construct only shows fluorescence of the red RFP while the green fluorescence signal of the EGFP is quenched due to the acidic pH within the lysosomal lumen. **(C)** Various scenarios of cells expressing the mRFP-EGFP-LC3 at different stages of autophagy. Within cells with a low autophagic flux most of the LC3 remains unlipidated and both RFP and EGFP fluorescence signals result in a yellow signal of the cytoplasm. Only a few autophagosomes (yellow vesicles) and autolysosomes (red vesicles) are visible. Under high autophagic flux conditions LC3 is lipidated to LC3-II and the cytoplasm turns into a bright yellow. New autophagosomes are formed which rapidly fuse with lysosomes. There is an increase in the total number of vesicles and more red autolysosomes are visible. In case there is a blockade in the autophagic flux autophagosome formation may still occur but fusion with lysosomes is blocked. Therefore, the cytoplasm turns bright yellow as LC3 gets lipidated and only yellow autophagosomes but no red autolysosomes are visible. Figure adapted from(Lopez et al. 2018) using biorender.com.

Cells were grown on cover slips and transfected with mRFP-EGFP-tagged LC3 48 h prior the previously described autophagy assay was applied and analyzed by fluorescence microscopy (3.2.4.1). The results are presented in Figure 23.

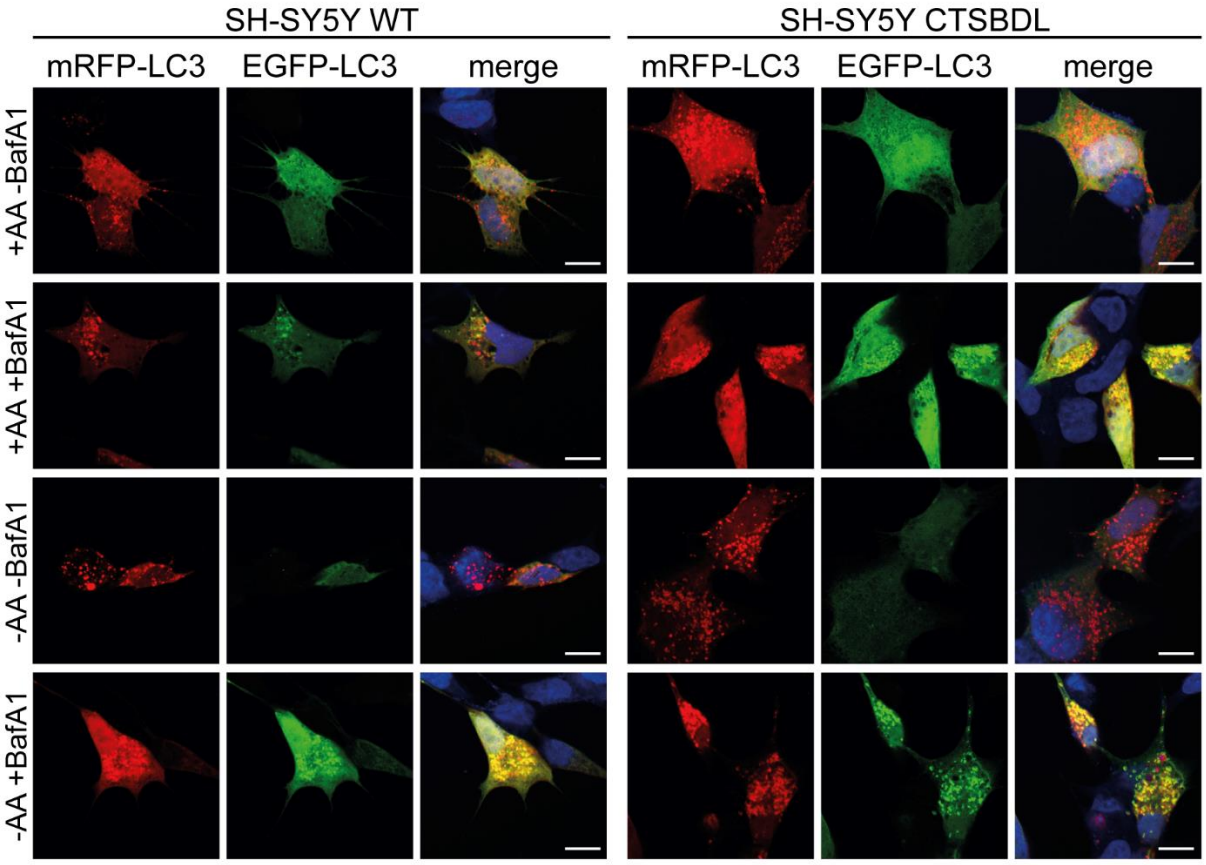


**Figure 23: Fusion of autophagosomes with lysosomes is unaffected in the SH-SY5Y CTSBDL-deficient cells.** Respective immunofluorescence images of SH-SY5Y WT and CTSBDL-deficient cells after transfection with a tandem mRFP-EGFP-LC3 reporter construct. Cells were grown on coverslips, transfected for 48 h with mRFP-EGFP-LC3 followed by an autophagy assay for 3 h. Cells were grown under endogenous conditions using EBSS and essential and non-essential amino acids (AA; first row), endogenous conditions with the lysosomal inhibitor Bafilomycin A1 (BafA1, 500 nM; second row), starvation conditions with EBSS only (third row) and starvation conditions with BafA1 (fourth row). Fluorescent signals were captured at 594 nm for RFP and 488 nm for EGFP. Scale bar: 10 µm

Under nutrient-rich conditions (+AA, -BafA1, Figure 23 first row) in SH-SY5Y WT cells the cytoplasm appeared yellow and red and yellow vesicles are observed. The cytoplasm in SH-SY5Y CTSBDL-deficient cells the cytoplasm was also yellow and there were more and bigger red vesicles indicating more lysosomes and an impaired autophagic flux when compared to WT cells. This also explained that under endogenous conditions autophagosomes were still formed and could fuse with lysosomes in the SH-SY5Y CTSBDL-deficient cells. On the other hand, it appeared that more autophagosomes were formed that rapidly fused with lysosomes. These lysosomes were not able to completely recycle their cargo as three of the main hydrolases are missing. If BafA1 was added (Figure 23, second row), the SH-SY5Y WT cytoplasm appeared faint yellow and both yellow autophagosomes and red

autolysosomes were detected. The SH-SY5Y CTSBDL-deficient cells had a stronger yellow cytoplasm and only yellow autophagosomes. The CTSBDL-deficiency led to a blockade in the autophagic flux while autophagy seemed to be higher in the SH-SY5Y WT cells. This could also be seen in the autophagy assay analyzed by immunoblot (Figure 21) as there was more lipidated LC3-II in the SH-SY5Y CTSBDL-deficient cells when compared to WT cells. Under starvation conditions (-AA, -BafA1, Figure 23, third row) the SH-SY5Y WT and CTSBDL-deficient cells shared the same appearance of fluorescent signals. The cytoplasm was faint yellow and there were only red autolysosomes. Most of the RFP-GFP-LC3 was lipidated (no more unlipidated LC3 in the cytoplasm) and all autophagosomes had fused with lysosomes. Both cell types rely on autophagy under these conditions as there is no nutrient supply from the outside. That is why in both cases autophagy is activated and the autophagic flux is high. Again, the SH-SY5Y CTSBDL-deficient cells had more autolysosomes as they were not completely able to recycle their cargo and it also confirmed that autophagosomes were still fusing with lysosomes. By increasing the stress level by adding BafA1 (Figure 23, fourth row) to starvation conditions both cell types mainly had yellow autophagosomes indicating a blockade in the autophagic flux. The SH-SY5Y WT cells showed a brighter yellow cytoplasm compared to the CTSBDL-deficient cell which indicated that there was more unlipidated LC3 and probably a lower autophagosome formation rate. Though, both cell types showed inhibition of the autophagic flux under starvation conditions with BafA1.

Conclusively, under nutrient-rich conditions the combined KO of CTSB, CTSD and CTSL in SH-SY5Y cells led to a mild decrease of the autophagic flux as there was more lipidated LC3 (LC3-II) and more autolysosomes compared to WT cells. However, under endogenous conditions (+AA, -BafA1) the autophagic flux was only mildly impaired as there was only 5.58% LC3-II present (Figure 21) when compared to the LC-II found under maximal autophagy inhibition (-AA, +BafA1).

## 4.5 SH-SY5Y CTSBDL-deficient cells have impaired proteolysis of endocytosed proteins

Autophagy represents a degradation pathway for intracellular material. Endocytosis is a way to degrade extracellular material (Settembre et al. 2013). Therefore, it should be investigated what happens to endocytosed proteins in the SH-SY5Y CTSBDL-deficient

cells. Bovine serum albumin (BSA) is a broadly used protein to examine endocytosis, its intracellular processing and analysis of enzymatic activity of proteins hydrolyzing BSA. CTSB, CTSD and CTSL can cleave BSA *in vitro*. Using a fluorophore-tagged BSA, different albumin fragmentation patterns were visible after in-gel fluorescence detection (Di Spiezio et al. 2021). One day after SH-SY5Y CTSBDL-deficient cells were seeded they were washed in PBS and incubated for up to 16 h with DMEM, 1% FBS, 1% P/S containing 15 µg/ml BSA Alexa Fluor 647 conjugate. Cells were then harvested and lysed in the dark to prevent bleaching, loaded on 15% SDS-gels and in-gel fluorescence was analyzed using the Amersham Typhoon Biomolecular Imager (3.2.3.4).

Figure 24A shows the fluorescent SDS-PAGE. The molecular weight of the BSA monomer is 66 kDa and its dimer 132 kDa (Marciano et al. 2022). These signals were both visible in the SH-SY5Y CTSBDL-deficient cells. Surprisingly, an additional BSA-AlexaFluor 647 fragment at 50 kDa appeared after 3 h and was stable over all the investigated time points. To compare the influence of the loss of CTSB, CTSD and CTSL a pulse-chase experiment was conducted on both SH-SY5Y WT and CTSBDL-deficient cells. As the additional 50 kDa BSA fragment appears after 3 h the idea was to capture the time point of its accumulation in the SH-SY5Y CTSBDL KO cells.

Therefore, cells were seeded one day prior the assay was conducted. Cells were incubated with DMEM, 1%FBS, 1% Pen/Strep containing 15 µg/ml BSA Alexa Fluor 647 conjugate for 2 h (pulse) and then chased for 0, 10, 20, 30, 60 and 120 min. Control cells were collected after 120 h without incubation with the BSA conjugate. The results are shown in Figure 24B. Both the monomer and dimer of BSA were detectable after 2 h. In SH-SY5Y WT cells the signal intensity for the BSA dimer and monomer got weaker after 30 min while in SH-SY5Y CTSBDL KO cells these signals were still stronger at 30 min but also weakened at later time points. Interestingly, in WT cells there were no smaller fragments than the BSA monomer in all time points, while the 50 kDa BSA fragment was detectable in the SH-SY5Y CTSBDL-deficient cells and got weaker after 60 min. These data indicate that endocytosed BSA was taken up and degraded in both SH-SY5Y WT and CTSBDL-deficient cells. However, the common loss of CTSB, CTSD and CTSL led to an additional 50 kDa BSA fragment pointing towards a deficiency in the proteolysis of BSA within lysosomes. Eventually, the 50 kDa fragments seemed to be degraded over time as the signal got weaker at 60-120 min

indicating that additional lysosomal hydrolases are degrading BSA and prevent accumulation of larger BSA peptide fragments.

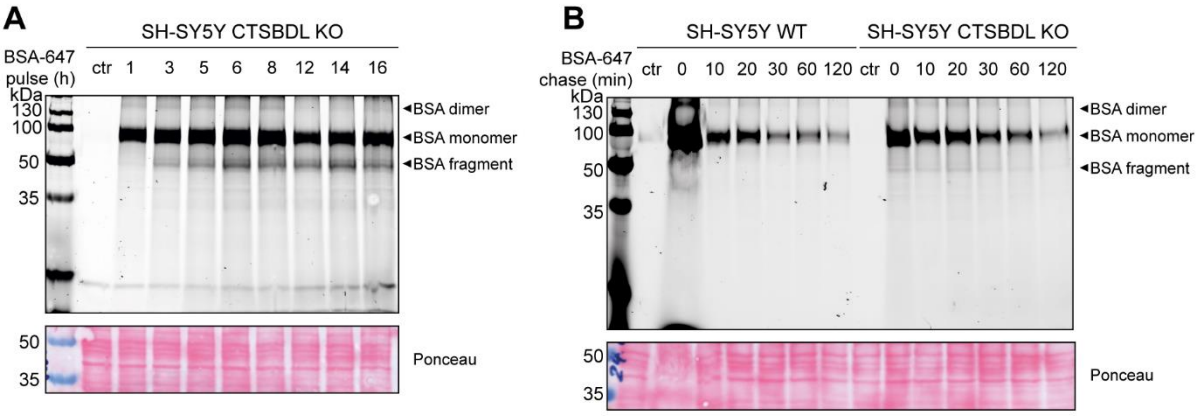


**Figure 24: SH-SY5Y CTSBDL-deficient cells accumulate a 50 kDa BSA fragment. (A)** SH-SY5Y CTSBDL-deficient cells were incubated with 15 µg/ml BSA Alexa Fluor 647 conjugate (Thermo Fisher Scientific) for 1, 3, 5, 6, 12, 14 and 16 h. The control (ctr) was harvested after 16 h without BSA Alexa Fluor 647 conjugate. Lysates were analyzed after SDS-PAGE by in-gel fluorescence detection using the Amersham Typhoon Biomolecular Imager. **(B)** SH-SY5Y WT and CTSBDL-deficient cells were incubated with 15 µg/ml BSA Alexa Fluor 647 conjugate for 2 h (pulse) and chased for 0, 10, 20, 30, 60 and 120 min. Controls were harvested 120 min after pulsing cells without the BSA conjugate. Lysates were analyzed after SDS-PAGE by in-gel fluorescence detection using the Amersham Typhoon biomolecular Imager. Ponceau S staining afterwards served as a loading control. kDa: kilodalton.

## 4.6 Consequences for the cellular proteome after a CTSBDL-deficiency in SH-SY5Y cells

The present data revealed that CTSBDL-deficiency in SH-SY5Y cells led to enlarged lysosomes filled with autofluorescent storage material but only to a mild impairment of the autophagic flux. The results from the BSA processing experiment (Figure 24) indicated that other lysosomal hydrolases are still functional and maintain general protein degradation, although there was accumulation of lysosomal storage material such as lipofuscin. To investigate proteins and peptides piling up within SH-SY5Y CTSBDL KO lysosomes a proteomie analysis was chosen. To this end SH-SY5Y WT and CTSBDL KO cells from clone #4 and #9 were seeded 24 h prior harvesting. Cells were then lysed in modified RIPA buffer (Table 10; 3.2.3.1) and six individual samples of each clone were sent to Dr. S. Lichtenthaler from the DZNE in Munich to perform proteomic analysis of whole cell lysates (3.2.3.8).

In Figure 25 volcano plots represent changes in the protein expression when SH-SY5Y CTSBDL-deficient cells (clone #4 and #9) were compared to WT cells. Overall, analysis revealed that expression of 213 proteins was upregulated and expression of 51

proteins was downregulated in both SH-SY5Y CTSBDL-deficient clones. Among the highest upregulated proteins there were lysosomal membrane proteins like LAMP1, LIMP2 (Lysosomal integral membrane protein 2) and LAMP2, the autophagy marker p62 (Sequestosome-1, SQSTM1), proteins involved in cell adhesion like ITGA1 (Integrin alpha-1) and ITGA2 (Integrin alpha-2) and proteins involved in neurodegenerative diseases like APP (Amyloid Precursor Protein), PLD3 (Phospholipase D3) and LRP1 (Low density lipoprotein receptor-related protein 1).

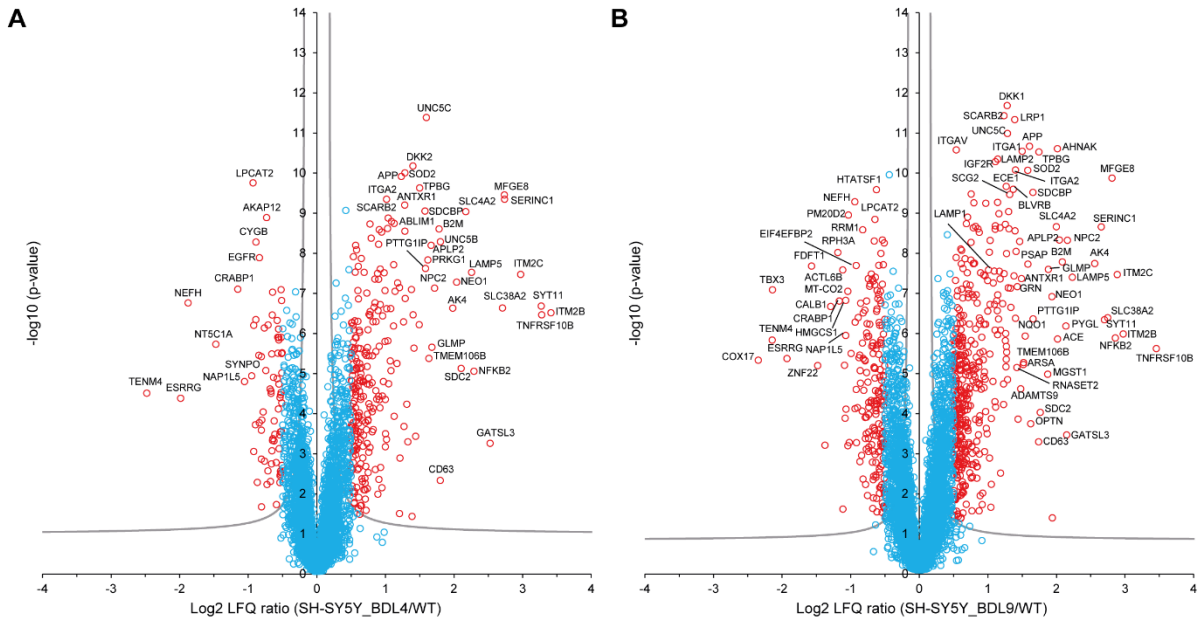


**Figure 25: Proteome analysis of SH-SY5Y WT and two CTSBDL-deficient cell lines reveals dysregulated protein expression. (A)** Volcano scatter plot of SH-SY5Y WT vs. CTSBDL KO clone #4 (BDL4) and **(B)** CTSBDL KO clone #9 (BDL9). Cells were lysed in modified RIPA lysis buffer (5 M NaCl, 0.5 M EDTA pH 8, 0.5 M Tris-HCl pH 8, 1 % Triton X-100, 0.5 % sodium deoxycholate, 0.1 % SDS) and supernatants collected and examined by proteomic analysis. For each cell line 6 individual samples were analyzed. The curved grey line represents the false discovery rate (FDR) horizon of 0.05. Red data points above the FDR horizon represents significantly increased or decreased expression of proteins in SH-SY5Y CTSBDL-triple KO cells compared to the control sample (SH-SY5Y WT). LFQ: label-free quantitation. Proteomic data were generated and analyzed by Dr. S. Lichtenthaler from the DZ NE in Munich.

The data set was further analyzed by the Kyoto Encyclopedia of Genes and Genomes (KEGG) pathway maps tool provided by Kanehisa Laboratories. Figure 26 shows an adapted overview of the lysosomal processes and points out differently regulated expression of lysosomal hydrolase classes, lysosomal membrane proteins or single proteins within the SH-SY5Y CTSBDL-deficient cell compared to WT cells. The overview depicts the transport of synthesized lysosomal enzymes, endocytosis and autophagy. Upregulated proteins due to a loss of CTSB, CTSD and CTSL are highlighted in red. Several lysosomal membrane proteins are upregulated like LAMP

and LIMP. Lysosomal proteases like Legumain (LGMN), Tripeptidyl-peptidase 1 (TPP1) and some glycosidases are also upregulated. The transport of synthesized lysosomal enzymes seems to remain unaffected.

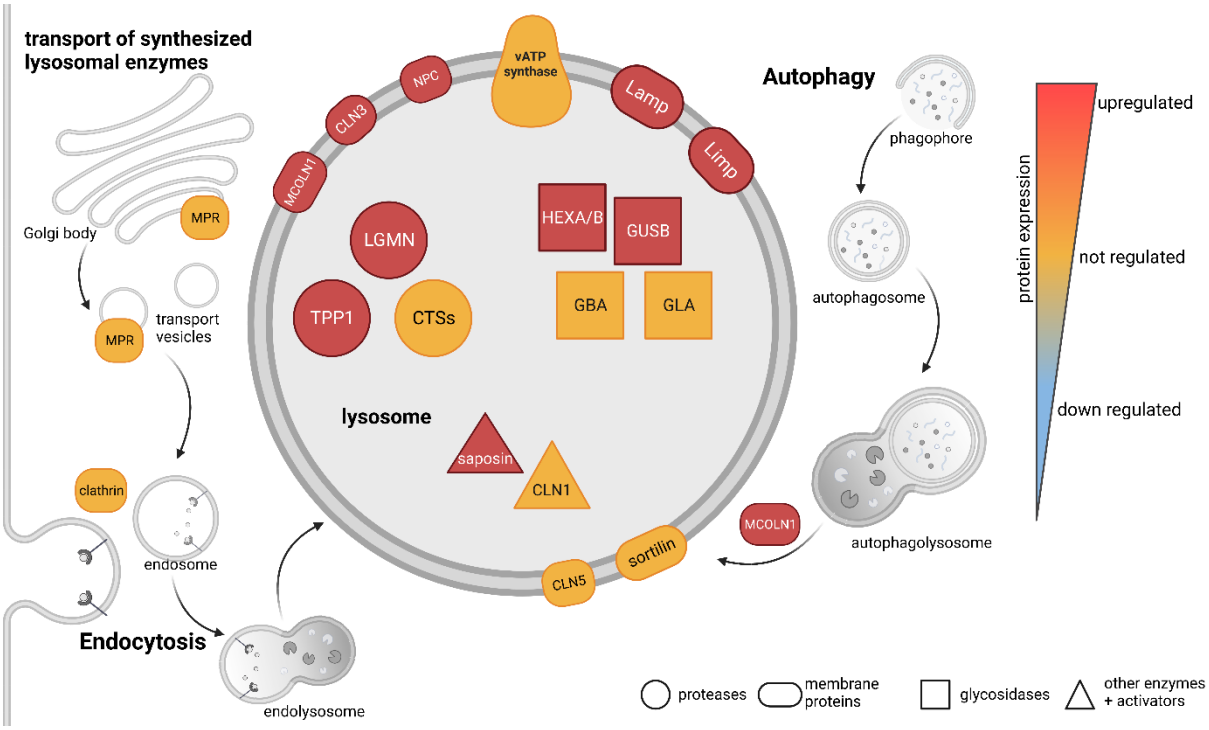


**Figure 26: Lysosomal pathway analysis of SH-SY5Y CTSBDL-deficient cells.** Schematic overview of altered levels of proteins and proteases involved in endocytosis, autophagy and the transport of synthesized lysosomal enzymes in SH-SY5Y CTSBDL-deficient cells compared to WT cells. CLN1 - Palmitoyl-protein Thioesterase 1, CLN3 - Ceroid-Lipofuscinosis Neuronal 3 Protein, CLN5 - Ceroid-Lipofuscinosis Neuronal 5 Protein, CTS – cathepsin, GBA – Glucocerebrosidase, GLA - α-Galactosidase, GUSB - β-glucuronidase, HEXA/B - Hexosaminidase A/B, LGMN – Legumain, MCOLN1 - Mucolipin-1, MPR - Mannose-6-phosphate Receptor, NPC - Niemann-Pick C1 Protein, TPP1 - Tripeptidyl-peptidase 1. Overview adjusted from Kyoto Encyclopedia of Genes and Genomes (KEGG).

To confirm the proteome data analysis, lysates of SH-SY5Y WT, CTSB KO, CTSD KO, CTSL KO and CTSBDL KO cells were analyzed by immunoblot. Lysates of four individual experiments were prepared and analyzed for p62, APP and ITGA2 (Figure 27). Quantifications revealed that p62 expression is significantly upregulated in CTSD KO (2.74-fold) and CTSL KO (2.86-fold) compared to WT cells. The CTSBDL KO cells only show a trend towards increased p62 expression levels (p=0.09).

An antibody directed against the N-terminus of APP revealed that in SH-SY5Y CTSBDL-deficient cells an additional fragment at ~17 kDa significantly accumulated 22-fold compared to the WT cells. Detecting APP with an antibody directed against the C-terminal site both levels of APP-C83 and APP-C99 fragments were significantly increased (5.0-fold) when compared to the WT control. Analyzing ITGA2 revealed a

trend towards increased expression levels (p=0.11) in the SH-SY5Y CTSBDL-deficient cells, however it was not significantly increased.

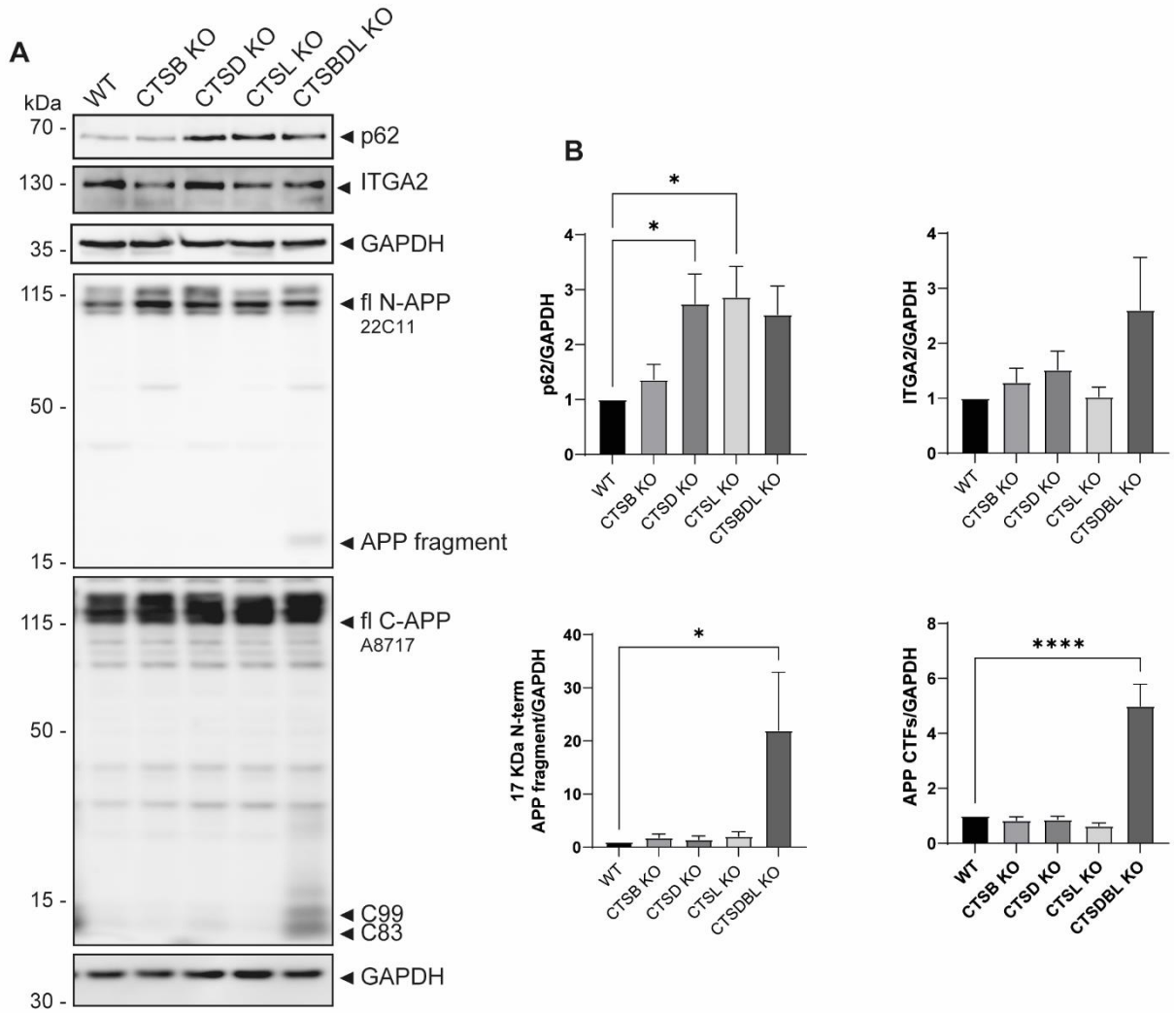


**Figure 27: Accumulation of APP N- and C-terminal fragments in SH-SY5Y CTSBDL-deficient cells. (A)** Respective immunoblot of SH-SY5 WT, CTSB KO, CTSD KO, CTSL KO and CTSBDL KO cells with antibodies directed against p62, N-terminus (22C11, invitrogen) and C-terminus (A8717, Sigma-Aldrich) of APP (Amyloid Precursor Protein) and ITGA2 (Integrin-alpha-2). GAPDH was used as loading control. **(B)** Quantification of four individual experimental sets of lysates from SH-SY5Y WT, CTSB, CTSD, CTSL and CTSBDL KO cells. Protein levels were normalized to GAPDH with WT set as one. Data represent the mean + SEM, one-way ANOVA with a Bonferroni's multiple comparison test with SH-SY5Y WT as reference. * p<0.05; **** p>0.0001. kDa: kilodalton.

Overall, proteome analysis revealed changes of the SH-SY5Y CTSBDL-deficient cells within the lysosomal pathway with upregulation of the expression of lysosomal membrane proteins like LAMP1 and LIMP2 but also lysosomal enzymes like Legumain and TPP1. The upregulated expression of the autophagy marker p62 could only be partially confirmed by immunoblot as there was only a tendency to increased expression levels.

Interestingly, APP was among the increased proteins and by immunoblot analysis an additional ~17 kDa N-terminal and both C-terminal APP fragments (C83, C99) appear to accumulate. Quantifications revealed that ITGA2 shows a tendency towards higher expression levels (p=0.12) (Figure 27).

Next, it was examined whether the upregulation of certain protein expressions was only due to the loss of CTSs or if by any chance indirect effects may have been involved. Therefore SH-SY5Y WT and CTSBDL-deficient cells were seeded one day prior transfection. Cells were transfected with pcDNA3.1 empty vector and/or pCDNA3.1-CTSB, pCDNA3.1-CTSD, pCDNA3.1-CTSL or all three CTSBDL encoding plasmids for 48 h (3.2.2.3). Cells were harvested and analyzed by immunoblot analysis (Figure 28). First, the transfection of each plasmid encoding for the referring CTS was successful as for example SH-SY5Y CTSBDL-deficient cells transfected with only pcDNA3.1-CTSB clearly showed signals for CTSB at the correct sizes (pro-form: 41 kDa, single chain form: 29 kDa, mature form: 25 kDa (Ishidoh and Kominami 2002). This was also proven for CTSD and CTSL, respectively.

The detection of the mature form of CTSB, CTSD and CTSL also indicated the rescue of the activity of the respective CTSs within the re-transfected SH-SY5Y CTSBDL-deficient cells. Analysis of the lysosomal marker LAMP1 revealed only a mild trend towards decreased protein expression levels by 40.73% after re-transfection of CTSB, CTSD and CTSL to the SH-SY5Y CTSBDL-deficient cells but did not reach WT expression level. The transfection was also prolonged to 72 h or 7 days and double transfections were performed. None of these approaches resulted in a WT-like lysosomal phenotype in fluorescence microscopy either (data not shown). Further analysis revealed a significant reduction of the ~17 kDa N-terminal APP fragment by 66.09% in the SH-SY5Y CTSBDL KO cells transfected with CTSB, CTSD and CTSL. The expression of the accumulating C-terminal APP fragments (CTFs) could also be partially rescued. Neither a 48 h- nor 72 h-transfection led to WT-expression levels of the ~17 kDa N-terminal fragment nor of the CTFs of APP. The expression of the autophagosome marker LC3-II could also only partially be rescued as immunoblot quantification revealed a tendency towards decreased LC3-II levels after all three CTSs were re-transfected. These results confirmed, that a loss of CTSB, CTSD and CTSL in SH-SY5Y led to dysregulation of certain proteins that had been found by proteome analysis (Figure 25). Also, it revealed that re-transfecting the missing CTSs

to the SH-SY5Y CTSBDL KO cells restored their activity. Upregulation in LAMP1 and LC3-II is possibly only a side effect as the cells have to adapt to the cellular stress and undegraded material. Probably all three cathepsins are required to degrade the ~17 kDa N-terminal APP fragment.

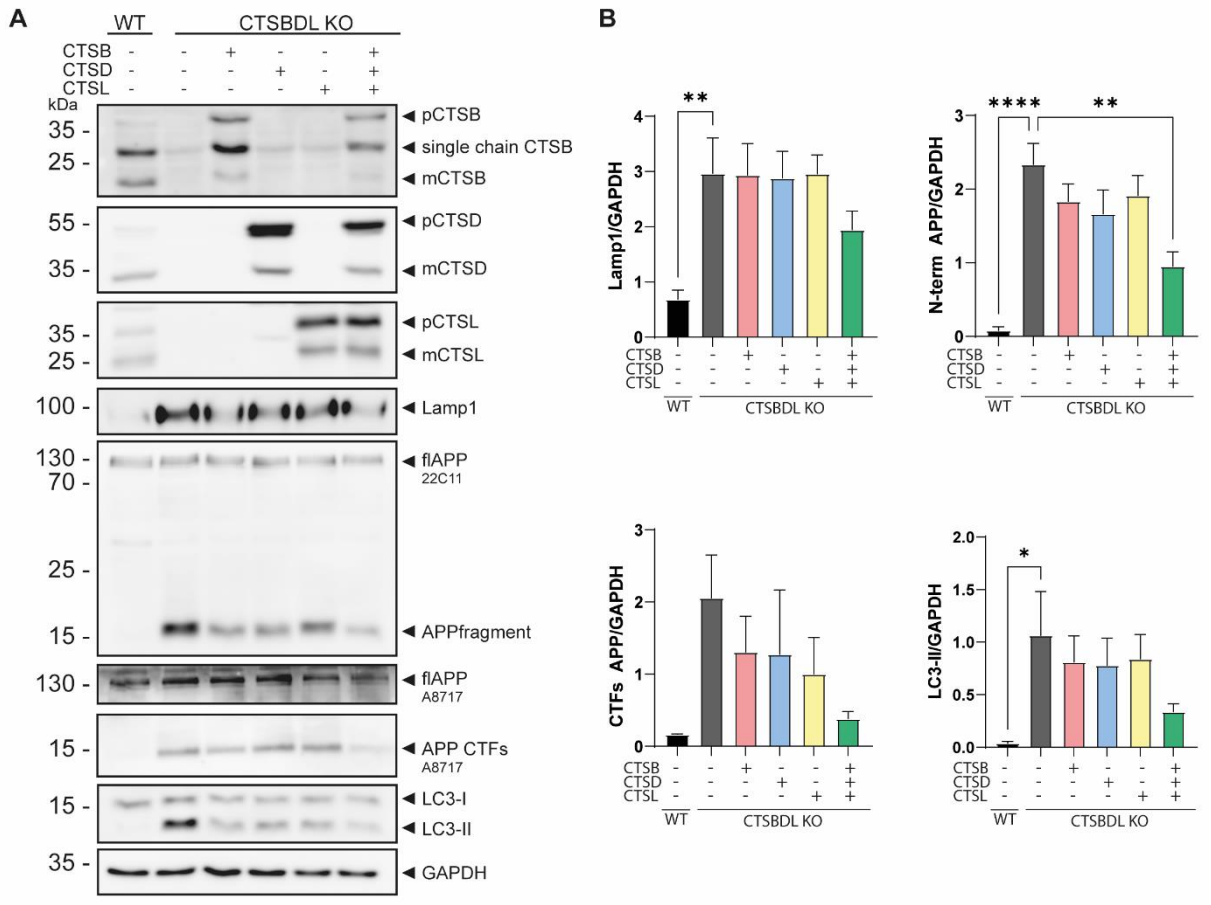


**Figure 28: The dysregulation of certain proteins in the SH-SY5Y CTSBDL-deficient cells can partially be rescued after re-transfection of CTSs. (A)** Respective immunoblot of SH-SY5Y WT and CTSBDL-deficient cells. Cells were transfected with pCDNA3.1-plasmids encoding for CTSB, CTSD, CTSL or empty vector as control for 48 h. Antibodies directed against CTSB, CTSD, CTSL, Lamp1, N-terminus of APP (22C11, Invitrogen), C-terminus of APP (A8717, Sigma-Aldrich) and LC3 were used and GAPDH served as loading control. **(B)** Quantitative analysis of 4-5 individual experiments. Protein levels were normalized to GAPDH. Data represent the mean + SEM, one-way ANOVA with a Bonferroni's multiple comparison test with SH-SY5Y CTSBDL transfected with empty vector (pcDNA3.1) as reference. * p<0.05; ** p<0.01; **** p>0.0001. kDa: kilodalton.

## 4.7 Amyloid-β, derived from the Amyloid Precursor Protein, is a known substrate of Cathepsin D

The Amyloid Precursor Protein (APP) is known to be relevant in Alzheimer's research as it is the precursor molecule for Amyloid-β (Aβ) which is accumulating and forming

amyloid plaques in Alzheimer's disease (AD) patients (Harmeier et al. 2009). Several proteases are able to proteolytically process APP by sequential cleavage (Delport and Hewer 2022). Among these, the major lysosomal hydrolase active within the brain - CTSD - has been of interest within the last years. CTSD has been connected to AD as there were lower activity of CTSD and lower Aβ1-42 levels found in AD patients (Papassotiropoulos et al. 2002; Suire et al. 2020). Therefore, CTSD was chosen to be further investigated to study its role in the APP and Aβ metabolism in different cellular and murine models.

CTSD was recently identified as the major intracellular Aβ-cleaving enzyme (Suire et al. 2020). This research seeks to examine whether boosting lysosomal proteolysis by adding recombinant human pro-CTSD (rhpro-CTSD) to the chosen model systems has a beneficial impact on reducing both intra- and extracellular levels of Aβ.

### 4.7.1 Recombinant human pro-CTSD gets self-activated under acidic pH conditions

Rhpro-CTSD does not exert any proteolytic activity until it is delivered to the acidic compartments by endocytosis. This feature makes it an attractive drug to use *in vitro* and *in vivo* as it only becomes enzymatically active within the correct organelle, e.g. the lysosomes. To activate rhpro-CTSD it was incubated in activity buffer at a lysosome-like pH containing the quenched CTSD-substrate (3.2.3.9).

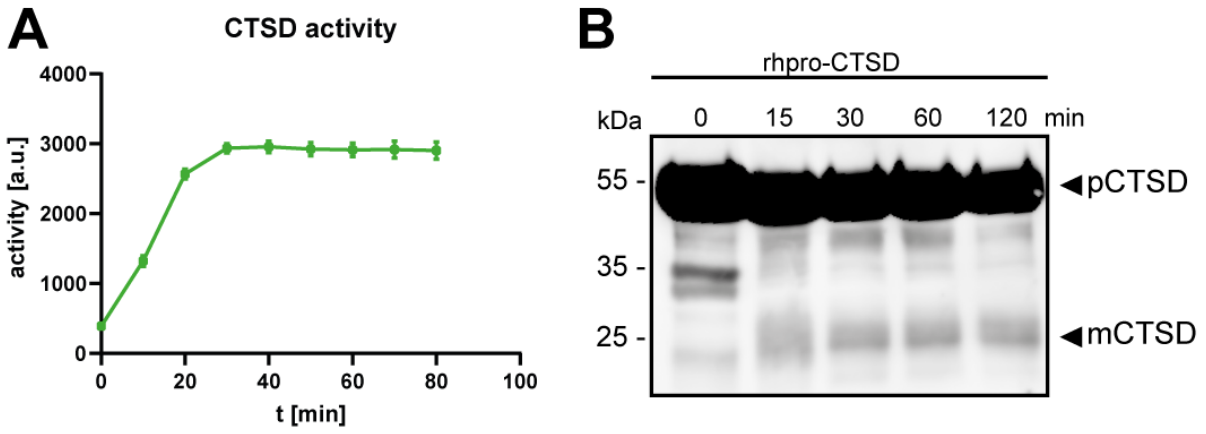


**Figure 29: Rhpro-CTSD gets self-activated at acidic pH. (A)** Activity assay of 0.2 µg/µl rhpro-CTSD incubated in activity buffer (50 mM sodium acetate (pH 5.5), 0.1 M NaCl, 1 mM EDTA, and 0.2% Triton X100; pH 4.5) containing 10 µM fluorogenic Cathepsin D & E substrate over 80 min at 37 °C. The fluorophore AMC (7-Amino-4-Methylcoumarin) is released upon proteolytic cleavage. Fluorescence was measured with a microtiter plate reader (exc: 360 nm; em: 440 nm) and activity is given in arbitrary units (a.u.). **(B)** 0.2 µg/µl rhpro-CTSD was incubated in activity buffer for 120 min at 37 °C. After time points 0, 15, 30, 60 and 120 min samples were boiled for 5 min at 95 °C with Laemmli buffer and analysed by immunoblot. The signal for the mature-form of CTSD (mCTSD) increases with time and is visible already after 15 min indicating its activation.

After CTSD cleaved the substrate the AMC (7-Amino-4-Methylcoumarin)-fluorescence at an excitation of 360 nm could be measured. The activation over time of rhpro-CTSD is presented in Figure 29A. The activity of CTSD increased over time and the maximal activity was reached after approximately 30 min and it was stable over all chosen time points. Additionally, 0.2 µg/µl rhpro-CTSD was incubated in activity buffer for 120 min at 37 °C. After time points of 0, 15, 30, 60 and 120 min samples were boiled in Laemmli buffer for 5 min at 95 °C and analyzed by immunoblot (Figure 29B). Both the activity assay and immunoblot analysis demonstrated that rhpro-CTSD got self-activated at lower pH after 10-15 min and the mature form was stable over time.

### 4.7.2 Human Aβ1-42 is a substrate of human CTSD

Having established the activation of rhpro-CTSD under acidic conditions, it was next attempted to analyze the cleavage sites of human CTSD in human Aβ1-42. To this end rhpro-CTSD was pre-activated in activity buffer at 37°C for a minimum of 30 min (3.2.3.10). Afterwards, 2 µg of pre-activated CTSD was incubated with 100 µM human Aβ1-42 for 15, 30 and 60 min including a PepA control to inhibit CTSD. Specific cleavage fragments were analyzed by liquid chromatography mass spectrometry (LC-MS) in collaboration with Dr. A. Tholey at the Institute of Experimental Medicine Kiel (Figure 30). LC-MS data revealed that Aβ1-42 is partly oxidized (Met35) at time point 0 min which is a common finding in methionine-containing peptides at elevated incubation times (Figure 30A). After 15 min of incubation of Aβ1-42 with pre-activated rhCTSD, five abundant Aβ fragments were identified (Figure 30; Figure 52 in appendix). These fragments were also abundant after 30 and 60 min but in different prevalence. Hydrolysis at Phe19 led to two peptides with masses of 2314.50 Da (average mass) and 2217.61 Da, representing C- and N-terminal cleavage products. The C-terminal product was further proteolytically cleaved at Leu34. The N-terminal fragment was additionally cleaved after Leu17 and Phe20. The control samples co-incubated with PepA revealed no cleavage products after 60 min proving the specifity of CTSD-cleavage and no unspecific degradation of the Aβ1-42 due to used conditions. In summary, these results prove that human Aβ1-42 is a substrate of human CTSD under the chosen *in vitro* conditions.

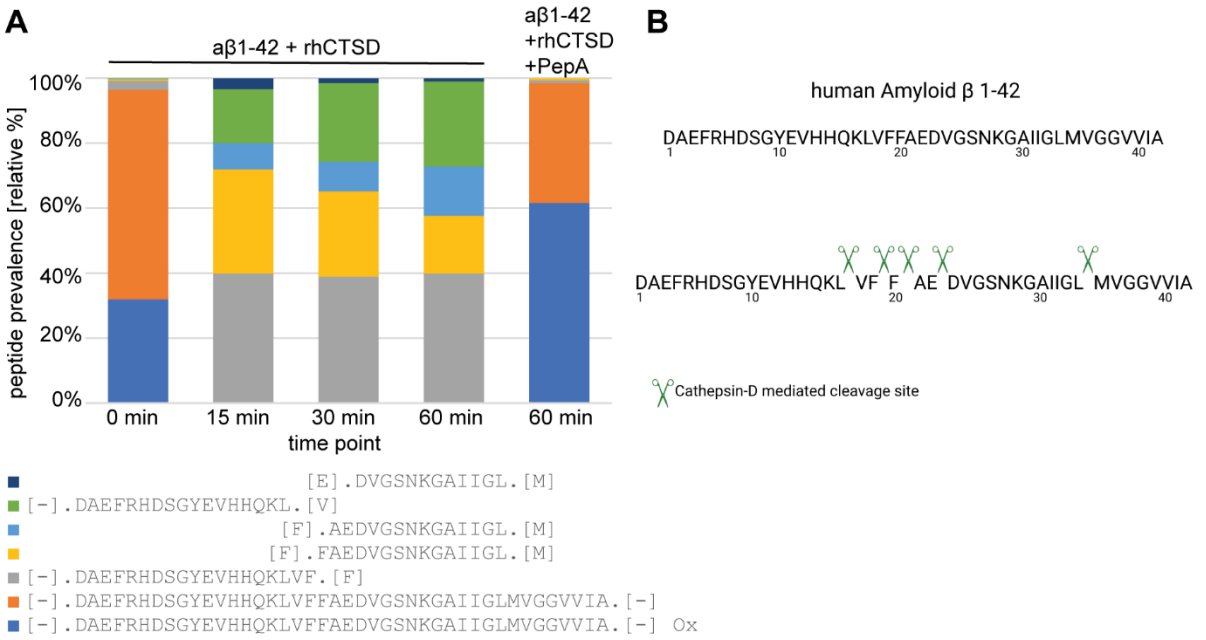


**Figure 30: *In vitro* digestion of human Aβ1-42 by rhCTSD. (A)** Most abundant peptides identified following enzymatic digestion of Aβ1-42 after 0 min (control), 15 min, 30 min, or 60 min, or protease treatment plus the addition of pepstatin A (PepA, 60 min. incubation) by mass spectrometry. Peptides detected with more than 9 peptide spectral matches (PSM) are shown, peptide prevalence was plotted as a percentage of the total PSM counts for each time point/treatment. Ox: oxidized. Analyzed by *A.Tholey* at the Institute of Experimental Medicine Kiel. **(B)** Determined cleavage sites of rhCTSD within human Aβ1-42.

## 4.8 Intracranial dosing of rhpro-CTSD in a CLN10 mouse model does not affect the expression of mouse Aβ species

Lately, Marques et al. and Prieto Huarcaya and Drobny et al. demonstrated the promising effects of a novel type of enzyme-replacement therapy (ERT) in Neuronal Ceroid Lipofuscinosis-10 (CLN-10) mice. The therapy improved the autophagic flux, reduced neuroinflammation and accumulated storage material like saposins or α-synuclein typically found in CLN-10 and Parkinson's disease (Marques et al. 2020; Prieto Huarcaya et al. 2022). By proving that pre-activated rhpro-CTSD is able to proteolytically process human Aβ1-42 *in vitro,* the next question to be answered was if rhpro-CTSD also has an impact on APP and Aβ peptide metabolism *in vivo*. Therefore, the CLN-10 mouse model which is characterized by a CTSD-deficiency was chosen for the next analyses. CLN-10 mice are referred to as CTSD KO mice.

### 4.8.1 After intracranial injection rhpro-CTSD is endocytosed and activated in neurons and microglia of CTSD-deficient mice

A schematic overview of the used intracranial injection method and the schedule of dosing of rhpro-CTSD to CTSD KO mice is presented in Figure 31A. Mice were intracerebroventricular (ICV) injected with 0.1 mg rhpro-CTSD at postnatal day 1 (P1) into the left hemisphere and at P20 into the right hemisphere (3.2.5.3). Mice were transcardially perfused (3.2.5.6) with 0.1 M PB at P22 and samples were collected and processed. The body weight gain of P19 to P22 injected mice was determined (Figure 31B). While WT mice do gain weight over time, CTSD KO mice treated with PBS do not. Injecting rhpro-CTSD to the CTSD KO mice led to a positive increase in weight gain as seen in WT mice indicating a beneficial effect of rhpro-CTSD on the overall condition in rhpro-CTSD-dosed mice.

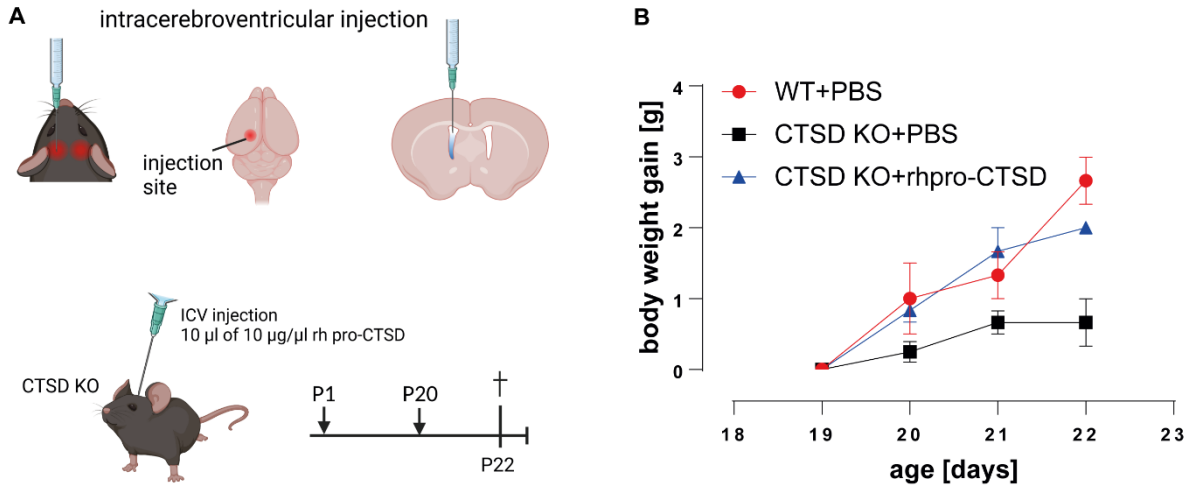


**Figure 31: Principal of intracerebroventricular injections of rhpro-CTSD and beneficial effects on body weight gain in CTSD KO mice. (A)** Intracerebroventricular (ICV) injection sites of rhpro-CTSD in mice and injection schedule for the CTSD KO mice. **(B)** Body weight gain in grams (g) from day 19 to 22 of WT and CTSD KO mice injected with PBS and CTSD KO injected with 0.1 mg rhpro-CTSD at P1 and P20.

Next, immunostainings and immunoblots were prepared to visualize and identify the cells that took up and maturated rhpro-CTSD after ICV injections. For immunostainings, CTSD KO mice were transcardially perfused with 0.1 M PB and one hemisphere was fixed in 4% PFA for at least for 4 h (3.2.4.3). Brains were sagittally cut into 35 µm sections and stained for the neuronal marker Map2 (microtubule-associated protein 2), the microglial marker Iba-1 (ionized calcium-binding adapter molecule 1) and CTSD (3.2.4.4). Figure 32A depicts immunostainings of the cortex of P22 CTSD KO mice injected with 0.1 mg rhpro-CTSD at P1 and P20. Both, neurons (Map2-

positive cells, green) and microglia (Iba1-positive cells, red) were able to take up rhpro-CTSD (CTSD, white). Overall, the rhpro-CTSD was visible in the entire CTSD KO mouse cortex demonstrating efficient uptake in the mouse brain.

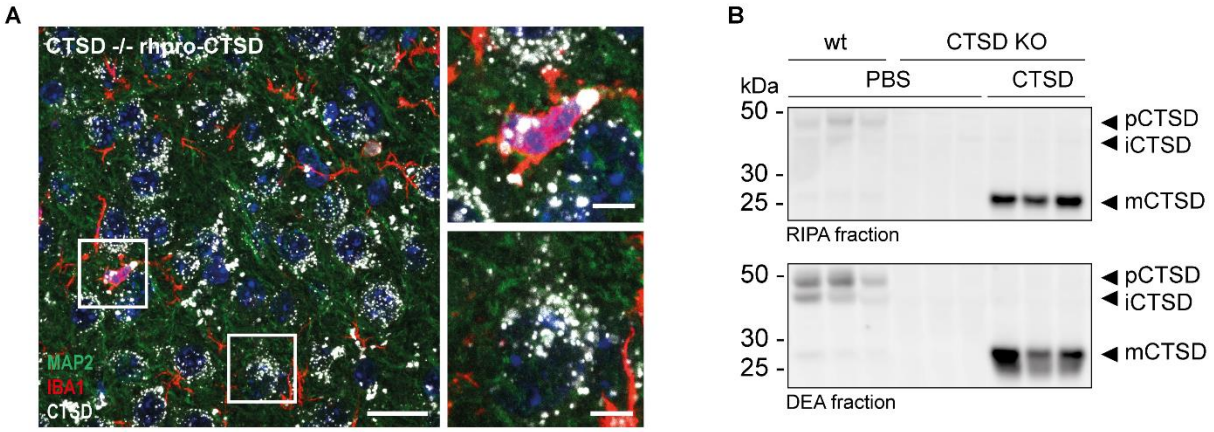


**Figure 32: Rhpro-CTSD ICV-injected to CTSD KO mice is taken up and matured by neurons and microglia. (A)** Immunohistochemistry of the cortex of P22 CTSD-deficient mice injected with 0.1 mg rhpro-CTSD at P1 and P20 was stained for the neuronal marker MAP2, the microglia marker Iba1 and CTSD. Nuclei are stained with DAPI. Scale bar: large image: 20 µm, inserts: 5 µm. Picture taken by *Dr. A. Di Spiezio*. **(B)** Immunoblot of RIPA and DEA lysates derived from P22 CTSD KO mice injected with 0.1 mg rhpro-CTSD at P1 and P20. A well-established CTSD antibody was used to detect CTSD (pro-form: pCTSD, intermediate single chain form: iCTSD, mature form: mCTSD). kDa: kilodalton

To further analyze the brain tissue in regards of the processing of rhpro-CTSD one hemisphere was snap frozen in liquid nitrogen after perfusion of the mice with 0.1 M PB (3.2.5.6). RIPA and DEA fractions were prepared as described in 3.2.3.2. Rhpro-CTSD maturation was analyzed by immunoblot (Figure 32B). WT mice expressed pro-CTSD and mature-CTSD (mCTSD) as seen in the DEA fraction. CTSD KO mice injected with PBS did not express CTSD in any form confirming the genotype of the mice. After ICV-injections of 0.1 mg rhpro-CTSD at P1 and P20 both RIPA and DEA lysate analysis revealed uptake and processing to the mature form of CTSD as only the mCTSD (34 kDa) was detectable. These findings indicate a fast processing of the rhpro-CTSD as no pro-form of CTSD was detectable in the CTSD KO mice treated with rhpro-CTSD. In summary, CTSD KO mice ICV-injected with rhpro-CTSD take up the enzyme into neurons and microglia where it is maturated to its proteolytically active form.

### 4.8.2 Intracranial dosing of CTSD-deficient mice with rhpro-CTSD does not alter their APP and Aβ metabolites

Having provided information that neurons and microglia are able to take up and process rhpro-CTSD into its mature active form, the next step was to analyze the APP

and Aβ metabolism in mice after intracranial application of the pro enzyme. Therefore, DEA and RIPA lysates of brain tissue derived from P22 WT and CTSD-deficient mice injected with either PBS or 0.1 mg rhpro-CTSD at P1 and P20 were prepared and analyzed by immunoblot (Figure 33).

Quantitative and statistical analysis of the full-length APP did not reveal any differences between the WT and the CTSD-deficient mice. There seemed to be a slight increase in both APP C-terminal fragments (CTFs) APP-C83 (predicted size: ~10 kDa, (uniprot.org, human APP: P05067, ID: PRO_0000000094) and APP-C99 (predicted size: ~11 kDa, (uniprot.org, human APP: P05067, ID: PRO_0000000091) by ~30 % in the CTSD-deficient mice. However, these findings were not statistically significant. Re-addition of CTSD led to a trend towards decreased full-length APP (predicted size ~90 kDa, uniprot.org, ID: P05067-1) levels by ~30 % and a significant decrease in the APP-C83 fragment by ~40 % indicating degradation and lysosomal turnover by CTSD. However, there was no effect on the APP-C99 fragment. A CTSD-deficiency in mice led towards lower levels of both soluble APP fragments sAPPα (~76 kDa, uniprot.org, human APP: P05067, ID: PRO_0000000089) and sAPPβ (~75 kDa, uniprot.org, human APP: P05067, ID: PRO_0000000090) by ~30 % each. However, these findings were not statistically significant. Treatment with rhpro-CTSD did not have any effect on sAPPα levels but showed a trend towards sAPPβ expression levels comparable to the levels found in WT mice. Endogenously expressed Aβ of P22 WT and CTSD-deficient mice in both RIPA and DEA samples was not detectable by immunoblot analysis (Figure 26). Therefore, ELISA and MSD analysis, an electrochemiluminescence-based ultra-sensitive assay to detect Aβ species (3.2.3.6; 3.2.3.7), was performed to detect endogenous levels of Aβ1-34, Aβ1-38, Aβ1-40 and Aβ1-42 (Figure 34).

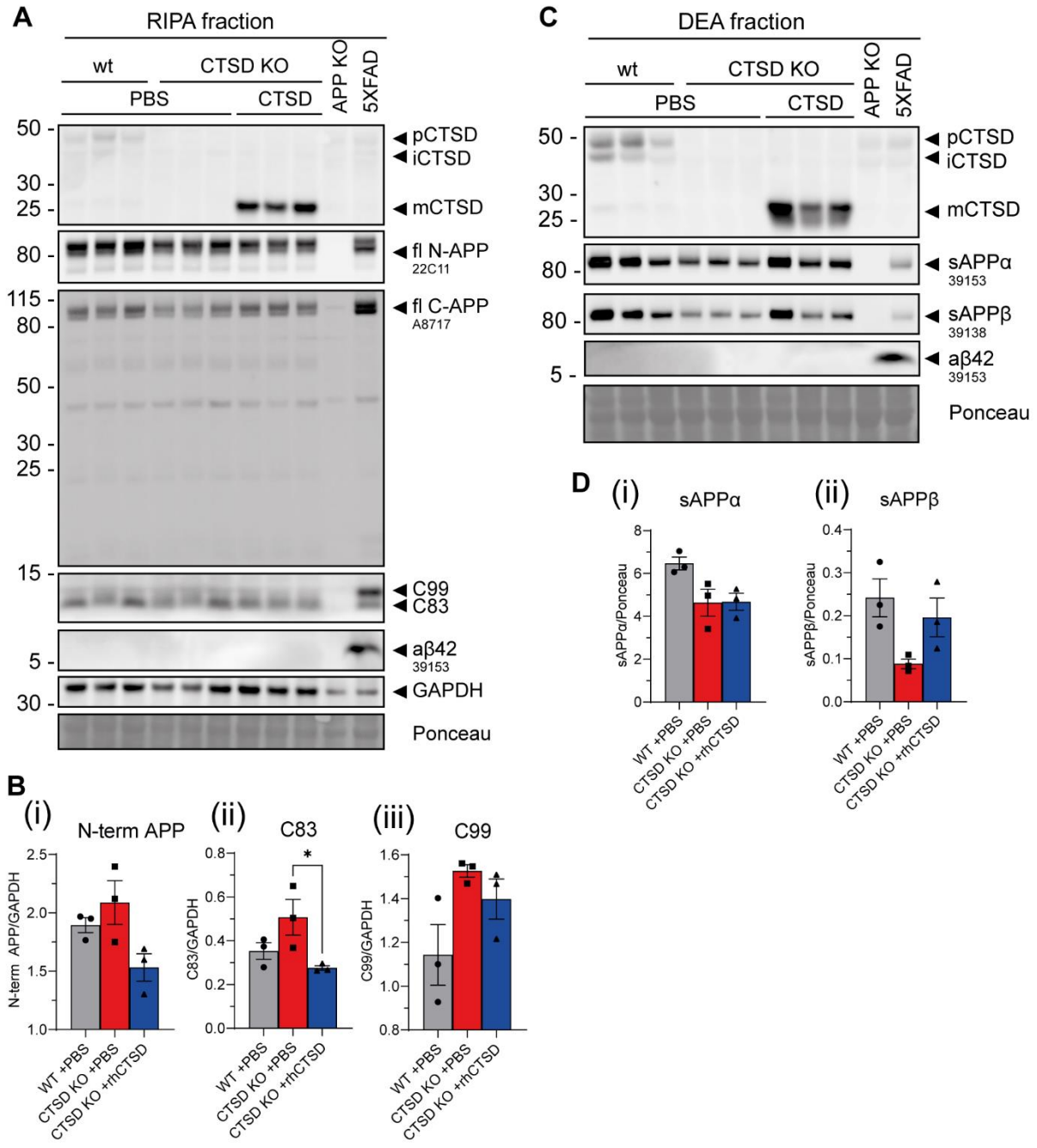


**Figure 33: Rhpro-CTSD treatment of CTSD KO mice does not alter their APP metabolism.** **(A)** Immunoblot of RIPA brain lysates of P22 WT mice treated with PBS and CTSD-deficient mice injected with either PBS or 0.1 mg rhpro-CSTD. Antibodies directed against CTSD, the N-terminus of APP (22C11, Thermo Fisher Scientific), the C-terminus of APP (A8717, Sigma-Aldrich), Aβ1-42 (39153-50, Covance) and GAPDH were used. Brain lysates derived from APP KO and 5xFAD served as antibody controls. **(B)** Quantifications of (i) full-length APP (N-terminal APP antibody) and C-terminal fragments of APP (ii) C83 and (iii) C99. GAPDH was used as reference loading control (n = 3). **(C)** Immunoblot of DEA brain samples of P22 WT mice injected with PBS or 0.1 mg rhpro-CTSD. Antibodies directed against epitopes of CTSD, sAPPα and Aβ1–42 (39153-50, Covance), sAPPβ (39138, Covance) and GAPDH were used. Brain lysates derived from APP KO and 5xFAD served as antibody controls. **(D)** Quantification of (i) sAPPα and (ii) sAPPβ normalized to Ponceau S staining (n = 3). Data represent mean ± SEM. Statistical analysis was performed by using one-way ANOVA with a Tukey's multiple comparison test. * $p < 0.05$.

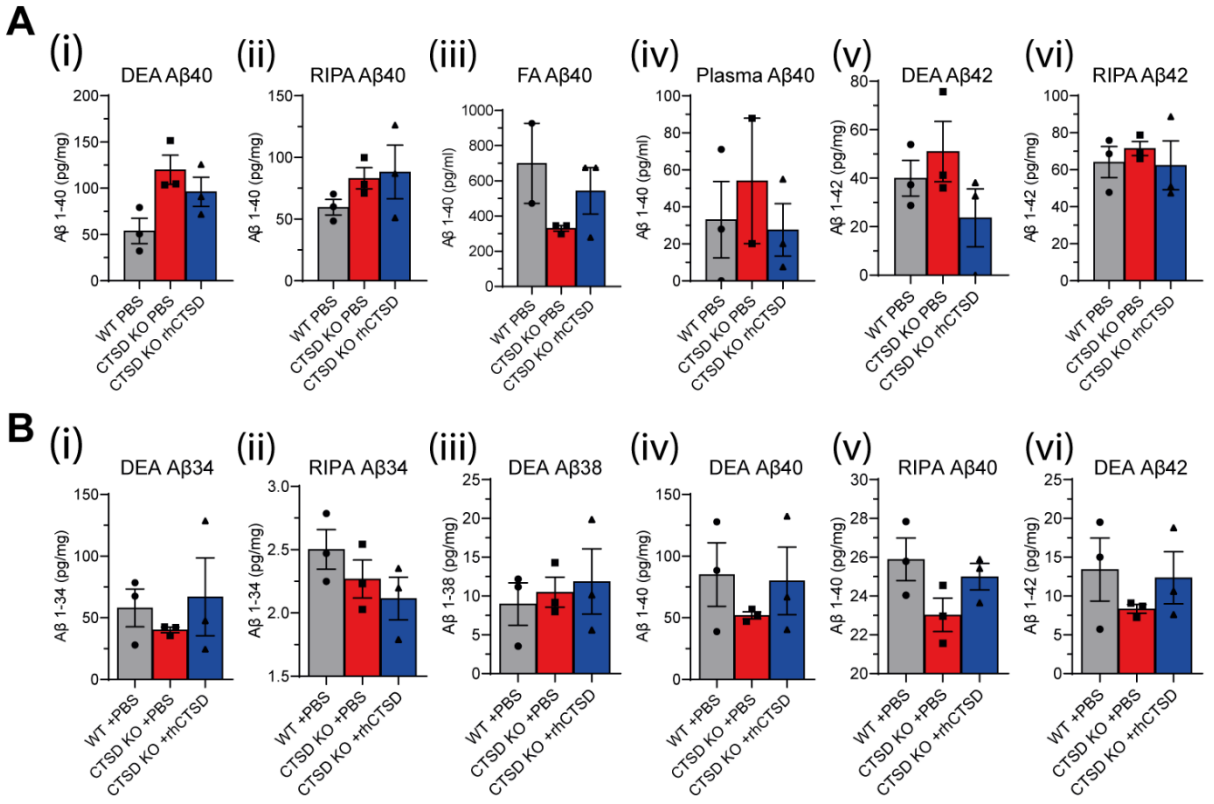


**Figure 34: Aβ species in CTSD-deficient mice treated with rhpro-CTSD are not altered. (A)** Aβ1-40 and Aβ1-42 in pg/mg analyzed by ELISA of DEA, RIPA and FA brain samples and plasma from P22 WT mice injected with PBS and CTSD-deficient mice with PBS or 0.1 mg rhpro-CTSD (n = 3). **(B)** Meso Scale Discovery (MSD) analysis of Aβ1-34, Aβ1-38, Aβ1-40 and Aβ1-42 levels of DEA and RIPA samples derived from brains of P22 WT mice injected with PBS and CTSD-deficient mice with PBS or 0.1 mg rhpro-CTSD (n = 3). MSD data was measured and analyzed by *I. Ulku* (McGill University, Montreal). Data represent mean ± SEM.

A CTSD-deficiency in mice did not lead to significant changes in all detected and analyzed Aβ species. There were also no changes upon rhpro-CTSD treatment detectable in these brain lysates indicating that CTSD did not alter the Aβ metabolism in P22 mice. It is of note that not all Aβ species were detectable in all samples. There was no Aβ1-42 detectable in the FA and plasma samples by ELISA. Aβ1-38 and Aβ1-42 was not detectable in RIPA lysates analyzed by MSD suggesting that P22 mice did not have any insoluble Aβ1-42 accumulates or the half-life within plasma samples is too short and that the age of 22 days is too young to study Aβ metabolites in these mouse models.

Taken together, the results from immunostainings propose that intracranially injected rhpro-CTSD to CTSD-deficient mice is endocytosed by microglia and neurons. Immunoblots revealed that rhpro-CTSD became maturated and activated within these cell types. ELISA and MSD analysis showed that rhpro-CTSD did not have an effect

on investigated Aβ species. In summary, a CTSD-deficiency in mice does not lead to significant changes in the APP and Aβ metabolism and a treatment by intracranial application of rhpro-CTSD could not reveal any beneficial changes.

## 4.9 Inhibition of CTSD in HEK APP overexpressing cells leads to an increase of intracellular Aβ1-42

As AD develops and progresses with age, analysis of CTSD-deficient mice is not sufficient to follow up the changes in the APP metabolism and Aβ accumulation as these mice die at young age and do not develop typical AD-related pathology (Saftig et al. 1995; Koike 2000). Therefore, human embryonic kidney (HEK) cells with overexpression of human APP (hAPP) or the Swedish mutant APP (APPswe; harboring a mutation in the cleavage site of APP (KM>NL) for higher affinity of BACE1 resulting in higher sAPPβ and Aβ levels) were chosen to further investigate the effects of additional CTSD activity on human APP and Aβ.

### 4.9.1 Rhpro-CTSD becomes activated within HEK cells

The intracranial injection of rhpro-CTSD in CTSD-deficient mice revealed endocytosis and maturation of CTSD in neurons and microglia (Figure 32). To also prove the uptake by endocytosis in HEK APPswe cells, cells were incubated with 20 µg/ml rhpro-CTSD in presence or absence Pep A for 48 h (3.1.3). CTSD-activity within the cell lysates and the respective supplemented supernatant was analyzed by an activity assay over 90 min (3.2.3.9) and is presented in Figure 35. In APPswe control cell lysates (black line) endogenous CTSD activity could be revealed. An increase in the fluorogenic signal derived from the cleaved fluorogenic CTSD substrate over time was observed. The maximum activity was not yet reached after 90 min. After incubating cells with 20 µg/ml rhpro-CTSD (dark green line) for 48 h the enzymatic activity rose faster indicating a higher enzymatic activity of CTSD compared to the untreated control cells. This activity was almost comparable to the activity measured in the pre-activated rhpro-CTSD control (light green line) and indicates endocytosis and delivery to the lysosomes of the rhpro-CTSD where it gets correctly processed and activated due to the acidic lysosomal pH. PepA application (red line) caused an inhibition of the enzymatic activity (dark blue line). As expected, the negative control sample where pre-activated rhpro-

CTSD was incubated with PepA (light blue line) did also not show enzymatic activity. Both endogenous and boosted CTSD activity was inhibited by PepA in HEK APPswe cells (Figure 35 A). To exclude whether rhpro-CTSD added to the supernatant could get self-activated or the endocytosed and activated CTSD might be exocytosed into the supernatant, the CTSD activity assay was also performed with the supernatant of the rhpro-CTSD-treated HEK APPswe cells (Figure 35 B). The activity assay revealed that only the HEK APPswe cells treated with rhpro-CTSD for 48 h exerted an increase of the enzymatic activity of CTSD over time. This proved that rhpro-CTSD was not exocytosed by the cells but was only activated due to the lysosomal pH 4.5 of the activity buffer. It also confirmed that enough rhpro-CTSD remained within the supernatant after 48 h and that there was no limitation of extracellularly given enzyme in this set up. Taken together, HEK APPswe cells are able to endocytose, maturate and activate extracellularly dosed rhpro-CTSD.

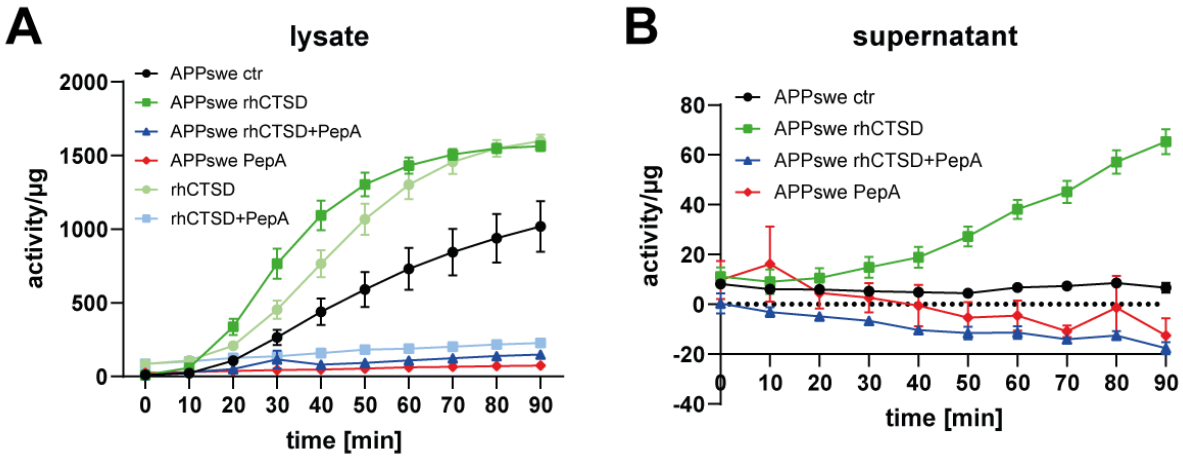


**Figure 35: CTSD activity assay of HEK APPswe cell lysates and supernatant. (A)** CTSD activity in activity/µg assayed with the fluorogenic CTSD substrate Mca-GKPILFRLK-Dnp in HEK APPswe cell lysates and **(B)** the respective supernatant over a time period of 90 min. Pre-activated rhpro-CTSD was used as positive control and the aspartate protease inhibitor pepstatin A (Pep A) was used as negative control. Data are represented as mean ± SEM.

### 4.9.2 Inhibition of CTSD in HEK APPswe cells increases intracellular Aβ1-42

After having shown that dosed rhpro-CTSD is endocytosed and activated within HEK APPswe cells, the next aim was to investigate its effect on APP and Aβ metabolism *in vitro*. HEK WT, hAPP and APPswe cells were incubated with 20 µg/ml rhproCTSD with or without PepA for 48 h and collected together with their corresponding supernatants (3.2.3.1) and analyzed by immunoblot (3.2.3.4; 3.2.3.5).

Figure 36 shows a representative immunoblot and the quantification of 7 conducted experiments. As indicated by the results of the CTSD activity assay (Figure 35) the extracellularly provided rhpro-CTSD (54 kDa) was taken up and processed into its mature active form (m-CTSD, 34 kDa) by HEK WT, hAPP and APPswe cells. HEK APPswe cells showed the highest expression of full-length APP and higher amounts of the APP CTFs C83 and C99. These cells were used to quantify the APP fragments and Aβ species.

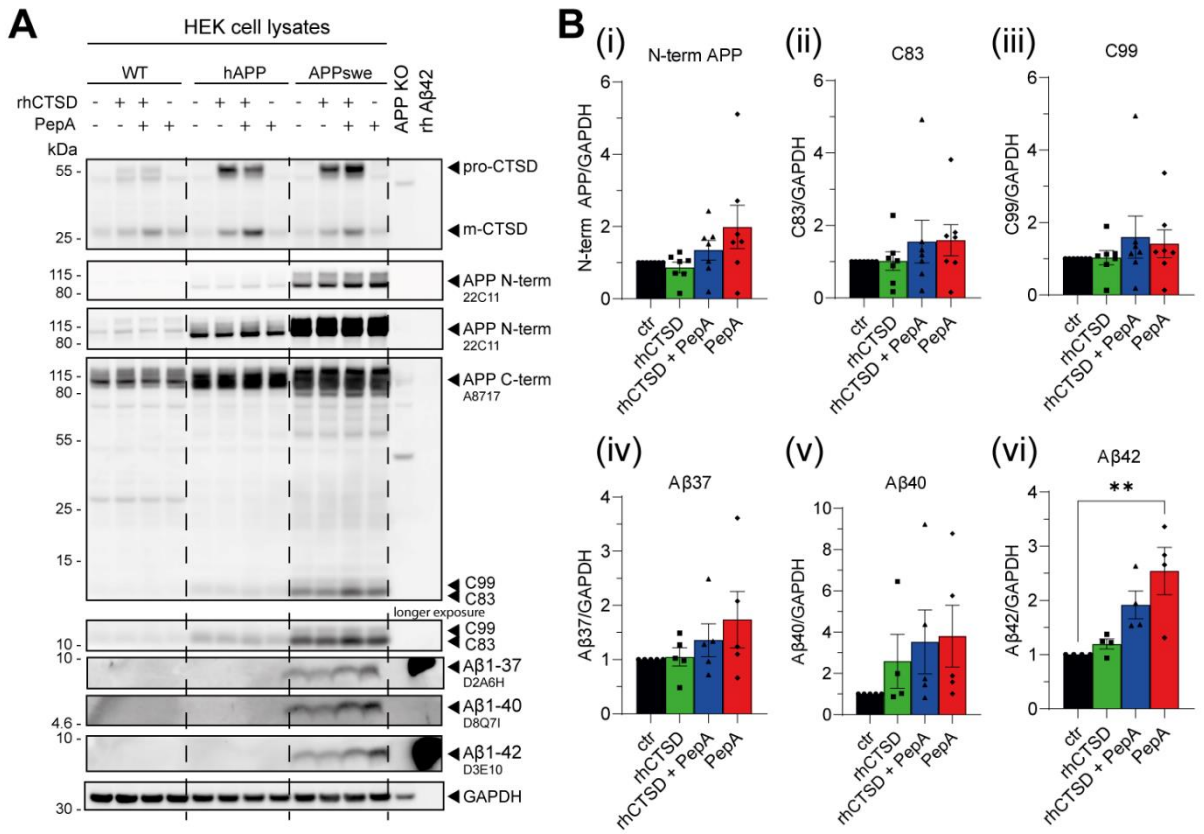


**Figure 36: Inhibition of CTSD increases intracellular Aβ1-42 in HEK APPswe cells. (A)** Immunoblot of cell lysates of HEK WT, hAPP and APPswe cells treated with 20 µg/ml rhpro-CTSD in presence or absence of 10 µg/ml Pepstatin A (PepA). Brain lysates derived from APP KO mice (provided by Ulrike Müller, University of Heidelberg) and recombinant human Aβ1-42 protein served as antibody controls. Antibodies directed against CTSD, the N-terminus of APP (22C11, Thermo Fisher Scientific), the C-terminus of APP (A8717, Sigma-Aldrich), Aβ1-37, Aβ1-40 and Aβ1-42 (β-amyloid sample kit, 85314, Cell Signaling) and GAPDH were used. **(B)** Quantifications of full-length APP (N-terminal antibody), APP CTFs C83 and C99 and Aβ fragments of cell lysates shown in (A). GAPDH served as loading control with control cells sat as one (n = 4–7). Data represent mean ± SEM. Statistical analysis was performed by using one-way ANOVA with a Tukey's multiple comparison test. ** $p < 0.01$.

Overall, full-length APP, APP CTFs C83 and C99 were not altered by treatment with rhpro-CTSD regardless of treatment with PepA. The quantification of Aβ1-37 (predicted size: 4.0 kDa, (Wiltfang et al. 2001)) and Aβ1-40 (predicted size: 4.3 kDa, (Wiltfang et al. 2001)) shows a trend towards increased levels after inhibition of CTSD with PepA. PepA treatment significantly increased Aβ1-42 levels (predicted size:

4.5 kDa, (Wiltfang et al. 2001)). Inhibition of CTSD led to increased Aβ1-42 levels by 1.92-2.54-fold (rhpro-CTSD + PepA vs PepA) compared to WT levels. These data indicate that an increased CTSD activity does not alter APP or Aβ metabolism in HEK APPswe cells. The effect of PepA on HEK APPswe cells also suggests that there might be another aspartate protease involved in generation of Aβ1-42 as CTSD alone does not have an effect on APP.

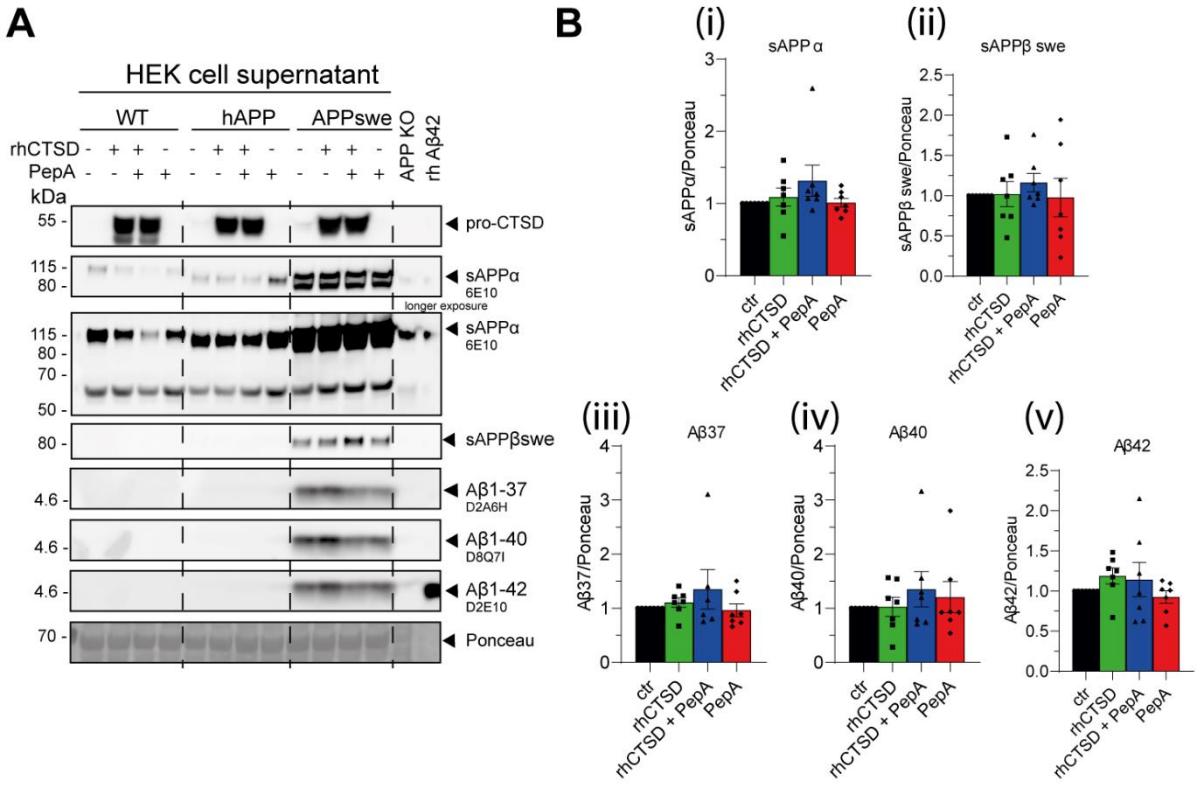


**Figure 37: Rhpro-CTSD application to cells has no effect on soluble APP fragments. (A)** Respective immunoblot of supernatant collected from cells shown in (Figure 36). Antibodies directed against CTSD, sAPPα (6E10, biolegend), sAPPβswe and Aβ1-37, Aβ1-40 and Aβ1-42 (β-amyloid sample kit, 85314, Cell Signaling) were used. Ponceau S staining was used to verify equal loading amounts. **(B)** Quantifications of samples from (A) with control cells set as one (n = 6–7). Ponceau S staining served as a loading control. Data represent mean ± SEM.

In addition, soluble APP fragments of HEK APPswe cells treated with rhpro-CTSD and PepA were analyzed (Figure 37). Soluble APP fragments were released into the supernatant which was collected from the cells after 48 h, spun down and investigated by immunoblot (3.2.3.4; 3.2.3.5). As the CTSD activity assay (Figure 35 B) revealed there was no auto-activated or exocytosed CTSD present in the rhpro-CTSD-supplemented supernatant. The soluble APP fragments sAPPα and sAPPβswe as well as Aβ1-37, Aβ1-40 and Aβ1-42 were released into the supernatant however, did not show statistically relevant differences compared to untreated cells. This indicates that there is no effect of rhCTSD on the soluble fragments of APP in HEK APPswe cells.

In summary, HEK WT, hAPP and APPswe cells are able to endocytose rhpro-CTSD where it is maturated and activated. An addition of CTSD does not have a relevant effect on the APP and Aβ metabolism in HEK APPswe cells. However, inhibition of CTSD (and other aspartate-proteases) by PepA increases the intracellular Aβ1-42 production within the cells.

## 4.10 Analysis of rhpro-CTSD uptake and Aβ clearance in an Alzheimer's disease mouse model

*In vitro* experiments with rhpro-CTSD and recombinant human Aβ (Figure 30) have shown the principle ability of CTSD to cleave Aβ1-42. These findings have not yet been studied in an approved mouse model as CTSD-KO mice do not exert AD-related pathologies. Analyzing APP and Aβ metabolites in HEK APPswe cells treated with rhpro-CTSD revealed no direct effect of CTSD applied to the cells. Interestingly, inhibition of CTSD led to an accumulation of Aβ1-42 within the cells (Figure 36) indicating and supporting the *in vitro* data that CTSD (Figure 30) may be involved in the degradation pathway of this plaque-prone Aβ fragment.

To better analyze the effects of rhpro-CTSD *in vivo*, 5xFAD mice expressing human APP mutations (Swedish: K670N/M671L, Florida: I716V, and London: V717I) and presenilin transgenes (M146L and L286V) were chosen as a suitable model to study AD-related pathologies (Oakley et al. 2006). These mutations are under the control of the *Thy1* promoter which has an estrogen response element (Sadleir et al. 2015). This feature explains the sex differences with females developing AD-related pathologies earlier than male mice. Therefore, only female 5xFAD mice were analyzed during this present study. 5xFAD mice develop Aβ plaques in the brain from 2-4 months of age followed by neuroinflammation and microgliosis (Forner et al. 2021).

### 4.10.1 Aβ1-42 accumulation in brains of two-months old 5xFAD mice

To investigate the time-point of Aβ formation and accumulation, DEA and RIPA lysates derived from WT, 5xFAD and APP KO mouse brains were prepared (3.2.3.2) and analyzed by immunoblot (Figure 38). 5xFAD mice had accumulated levels of the APP CTFs C83 and C99 compared to WT mice confirming a genetic-driven dysregulation of the amyloidogenic pathway resulting in soluble Aβ formation starting already at two

months of age (DEA samples). After three months the Aβ formation became more prominent as both DEA and RIPA lysates showed high expression of Aβ. Expression levels of soluble fragments like sAPPα and sAPPβ or even the full-length APP (N-APP) did not seem to be affected by the five AD-related mutations in the 5xFAD mice. Therefore, the time-points of one, two and three months of age were chosen to investigate any effect of intracranially injected rhpro-CTSD.

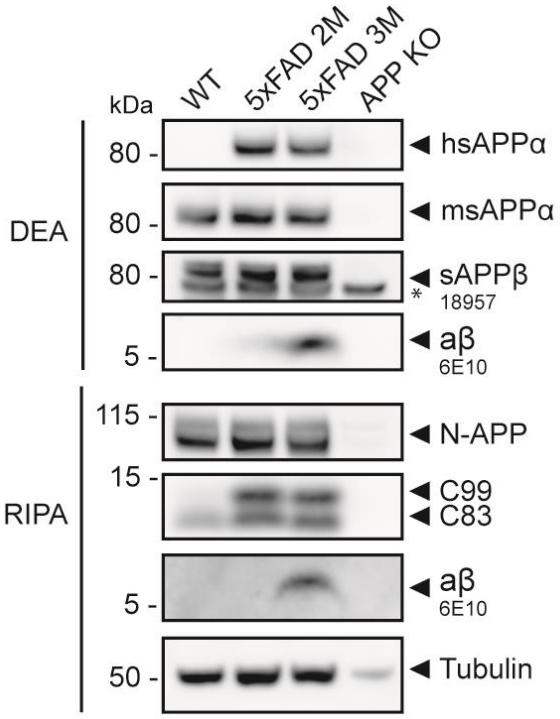


**Figure 38: Analyzing APP and Aβ in 5xFAD mice of different ages.** Immunoblot of DEA and RIPA brain lysates derived from of WT, two- and three-month-old (2M, 3M) 5xFAD and APP KO mice (samples provided by Ulrike Müller, University of Heidelberg). Antibodies directed against human and mouse soluble APPα (hsAPPα: 6E10, biolegend; msAPPα: 39153-50, Covance), sAPP (18957, IBL), the N-terminus of APP (22C11, Thermo Fisher Scientific), the C-terminus of APP (A8717, Sigma-Aldrich) and Aβ (6E10, biolegend) were used. Tubulin served as internal loading control.

As early dosing of CTSD KO mice with rhpro-CTSD at P1 and P20 showed longer-lasting activity after CTSD treatment for >31 days (Marques et al. 2020), the 5xFAD were also dosed with rhpro-CTSD at P1 and P20. Analysis was done at one, two and three months of age (Figure 39).

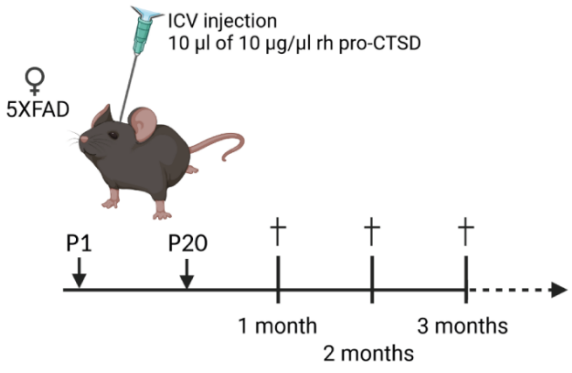


**Figure 39: Injection schedule for 5xFAD mice with rhpro-CTSD.** 5xFAD mice were intracerebroventricular (ICV) injected at P1 and P20 with 0.1 mg/ml rhpro-CTSD and sacrificed for analysis after one, two and three months of age.

### 4.10.2 Effect of intracranial rhpro-CTSD application on the APP and Aβ metabolism in one-month old 5xFAD mice

First, mice of one month of age were analyzed. Figure 40 shows the immunoblot and the quantitative analysis of WT mice injected with PBS and 5xFAD mice either injected with PBS or 0.1 mg/ml rhpro-CTSD at P1 and P20. The immunoblot reveals the uptake and maturation of the rhpro-CTSD in 5xFAD mice demonstrating a successful delivery and activation of the enzyme (Figure 32). Investigations on APP CTFs and soluble fragments did not reveal any changes or benefits upon rhpro-CTSD treatment in the one-month old 5xFAD mice. There was an upregulation of Aβ in the 5xFAD (Figure 40) compared to WT mice. However, rhpro-CTSD treatment did not alter the expression levels of Aβ, indicating no direct effect of CTSD on Aβ. Formic acid (FA) fractions which supposed to contain insoluble proteins and plaque-like structures, were also analyzed. However, no Aβ could be found indicating that there are no insoluble Aβ species or plaques in the one-month old 5xFAD mice.

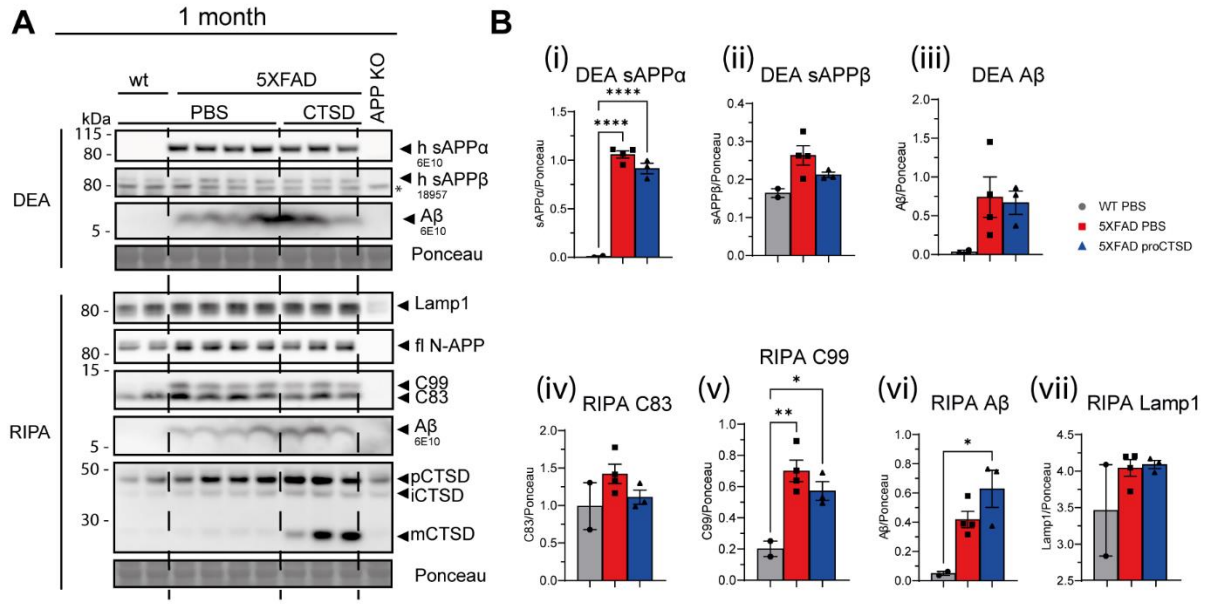


**Figure 40: ICV injection of rhpro-CTSD of 5xFAD mice does not alter APP or Aβ metabolites after one month. (A)** Immunoblot of DEA and RIPA protein fractions from brain hemispheres of one-month-old female WT and 5xFAD mice ICV injected with either PBS or 0.1 mg rhpro-CTSD at P1 and P20. Antibodies detecting CTSD, LAMP1, human sAPPα (hsAPPα: 6E10), sAPPβ (18957, IBL), the N-terminus of APP (22C11, Thermo Fisher Scientific), the C-terminus of APP (A8717, Sigma-Aldrich) and Aβ (6E10, biolegend) were used. Brain lysate of an APP KO mice was used as antibody control for APP antibodies. Ponceau S staining served as a loading control. **(B)** Quantitative analysis of one-month-old female 5xFAD shown in (A) (n = 2–4). Data represent mean ± SEM. Statistical analysis was performed by using one-way ANOVA with a Tukey's multiple comparison test. **** $p < 0{,}001$, ** $p < 0.01$, * $p < 0.05$.

ELISA analysis was performed to investigate the levels of Aβ1-40 and Aβ1-42 in DEA, RIPA, FA and CSF samples (Figure 41, 3.2.3.6). Neither DEA, RIPA nor FA samples revealed any effects upon rhpro-CTSD treatment of the 5xFAD mice. In CSF samples there was a trend detectable indicating increased Aβ1-40 levels and a significant upregulation of Aβ1-42.

In summary, in one-month old 5xFAD the rhpro-CTSD-dosing did not have any obvious effects on the APP and Aβ metabolism. Noteworthy, there seems to be a rather increased release of Aβ into the CSF.

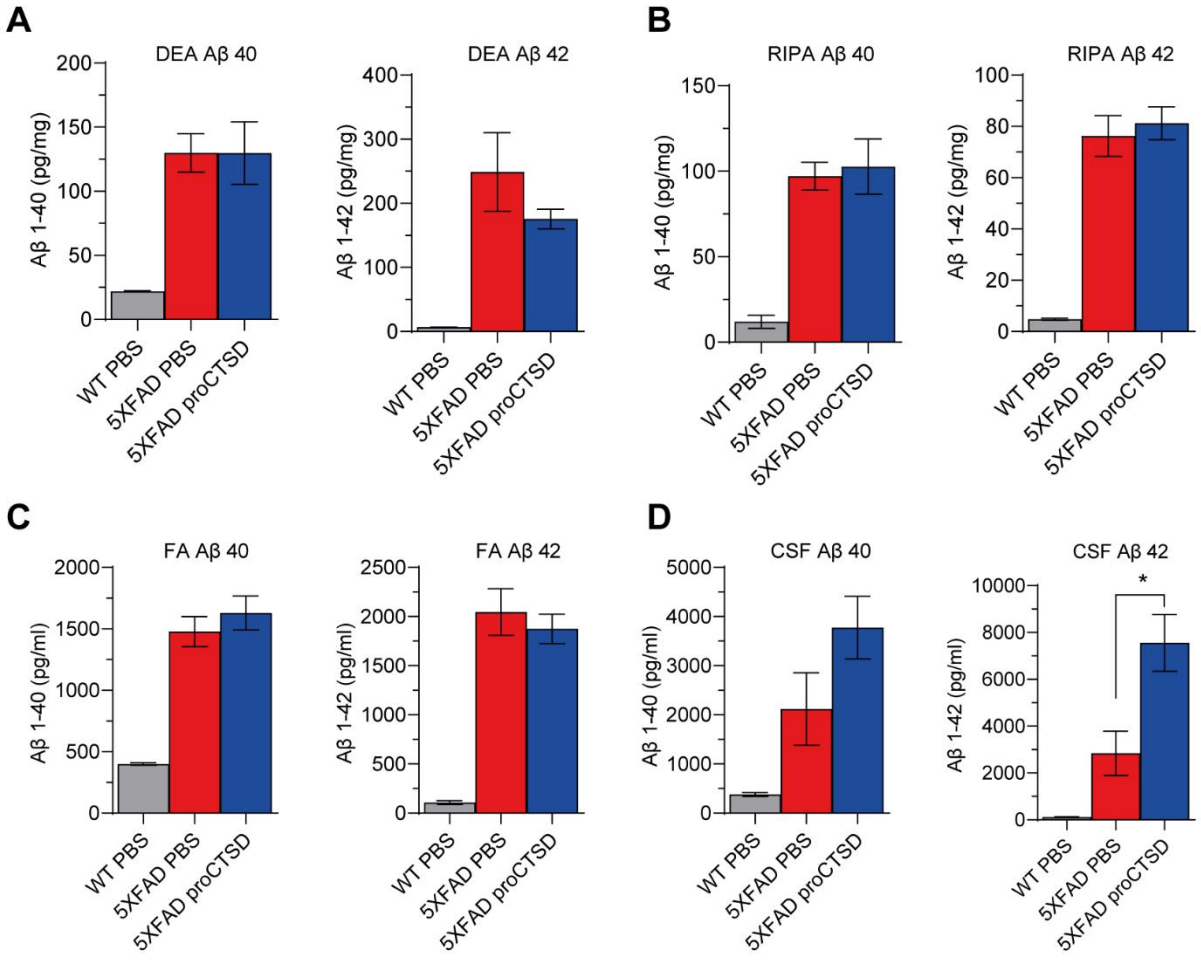


**Figure 41: Aβ1-40 and Aβ1-42 expressopn is upregulated in the CSF of rhpro-CTSD-treated 5xFAD mice.** ELISA analysis of Aβ1-40 and Aβ1-42 of **(A)** DEA, **(B)** RIPA, **(C)** FA and **(D)** CSF samples derived from brain of one-month old WT mice injected with PBS and 5xFAD mice either injected with PBS or 0.1 mg/ml rhpro-CTSD at P1 and P20 (WT: n = 2, 5xFAD: n = 3–4). Data represent mean ± SEM. Statistical analysis was performed by using one-way ANOVA with a Tukey's multiple comparison test. * $p < 0.05$.

### 4.10.3 Effect of rhpro-CTSD application on the APP and Aβ metabolism in two-month old 5xFAD mice

Rhpro-CTSD- and PBS-treated animals of two months of age were perfused with 0.1 M PB and investigated by immunoblot and ELISA. Figure 42 shows the immunoblot and its quantitative analysis. The CTSD levels in the RIPA lysates revealed that there was no activity of additional CTSD after two months of age in the rhpro-CTSD-injected 5xFAD animals. As noticed in the one-month old 5xFAD mice, there was no change in the levels of the soluble fragments sAPPα, sAPPβ or soluble Aβ (DEA fraction) and no differences in the APP CTFs C83 and C99 in 5xFAD mice of two-months of age.

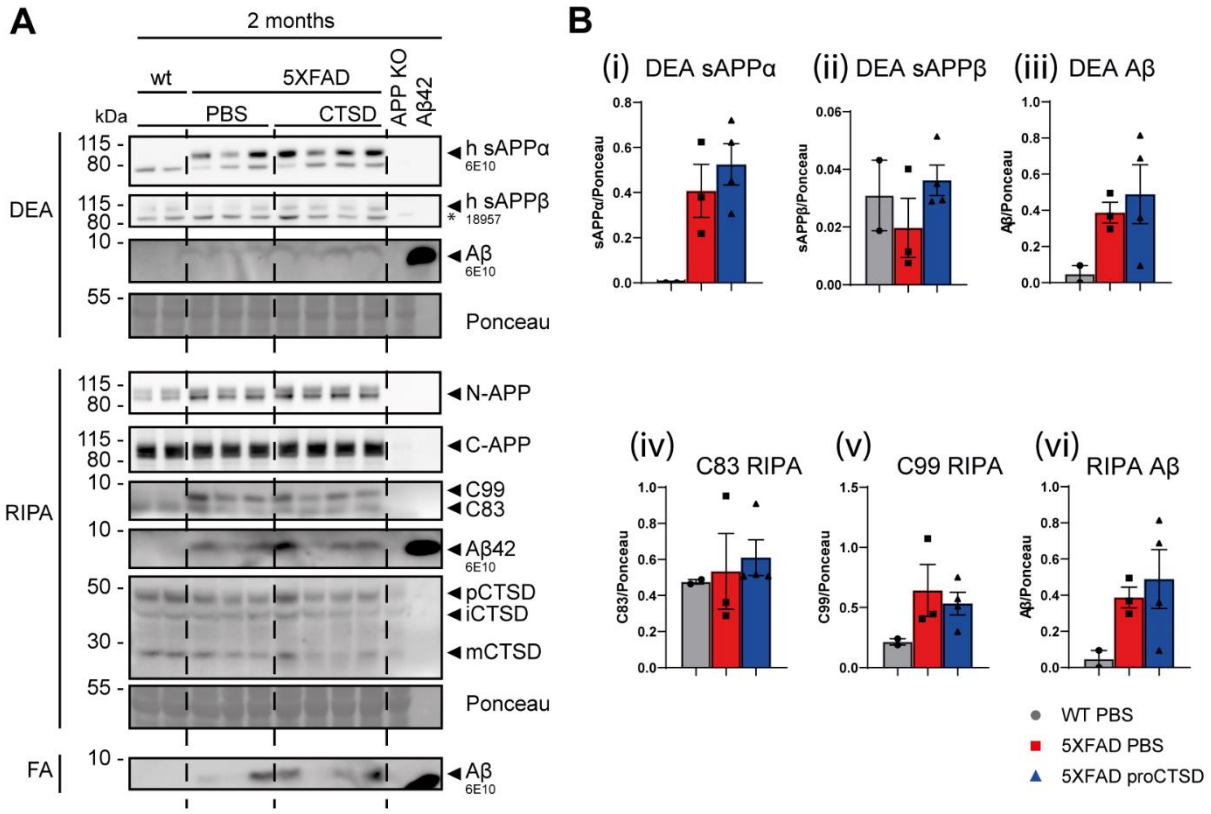


**Figure 42: ICV injection of rhpro-CTSD of 5xFAD mice does not alter APP or Aβ metabolites after two months. (A)** Immunoblot of DEA, RIPA and FA protein fractions from brain hemispheres of two-months old female WT and 5xFAD mice ICV injected with either PBS or 0.1 mg rhpro-CTSD at P1 and P20. Antibodies detecting CTSD, human sAPPα (hsAPPα: 6E10), sAPPβ (18957, IBL), the N-terminus of APP (22C11, Thermo Fisher Scientific), the C-terminus of APP (A8717, Sigma-Aldrich) and Aβ (6E10, biolegend) were used. Brain lysate of an APP KO mice was used as antibody control for APP antibodies. Ponceau S staining served as a loading control. **(B)** Quantitative analysis of two-months old female 5xFAD shown in (A) (n = 2–4). Data represent mean ± SEM.

ELISA analysis (3.2.3.6) revealed trends towards increased levels of Aβ1-40 and Aβ1-42 in DEA, RIPA and particularly in the FA fraction. Additional activity of CTSD seemed to rather elevate Aβ levels in the brain of 5xFAD mice than degrading Aβ1-42 into smaller Aβ species as hypothesized.

In summary, two-month old 5xFAD injected with rhpro-CTSD at P1 and P20 did not have elevated active CTSD levels and showed a trend towards increased levels of Aβ1-40 and Aβ1-42 as determined by ELISA. In addition, the investigated APP fragments sAPPα, sAPPβ, C83 and C99 were not affected by dosing 5xFAD with rhpro-CTSD at early age.

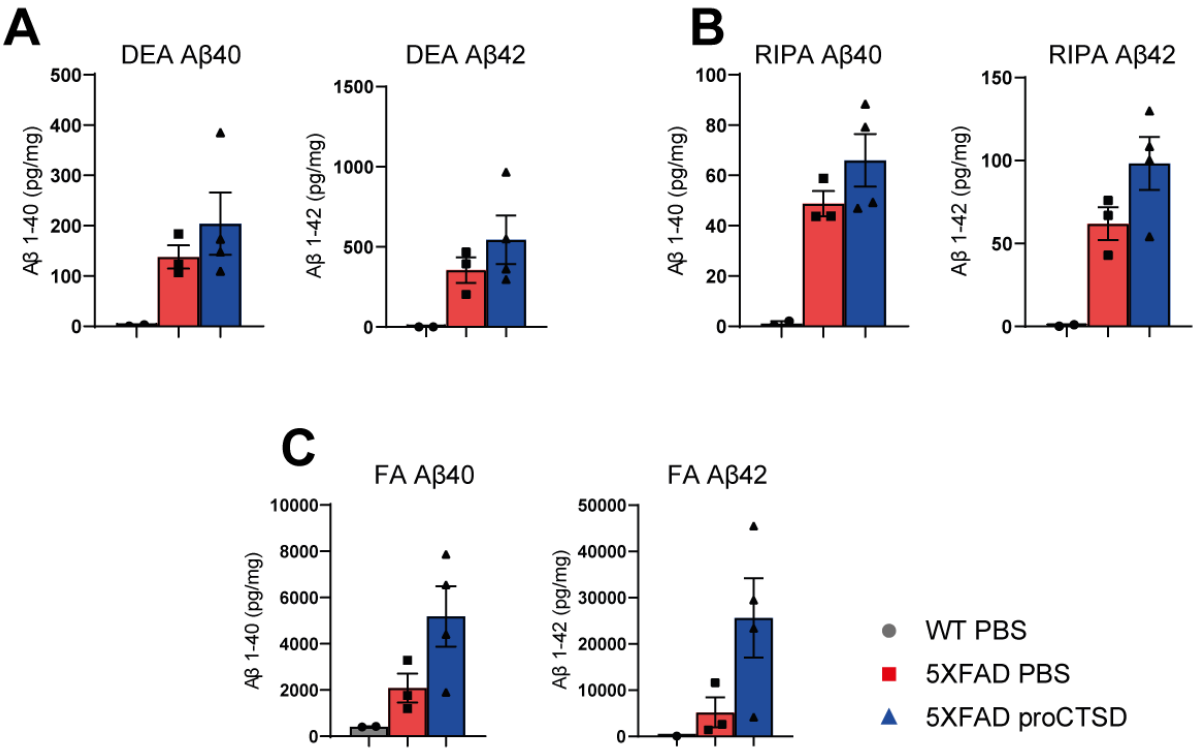


**Figure 43: Aβ1-40 and Aβ1-42 levels are upregulated in the brains of rhpro-CTSD-treated 5xFAD mice.** ELISA analysis of Aβ1-40 and Aβ1-42 in pg/µg(protein) of **(A)** DEA, **(B)** RIPA and **(C)** FA samples derived from brain of two-months old WT mice injected with PBS and 5xFAD mice either injected with PBS or 0.1 mg/ml rhpro-CTSD at P1 and P20 (WT: n = 2, 5xFAD: n = 3–4). Data represent mean ± SEM.

### 4.10.4 Effect of rhpro-CTSD on the APP and Aβ metabolism in three-month old 5xFAD mice

The last time-point chosen to analyze rhpro-CTSD treated 5xFAD mice was three months of age. Similar to the rhpro-CTSD-dosed one- and two-month old mice, the three-months old mice were perfused with 0.1 M PB and brains were investigated by immunoblot and ELISA (Figure 44 and Figure 45 A). In addition, MSD analysis for smaller Aβ species was performed in collaboration with *I. Ulku* at the University of Montreal (Figure 45 B).

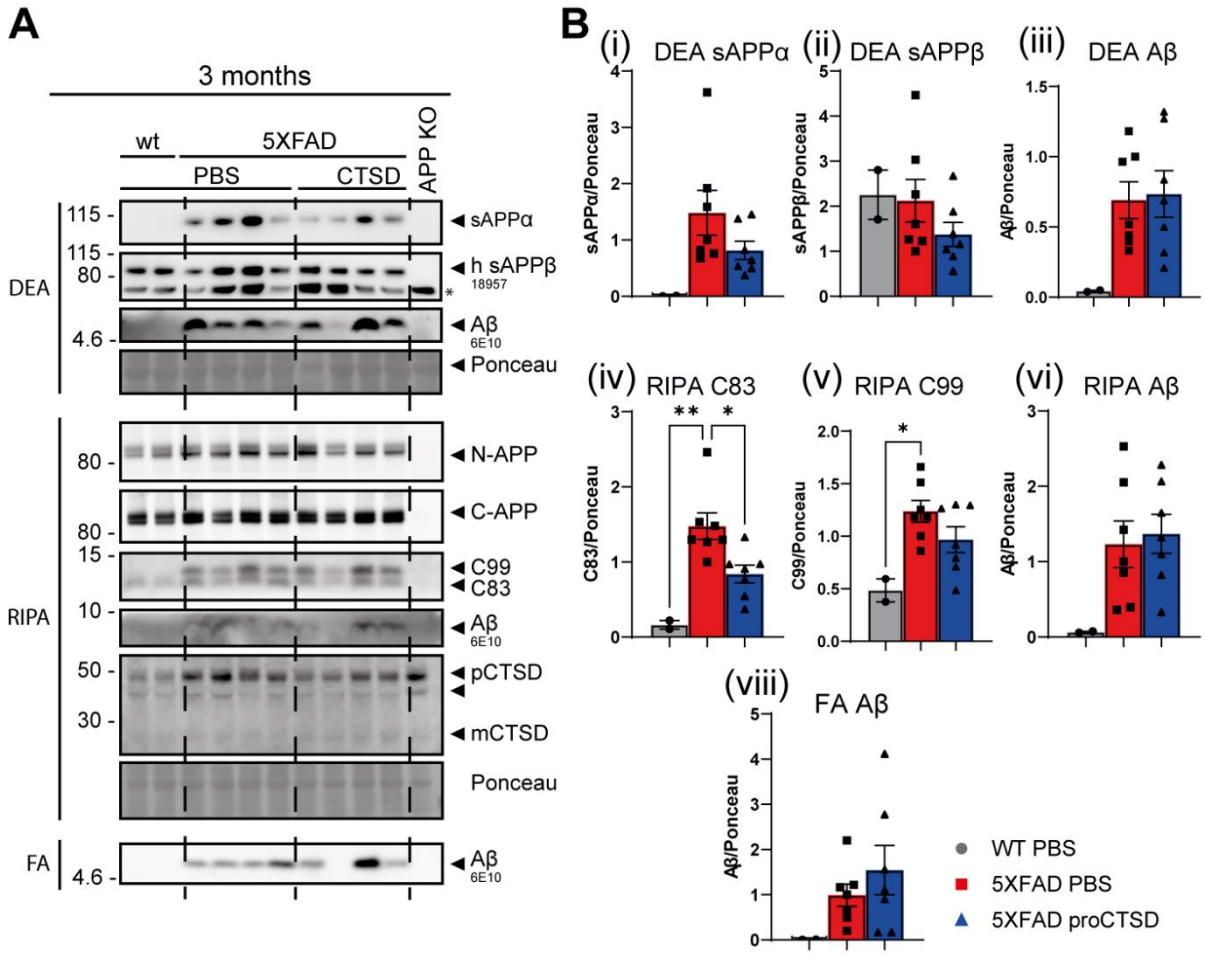


**Figure 44: Intracranial injection of rhpro-CTSD of 5xFAD mice does not alter APP or Aβ metabolites after three months of age. (A)** Respective immunoblot of DEA, RIPA and FA protein fractions from brain hemispheres of three-months old female WT and 5xFAD mice ICV injected with either PBS or 0.1 mg rhpro-CTSD at P1 and P20. Antibodies detecting CTSD, human sAPPα (hsAPPα: 6E10), sAPPβ (18957, IBL), the N-terminus of APP (22C11, Thermo Fisher Scientific), the C-terminus of APP (A8717, Sigma-Aldrich) and Aβ (6E10, biolegend) were used. Brain lysate of an APP KO mice was used as antibody control for APP antibodies. Ponceau S staining served as loading control. **(B)** Quantitative analysis of three-months old female 5xFAD shown in (A) (n = 2–4). Data represent mean ± SEM. Statistical analysis was performed by using one-way ANOVA with a Tukey's multiple comparison test. ** $p < 0.01$, * $p < 0.05$.

As already noted in CTSD-dosed 5xFAD of two-months of age, no elevated levels of active CTSD could be found after three months. Similarly, as in the one- and two-month old CTSD-dosed 5xFAD mice the sAPPα and sAPPβ fragments as well as soluble Aβ were not affected by rhpro-CTSD dosing at P1 and P20. By looking at the APP CTFs a statistically significant decrease of ~45 % of the APP-C83 fragment upon CTSD treatment was observed indicating degradation by CTSD or secondary effects induced by the elevated CTSD levels at early age. Other species of APP as well as Aβ in all three fractions (RIPA, DEA. FA) were not altered after dosing 5xFAD mice with rhpro-CTSD. Deeper analysis of the different Aβ species by ELISA or MSD analysis did not reveal any remarkable changes upon rhpro-CTSD treatment (Figure 45).

In summary, the data collected by immunoblot from the one-, two- and three-month old mice indicate that rhpro-CTSD was internalized into the neurons of 5xFAD mice, processed into its active form but appeared to exert a stability which does not last for three months. Rhpro-CTSD dosing did not alter APP or Aβ metabolism and metabolites to a considerable degree. Data retrieved from immunoblot, ELISA and MSD analysis suggest that CTSD is not able to reduce Aβ burden in the brains of the 5xFAD mice. However, the analysis methods used do not reveal evidence on how plaque morphology and number or neuroinflammation might be affected after rhpro-CTSD treatment.

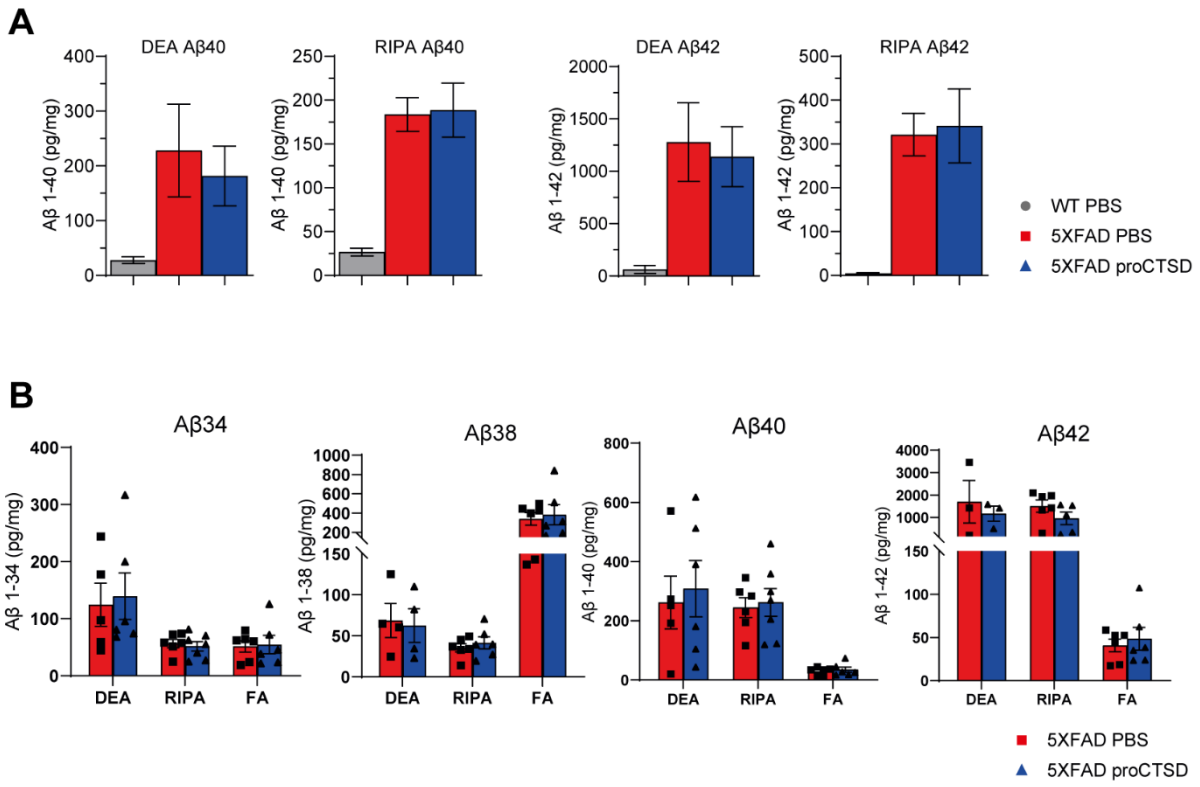


**Figure 45: Rhpro-CTSD dosing to 5xFAD mice at early age does not affect the levels of Aβ species after three months of age. (A)** ELISA analysis of Aβ1-40 and Aβ1-42 of DEA and RIPA samples derived from brains of P22 WT mice injected with PBS and CTSD-deficient mice with PBS or 0.1 mg rhpro-CTSD (WT: n = 2, 5xFAD: n = 7). **(B)** Meso Scale Discovery (MSD) analysis of Aβ1-34, Aβ1-38, Aβ1-40 and Aβ1-42 levels of DEA, RIPA and FA samples. MSD data was measured and analyzed by *Irem Ulku* (McGill University, Montreal). Data represent mean ± SEM.

### 4.10.5 Plaque morphology and neuroinflammation are not affected after rhpro-CTSD treatment in 5xFAD mice

Although immunoblot, ELISA and MSD analysis could not reveal striking effects of rhpro-CTSD ICV-dosed 5xFAD mice, these methods could not be used to analyze Aβ plaque size and amount or how neuroinflammation in the brain following Aβ-deposition

might be affected. Therefore, brains of PBS and rhpro-CTSD-dosed 5xFAD mice were sagittally cut into 35 µm sections and stained with different antibodies directed against Aβ and neuroinflammatory markers like GFAP or Iba1 (3.1.4).

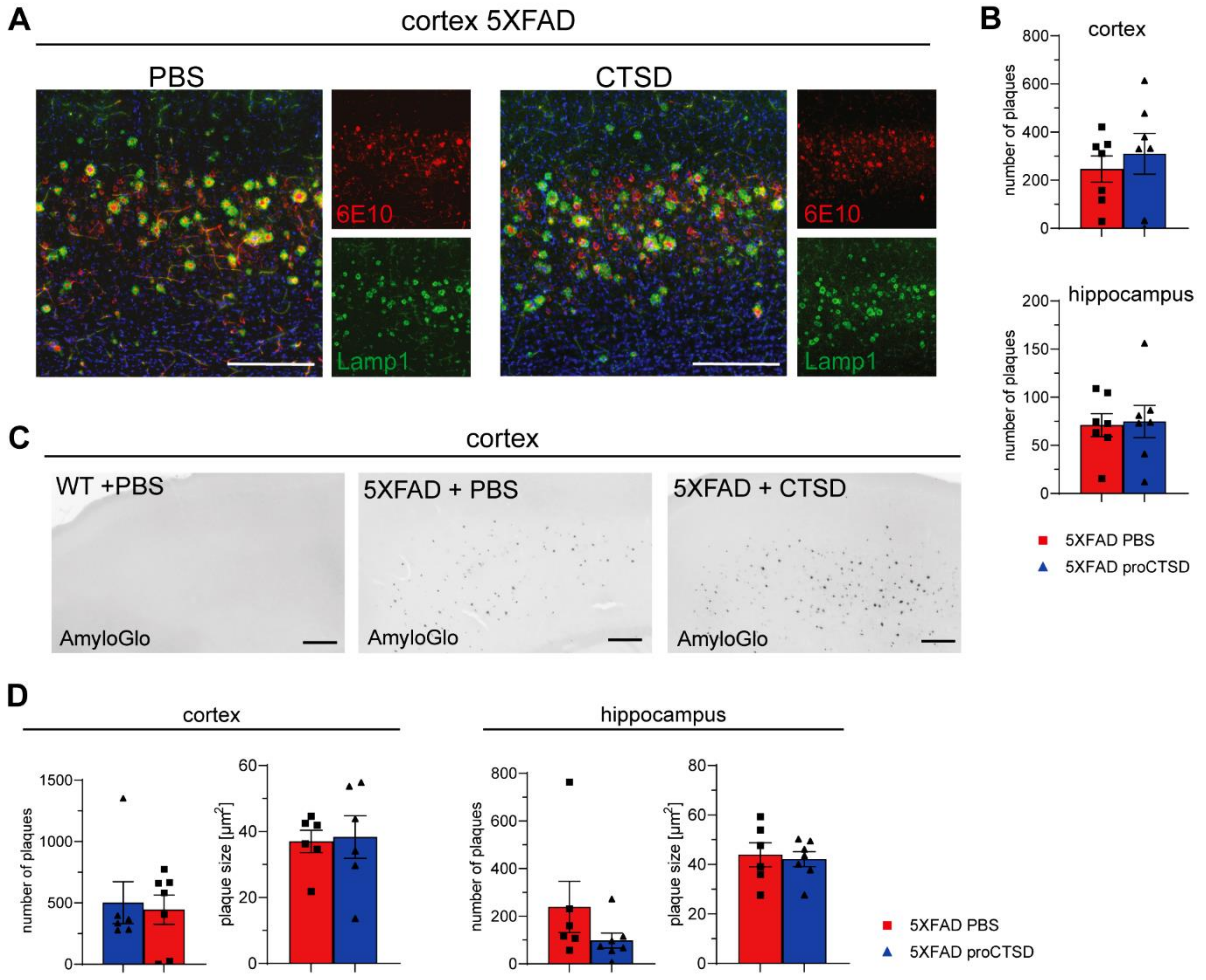


**Figure 46: ICV injection of rhpro-CTSD of 5xFAD mice does not lead to a benefit in relation to clearing Aβ. (A)** Respective immunostainings of cortices of three-months old 5xFAD injected with either PBS or 0.1 mg rhpro-CTSD at P1 and P20. Antibodies directed against the lysosomal marker LAMP1 (green, 1D4B, DSHB) and Aβ (red, 6E10, biolegend) and DAPI (blue) were used. Scale bar: 500 µm. **(B)** Number of Aβ plaques in cortex and hippocampus of three-months old female 5xFAD mice double injected with either PBS or 0.1 mg rhCTSD (n = 7). **(C)** respective staining of Aβ plaques with Amylo-Glo RTD Amyloid Plaque Stain Reagent (Biosensis) from cortex of three-months old female 5xFAD mice. Scale bar: 200 µm. **(D)** Number and size (µm2) of Aβ plaques from cortex and hippocampus (n=7). Data represent mean ± SEM.

First, the possible effects of ICV-dosed rhpro-CTSD on plaque formation were investigated to address the hypothesis that early dosing of rhpro-CTSD is beneficial in removing plaque-prone Aβ species resulting in smaller or less plaques within the brains of treated 5xFAD mice. Therefore, brain sections of three-months old 5xFAD mice injected either with PBS or rhpro-CTSD were stained with the anti-Aβ and anti-LAMP1-antibodies to stain plaques surrounded by lysosomes (Gowrishankar et al. 2015). Such Aβ plaques have been counted in cortex and hippocampus.

A respective immunostaining and the analysis of seven individuals is shown in Figure 46. The analysis shows that there are no major differences in the number of Aβ plaques in the cortex or hippocampus of rhpro-CTSD treated 5xFAD mice. Within the cortex, 5xFAD mice injected with PBS had 246 plaques on average while the ones dosed with rhpro-CTSD had 310 plaques. In the hippocampus, 5xFAD injected with PBS had 71 while the ones treated with rhpo-CTSD had 75.

Since the 6E10 antibody also stains the sAPPα (Cuchillo-Ibañez et al. 2015) and to get a better contrast of plaques within the brain, AmyloGlo staining was used to stain Aβ plaques only (Schmued et al. 2012). Staining in cortex and hippocampus of three-month old WT and 5xFAD mice either treated with PBS or rhpro-CTSD could not reveal any effect of the rhpro-CTSD on plaque number or size (Figure 46C). Within the cortex, there were on average 502 plaques with an average size of 37 µm² in 5xFAD injected with PBS. The 5xFAD dosed with rhpro-CTSD had 445 plaques with an average size of 38 µm². In the hippocampus, 5xFAD mice injected with PBS had 239 plaques with a mean size of 44 µm² while the 5xFAD mice treated with rhpro-CTSD had 98 plaques with an average size of 42 µm². However, statistical tests did not reveal differences. These data are in line with the previously described results that rhpro-CTSD dosing at P1 and P20 did not alter APP or Aβ metabolism in 5xFAD mice after three months.

Neuroinflammation, another major hallmark of AD is caused by misfolded and aggregated proteins that bind to microglia and astroglia receptors resulting in a neuroinflammatory response (Heneka et al. 2015; Leng and Edison 2021). Microglia phagocytose pathogens and cellular debris within the brain and protect synapses for precise maintenance. (Ji et al. 2013). The shape of microglia can change from a highly ramified form to an amoeboid form upon pathological activation or to a low ramified shape due to aging (Leng and Edison 2021). Interestingly, amyloid plaque-associated microglia seem to be less ramified and smaller in size, whereas plaque-distant microglia remained ramified and larger in size. To analyze microglia in three-month old WT and 5xFAD mice injected with either PBS or rhpro-CTSD at P1 and P20, brain sections were stained with Iba-1 and the ramification of microglia of seven individuals per group was analyzed by using Sholl analysis (Ferreira et al. 2014). Using this analysis, the ramification of microglia was determined by counting the intersections in regards of the distance to the cell body. The higher the number of intersections the higher the ramification of the microglia.

A slight increase in the ramification of the PBS- or rhpro-CTSD-treated 5xFAD when compared to WT mice in the cortex was observed. Both, PBS- and rhpro-CTSD mice display higher ramification closer to the cell body (4.4-14.3 µm). There were 5 to 9 intersections in 5xFAD mice while WT mice had 4 to 5 intersections. However, these differences were not significant. In the hippocampus the ramification of 5xFAD with PBS or rhpro-CTSD was not altered compared to WT mice. Like described in the previous findings, the treatment with rhpro-CTSD did not have an effect on the morphology and function of microglia.

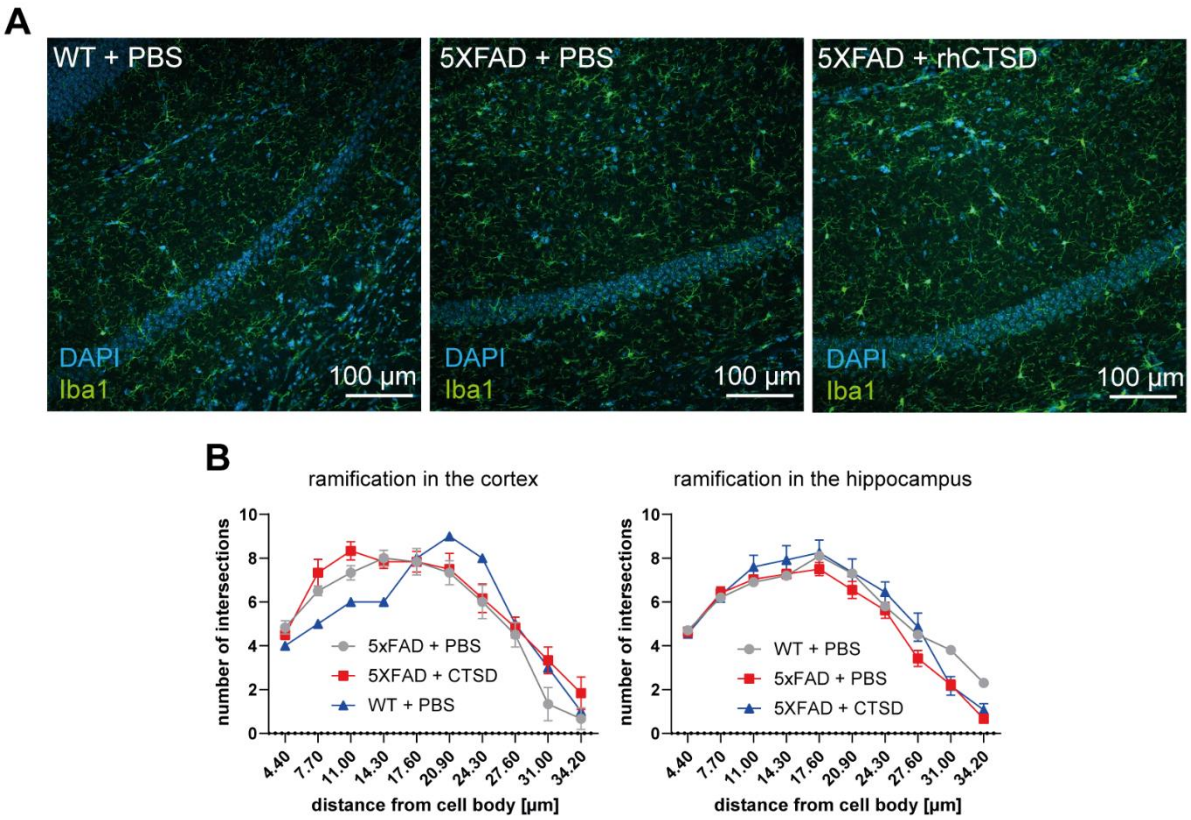


**Figure 47: No beneficial effect of rhpro-CTSD treatment in 5xFAD mice on microgliosis. (A)** Respective immunostaining of cortices of three-months old WT injected with PBS and 5xFAD injected with either PBS or 0.1 mg rhpro-CTSD at P1 and P20. Anti-Iba1 was used to stain microglia within the brains. Scale bar: 100 µm. **(B)** Ramification analysis of microglia (Iba-1 positive) in three-month old WT and 5xFAD mice treated with PBS or rhpro-CTSD.

While activated microglia internalize pathogens, astrocytes contribute to the maintenance of cerebral blood flow, neurotransmitter homeostasis and metabolic support for synapses (Leng and Edison 2021). GFAP is expressed in the cytoskeleton of astrocytes and is associated with Aβ burden, neurodegeneration and is upregulated in AD brains (Cicognola et al. 2021; Shir et al. 2022). To analyze three-month old 5xFAD mice treated with rhpro-CTSD, brain sections of seven mice were stained with

anti-GFAP and the GFAP-positive areas were determined using ImageJ (3.2.4.4; 3.2.6.3).

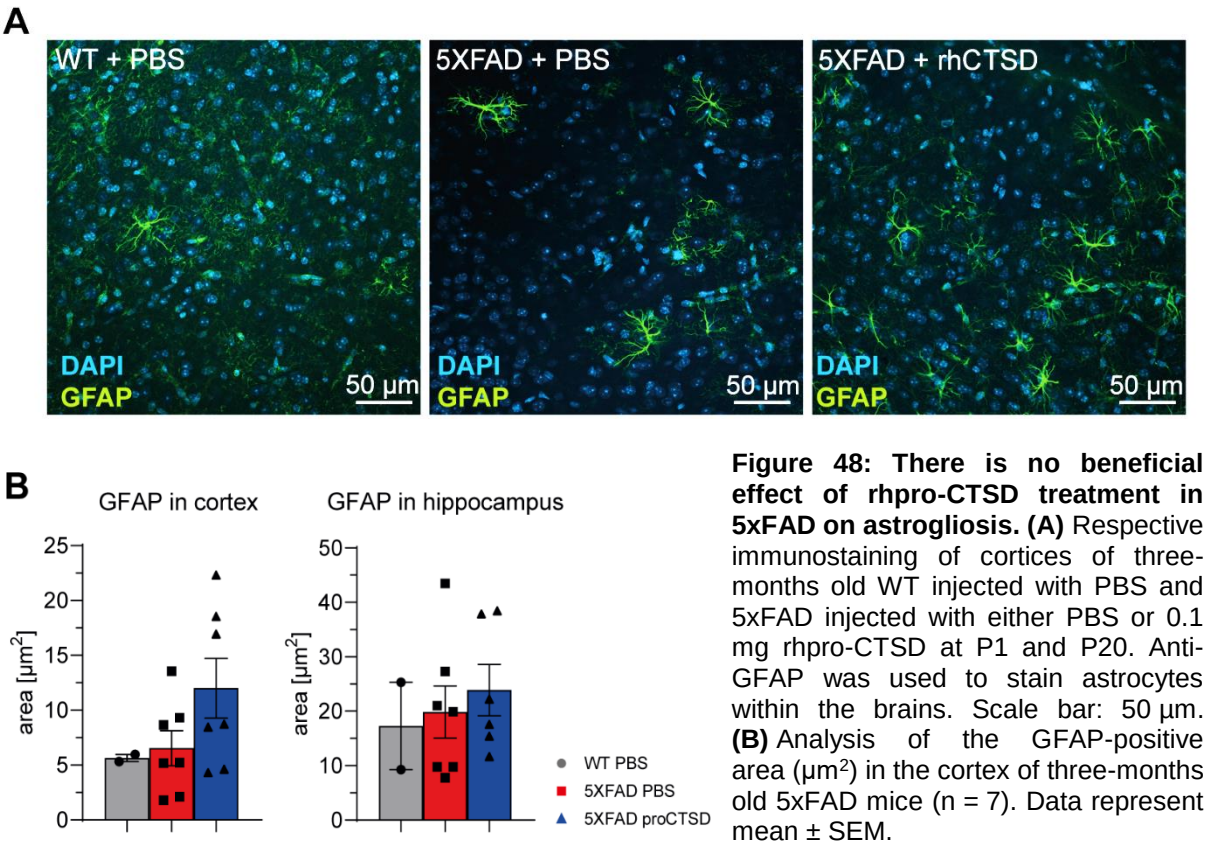


**Figure 48: There is no beneficial effect of rhpro-CTSD treatment in 5xFAD on astrogliosis. (A)** Respective immunostaining of cortices of three-months old WT injected with PBS and 5xFAD injected with either PBS or 0.1 mg rhpro-CTSD at P1 and P20. Anti-GFAP was used to stain astrocytes within the brains. Scale bar: 50 µm. **(B)** Analysis of the GFAP-positive area (µm²) in the cortex of three-months old 5xFAD mice (n = 7). Data represent mean ± SEM.

Figure 48 shows respective immunostainings of three-month old WT and 5xFAD mice either treated with PBS or rhpro-CTSD at P1 and P20 and the documentation of the analyzed GFAP-positive areas. The dosed three-month old 5xFAD mice did not show any increase in GFAP when compared to WT mice, indicating no astrogliosis. However, rhpro-CSTD treatment did not alter the astroglia expression at this stage as the area of GFAP in the cortex and hippocampus remains unaffected. Taken together, rhpro-CTSD treatment in mice did not have beneficial effects on the plaque burden or neuroinflammatory markers Iba-1 and GFAP, respectively.

# 5 Discussion

## 5.1 Cathepsins are differently expressed in SH-SY5Y and HeLa cells

During this work CTSB, CTSD, and CTSL were revealed as the three major lysosomal endopeptidases active in HeLa and SH-SY5Y cells. While RNA and protein expression data suggested similar distribution of CTSB and CTSD in SH-SY5Y and HeLa cells, there is less CTSL expressed in the SH-SY5Y cells as compared to HeLa cells. In human brain, Hsu et al. determined the protein expression of CTSD with up to 49%, CTSB with up to 32% and CTSL with up to 9% of the overall CTS expression pointing out their abundance and their important functions and activities within this organ (Hsu et al. 2018). Liu and Doray used RNA expression levels obtained from the data of the Human Protein Atlas to show that in HeLa cells CTSL, CTSZ and CTSB are the highest expressed CTSs besides CTSD (Liu and Doray 2021). Additionally, in this study differences in their enzymatic activities could be proven in HeLa and SH-SY5Y cells using the activity-based probe (ABP) BMV-109 for CTSB and CTSL as well with an enzymatic cleavage assay for CTSD. Despite their ubiquitous expression, members of the CTS family appear to be delicately coordinated within the lysosomal enzyme pool. This coordination varies across different tissues and cell types. CTSs also modulate each other's maturation (Laurent-Matha et al. 2006; Katunuma 2010) but can also replace or substitute their enzymatic activity (Felbor et al. 2002; Aghdassi et al. 2018; Iwama et al. 2021). They seem to have different individual but also redundant functions and might act in a hierarchical manner.

## 5.2 Cathepsin-deficiencies differently influence the lysosomal phenotype and accumulation of autofluorescent storage material

While CTSB-KO mice did not present an obvious phenotype, are viable and fertile (Deussing et al. 1998), CTSL-KO mice showed phenotypic changes in the skin (Roth et al. 2000), thymus (Nakagawa et al. 1998), or thyroid gland (Friedrichs et al. 2003). Both CTSB and CTSL separately disrupted the progression of tumor invasion and seem to have non-redundant functions within this process (Gocheva and Joyce 2007). Interestingly, in the central nervous system (CNS) both cysteine-type proteases CTSB and CTSL seem to share overlapping substrates and redundant functions as only a double KO of both CTSB and CTSL led to severe brain atrophy and neurodegeneration

causing an early death (Felbor et al. 2002). In the same study an enlargement of endosomal and lysosomal compartments increasing age-dependently within the CTSBL-double KO mice was described (Felbor et al. 2002). Mouse embryonic fibroblasts (MEFs) depleted for either CTSB or CTSL did show significantly increased LAMP1 expression levels comparable to the LAMP1 expression found in MEF CTSBL double knockout pointing towards the presence of lysosomal storage material (Cermak et al. 2016). However, mice lacking CTSB or CTSL in the pancreas did not show altered LAMP2 expression (Iwama et al. 2021). These findings support the hypothesis of a tissue-specific redundancy of CTSB and CTSL. In fact, CTSB and CTSL share similarities and also differences in their substrate recognition patterns (Poreba et al. 2018; Poreba et al. 2019). CTSB for example is involved in the cleavage of fibronectin (Wyczalkowska-Tomasik et al. 2015) while CTSL is capable in cleaving elastin, an important component of the extracellular matrix, 100-fold better than CTSB (Chapman et al. 1994). The human neuroblastoma single SH-SY5Y CTSB- and CTSL-KO cells analyzed during this work did not show an altered lysosomal LAMP1 expression nor an increased lysosomal size indicating a redundant function of both CTSB and CTSL within this human neuroblastoma cell line.

A CTSD-deficiency or CTSD mutations in mice and humans has fatal consequences since patients suffer from neuronal ceroid lipofuscinosis type 10 (NCL10) – a serious lysosomal storage disorder. This disease is characterized by severe progressive neurodegeneration often causing early lethality (Saftig et al. 1995; Steinfeld et al. 2006). Lysosomes of Schwann cells from NCL10 patients and of neurons from CTSD-knockout mice were significantly enlarged and filled with autofluorescent storage material composed of granular osmiophilic deposits and myelin-like lamellar structures pointing towards a strong lysosomal dysfunction and a non-redundant and specific function of CTSD within the CNS (Koike 2000; Tyynelä et al. 2000; Steinfeld et al. 2006). MEF cells and mouse liver, spleen, and brain lysates deficient in CTSD expressed elevated levels of LAMP1 and had enlarged lysosomes (Marques et al. 2020). However, a pancreas-specific CTSD-KO in mice did not show altered LAMP2 levels indicating that also CTSD functions may be compensated by other lysosomal proteases within this tissue (Iwama et al. 2021).

SH-SY5Y CTSD-deficient cells generated by CRISPR/Cas9 depletion in this study did not express higher LAMP1 protein levels and show some lysosomes mildly but

insignificantly increased in size. This might indicate that other proteases are still capable in processing substrates that are usually degraded by CTSD within this neuron-like cell line. However, the slightly enlarged lysosomes could also point towards specific substrates that might accumulate within the CTSD-depleted lysosomes. CTSD may also be required to initiate degradation of certain proteins for other lysosomal proteases to continue their degradation. All forms of NCL share features like selective neuronal loss and damage most pronounced within the retina and brain. Neuroinflammation and aggregation of autofluorescent ceroid lipofuscin are further hall marks of the disease (Jalanko and Braulke 2009). Interestingly, microscopy analysis of autofluorescent signals within the SH-SY5Y CTSD-deficient cells revealed some fluorescent storage material within lysosomes which supports the special importance of CTSD within the CNS. Besides, the CTSBDL-triple knockout SH-SY5Y cells presented even more autofluorescent storage material. This material could likely represent lipofuscin, a highly oxidized cross-linked aggregated mixture of protein and lipid which also accumulates with aging (Jung et al. 2007) within lysosomes. The finding in the multiple knockout cell lines indicates a stronger dysregulation of lysosomal enzyme activity and higher amount of accumulated lysosomal storage material. In addition, transmission electron microscopy (TEM) images from SH-SY5Y CTSBDL-deficient cells revealed enlarged lysosomes filled with electron dense material. A combined deficiency of CTSB, CTSD and CTSL in cells has not yet been described to date. Since CTSBDL-triple deficient mice would most likely not be viable or fertile one relies on such cellular studies and an *in vivo* analysis to analyze the redundant functions of these three enzymes is likely not feasible.

Recently, Iwama et al. created pancreas-specific (-Δpan) single and also double CTS-KO mice with the combinations CTSBD-Δpan, CTSBL-Δpan and CTSDL-Δpan (Iwama et al. 2021). All mice were viable but CTSBD-Δpan-deficient mice showed a significant lower weight as compared to wildtype littermates. After two months of age CTSBD-Δpan-deficient mice developed increased numbers of cytoplasmic vacuoles in the pancreas which might originate from lysosomes (Iwama et al. 2021; Huang et al. 2020). Electron microscopy images of pancreatic acinar cells from CTSBD-Δpan-deficient mice revealed large numbers of autolysosome-like structures (Iwama et al. 2021). This study could demonstrate that only a combined loss of CTSB and CTSD in

the pancreas is causing an enlargement of lysosomes and that both CTSB and CTSD play an important role in the lysosomal/autophagic clearance in the pancreas.

During this work, the SH-SY5Y CTSBDL-triple deficient cells also showed significantly increased lysosomes and LAMP1 expression which surprisingly could not be rescued by re-transfecting single or all three missing CTSs. Re-transfection of a single CTS protease to the SH-SY5Y CTSBDL-triple-deficient cells would essentially lead to a double-CTS-knockout mutant (similar to experiments described by Iwama et al.) but also failed to reduce the observed increase of LAMP1 expression in the triple cathepsin-lacking cells. This might indicate that CTSB, CTSD and CTSL sequentially process substrates in a hierarchical manner in the SH-SY5Y cells. Substrates need to be proteolyzed by one CTS prior the next CTS gets access to the same substrate polypeptide.

However, there are also some technical limitations to be considered when interpreting these data. Not all cells may have been transfected and not all plasmids may have reached the same cell to efficiently restore the lysosomal phenotype. Since it was not possible to stain three different CTSs in parallel as well as lysosomal markers and to perform an analysis of autofluorescence at the same time the interpretation of the microscopy analysis was limited. Despite of these limitations a mild trend towards lowered LAMP1 expression after re-addition of CTSB, CTSD and CTSL to the SH-SY5Y CTSBDL-deficient cells was observed suggesting a partial restoration of the lysosomal activity and tendencies towards fully functional degradation of the accumulated and endocytosed substrates.

### 5.3 CTSBDL-triple deficiency leads to mild impairment of the autophagic flux

Loss of protease activity, enlarged lysosomes and accumulated storage material are often associated with a reduced autophagic flow (Ballabio and Gieselmann 2009; Jalanko and Braulke 2009). In a previous study, the expression of the autophagy marker LC3-II, which represents a lipidated form of LC3-I associated with autophagosomal membranes throughout the autophagic maturation (Mizushima et al. 2010; Klionsky et al. 2016), was not altered in MEFs deficient in CTSB but significantly upregulated in MEFs deficient in CTSL or CTSBL KO (Cermak et al. 2016). Iwama et al. also analyzed LC3-II in their CTS-Δpan mice and found upregulated LC3-II protein

levels in CTSBD-Δpan mice (Iwama et al. 2021). Analyzing neural stem cell-derived astrocytes and brain lysates from CTSD-deficient mice, also revealed higher LC3-II levels (Marques et al. 2020; Di Spiezio et al. 2021). Therefore, autophagy seems to be differently affected in organs and especially CTSD is important for autophagic degradation within the brain but apparently not in pancreas. Treating CTSD-deficient mice with recombinant human (rh)-proCTSB or rh-proCTSL could partially decrease the LC3-II accumulation caused by deficiency of the aspartyl-protease CTSD indicating a partial functional compensation by both cysteine-proteases (Di Spiezio et al. 2021). Within this work, SH-SY5Y CTSD KO cells showed an accumulation of LC3-II indicating again the special role of CTSD. Importantly, a CTSBDL-triple deficiency in SH-SY5Y led to further increased accumulation of LC3-II suggesting that the combined degradation by the three major cathepsins is required for the efficient autophagic degradation. However, autophagic flux assays revealed a rather mild impairment of this process. Data obtained from RFP-GFP-LC3-transfected SH-SY5Y cells combined with an autophagic flux assay suggest an accumulation of autolysosomes after CTBDL-triple knockout and after starvation combined with BafA1-treatment. These data are in line with the findings from Tanida and colleagues reporting that HeLa cells have a slightly increased LC3-II expression upon inhibition of aspartyl- and cysteine-type lysosomal hydrolases using PepA/E64D treatment as compared to non-treated cells (Tanida et al. 2005). It was also demonstrated that HEK cells have lower LC3-II expression levels after PepA/E64D treatment (Tanida et al. 2005), which again reflects the cell type-specific functions of CTSs. However, in both cell types autolysosomes accumulated upon starvation and treatment with PepA/E64D indicating LC3-II is mainly turned-over by lysosomal hydrolases after formation of autolysosomes.

SH-SY5Y CTSBDL-triple deficient cells revealed accumulation of LC3-II upon starvation and there is probably an accumulation of autolysosomes. However, CTSB, CTSD and CTSL seem to not be the only lysosomal hydrolases able to degrade LC3-II as its level is even further increased after BafA1 treatment (maximal lysosomal inhibition of proteolytic activity). This indicates that despite the lack of three major lysosomal hydrolases other proteases are still capable in hydrolyzing substrates such as LC3-II. From preliminary peptidome analysis retrieved from HeLa lysosomes lacking CTSB, CTSD, CTSL and CTSZ (data not published) it is known that enlarged lysosomes are filled with a lower number of peptides compared to lysosomes of HeLa

WT cells. These peptides differ in size as single amino acids are still cleaved off from the C-terminus (“peptide ladders”) suggesting the activity of exopeptidases to be responsible for the “trimming” of these peptides. Therefore, sufficient free amino acids and small peptides are available and may be released (e.g. through the lysosomal amino acid transporter SLC38A9 (Wyant et al. 2017)) released into the cytoplasm stimulating mTOR (mammalian target of rapamycin) activity and reduce the induction of autophagy after transcription factor EB (TFEB) phosphorylation in most cells (Kobayashi 2015; Wyant et al. 2017).

In fact, proteome analysis of CTSBDL-deficient SH-SY5Y cells revealed significant upregulation of the endopeptidase Legumain, the lysosomal exopeptidase Dipeptidyl-peptidase 7 (DPP7) and the exopeptidases Tripeptidyl-peptidase 1 (TPP1) and TPP3 indicating a compensatory effect for the loss of the three major lysosomal hydrolases in SH-SY5Y cells. Unfortunately, peptidome analysis of the SH-SY5Y CTSBDL-deficient cells was not yet possible as their lysosomes seem to be too fragile for their enrichment. Interestingly, by proteome analysis Galectin 1 (Gal1) and Gal3 were found upregulated in the SH-SY5Y CTSBDL-deficient cells. Among other functions, Galectins recognize galactose-containing glycoconjugates found in luminal membranes of different intracellular organs including lysosomes (Ludger et al. 2018). Since Gal1 is able to bind the carbohydrates of LAMP1 and LAMP2 during lysosomal damage (Dimitroff 2015) higher protein expression of LAMP1 and LAMP2 as found in the SH-SY5Y CTSBDL-KO cells could cause the higher abundance of Gal1 within these cells. On the other hand, Gal3 is involved in the repair of damaged lysosomes (Jia et al. 2020). This might explain the difficulties in isolation of lysosomes from SH-SY5Y CTSBDL-deficient cell as overexpressed LAMP1 might cause an upregulation of Gal3.

Besides LC3, p62/SQSTM1 (sequestosome-1) is another marker for autophagy that is often investigated (Klionsky et al. 2016; Mizushima et al. 2010). In CTSB-, CTSD- or CTSL-Δpan mice no upregulation of p62 (Iwama et al. 2021) was observed. Again only the combined loss of CTSD and CTSL within the pancreas led to increased p62 levels together with increased LC3-II levels indicating an impairment of autophagy (Iwama et al. 2021). However, p62 protein levels usually decrease upon short-term starvation and are then restored by transcriptional upregulation induced by released amino acids from the lysosome (Sahani et al. 2014). In SH-SY5Y CTSD KO and CTSL KO cells the

expression of p62 was also significantly upregulated. Proteome data derived from SH-SY5Y CTSBDL-triple deficient cells also revealed a significant upregulation of p62.

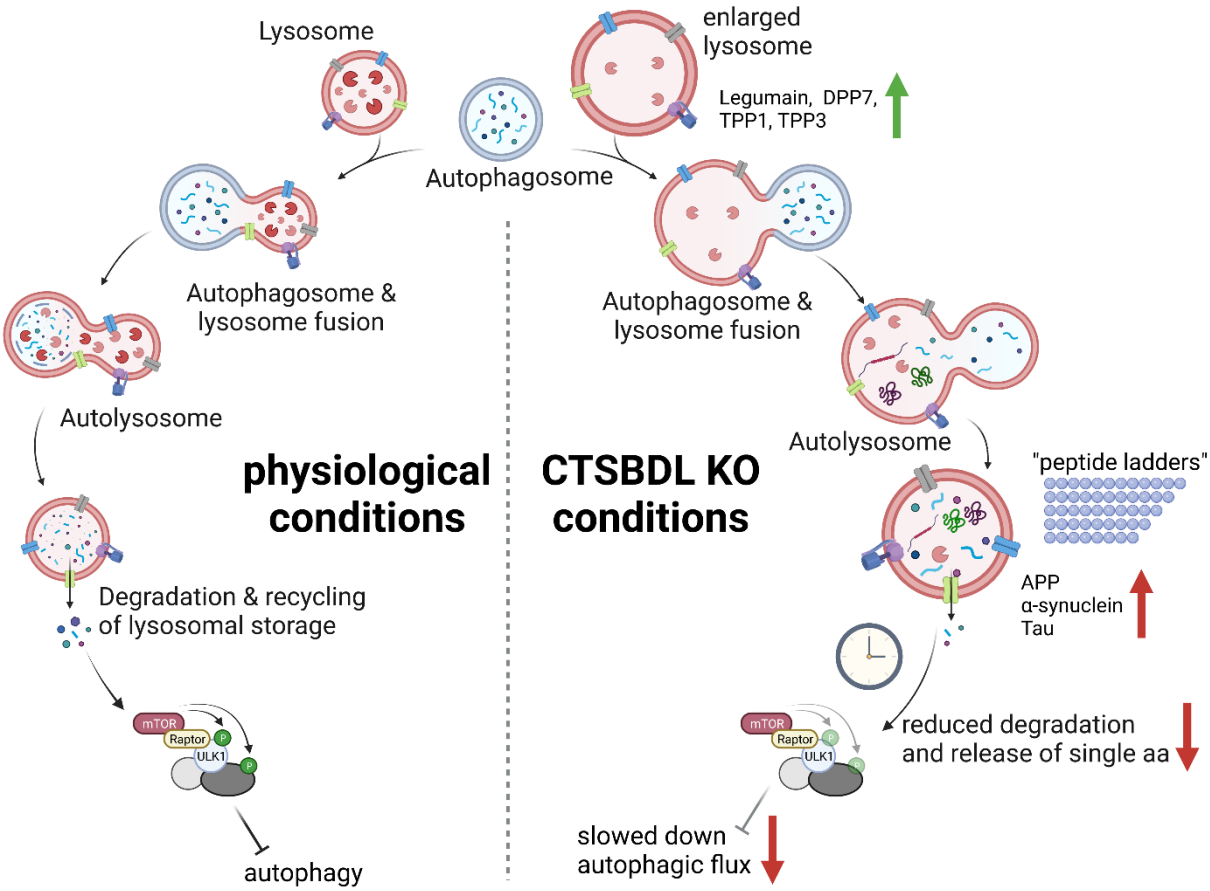


**Figure 49: Impacts of a deficiency of CTSB, CTSD and CTSL in SH-SY5Y cells on the autophagic pathway.** Under physiological conditions lysosomes and autophagosomes fuse to form autolysosomes. Lysosomal hydrolases are able to degrade storage material. Amino acids and small peptides are released into the cytosol and can activate mTORC1 which in turn blocks autophagy. Under CTSBDL-deficiency lysosomes are enlarged and lysosomal hydrolases like the endopeptidase Legumain and exopeptidases like DPP7, TPP1 and TPP3 are upregulated. Lysosomes can still fuse with autophagosomes to form autolysosomes. Protein expression associated with neurodegenerative diseases like APP, Tau and α-synuclein are found to be upregulated. Exopeptidases are still capable in degrading proteins resulting in peptides with sequences differing in single amino acids ("peptide ladders") which cannot be fully degraded by the lysosomal hydrolases. As single amino acids can still be released from the lysosome they can therefore activate mTORC to inhibit autophagy. This process seems to be slowed down as bulk proteolysis in the absence of CTSB, CTSD and CTSL is slowed down. mTOR - mammalian Target of Rapamycin, ULK1 - Unc-51 like autophagy activating kinase, DPP7 – Di-peptidyl-peptidase 7, TPP1 - Tripeptidyl-peptidase 1, TPP3 - Tripeptidyl-peptidase 3, APP – Amyloid Precursor Protein, aa – amino acid

Together with the unaltered expression of LC3-II in the single CTSD KO and CTSL KO SH-SY5Y cells, it suggests that autophagy is probably not severely disturbed in these cells. Unlike the single CTSD and CTSL KO, CTSBDL-triple deficiency led to mild

impairment of the autophagic flux as a result of accumulation of both LC3-II and partially p62. Probably, p62 levels are increased as p62 can bind to LC3-II during the formation of autophagosomes. While the main CTSs are missing both LC3-II and p62 cannot be degraded. It could also be that single amino acids are still released causing upregulation of the p62 synthesis (Sahani et al. 2014).

Figure 49 depicts a proposed model of the impacts of a deficiency of CTSB, CTSD and CTSL in SH-SY5Y cells and summarizes the major aspects regarding the impairment of the autophagic flux in the absence of the major lysosomal proteases discovered during this study.

## 5.4 CTSB, CTSD and CTSL can partially compensate for each other sharing the same substrates

Surprisingly the deficiency of three major cathepsins only mildly impaired autophagy. Endocytosis is a central pathway to transport molecules to the lysosome for degradation. Proteome analysis in combination with a KEGG (Kyoto Encyclopedia of Genes and Genomes) *in silico* pathway analysis revealed that proteins and enzymes involved in the regulation of endocytosis are not affected by the loss of CTSB, CTSD, and CTSL in SH-SY5Y cells. BSA-AlexaFluor 647 was similarly endocytosed by both WT and CTBDL-deficient SH-SY5Y cells and processed, indicating successful delivery of the BSA to the lysosomes. However, an appearance of a 50 kDa fragment found in the SH-SY5Y CTSBDL KO cells indicated its possible accumulation within the lysosomes. Notably, this fragment is still proteolyzed as the signal intensity fainted with time. This finding is in line with the available peptidome data revealing those “peptide ladders” due to compensatory overexpression of exopeptidases. The expression of exopeptidases like Tripeptidyl-peptidase 1 (TPP1), TPP3, Dipeptidyl-peptidase 7 (DPP7) were found to be upregulated by proteome analysis pointing towards alternative cleavage events in the experiment where BSA was analyzed as a substrate. In general, proteome data were gained from whole cell lysates. Dysregulated protein abundance could either mean up- or down-regulation or less degradation within the lysosome caused by the loss of the cathepsins’ activity in the SH-SY5Y cells. Upregulation of lysosomal enzymes like TPP1, TPP3, DPP7, and also Legumain indicate such compensatory consequences as a response for the missing activity of CTSB, CTSD and CTSL. The protein expression and maturation of CTSB, CTSD and

CTSL was not affected after only one specific of these cathepsins was depleted in the SH-SY5Y cell. The appearance of the respective mature form of the cathepsins seemed to remain unaffected by the lack of a single cathepsin.

Several independent studies addressed the compensatory effects by other lysosomal hydrolases caused by the loss of certain CTSs. The analysis of MEFs and mouse thyroid samples deficient in CTSL revealed an upregulation of CTSD, while CTSB remained unaffected (Friedrichs et al. 2003; Dennemärker et al. 2010). CTSBL-deficient mice also showed an increased CTSD protein expression (Felbor et al. 2002). Additionally, proteome analysis of lysosomes isolated from mouse brains deficient in CTSB and CTSL revealed an upregulation of the lysosomal enzymes CTSD, hexosaminidases A and B and Palmitoyl-protein Thioesterase 1 (PPT1) (Stahl et al. 2007). Tholen et al. analyzed skin samples from mice deficient in either CTSB or CTSL (Tholen et al. 2013). They found upregulated CTSZ protein levels in CTSB KO mice and upregulated CTSB, CTSD and CTSZ levels in CTSL KO mice. All these data support the idea of compensatory effects caused by the loss of a certain CTSs. As stated before CTSB, CTSD and CTSL act in concert and are precisely regulated within the lysosomal enzyme network. Therefore, proteomic data collected from SH-SY5Y CTSBDL-deficient cells would possibly contribute to this hypothesis and strengthen the idea of their delicate interplay. How this interplay is regulated, however remains largely unknown.

### 5.5 CTSB, CTSD and CTSL are involved in APP degradation

The SH-SY5Y CTSBDL-cell-derived microscopy and proteomic data pointed towards accumulation of lysosomal storage material. Upregulated protein levels of Integrin subunit α2 (ITGA2) and the Amyloid Precursor Protein (APP) were found. Immunoblot analysis could confirm an increased expression of C- and N-terminal APP fragments. There was a tendency towards an increased ITGA2 protein expression in the SH-SY5Y CTSBDL-deficient cells. Interestingly, SK-N-SH cells (neuroblastoma cell line, SH-SY5Y are cloned from this cell line) treated with the pan-Cathepsin inhibitor K777 also showed upregulated ITGA1 (homolog to ITGA2) and upregulated APP protein expression levels (Halakos et al. 2021).

ITGA2, a collagen receptor, is commonly overexpressed within neuroblastoma cells (Semeniak et al. 2019; Hee et al. 2020). It was demonstrated that collagen biosynthesis seems to be promoted by CTSB in bronchiolitis oblitrans syndrome (Morrone et al. 2021) while secreted CTSL could be involved in the hydrolysis of collagen XVIII (COL18A1) during angiogenesis (Felbor et al. 2000). The loss of CTSB and CTSL possibly leads to a dysregulation in the collagen metabolism causing either an upregulation of expression of the collagen receptor ITGA2 if there are higher levels of collagen or an increase in the endocytosis of ITGA2 to degrade the receptor when collagen levels are low. Indeed, proteome data revealed some upregulated collagen protein levels in the SH-SY5Y CTSBDL-deficient cells compared to wildtype cells like COL4A2 and COL6A1. As receptor and ligand (collagen and ITGA2) are bound and endocytosed ending up within lysosomes, the lack of CTSs could cause an increase in both proteins.

APP on the other hand is not necessarily a new substrate for CTSB, CTSD and CTSL (Oberstein et al. 2020; Suire et al. 2020; Wang et al. 2015) but the accumulation of a 17 kDa N-terminal APP fragment in the SH-SY5Y CTSBDL-deficient cells might be of specific interest. As stated before, CTSB, CTSD and CTSL play an important role in the brain and APP is also mainly expressed this organ. Pathophysiological cleavage leads to generation of Amyloid-β (Aβ) which is prone to aggregate in Alzheimer's disease (AD) patients (Knopman et al. 2021). Previously it could already be shown that a deficiency of CTSB, CTSL or both led to accumulation of the APP C-terminal fragments (CTFs) C83 and C99 in MEFs (Cermak et al. 2016). Cermak and colleagues also treated CHO WT cell with Pepstatin A (aspartyl-protease inhibitor) which did not lead to an accumulation of the C83 and C99 APP CTFs (Cermak et al. 2016). During this study, APP CTFs were only upregulated in the CTSBDL-deficient SH-SY5Y cells but not in any of the single CTS KO cells supporting Cermak and colleagues' findings that only the loss of more than one CTSs leads to accumulation of the APP CTFs. Lauritzen et al. demonstrated that lysosomal cathepsins are involved in the degradation of APP CTFs through autophagy (Lauritzen et al. 2016). Conversely, the loss of three major CTSs should lead to an accumulation of these fragments causing a disturbed degradation. By re-addition of single cathepsins to the SH-SY5Y CTSBDL-deficient cells the expression of both APP CTFs remained high, i.e. no prominent reduction of the level of these fragments was observed. However, re-transfection of all

three cathepsins in parallel led to lowered APP CTF protein levels suggesting that the APP CTF increase in CTSBDL-deficient SH-SY5Y cells was rescuable. The major degradation of the C83 and C99 APP fragments is indeed mediated by the common activities of CTSB, CTSD and CTSL.

The 17 kDa N-terminal fragment might be of interest as the N-terminal part of APP is usually released as soluble APP (e.g. sAPPα and sAPPβ) into the cytosol (Chow et al. 2010). Soluble APPα (sAPPα) is internalized by endocytosis and delivered to lysosomes by receptor-mediated transport mainly through LRP1 (Kounnas et al. 1995). Soluble APPβ also interacts with the LRP family indicating the same endocytic degradation pathway (Guo et al. 2021). Interestingly, LRP1 was also among the upregulated proteins found in proteome analysis of the SH-SY5Y CTSBDL-deficient cells. This might indicate an increased transport of the soluble APP fragments to the lysosomes. Since here, the major cathepsins are missing, an N-terminal-fragment of APP is able to accumulate. This fragment can be partially degraded after re-transfection of CTSB, CTSD or CTSL to the but again the activity of all three cathepsins was required to completely hydrolyze and reduce the appearance of this N-terminal polypeptide as visualized in immunoblot experiments. This again indicates a hierarchical and precise interplay of CTSB, CTSD and CTSL within the lysosomal network.

In addition to APP, other proteins related to neurodegenerative diseases were found to be upregulated in the SH-SY5Y CTSBDL-deficient cell lines by proteomic analysis. The expression of Tau, a central microtubule interacting protein accumulating and forming fibrils in AD patients (Knopman et al. 2021), and α-synuclein, a protein found to be aggregated in patients suffering from Parkinson’s disease (PD) (Baba et al. 1998), were upregulated when the three cathepsins are deficient.

## 5.6 Recombinant human Cathepsin D cleaves recombinant Aβ1-42 in vitro

Among the lysosomal proteinases CTSD has received particular attention. Based on *in vivo* data it was concluded that CTSD exerts roles in murine brain development and neuronal homeostasis (Benes et al. 2008; Di Domenico et al. 2016). CTSD may also be beneficial to support the degradation of aggregated and toxic proteins delivered to the lysosome as has been observed in Alzheimer’s disease (Di Domenico et al. 2016).

Early and often initiating factors in Alzheimer's disease are the generation and reduced clearance of Amyloid-β 1-42 (Aβ1-42) (Selkoe und Hardy 2016). Since CTSD may be involved as an intracellular Aβ hydrolyzing protease (Suire et al. 2020), this study aimed to shed more light on the potential beneficial role of CTSD in the regulation of the APP and Aβ metabolism.

In this study it could be demonstrated that recombinant human CTSD is able to cleave human Aβ1-42 in an *in vitro* set up. CTSD prefers hydrophobic residues at P1 (Pimenta et al. 2001; Sun et al. 2013) which are also present and used in human Aβ1-42 at positions Leu17, Phe19, Phe20, and Leu34, respectively. Another additional cleavage event was discovered at position Glu22. These CTSD-mediated cleavage positions were analyzed by LC-MS and confirmed data generated by Hamazaki et al. who identified the same cleavage sites of CTSD in Aβ1-42 at positions Leu34 and Phe19 (Hamazaki 1996). An independent study found the cleavage sites in human Aβ1-42 at positions Phe19, Phe20 and Leu34 (Suire et al. 2020). Interestingly, the cleavage events after Leu17 and Glu22 observed during the present work have not yet been described. Leucin is a hydrophobic amino acid which is a preferred residue at position P1 in the cleavage pocket of CTSD (Pimenta et al. 2001; Sun et al. 2013). Glutamic acid is an acidic amino acid which was previously found to be favored by CTSD at position P3 in combination with leucin in synthetic peptides (Pimenta et al. 2001) and might represent a cleavage site for position P1 in Aβ1-42 by CTSD. However, the fragment generated after Glu22 cleavage was found to be the less abundant one indicating a lower affinity for CTSD to cleave after glutamic acid. Taken together, LC-MS data confirm that CTSD has the potential to hydrolyze human Aβ1-42 *in vitro* to generate smaller fragments that might be less prone to aggregate and could possibly contribute to the clearance of toxic Aβ1-42 peptides by other endo- and exopeptidases.

### 5.7 Intracranial dosing of rhpro-CTSD to CTSD-deficient mice did not alter the amount of Aβ-species

Several studies already connected a dysfunctional lysosome-autophagy system to ageing or the development of AD and other neurodegenerative disorders (Aman et al. 2021; Liu und Li 2019; Zhang et al. 2009). Yang et al. showed that a deficiency of the lysosomal cysteine-protease inhibitor cystatin B in an AD-mouse model TgCRND8

(overexpressing APP695 including the APP-Swe K670N, M671L and APP-Ind V717F mutations (Chishti et al. 2001)) led to a clear reduction of Aβ levels within the brain (Yang et al. 2011). In an independent study five different murine AD models were analyzed and it was revealed that a declined acidification of neuronal lysosomes and therefore less active lysosomal hydrolases contributed to the aggregation of Aβ (Lee et al. 2022). In agreement, a reduced expression or modifications of subunits of the v-ATPase, which is responsible for lysosomal acidification (Song et al. 2020), were functionally linked to the pathology (intracellular neurofibrillary tangles and extracellular Aβ aggregates), observed in AD patients and AD-related mouse models (Johnson et al. 2020; Lee et al. 2010; Wolfe et al. 2013). A potential impairment of lysosomal protease function could be an important trigger to accelerate the molecular Aβ-related pathology in AD and an additional supply with active lysosomal proteases may be considered to be protective in this pathological cascade. With CTSD as the main lysosomal cathepsin active at low pH within the CNS analysis on the proteolysis of APP and Aβ has been of interest (Vidoni et al. 2016; Suire und Leissring 2021).

Marques et al. demonstrated the successful application of a modified type of an enzyme replacement therapy (ERT) in CTSD-deficient mice, a mouse model for human neuronal ceroid lipofuscinosis (Marques et al. 2020). Application of recombinant pro-CTSD reduced accumulated storage material, improved neuropathology and increased the lifespan of the treated mice. Interestingly, CTSD-deficient mice when treated with rhpro-CTSD also showed decreased α-synuclein levels and endo-lysosome and autophagy function were restored after treatment (Prieto Huarcaya et al. 2022). As insoluble Aβ levels from cerebral extracts of CTSD-deficient mice seemed to be higher (Suire et al. 2020), this treatment-strategy, i.e. delivery of pro-CTSD into the brain, might also be beneficial in the clearance of different types of Aβ forms to prevent or delay the Aβ plaque burden.

During this work it could be revealed that rhpro-CTSD dosing to CTSD-deficient mice led to a successful delivery of the enzyme to the lysosome and led to the maturation of the CTSD pro-peptide into its active form. Despite of the successful lysosomal delivery the levels of full-length APP and APP C-terminal fragments (CTFs) C83 and C99 were not altered in the rhpro-CTSD-treated mice compared to PBS treated ones. As an interesting side-finding it was observed that CTSD-deficient mice show a tendency towards lower soluble APPβ levels, the precursor for Aβ, compared to WT

mice. However, it could not be confirmed that this resulted in changed Aβ levels in CTSD-deficient mice. Since early studies suggest that CTSD may also directly act as β- or γ-secretase and could potentially cleave APP at the respective cleavage sites of BACE1 or Presenilin (Schechter und Ziv 2008; Sadik et al. 1999), one may also have expected changes in the processing of APP and levels of Aβ-peptide which were not found after administration of pro-CTSD. Furthermore, it has been reported that both, BACE1 and CTSD show a lower activity towards wildtype Aβ and a higher activity towards mutated “Swedish” Aβ also indicating that CTSD may be involved in the amyloidogenic pathway (Schechter und Ziv 2008). Additionally, the proposed γ-secretase activity of CTSD was found in experiments where CTSD was incubated with an 100-amino acid APP C-terminal fragment (C-100) containing the cytoplasmic domain of APP and parts of Aβ (Sadik et al. 1999). The experiments at this time suggested that CTSD acts as γ-secretase *in vitro*, however there is no evidence for an *in vivo* γ-secretase activity. A direct involvement of CTSD in APP processing was excluded since virus-mediated expression of human APP in CTSD-deficient neurons did not result in an altered cleavage pattern and Aβ generation as compared to transduced neurons from wildtype mice (Saftig et al. 1996)

### 5.8 Rhpro-CTSD treatment does not alter the processing of APP in HEK cells

Treating HEK cells expressing the Swedish APP variant with rhpro-CTSD led to a successful delivery of the enzyme to lysosomes as revealed by the analysis of the enzymatic activity and the processing of CTSD to the mature form. Despite of the established lysosomal activity of CTSD the rhpro-CTSD treated cells did neither show an altered proteolytic processing of APP nor a different abundance and type of Aβ species. In this context it is interesting to note that the dosed CTSD did not show a higher affinity towards mutated “Swedish” Aβ, as previously suggested by Schechter and colleagues (Schechter and Ziv 2008). In such a case one would have expected more generation of sAPPβ-Swe and C99 APP fragment. There was also no change in soluble or insoluble Aβ1-40 or Aβ1-42 upon CTSD treatment in the HEK cells expressing Swedish APP. Additionally, the level of Aβ and sAPPβswe in the cell supernatants were not altered. This strongly suggests that CTSD does not directly or

indirectly exert β- or γ-secretase activity in the used experimental setup as previously suggested (Schechter and Ziv 2008; Sadik et al. 1999)

## 5.9 Intracranial injection of rhpro-CTSD does not alter the APP processing in 5xFAD mice

During this work, 5xFAD mice were intracranially dosed with rhpro-CTSD at early age to boost lysosomal CTSD activity as early as possible and were analyzed at different ages.

APP is cleaved by the α-secretase ADAM10 at or on its way to the cell surface which leads to a soluble APPα and a membrane-bound APP C-terminal fragment (C83) (Jorissen et al. 2010; Haass and Willem 2019). However, the majority of APP is transported to the endosomes and lysosomes (Wang et al. 2017). Within the endosomal compartments β-secretase (BACE-1) further cleave APP (Kumar-Singh 2008; Whyte et al. 2020). The resulting membrane-bound but also soluble APP fragments may be subject to proteolytic cleavage by lysosomal proteases after endosome-lysosome fusion (Figure 50, left). Full-length APP, N-and C-terminal APP fragments and Aβ can all end up in lysosomes and may get in contact with the exogenously provided rhpro-CTSD (Figure 50, right). By injecting rhpro-CTSD to 5xFAD mice, the enzyme is recognized by different types of receptors including Low Densitiy Lipoprotein Receptor Related Protein 1 (LRP1) and Mannose-6-phosphate Receptor (MPR) (Drobny et al. 2022) and endocytosed. During the endocytic maturation CTSD gets activated within the lysosomes due to the acidic pH and processing by CTSB and CTSL (Laurent-Matha et al. 2006; Erickson et al. 2013). Such lysosomes with an increased CTSD protein level and activity may fuse to endosomes containing APP, N- and C-terminal APP-fragments including Aβ and could hypothetically better hydrolyze these APP-derived polypeptides including Aβ.

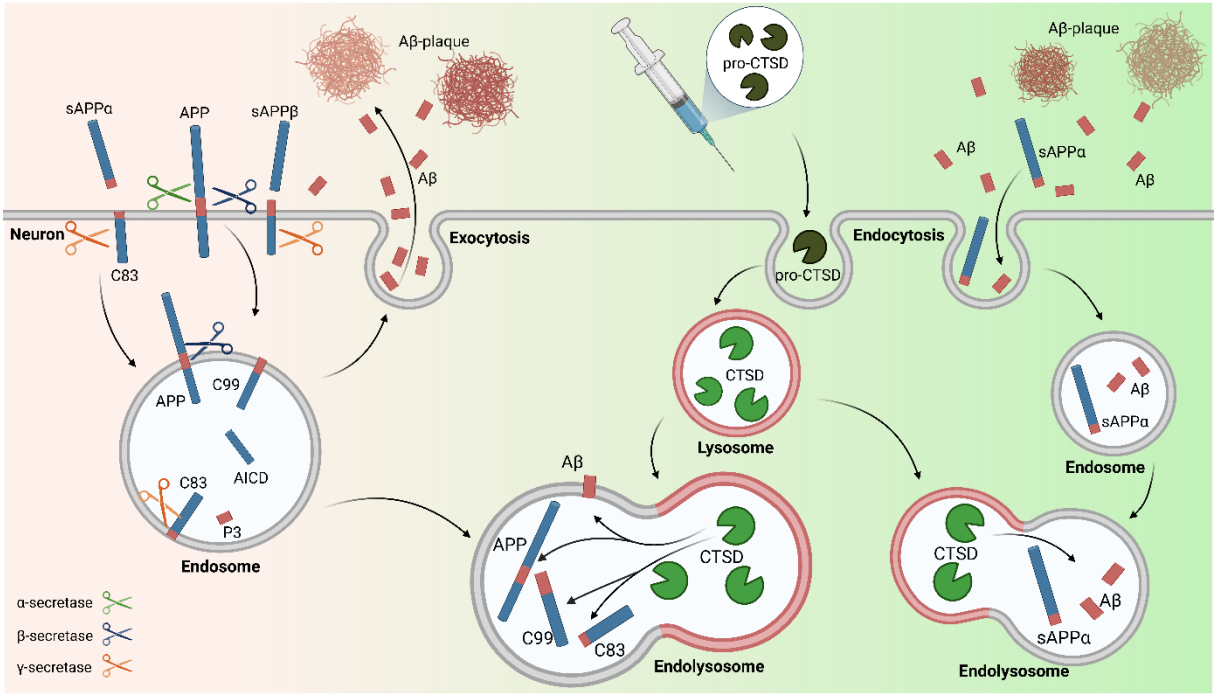


**Figure 50: How could intracranially injected CTSD cleave APP and Aβ?** Schematic overview of APP cleavage events by α-, β- and γ-secretases and the generated APP fragments. APP can be cleaved at the cell surface by α-, β- and γ-secretases and release soluble APP fragments including Aβ . Within the endosome β-secretases further cleave APP. The Aβ peptide is either released at the plasma membrane after β- and γ-secretase cleavage or after exocytosis. Aβ is able to form extracellular plaques or gets endocytosed by endosomes which can fuse with lysosomes. Intracranially dosed pro-Cathepsin D (pro-CTSD) is endocytosed by the neurons and activated within the lysosomes to form mature CTSD. The lysosomes with boosted CTSD activity can fuse with endosomes containing APP, N- and C-terminal APP fragments and Aβ.

The half-life of CTSD was not long enough to maintain higher enzymatic activity in the 5xFAD mice at three months of age, i.e. 2.5 months after the last dosing. Marques et al. determined the half-life of CTSD to be longer than 72h for CTSD in MEF cells (Marques et al. 2020). A considerable amount of CTSD protein and activity could still be determined until postnatal day 34 (P34), which was 15 days after the last injection, within the brain of rhpro-treated CTSD-deficient mice (Marques et al. 2020). This indicates that the activity of recombinant CTSD within the brain of mice lasts at least for 15 days. However, in this study the 5xFAD mice treated with rhpro-CTSD did not exert a measurable enzymatic CTSD activity 42 to 72 days after the last dosing. In the mice analyzed at two and three months of age the concentration of the exogenously added CTSD was below the detection limit. Other clinically approved enzyme replacement therapy (ERT) strategies suggest treatment every other (e.g. velaglucerase alfa for Type I Gaucher disease) to every second week (e.g. cerliponase alfa for CLN2) to maintain sufficient enzymatic activity of the replaced enzyme (Ratko

et al. 2013). Therefore, injecting rhpro-CTSD to 5xFAD at P1 and P20 may not be sufficient to maintain enzymatic activity for more than two months of age.

The initial idea that dosing 5xFAD mice with rhpro-CTSD at early age (P1 and P20) could reduce Aβ plaque appearance could not be confirmed as this chosen treatment strategy failed to prevent or postpone Aβ peptide generation and plaque formation.

Analyzing 5xFAD mice at one month of age, i.e. 8 days after the last dosing at P20, revealed no striking differences in the expression levels of soluble or membrane-bound APP fragments. There was a slight but significant reduction of the soluble APPα and the APP C-terminal C99-fragment after rhpro-CTSD dosing. It is conceivable that the boosted lysosomal CTSD activity contributed to a reduction of the APP-C99 fragment due to cleavage events of CTSD within APP-C99 which have been described by Sadik et al. in an 100-amino acid long C-terminal fragment (C-100) containing the cytoplasmic domain of APP and parts of Aβ after incubation with recombinant CTSD (Sadik et al. 1999). SH-SY5Y CTSBDL-deficient cells analyzed in this study revealed upregulation of both C-terminal APP fragments C83 and C99 when compared to their respective wildtype cell line. Re-transfection of CTSD to these SH-SY5Y CTSBDL-deficient cells led to a reduction of both C-terminal fragments indicating that CTSD is able to hydrolyze both APP-C83 and APP-C99. Notably, both sequences of the C-terminal APP-C99 (uniprot.org, human APP: P05067, ID: PRO_0000000091) and the APP-C83 (uniprot.org, human APP: P05067, ID: PRO_0000000094) contain possible cleavage sites for CTSD as both contain the favored Phe-Phe bond and Leu residues fitting in the cleavage pocket of CTSD (Pimenta et al. 2001; Sun et al. 2013). CTSD cleavage sites in the soluble APP fragments were also identified by *in vitro* assays (Dreyer et al. 1994). There is not much known about the affinity of CTSD towards the different APP fragments, however it is not the only lysosomal enzyme that is able to cleave APP. Other cathepsins like CTSB or CTSL can also proteolyze APP (Schechter and Ziv 2011; Cermak et al. 2016) which was also analyzed in this study in the SH-SY5Y CTSBDL-deficient cells after re-transfection with CTSB or CTSL.

Analyzing mice of two and three months of age, i.e. 42 or 70 days after the last dosing, did not reveal obvious differences in the processing of APP. The analysis of insoluble Aβ within the formic acid fractions which should indicate the presence of Aβ plaques

did also not reveal a reduction of these Aβ forms. This might again be due to the fact that the dosed CTSD is not stable over longer periods of time.

### 5.10 Aβ levels are surprisingly elevated in the CSF of 5xFAD mice after rhpro-CTSD dosing

A non-expected effect was observed in the cerebrospinal fluid (CSF) of rhpro-CTSD-treated one-month old 5xFAD mice. Here, the level of Aβ1-42 was found to be 2.7-fold increased after rhpro-CTSD treatment. Also, a clear tendency towards an elevated amount of Aβ1-40 was found. Amyloid-β can be cleared from the brain through the interstitial fluid (ISF) followed by transport mediated by Low Density Lipoprotein Receptor-related Protein 1 (LRP1) through the blood-brain barrier (BBB) but also by perivascular transport into the cerebrospinal fluid (CSF) (Figure 51, left) (Kumar-Singh 2008; Spies et al. 2012; Menéndez González 2017). While the levels of CTSD were found to be upregulated in the CSF of AD patients (Schwagerl et al. 1995), there are reduced levels of Aβ1-42 in the CSF compared to the Aβ1-40 levels in AD patients (Spies et al. 2012; Teunissen et al. 2018). The elevated Aβ1-42 levels found in the CSF of one-month old 5xFAD mice after CTSD treatment might indicate an upregulated generation of those peptides as CTSD is also thought to exert β-secretase activity (Schechter and Ziv 2008). However, DEA or RIPA fractions from those mice did not show altered expression of soluble or membrane-bound APP fragments.

While Aβ1-42 is more prone to aggregate to form Amyloid-β plaques residing in the brain, Aβ1-40 is more efficiently cleared from the brain by LRP1 (Deane et al. 2009; Spies et al. 2012). In this study, proteome analysis of the SH-SY5Y CTSBDL-triple-deficient cells compared to wildtype cells revealed an upregulation of LRP1. When now rhpro-CTSD-dosing in 5xFAD leads to increased CTSD protein levels and activity, this might also cause a reduced expression of LRP1 at the blood-brain-barrier or the blood-CSF-barrier. Therefore, an upregulated CTSD activity might also cause a decreased clearance through the BBB via LRP1 and the majority of Aβ1-42 and Aβ1-40 remains in the CSF (Figure 51, right).

The early rhpro-CTSD-treatment could possibly also lead to reduced Aβ-plaque formation in the one-month-old 5xFAD. However, the effects of CTSD on elevated Aβ levels found in the CSF on one-month old mice needs to be further elucidated.

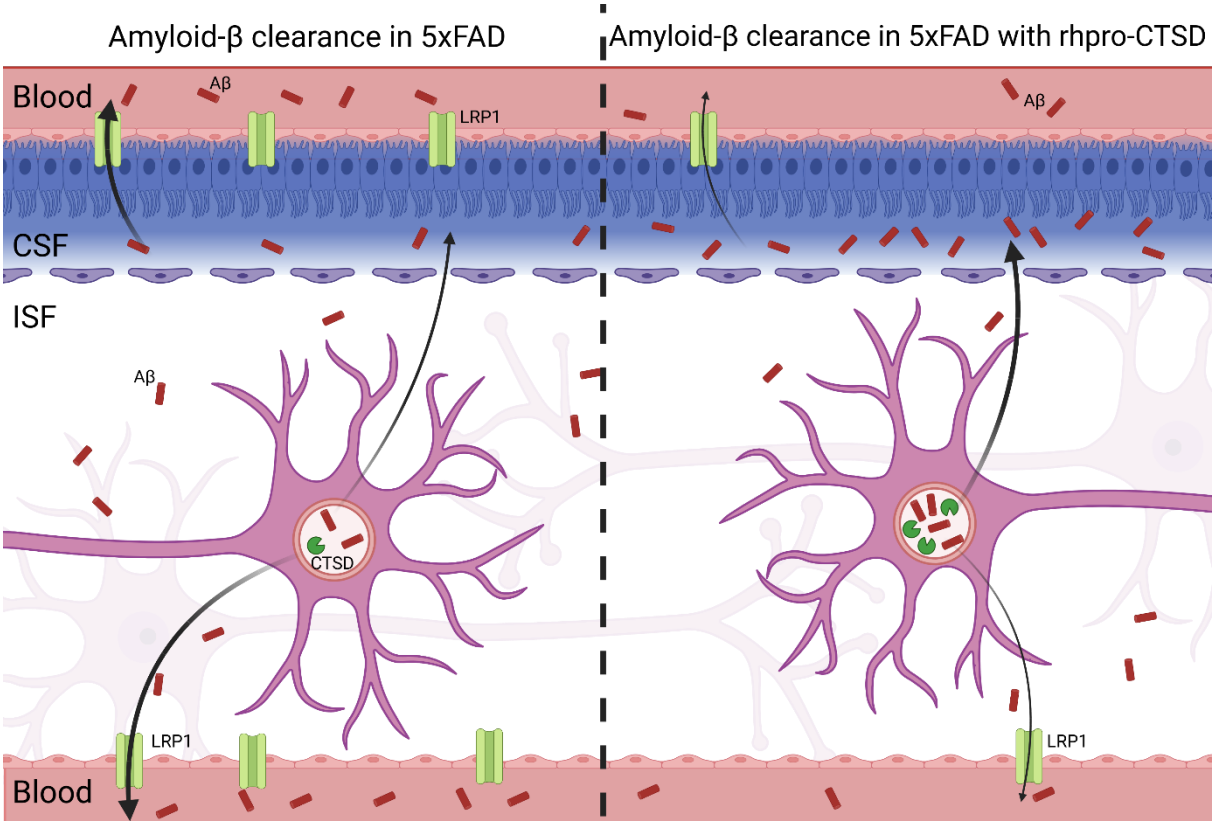


**Figure 51: The influence of rhpro-CTSD on Amyloid-β clearance in the brain.** Amyloid β can be cleared from the brain through the interstitial fluid (ISF) followed by active transport through the Low density Lipoprotein Receptor-related Protein 1 (LRP1) into the blood or passive transport through the cerebrospinal fluid (CSF) followed by LRP1-mediated transport into the blood (left). The majority of Amyloid β is cleared from the brain via LRP1. When 5xFAD are dosed with rhpro-CTSD (right) there seems to be an increased generation or presence of Aβ1-40 and Aβ 1-42. Additionally, the expression of LRP1 might be reduced (possibly by endocytic degradation modified by CTSD) indicating accumulation of Amyloid-β species in the CSF.

## 5.11 Amyloid-β-containing plaque load and neuroinflammation are not altered after rhpro-CTSD dosing to 5xFAD mice

Rhpro-CTSD treatment did not alter the Aβ-containing plaque number, size and morphology in the analyzed three-month old 5xFAD mice, i.e. after 70 days of the last injection at P20. Lysosome-like organelles massively accumulate around Aβ-containing plaques (Gowrishankar et al. 2015). Those LAMP1-positive lysosomes are apparently unable to efficiently degrade plaque components including Aβ. Those lysosomes are located within swollen axons which are in contact with Amyloid-plaques (Gowrishankar et al. 2015). Within these swollen axons the lysosomal CTSB, CTSD and CTSL were not detected (Gowrishankar et al. 2015). A possible local impairment of the lysosome transport within axons caused by Aβ deposits was suggested

(Gowrishankar et al. 2015). Interestingly, also an impaired lysosomal acidification of lysosomes surrounding Aβ plaques was revealed (Lee et al. 2022). Here, it was speculated that the faulty acidification occurs prior Aβ deposition in the brain and therefore is causing the intraluminal lysosomal Aβ accumulation (Lee et al. 2022). The impaired acidification is possibly caused by a lowered v-ATPase activity and leads to inactivity of most lysosomal proteases including CTSD (Lee et al. 2022).

LAMP1-positive vesicles accumulating around Aβ plaques were also found in the 5xFAD mice during this present work. The v-ATPase and CTSD activity or lysosomal pH of the lysosomes surrounding Aβ plaques could not be determined during this study. It is conceivable that the dosed CTSD does not reach these lysosomes surrounding Aβ plaques or that the intra-lysosomal pH is too low to activate CTSD to properly assist in the degradation of Aβ.

Neuroinflammatory markers like Iba1 and GFAP were not altered upon CTSD treatment in 5xFAD mice. In CTSD-deficient mice, both astrocyte and microglia activity was found upregulated (Suzuki et al. 2022). Disease associated microglia (DAM) which are found and activated in AD patients express high levels of CTSD (Muzio et al. 2021). Therefore, there seems to be different functions of CTSD in microglia as a deficiency but also an increase of CTSD in the brain can cause activation of microglia. More research is needed to further elucidate CTSD’s function on microglia or astrocyte activation. Microglia was not upregulated after rhpro-CTSD-dosing int the 5xFAD mice as analyzed in this study.

Astrocyte activity can be induced due to the presence of Aβ deposits (Escartin et al. 2021). In 5xFAD mouse model used during this study such an induction of astrocyte activity was not observed. An early dosing with rhpro-CTSD did also not have an influence on the activation status of astrocytes. As a reason, that three-month-old 5xFAD mice treated with rhpro-CTSD at P1 and P20 did not show any change in microglia or astrocyte activity one could assume that there is no additional CTSD enzyme activity in the brain 70 days after the last dosing at P20. Since rhpro-CTSD dosing to 5xFAD mice failed to reduce the Aβ load within the brain, it is therefore not too surprising that a reduction of the activation of astrocytes and also microglia was not observed.

# 6 Outlook

Multiple CTSBDL-deficient SH-SY5Y cell lines were generated and analyzed regarding phenotypic and morphological changes of their lysosomes and the consequences of the loss of the major cathepsins for the autophagic pathway, the substrate usage and the lysosomal storage.

These cell lines could be suitable for studies on the metabolic regulation in lysosomal storage disorders or neurodegenerative diseases as proteins like APP, Tau, LRP1 or α-synuclein were found to be upregulated in proteomic analysis. Those proteins are connected to severe diseases like Alzheimer's or Parkinson's disease. It could therefore also function as a cellular model to study on possible drugs targeting those proteins for further therapies. For example recent approaches that specifically target substrates for protein degradation, e.g. Autophagy-targeting chimera (AUTAC) and Proteolysis targeting chimera (PROTAC) (Pei et al. 2021; Sakamoto et al. 2001; Zengerle et al. 2015) could be helpful to find new treatment strategies for neurodegenerative disorders. These molecules consist of two protein-binding domains: one domain binds to the substrate while another domain either binds to LC3 (to target the substrate to the autophagosome, AUTAC) or to the E3-Ligase (to target the substrate to the proteasome, PROTAC). The target is then either transported to the autophagosome via LC3 or is ubiquitinated and degraded through the proteasome.

To further analyze the lysosomal peptide load in the SH-SY5Y CTSBDL-deficient lysosomes, it would be interesting to isolate lysosomes by lysosomal immunoprecipitation using tagged versions of the lysosomal membrane protein TMEM192 (Singh et al. 2020). Once, lysosomes of the SH-SY5Y CTSBDL-deficient cells are isolated, proteome and peptidome analysis would provide better insights into the non-utilized lysosomal substrate variety in the SH-SY5Y CTSBDL-deficient lysosomes. To further confirm possible new protein/peptide substrates for the respective cathepsins, one could create stably re-transfected SH-SY5Y cell lines with either one or all three missing CTSs re-expressed followed by proteome or peptidome analysis to find possible new CTS-specific substrates or unique and individual cleavage preferences. This could also help to better understand the hierarchy of cleavage events of the different CTSs.

## Outlook

CTSD might play a special role in Alzheimer's disease and APP processing, Aβ degradation and clearance. The *in vitro* and *in vivo* models analyzed during this work could partly confirm the involvement of CTSD in the Aβ processing. However, detailed *in vivo* analysis failed to demonstrate beneficial therapeutic effects after exogenously adding cathepsin D to cells and mice. This might be due to the use of an AD mouse model (5xFAD) with a rapidly progressing neuropathology. A therapeutic approach with only two injections at early age could not reveal a postponed development of the Aβ burden in those mice. The recently approved enzyme replacement therapy for CLN2 works with weekly dosing of tripeptidyl peptidase 1 (TPP1) to patients caring mutations in *TPP1* (Markham 2017; Kohlschütter et al. 2019). Rhpro-CTSD dosing could possibly reduce the Aβ burden in a less severe AD mouse model (e.g. APPlon mice) developing Aβ plaques at ten months of age (later than 5xFAD mice which develop Aβ plaques already at three months of age) with weekly intracerebroventricular injections. Another treatment strategy could be a combined treatment with CTSB, CTSD and CTSL as suggested by Di Spiezio et al. due to the hierarchical cleavage process of CTSB and CTSL on protein aggregates (Di Spiezio et al. 2021).

# 7 Summary

Lysosomal hydrolases are capable of degrading proteins and peptides that enter the compartment by endocytosis, phagocytosis and autophagy. Cathepsins (CTS) are acid lysosomal proteases classified by their structure and catalytic mechanisms. Deficiency or impairment of CTSs are associated with the development of lysosomal storage diseases, neurodegeneration and cancer. Despite the essential role of CTSs for lysosomal proteolysis, there is a need to understand how CTS are functionally embedded in the network of lysosomal proteases and protein degradation pathways.

This study focused on the major and most abundant CTSs expressed in human neuroblastoma-derived SH-SY5Y cells. Using CRISPR/Cas9 editing, CTSB-, CTSD-, CTSL-, and CTSBDL-triple deficient (KO) SH-SY5Y cells were generated. The detailed investigations of these cell lines revealed significantly enlarged lysosomes and accumulated lysosomal storage material in multiple CTS-deficient cell lines. Despite the lack of the three major CTSs assays addressing the autophagic flux pointed towards an only mild impairment. Endocytosed serum albumin was slower degraded in the triple KO cells, suggesting that the remaining active lysosomal hydrolases are still capable to contribute to the lysosomal protein degradation. To obtain insight into the substrate usage of the different CTSs, proteome analysis of whole-cell lysates from wildtype and CTS-depleted cells was performed. The proteome analysis revealed some overexpressed proteins which can be assigned to the autophagic system like LC3 or p62. In addition, amyloid precursor protein (APP) and APP fragments, which are linked to amyloid-beta (Aβ) peptide production later forming plaques in Alzheimer's disease (AD), are processed through CTS-mediated cleavages.

Hence, another focus of this work was the analysis of the possible beneficial function of cathepsin D (CTSD) in AD. Based on a recent study that could reveal that dosing recombinant CTSD has a therapeutic effect in a murine model of Neuronal Ceroid Lipofuscinosis type 10 and in cells and mice storing α-synuclein it was envisaged that CTSD may exert a similar benefit in AD models. Here, it was aimed to reduce or delay AD-related hallmarks such as Aβ plaque burden, neuroinflammation, and microgliosis by boosting the lysosomal protein turnover with recombinant human pro-CTSD (rhpro-CTSD). The previously established method to intracranially inject rhpro-CTSD to young mice was adapted to deliver high concentrations of CTSD to lysosomes of cells within

the mouse brain. Careful monitoring revealed uptake and maturation of the pro-CTSD enzyme to its mature and active form. Despite successful delivery, no evidence of CTSD having therapeutic effects on APP cleavage, Aβ burden, neuroinflammation, and microgliosis was found, ruling CTSD out as a suitable drug target for the treatment of AD.

# 8 Zusammenfassung

Lysosomale Hydrolasen sind in der Lage Proteine und Peptide, die das Organell über Endozytose, Phagozytose oder Autophagie erreichen, zu degradieren. Cathepsine (CTS) sind saure lysosomale Proteasen, die durch ihre Struktur und ihren katalytischen Mechanismus klassifiziert werden können. Der Verlust oder eine beeinträchtigte Funktion der Cathepsine ist mit der Entstehung lysosomaler Speicherstoff-erkrankungen, Neurodegeneration oder auch Krebs assoziiert. Trotz ihrer essentiellen Rolle in der lysosomalen Proteolyse, besteht die Notwendigkeit zu verstehen, wie Cathepsine funktional in das Netzwerk der lysosomalen Proteasen und der Proteinabbauwege integriert sind.

Diese Arbeit fokussierte sich auf die wichtigsten und am häufigsten exprimierten Cathepsine in SH-SY5Y Zellen, die von einem Neuroblastom abstammen. Mithilfe der CRISPR/Cas9-Methode, wurden SH-SY5Y Zelllinien generiert, denen CTSB, CTSD, CTSL oder alle drei Cathepsine fehlen. Die detaillierte Untersuchung dieser Zelllinien ergab, dass die SH-SY5Y CTSBDL-defizienten Zellen signifikant vergrößerte Lysosomen mit akkumuliertem Speichermaterial besitzen. Trotz des Verlusts der Haupt-Cathepsine, wiesen Experimente auf eine nur geringe Beeinträchtigung des Autophagie-Flusses auf. In den SH-SY5Y CTSBDL-defizienten Zellen wurde endozytiertes Serumalbumin langsamer abgebaut, was darauf hindeutet, dass die übrigen aktiven Hydrolasen noch ausreichend zur Funktionalität der lysosomalen Proteindegradierung beitragen. Um einen Einblick in die gemeinsame Substratnutzung der verschiedenen Cathepsine zu bekommen, wurde das Proteom der CTSBDL-defizienten SH-SY5Y Zelllinien im Vergleich zum Wildtyp analysiert. Unter den vermehrt vorhandenen Proteinen konnten die Autophagie-assoziierten Proteine LC3 und p62 gefunden werden. Weiterhin wurden das Amyloide Vorläuferprotein (APP) und dessen Fragmente gefunden, welche zur Amyloid-β Produktion beitragen und bei der Alzheimer Erkrankung eine Rolle spielen.

Ein weiterer Fokus dieser Arbeit lag bei der Analyse eines möglicherweise positiven Einflusses von CTSD bei der Alzheimer Erkrankung. Aktuelle Studien zeigten, dass die Verabreichung von rekombinantem CTSD eine therapeutische Wirkung bei einem murinen Mausmodell der Neuronalen Ceroid Lipofuszinose Typ 10, sowie bei Zellen und Mäusen, die α-Synuklein speichern, hat. Daher wurde vermutet, dass CTSD ähnliche Vorteile bei Alzheimer Mausmodellen haben könnte. Das Ziel war hier, die

Amyloid-β Plaques, Neuroinflammation und Mikrogliose durch die Gabe von rekombinantem humanen CTSD zu reduzieren. Die zuvor etablierte Methode, das Enzym intrakraniell zu injizieren wurde angepasst, um hohe Mengen von CTSD in die Lysosomen der Gehirnzellen zu bringen. Eine sorgfältige Analyse ergab, dass das pro-CTSD von den Lysosomen aufgenommen und aktiviert wurde. Trotz erfolgreicher Verabreichung, hatte CTSD keine therapeutische Wirkung auf die APP Prozessierung, die Amyloid-β Plaques, Neuroinflammation oder Mikrogliose. Daher scheint CTSD kein geeignetes Therapeutikum für die Behandlung der Alzheimer Erkrankung zu sein.

# 9 References

Adli, M. (2018): The CRISPR tool kit for genome editing and beyond. In *Nature communications* 9 (1), p. 1911. DOI: 10.1038/s41467-018-04252-2.

Aghdassi, Ali A.; John, Daniel S.; Sendler, Matthias; Weiss, F. Ulrich; Reinheckel, Thomas; Mayerle, Julia; Lerch, Markus M. (2018): Cathepsin D regulates cathepsin B activation and disease severity predominantly in inflammatory cells during experimental pancreatitis. In *The Journal of biological chemistry* 293 (3), pp. 1018–1029. DOI: 10.1074/jbc.M117.814772.

Andrew, Robert J.; Kellett, Katherine A. B.; Thinakaran, Gopal; Hooper, Nigel M. (2016): A Greek Tragedy. The Growing Complexity of Alzheimer Amyloid Precursor Protein Proteolysis. In *The Journal of biological chemistry* 291 (37), pp. 19235–19244. DOI: 10.1074/jbc.R116.746032.

Ao, X.; Zou, L.; Wu, Y. (2014): Regulation of autophagy by the Rab GTPase network. In *Cell death and differentiation* 21 (3), pp. 348–358. DOI: 10.1038/cdd.2013.187.

Ashtari, N.; Jiao, X.; Rahimi-Balaei, M.; Amiri, S.; Mehr, S. E.; Yeganeh, B.; Marzban, H. (2016): Lysosomal Acid Phosphatase Biosynthesis and Dysfunction: A Mini Review Focused on Lysosomal Enzyme Dysfunction in Brain. In *Current molecular medicine* 16 (5), pp. 439–446. DOI: 10.2174/1566524016666160429115834.

Baba, M.; Nakajo, S.; Tu, P. H.; Tomita, T.; Nakaya, K.; Lee, V. M. et al. (1998): Aggregation of alpha-synuclein in Lewy bodies of sporadic Parkinson's disease and dementia with Lewy bodies. In *The American journal of pathology* 152 (4), pp. 879–884.

Ballabio, Andrea; Gieselmann, Volkmar (2009): Lysosomal disorders: from storage to cellular damage. In *Biochimica et biophysica acta* 1793 (4), pp. 684–696. DOI: 10.1016/j.bbamcr.2008.12.001.

Becker-Pauly, Christoph; Pietrzik, Claus U. (2016): The Metalloprotease Meprin β Is an Alternative β-Secretase of APP. In *Frontiers in molecular neuroscience* 9, p. 159. DOI: 10.3389/fnmol.2016.00159.

References

Berg, J. M.; Tymoczko, J. L.; Gatto, G. J.; Stryer, L. (2018): Stryer Biochemie. Berlin, Heidelberg: Springer Berlin Heidelberg.

Bhagwat, Sonali R.; Hajela, Krishnan; Kumar, Amit (2018): Proteolysis to Identify Protease Substrates: Cleave to Decipher. In *Proteomics* 18 (13), e1800011. DOI: 10.1002/pmic.201800011.

Biedler, J. L.; Roffler-Tarlov, S.; Schachner, M.; Freedman, L. S. (1978): Multiple neurotransmitter synthesis by human neuroblastoma cell lines and clones. In *Cancer research* 38 (11 Pt 1), pp. 3751–3757.

Bilousova, Tina; Miller, Carol A.; Poon, Wayne W.; Vinters, Harry V.; Corrada, Maria; Kawas, Claudia et al. (2016): Synaptic Amyloid-β Oligomers Precede p-Tau and Differentiate High Pathology Control Cases. In *The American journal of pathology* 186 (1), pp. 185–198. DOI: 10.1016/j.ajpath.2015.09.018.

Bjørkøy, Geir; Lamark, Trond; Pankiv, Serhiy; Øvervatn, Aud; Brech, Andreas; Johansen, Terje (2009): Monitoring autophagic degradation of p62/SQSTM1. In *Methods in enzymology* 452, pp. 181–197. DOI: 10.1016/S0076-6879(08)03612-4.

Bond, Judith S. (2019): Proteases: History, discovery, and roles in health and disease. In *The Journal of biological chemistry* 294 (5), pp. 1643–1651. DOI: 10.1074/jbc.TM118.004156.

Bouhamdani, Nadia; Comeau, Dominique; Turcotte, Sandra (2021): A Compendium of Information on the Lysosome. In *Frontiers in cell and developmental biology* 9, p. 798262. DOI: 10.3389/fcell.2021.798262.

Brix, Klaudia; Dunkhorst, Anna; Mayer, Kristina; Jordans, Silvia (2008): Cysteine cathepsins: cellular roadmap to different functions. In *Biochimie* 90 (2), pp. 194–207. DOI: 10.1016/j.biochi.2007.07.024.

Brown, Madeleine R.; Radford, Sheena E.; Hewitt, Eric W. (2020): Modulation of β-Amyloid Fibril Formation in Alzheimer's Disease by Microglia and Infection. In *Frontiers in molecular neuroscience* 13, p. 609073. DOI: 10.3389/fnmol.2020.609073.

References

Brubaker, Sky W.; Bonham, Kevin S.; Zanoni, Ivan; Kagan, Jonathan C. (2015): Innate immune pattern recognition: a cell biological perspective. In *Annual review of immunology* 33, pp. 257–290. DOI: 10.1146/annurev-immunol-032414-112240.

Cabukusta, Birol; Neefjes, Jacques (2018): Mechanisms of lysosomal positioning and movement. In *Traffic (Copenhagen, Denmark)* 19 (10), pp. 761–769. DOI: 10.1111/tra.12587.

Caglic, Dejan; Pungercar, Jerica Rozman; Pejler, Gunnar; Turk, Vito; Turk, Boris (2007): Glycosaminoglycans facilitate procathepsin B activation through disruption of propeptide-mature enzyme interactions. In *The Journal of biological chemistry* 282 (45), pp. 33076–33085. DOI: 10.1074/jbc.M705761200.

Capell, A.; Steiner, H.; Willem, M.; Kaiser, H.; Meyer, C.; Walter, J. et al. (2000): Maturation and pro-peptide cleavage of beta-secretase. In *The Journal of biological chemistry* 275 (40), pp. 30849–30854. DOI: 10.1074/jbc.M003202200.

Casamento, Alessandra; Boucrot, Emmanuel (2020): Molecular mechanism of Fast Endophilin-Mediated Endocytosis. In *Biochemical Journal* 477 (12), pp. 2327–2345. DOI: 10.1042/BCJ20190342.

Cermak, Stjepko; Kosicek, Marko; Mladenovic-Djordjevic, Aleksandra; Smiljanic, Kosara; Kanazir, Selma; Hecimovic, Silva (2016): Loss of Cathepsin B and L Leads to Lysosomal Dysfunction, NPC-Like Cholesterol Sequestration and Accumulation of the Key Alzheimer's Proteins. In *PloS one* 11 (11), e0167428. DOI: 10.1371/journal.pone.0167428.

Chang, Howard H. Y.; Pannunzio, Nicholas R.; Adachi, Noritaka; Lieber, Michael R. (2017): Non-homologous DNA end joining and alternative pathways to double-strand break repair. In *Nature reviews. Molecular cell biology* 18 (8), pp. 495–506. DOI: 10.1038/nrm.2017.48.

Chapman, H. A.; Munger, J. S.; Shi, G. P. (1994): The role of thiol proteases in tissue injury and remodeling. In *American journal of respiratory and critical care medicine* 150 (6 Pt 2), S155-9. DOI: 10.1164/ajrccm/150.6_Pt_2.S155.

Chepyala, Surendhar Reddy; Liu, Xueyan; Yang, Ka; Wu, Zhiping; Breuer, Alex M.; Cho, Ji-Hoon et al. (2021): JUMPt: Comprehensive Protein Turnover Modeling

of In Vivo Pulse SILAC Data by Ordinary Differential Equations. In *Analytical chemistry* 93 (40), pp. 13495–13504. DOI: 10.1021/acs.analchem.1c02309.

Choi, Seulah; Kim, Donghoon; Kam, Tae-In; Yun, Seungpil; Kim, Sangjune; Park, Hyejin et al. (2015): Lysosomal Enzyme Glucocerebrosidase Protects against Aβ1-42 Oligomer-Induced Neurotoxicity. In *PloS one* 10 (12), e0143854. DOI: 10.1371/journal.pone.0143854.

Chow, Vivian W.; Mattson, Mark P.; Wong, Philip C.; Gleichmann, Marc (2010): An overview of APP processing enzymes and products. In *Neuromolecular medicine* 12 (1), pp. 1–12. DOI: 10.1007/s12017-009-8104-z.

Cicognola, Claudia; Janelidze, Shorena; Hertze, Joakim; Zetterberg, Henrik; Blennow, Kaj; Mattsson-Carlgren, Niklas; Hansson, Oskar (2021): Plasma glial fibrillary acidic protein detects Alzheimer pathology and predicts future conversion to Alzheimer dementia in patients with mild cognitive impairment. In *Alzheimer's research & therapy* 13 (1), p. 68. DOI: 10.1186/s13195-021-00804-9.

Ciechanover, A.; Elias, S.; Heller, H.; Ferber, S.; Hershko, A. (1980): Characterization of the heat-stable polypeptide of the ATP-dependent proteolytic system from reticulocytes. In *Journal of Biological Chemistry* 255 (16), pp. 7525–7528. DOI: 10.1016/S0021-9258(19)43856-8.

Ciechanover, Aaron (2005): Proteolysis: from the lysosome to ubiquitin and the proteasome. In *Nature reviews. Molecular cell biology* 6 (1), pp. 79–87. DOI: 10.1038/nrm1552.

Citron, M.; Oltersdorf, T.; Haass, C.; McConlogue, L.; Hung, A. Y.; Seubert, P. et al. (1992): Mutation of the beta-amyloid precursor protein in familial Alzheimer's disease increases beta-protein production. In *Nature* 360 (6405), pp. 672–674. DOI: 10.1038/360672a0.

Conant, David; Hsiau, Tim; Rossi, Nicholas; Oki, Jennifer; Maures, Travis; Waite, Kelsey et al. (2022): Inference of CRISPR Edits from Sanger Trace Data. In *The CRISPR journal* 5 (1), pp. 123–130. DOI: 10.1089/crispr.2021.0113.

Cox, Jürgen; Hein, Marco Y.; Luber, Christian A.; Paron, Igor; Nagaraj, Nagarjuna; Mann, Matthias (2014): Accurate proteome-wide label-free quantification by delayed normalization and maximal peptide ratio extraction, termed MaxLFQ. In

*Molecular & cellular proteomics : MCP* 13 (9), pp. 2513–2526. DOI: 10.1074/mcp.M113.031591.

Cuchillo-Ibañez, Inmaculada; Lopez-Font, Inmaculada; Boix-Amorós, Alba; Brinkmalm, Gunnar; Blennow, Kaj; Molinuevo, Jose-Luis; Sáez-Valero, Javier (2015): Heteromers of amyloid precursor protein in cerebrospinal fluid. In *Molecular neurodegeneration* 10, p. 2. DOI: 10.1186/1750-1326-10-2.

Cuda, Carla M.; Pope, Richard M.; Perlman, Harris (2016): The inflammatory role of phagocyte apoptotic pathways in rheumatic diseases. In *Nature reviews. Rheumatology* 12 (9), pp. 543–558. DOI: 10.1038/nrrheum.2016.132.

Dalbey, R. E.; Pei, D.; Ekici, Ö. D. (2017): Signal Peptidase Enzymology and Substrate Specificity Profiling. In *Methods in enzymology* 584, pp. 35–57. DOI: 10.1016/bs.mie.2016.09.025.

Dean, R. T.; Barrett, A. J. (1976): Lysosomes. In *Essays in biochemistry* 12, pp. 1–40.

Deane, R.; Bell, R. D.; Sagare, A.; Zlokovic, B. V. (2009): Clearance of amyloid-beta peptide across the blood-brain barrier: implication for therapies in Alzheimer's disease. In *CNS & neurological disorders drug targets* 8 (1), pp. 16–30. DOI: 10.2174/187152709787601867.

Delport, Alexandré; Hewer, Raymond (2022): The amyloid precursor protein: a converging point in Alzheimer's disease. In *Molecular neurobiology* 59 (7), pp. 4501–4516. DOI: 10.1007/s12035-022-02863-x.

Dennemärker, Julia; Lohmüller, Tobias; Müller, Sebastian; Aguilar, Stephanie Vargas; Tobin, Desmond J.; Peters, Christoph; Reinheckel, Thomas (2010): Impaired turnover of autophagolysosomes in cathepsin L deficiency. In *Biological chemistry* 391 (8), pp. 913–922. DOI: 10.1515/BC.2010.097.

Deretic, V. (2008): Autophagosome and phagosome edited by Vojo Deretic. Totowa NJ: Humana Press (Methods in molecular biology, 445).

Deussing, J.; Roth, W.; Saftig, P.; Peters, C.; Ploegh, H. L.; Villadangos, J. A. (1998): Cathepsins B and D are dispensable for major histocompatibility complex class II-mediated antigen presentation. In *Proceedings of the National Academy of Sciences of the United States of America* 95 (8), pp. 4516–4521. DOI: 10.1073/pnas.95.8.4516.

Di Spiezio, Alessandro; Marques, André R. A.; Schmidt, Lina; Thießen, Niklas; Gallwitz, Lisa; Fogh, Jens et al. (2021): Analysis of cathepsin B and cathepsin L treatment to clear toxic lysosomal protein aggregates in neuronal ceroid lipofuscinosis. In *Biochimica et biophysica acta. Molecular basis of disease* 1867 (10), p. 166205. DOI: 10.1016/j.bbadis.2021.166205.

Dikic, Ivan (2017): Proteasomal and Autophagic Degradation Systems. In *Annual review of biochemistry* 86, pp. 193–224. DOI: 10.1146/annurev-biochem-061516-044908.

Dimitroff, Charles J. (2015): Galectin-Binding O-Glycosylations as Regulators of Malignancy. In *Cancer research* 75 (16), pp. 3195–3202. DOI: 10.1158/0008-5472.CAN-15-0834.

Dissmeyer, N.; Rivas, S.; Graciet, E. (2017): Life and death of proteins after protease cleavage: protein degradation by the N-end rule pathway.

Dourlen, Pierre; Kilinc, Devrim; Malmanche, Nicolas; Chapuis, Julien; Lambert, Jean-Charles (2019): The new genetic landscape of Alzheimer's disease: from amyloid cascade to genetically driven synaptic failure hypothesis? In *Acta neuropathologica* 138 (2), pp. 221–236. DOI: 10.1007/s00401-019-02004-0.

Dreyer, R. N.; Bausch, K. M.; Fracasso, P.; Hammond, L. J.; Wunderlich, D.; Wirak, D. O. et al. (1994): Processing of the pre-beta-amyloid protein by cathepsin D is enhanced by a familial Alzheimer's disease mutation. In *European journal of biochemistry* 224 (2), pp. 265–271. DOI: 10.1111/j.1432-1033.1994.00265.x.

Drobny, Alice; Prieto Huarcaya, Susy; Dobert, Jan; Kluge, Annika; Bunk, Josina; Schlothauer, Theresia; Zunke, Friederike (2022): The role of lysosomal cathepsins in neurodegeneration: Mechanistic insights, diagnostic potential and therapeutic approaches. In *Biochimica et biophysica acta. Molecular cell research* 1869 (7), p. 119243. DOI: 10.1016/j.bbamcr.2022.119243.

Duve, C. de; Presman, B. C.; Gianetto, R.; Wattiaux, R.; Appelmans, F. (1955): Tissue fractionation studies. 6. Intracellular distribution patterns of enzymes in rat-liver tissue. In *The Biochemical journal* 60 (4), pp. 604–617. DOI: 10.1042/bj0600604.

Dyken, P.; Wisniewski, K. (1995): Classification of the neuronal ceroid-lipofuscinoses: expansion of the atypical forms. In *American journal of medical genetics* 57 (2), pp. 150–154. DOI: 10.1002/ajmg.1320570208.

Eden, Eran; Geva-Zatorsky, Naama; Issaeva, Irina; Cohen, Ariel; Dekel, Erez; Danon, Tamar et al. (2011): Proteome half-life dynamics in living human cells. In *Science (New York, N.Y.)* 331 (6018), pp. 764–768. DOI: 10.1126/science.1199784.

Elbialy, Abdalla (2021): In vivo autophagy quantification: Measuring LC3 and P62 puncta in 3D image system from zebrafish larvae. In *Journal of cellular biochemistry* 122 (10), pp. 1435–1444. DOI: 10.1002/jcb.30021.

Erickson, Ann H.; Isidoro, Ciro; Mach, Lukas; Mort, John S. (2013): Cathepsins: Getting in Shape for Lysosomal Proteolysis, pp. 127–173. DOI: 10.1007/978-3-7091-0885-7_4.

Escartin, Carole; Galea, Elena; Lakatos, András; O'Callaghan, James P.; Petzold, Gabor C.; Serrano-Pozo, Alberto et al. (2021): Reactive astrocyte nomenclature, definitions, and future directions. In *Nature neuroscience* 24 (3), pp. 312–325. DOI: 10.1038/s41593-020-00783-4.

Eskelinen, Eeva-Liisa; Tanaka, Yoshitaka; Saftig, Paul (2003): At the acidic edge: emerging functions for lysosomal membrane proteins. In *Trends in cell biology* 13 (3), pp. 137–145. DOI: 10.1016/s0962-8924(03)00005-9.

Felbor, U.; Dreier, L.; Bryant, R. A.; Ploegh, H. L.; Olsen, B. R.; Mothes, W. (2000): Secreted cathepsin L generates endostatin from collagen XVIII. In *The EMBO journal* 19 (6), pp. 1187–1194. DOI: 10.1093/emboj/19.6.1187.

Felbor, Ute; Kessler, Benedikt; Mothes, Walther; Goebel, Hans H.; Ploegh, Hidde L.; Bronson, Roderick T.; Olsen, Bjorn R. (2002): Neuronal loss and brain atrophy in mice lacking cathepsins B and L. In *Proceedings of the National Academy of Sciences of the United States of America* 99 (12), pp. 7883–7888. DOI: 10.1073/pnas.112632299.

Ferreira, Tiago A.; Blackman, Arne V.; Oyrer, Julia; Jayabal, Sriram; Chung, Andrew J.; Watt, Alanna J. et al. (2014): Neuronal morphometry directly from bitmap images. In *Nature methods* 11 (10), pp. 982–984. DOI: 10.1038/nmeth.3125.

References

Figura, K. von; Hasilik, A. (1986): Lysosomal enzymes and their receptors. In *Annual review of biochemistry* 55, pp. 167–193. DOI: 10.1146/annurev.bi.55.070186.001123.

Forgac, M. (1999): The vacuolar H+-ATPase of clathrin-coated vesicles is reversibly inhibited by S-nitrosoglutathione. In *The Journal of biological chemistry* 274 (3), pp. 1301–1305. DOI: 10.1074/jbc.274.3.1301.

Forner, Stefania; Kawauchi, Shimako; Balderrama-Gutierrez, Gabriela; Kramár, Enikö A.; Matheos, Dina P.; Phan, Jimmy et al. (2021): Systematic phenotyping and characterization of the 5xFAD mouse model of Alzheimer's disease. In *Sci Data* 8 (1). DOI: 10.1038/s41597-021-01054-y.

Friedrichs, Bianca; Tepel, Carmen; Reinheckel, Thomas; Deussing, Jan; Figura, Kurt von; Herzog, Volker et al. (2003): Thyroid functions of mouse cathepsins B, K, and L. In *The Journal of clinical investigation* 111 (11), pp. 1733–1745. DOI: 10.1172/JCI15990.

Fritchie, Karen; Siintola, Eija; Armao, Diane; Lehesjoki, Anna-Elina; Marino, Thomas; Powell, Cynthia et al. (2009): Novel mutation and the first prenatal screening of cathepsin D deficiency (CLN10). In *Acta neuropathologica* 117 (2), pp. 201–208. DOI: 10.1007/s00401-008-0426-7.

Fukuda, M. (1991): Lysosomal membrane glycoproteins. Structure, biosynthesis, and intracellular trafficking. In *Journal of Biological Chemistry* 266 (32), pp. 21327–21330. DOI: 10.1016/S0021-9258(18)54636-6.

Galjart, N. J.; Morreau, H.; Willemsen, R.; Gillemans, N.; Bonten, E. J.; d'Azzo, A. (1991): Human lysosomal protective protein has cathepsin A-like activity distinct from its protective function. In *Journal of Biological Chemistry* 266 (22), pp. 14754–14762. DOI: 10.1016/S0021-9258(18)98751-X.

Gieselmann, V.; Hasilik, A.; Figura, K. von (1985): Processing of human cathepsin D in lysosomes in vitro. In *Journal of Biological Chemistry* 260 (5), pp. 3215–3220. DOI: 10.1016/S0021-9258(18)89493-5.

Gireud-Goss, Monica; Mack, Alexis F.; McCullough, Louise D.; Urayama, Akihiko (2021): Cerebral Amyloid Angiopathy and Blood-Brain Barrier Dysfunction. In *The Neuroscientist : a review journal bringing neurobiology, neurology and psychiatry* 27 (6), pp. 668–684. DOI: 10.1177/1073858420954811.

Gocheva, Vasilena; Joyce, Johanna A. (2007): Cysteine cathepsins and the cutting edge of cancer invasion. In *Cell cycle (Georgetown, Tex.)* 6 (1), pp. 60–64. DOI: 10.4161/cc.6.1.3669.

Goettlich-Riemann, W.; Young, J. O.; Tappel, A. L. (1971): Cathepsins D, A and B, and the effect of pH in the pathway of protein hydrolysis. In *Biochimica et biophysica acta* 243 (1), pp. 137–146. DOI: 10.1016/0005-2795(71)90047-X.

Golde, Todd E. (2022): Alzheimer's disease - the journey of a healthy brain into organ failure. In *Molecular neurodegeneration* 17 (1), p. 18. DOI: 10.1186/s13024-022-00523-1.

Gowrishankar, Swetha; Yuan, Peng; Wu, Yumei; Schrag, Matthew; Paradise, Summer; Grutzendler, Jaime et al. (2015): Massive accumulation of luminal protease-deficient axonal lysosomes at Alzheimer's disease amyloid plaques. In *Proceedings of the National Academy of Sciences of the United States of America* 112 (28), E3699-708. DOI: 10.1073/pnas.1510329112.

Guay, J.; Falgueyret, J. P.; Ducret, A.; Percival, M. D.; Mancini, J. A. (2000): Potency and selectivity of inhibition of cathepsin K, L and S by their respective propeptides. In *European journal of biochemistry* 267 (20), pp. 6311–6318. DOI: 10.1046/j.1432-1327.2000.01730.x.

Guo, Yanjun; Wang, Qinqiu; Chen, Shenghui; Xu, Chengfu (2021): Functions of amyloid precursor protein in metabolic diseases. In *Metabolism: clinical and experimental* 115, p. 154454. DOI: 10.1016/j.metabol.2020.154454.

Haass, C.; Hung, A. Y.; Schlossmacher, M. G.; Teplow, D. B.; Selkoe, D. J. (1993): beta-Amyloid peptide and a 3-kDa fragment are derived by distinct cellular mechanisms. In *Journal of Biological Chemistry* 268 (5), pp. 3021–3024. DOI: 10.1016/S0021-9258(18)53650-4.

Haass, Christian; Kaether, Christoph; Thinakaran, Gopal; Sisodia, Sangram (2012): Trafficking and proteolytic processing of APP. In *Cold Spring Harbor perspectives in medicine* 2 (5), a006270. DOI: 10.1101/cshperspect.a006270.

Haass, Christian; Willem, Michael (2019): Secreted APP Modulates Synaptic Activity: A Novel Target for Therapeutic Intervention? In *Neuron* 101 (4), pp. 557–559. DOI: 10.1016/j.neuron.2019.01.058.

Halakos, Effie G.; Connell, Andrew J.; Glazewski, Lisa; Wei, Shuo; Mason, Robert W. (2021): Bottom up proteomics identifies neuronal differentiation pathway networks activated by cathepsin inhibition treatment in neuroblastoma cells that are enhanced by concurrent 13-cis retinoic acid treatment. In *Journal of proteomics* 232, p. 104068. DOI: 10.1016/j.jprot.2020.104068.

Halangk, W.; Lerch, M. M.; Brandt-Nedelev, B.; Roth, W.; Ruthenbuerger, M.; Reinheckel, T. et al. (2000): Role of cathepsin B in intracellular trypsinogen activation and the onset of acute pancreatitis. In *The Journal of clinical investigation* 106 (6), pp. 773–781. DOI: 10.1172/JCI9411.

Hamazaki, H. (1996): Cathepsin D is involved in the clearance of Alzheimer's beta-amyloid protein. In *FEBS letters* 396 (2-3), pp. 139–142. DOI: 10.1016/0014-5793(96)01087-3.

Hammond, Dean E.; Simpson, Deborah M.; Franco, Catarina; Wright Muelas, Marina; Waters, John; Ludwig, R. W. et al. (2022): Harmonizing Labeling and Analytical Strategies to Obtain Protein Turnover Rates in Intact Adult Animals. In *Molecular & cellular proteomics : MCP* 21 (7), p. 100252. DOI: 10.1016/j.mcpro.2022.100252.

Harmeier, Anja; Wozny, Christian; Rost, Benjamin R.; Munter, Lisa-Marie; Hua, Haiqing; Georgiev, Oleg et al. (2009): Role of amyloid-beta glycine 33 in oligomerization, toxicity, and neuronal plasticity. In *The Journal of neuroscience : the official journal of the Society for Neuroscience* 29 (23), pp. 7582–7590. DOI: 10.1523/JNEUROSCI.1336-09.2009.

Hee, Esther; Wong, Meng Kang; Tan, Sheng Hui; Choo, Zhang'E; Kuick, Chik Hong; Ling, Sharon et al. (2020): Neuroblastoma patient-derived cultures are enriched for a mesenchymal gene signature and reflect individual drug response. In *Cancer science* 111 (10), pp. 3780–3792. DOI: 10.1111/cas.14610.

Heneka, Michael T.; Carson, Monica J.; El Khoury, Joseph; Landreth, Gary E.; Brosseron, Frederic; Feinstein, Douglas L. et al. (2015): Neuroinflammation in Alzheimer's disease. In *The Lancet. Neurology* 14 (4), pp. 388–405. DOI: 10.1016/S1474-4422(15)70016-5.

Henne, William Mike; Stenmark, Harald; Emr, Scott D. (2013): Molecular mechanisms of the membrane sculpting ESCRT pathway. In *Cold Spring Harbor perspectives in biology* 5 (9). DOI: 10.1101/cshperspect.a016766.

Holtzman, David M.; Morris, John C.; Goate, Alison M. (2011): Alzheimer's disease: the challenge of the second century. In *Science translational medicine* 3 (77), 77sr1. DOI: 10.1126/scitranslmed.3002369.

Hook, Gregory; Hook, Vivian; Kindy, Mark (2011): The cysteine protease inhibitor, E64d, reduces brain amyloid-β and improves memory deficits in Alzheimer's disease animal models by inhibiting cathepsin B, but not BACE1, β-secretase activity. In *Journal of Alzheimer's disease : JAD* 26 (2), pp. 387–408. DOI: 10.3233/JAD-2011-110101.

Hsu, Amy; Podvin, Sonia; Hook, Vivian (2018): Lysosomal Cathepsin Protease Gene Expression Profiles in the Human Brain During Normal Development. In *Journal of molecular neuroscience : MN* 65 (4), pp. 420–431. DOI: 10.1007/s12031-018-1110-6.

Huang, F. L.; Tappel, A. L. (1971): Action of cathepsins C and D in protein hydrolysis. In *Biochimica et biophysica acta* 236 (3), pp. 739–748. DOI: 10.1016/0005-2795(71)90259-5.

Huang, Youhua; Zhang, Ya; Liu, Zetian; Liu, Chuanhe; Zheng, Jiaying; Qin, Qiwei; Huang, Xiaohong (2020): Autophagy Participates in Lysosomal Vacuolation-Mediated Cell Death in RGNNV-Infected Cells. In *Frontiers in microbiology* 11, p. 790. DOI: 10.3389/fmicb.2020.00790.

Ishidoh, Kazumi; Kominami, Eiki (2002): Processing and activation of lysosomal proteinases. In *Biological chemistry* 383 (12), pp. 1827–1831. DOI: 10.1515/BC.2002.206.

Iwama, Hideaki; Mehanna, Sally; Imasaka, Mai; Hashidume, Shinsuke; Nishiura, Hiroshi; Yamamura, Ken-Ichi et al. (2021): Cathepsin B and D deficiency in the mouse pancreas induces impaired autophagy and chronic pancreatitis. In *Scientific reports* 11 (1), p. 6596. DOI: 10.1038/s41598-021-85898-9.

Jalanko, Anu; Braulke, Thomas (2009): Neuronal ceroid lipofuscinoses. In *Biochimica et biophysica acta* 1793 (4), pp. 697–709. DOI: 10.1016/j.bbamcr.2008.11.004.

Ji, K.; Akgul, G.; Wollmuth, L. P.; Tsirka, S. E. (2013): Microglia actively regulate the number of functional synapses (8).

Jia, Jingyue; Claude-Taupin, Aurore; Gu, Yuexi; Choi, Seong Won; Peters, Ryan; Bissa, Bhawana et al. (2020): Galectin-3 Coordinates a Cellular System for Lysosomal Repair and Removal. In *Developmental cell* 52 (1), 69-87.e8. DOI: 10.1016/j.devcel.2019.10.025.

Jinek, Martin; Chylinski, Krzysztof; Fonfara, Ines; Hauer, Michael; Doudna, Jennifer A.; Charpentier, Emmanuelle (2012): A programmable dual-RNA-guided DNA endonuclease in adaptive bacterial immunity. In *Science (New York, N.Y.)* 337 (6096), pp. 816–821. DOI: 10.1126/science.1225829.

Jonsson, Thorlakur; Atwal, Jasvinder K.; Steinberg, Stacy; Snaedal, Jon; Jonsson, Palmi V.; Bjornsson, Sigurbjorn et al. (2012): A mutation in APP protects against Alzheimer's disease and age-related cognitive decline. In *Nature* 488 (7409), pp. 96–99. DOI: 10.1038/nature11283.

Jorissen, Ellen; Prox, Johannes; Bernreuther, Christian; Weber, Silvio; Schwanbeck, Ralf; Serneels, Lutgarde et al. (2010): The disintegrin/metalloproteinase ADAM10 is essential for the establishment of the brain cortex. In *The Journal of neuroscience : the official journal of the Society for Neuroscience* 30 (14), pp. 4833–4844. DOI: 10.1523/JNEUROSCI.5221-09.2010.

Jung, Tobias; Bader, Nicolle; Grune, Tilman (2007): Lipofuscin: formation, distribution, and metabolic consequences. In *Annals of the New York Academy of Sciences* 1119, pp. 97–111. DOI: 10.1196/annals.1404.008.

Kageyama, Shun; Gudmundsson, Sigurdur Runar; Sou, Yu-Shin; Ichimura, Yoshinobu; Tamura, Naoki; Kazuno, Saiko et al. (2021): p62/SQSTM1-droplet serves as a platform for autophagosome formation and anti-oxidative stress response. In *Nature communications* 12 (1), p. 16. DOI: 10.1038/s41467-020-20185-1.

Kaksonen, Marko; Roux, Aurélien (2018): Mechanisms of clathrin-mediated endocytosis. In *Nature reviews. Molecular cell biology* 19 (5), pp. 313–326. DOI: 10.1038/nrm.2017.132.

Karlsson, Max; Zhang, Cheng; Méar, Loren; Zhong, Wen; Digre, Andreas; Katona, Borbala et al. (2021): A single-cell type transcriptomics map of human tissues. In *Science advances* 7 (31). DOI: 10.1126/sciadv.abh2169.

Katunuma, Nobuhiko (2010): Posttranslational processing and modification of cathepsins and cystatins. In *Journal of signal transduction* 2010, p. 375345. DOI: 10.1155/2010/375345.

Ketterer, Stephanie; Mitschke, Julia; Ketscher, Anett; Schlimpert, Manuel; Reichardt, Wilfried; Baeuerle, Natascha et al. (2020): Cathepsin D deficiency in mammary epithelium transiently stalls breast cancer by interference with mTORC1 signaling. In *Nature communications* 11 (1), p. 5133. DOI: 10.1038/s41467-020-18935-2.

Kimura, Shunsuke; Noda, Takeshi; Yoshimori, Tamotsu (2007): Dissection of the autophagosome maturation process by a novel reporter protein, tandem fluorescent-tagged LC3. In *Autophagy* 3 (5), pp. 452–460. DOI: 10.4161/auto.4451.

Kitamoto, Shiro; Sukhova, Galina K.; Sun, Jiusong; Yang, Min; Libby, Peter; Love, Victoria et al. (2007): Cathepsin L deficiency reduces diet-induced atherosclerosis in low-density lipoprotein receptor-knockout mice. In *Circulation* 115 (15), pp. 2065–2075. DOI: 10.1161/CIRCULATIONAHA.107.688523.

Klionsky, Daniel J.; Abdelmohsen, Kotb; Abe, Akihisa; Abedin, Md Joynal; Abeliovich, Hagai; Acevedo Arozena, Abraham et al. (2016): Guidelines for the use and interpretation of assays for monitoring autophagy (3rd edition). In *Autophagy* 12 (1), pp. 1–222. DOI: 10.1080/15548627.2015.1100356.

Knopman, David S.; Amieva, Helene; Petersen, Ronald C.; Chételat, Gäel; Holtzman, David M.; Hyman, Bradley T. et al. (2021): Alzheimer disease. In *Nature reviews. Disease primers* 7 (1), p. 33. DOI: 10.1038/s41572-021-00269-y.

Kobayashi, Satoru (2015): Choose Delicately and Reuse Adequately: The Newly Revealed Process of Autophagy. In *Biological & pharmaceutical bulletin* 38 (8), pp. 1098–1103. DOI: 10.1248/bpb.b15-00096.

Kohlschütter, Alfried; Schulz, Angela; Bartsch, Udo; Storch, Stephan (2019): Current and Emerging Treatment Strategies for Neuronal Ceroid Lipofuscinoses. In *CNS drugs* 33 (4), pp. 315–325. DOI: 10.1007/s40263-019-00620-8.

Koike, M. (2000): Cathepsin D deficiency induces lysosomal storage with ceroid lipofuscin in mouse CNS neurons. In *Neuroscience Research* 38, S29. DOI: 10.1016/S0168-0102(00)81020-2.

Konietzko, Uwe (2012): AICD nuclear signaling and its possible contribution to Alzheimer's disease. In *Current Alzheimer research* 9 (2), pp. 200–216. DOI: 10.2174/156720512799361673.

Kounnas, M. Z.; Moir, R. D.; Rebeck, G. W.; Bush, A. I.; Argraves, W. S.; Tanzi, R. E. et al. (1995): LDL receptor-related protein, a multifunctional ApoE receptor, binds secreted beta-amyloid precursor protein and mediates its degradation. In *Cell* 82 (2), pp. 331–340. DOI: 10.1016/0092-8674(95)90320-8.

Kumar, Kushal; Kumar, Ashwani; Keegan, Richard M.; Deshmukh, Rahul (2018): Recent advances in the neurobiology and neuropharmacology of Alzheimer's disease. In *Biomedicine & pharmacotherapy = Biomedecine & pharmacotherapie* 98, pp. 297–307. DOI: 10.1016/j.biopha.2017.12.053.

Kumar-Singh, S. (2008): Cerebral amyloid angiopathy: pathogenetic mechanisms and link to dense amyloid plaques. In *Genes, brain, and behavior* 7 Suppl 1, pp. 67–82. DOI: 10.1111/j.1601-183X.2007.00380.x.

Laurent-Matha, Valérie; Derocq, Danielle; Prébois, Christine; Katunuma, Nobuhiko; Liaudet-Coopman, Emmanuelle (2006): Processing of human cathepsin D is independent of its catalytic function and auto-activation: involvement of cathepsins L and B. In *Journal of biochemistry* 139 (3), pp. 363–371. DOI: 10.1093/jb/mvj037.

Lauritzen, Inger; Pardossi-Piquard, Raphaëlle; Bourgeois, Alexandre; Pagnotta, Sophie; Biferi, Maria-Grazia; Barkats, Martine et al. (2016): Intraneuronal aggregation of the β-CTF fragment of APP (C99) induces Aβ-independent lysosomal-autophagic pathology. In *Acta neuropathologica* 132 (2), pp. 257–276. DOI: 10.1007/s00401-016-1577-6.

Lee, Ju-Hyun; Yang, Dun-Sheng; Goulbourne, Chris N.; Im, Eunju; Stavrides, Philip; Pensalfini, Anna et al. (2022): Faulty autolysosome acidification in Alzheimer's disease mouse models induces autophagic build-up of Aβ in neurons, yielding senile plaques. In *Nature neuroscience* 25 (6), pp. 688–701. DOI: 10.1038/s41593-022-01084-8.

Leng, Fangda; Edison, Paul (2021): Neuroinflammation and microglial activation in Alzheimer disease: where do we go from here? In *Nature reviews. Neurology* 17 (3), pp. 157–172. DOI: 10.1038/s41582-020-00435-y.

Liu, Lin; Doray, Balraj (2021): Elevated mRNA expression and defective processing of cathepsin D in HeLa cells lacking the mannose 6-phosphate pathway. In *FEBS open bio* 11 (6), pp. 1695–1703. DOI: 10.1002/2211-5463.13169.

Long, Justin M.; Holtzman, David M. (2019): Alzheimer Disease. An Update on Pathobiology and Treatment Strategies. In *Cell* 179 (2), pp. 312–339. DOI: 10.1016/j.cell.2019.09.001.

Lopez, Ana; Fleming, Angeleen; Rubinsztein, David C. (2018): Seeing is believing: methods to monitor vertebrate autophagy in vivo. In *Open biology* 8 (10). DOI: 10.1098/rsob.180106.

López-Ornelas, Adolfo; Jiménez, Adriana; Pérez-Sánchez, Gilberto; Rodríguez-Pérez, Citlali Ekaterina; Corzo-Cruz, Alejandro; Velasco, Iván; Estudillo, Enrique (2022): The Impairment of Blood-Brain Barrier in Alzheimer's Disease: Challenges and Opportunities with Stem Cells. In *International journal of molecular sciences* 23 (17). DOI: 10.3390/ijms231710136.

López-Otín, Carlos; Bond, Judith S. (2008): Proteases: multifunctional enzymes in life and disease. In *The Journal of biological chemistry* 283 (45), pp. 30433–30437. DOI: 10.1074/jbc.R800035200.

Ludger, Johannes; Ralf, Jacob; Hakon, Leffler (2018): Galectins at a glance. In *Journal of cell science* 131 (9). DOI: 10.1242/jcs.208884.

Magini, Alessandro; Polchi, Alice; Tozzi, Alessandro; Tancini, Brunella; Tantucci, Michela; Urbanelli, Lorena et al. (2015): Abnormal cortical lysosomal β-hexosaminidase and β-galactosidase activity at post-synaptic sites during Alzheimer's disease progression. In *The international journal of biochemistry & cell biology* 58, pp. 62–70. DOI: 10.1016/j.biocel.2014.11.001.

Majumder, Parijat; Baumeister, Wolfgang (2019): Proteasomes: unfoldase-assisted protein degradation machines. In *Biological chemistry* 401 (1), pp. 183–199. DOI: 10.1515/hsz-2019-0344.

Marciano, Shir; Dey, Debabrata; Listov, Dina; Fleishman, Sarel J.; Sonn-Segev, Adar; Mertens, Haydyn et al. (2022): Protein quaternary structures in solution are a mixture of multiple forms. In *Chemical science* 13 (39), pp. 11680–11695. DOI: 10.1039/d2sc02794a.

Markham, Anthony (2017): Cerliponase Alfa: First Global Approval. In *Drugs* 77 (11), pp. 1247–1249. DOI: 10.1007/s40265-017-0771-8.

Marques, André R. A.; Di Spiezio, Alessandro; Thießen, Niklas; Schmidt, Lina; Grötzinger, Joachim; Lüllmann-Rauch, Renate et al. (2020): Enzyme replacement therapy with recombinant pro-CTSD (cathepsin D) corrects defective proteolysis and autophagy in neuronal ceroid lipofuscinosis. In *Autophagy* 16 (5), pp. 811–825. DOI: 10.1080/15548627.2019.1637200.

Marques, André R. A.; Saftig, Paul (2019): Lysosomal storage disorders - challenges, concepts and avenues for therapy: beyond rare diseases. In *Journal of cell science* 132 (2). DOI: 10.1242/jcs.221739.

Masters, C. L.; Multhaup, G.; Simms, G.; Pottgiesser, J.; Martins, R. N.; Beyreuther, K. (1985): Neuronal origin of a cerebral amyloid: neurofibrillary tangles of Alzheimer's disease contain the same protein as the amyloid of plaque cores and blood vessels. In *The EMBO journal* 4 (11), pp. 2757–2763. DOI: 10.1002/j.1460-2075.1985.tb04000.x.

Mauvezin, Caroline; Nagy, Péter; Juhász, Gábor; Neufeld, Thomas P. (2015): Autophagosome-lysosome fusion is independent of V-ATPase-mediated acidification. In *Nature communications* 6, p. 7007. DOI: 10.1038/ncomms8007.

McDermott, J. R.; Gibson, A. M. (1996): Degradation of Alzheimer's beta-amyloid protein by human cathepsin D. In *Neuroreport* 7 (13), pp. 2163–2166. DOI: 10.1097/00001756-199609020-00021.

McGuire, Micheal J.; Lipeky, Peter E.; Thiele, Dwain L. (1992): Purification and Characterization of Dipeptidyl Peptidase I from Human Spleen. In *Archives of biochemistry and biophysics* (295), pp. 280–288.

Ménard, R.; Carmona, E.; Takebe, S.; Dufour, E.; Plouffe, C.; Mason, P.; Mort, J. S. (1998): Autocatalytic processing of recombinant human procathepsin L. Contribution of both intermolecular and unimolecular events in the processing

of procathepsin L in vitro. In *The Journal of biological chemistry* 273 (8), pp. 4478–4484. DOI: 10.1074/jbc.273.8.4478.

Menéndez González, Manuel (2017): Mechanical Dilution of Beta-amyloid Peptide and Phosphorylated Tau Protein in Alzheimer's Disease: Too Simple to be True? In *Cureus* 9 (2), e1062. DOI: 10.7759/cureus.1062.

Mijanovic, Olja; Petushkova, Anastasiia I.; Brankovic, Ana; Turk, Boris; Solovieva, Anna B.; Nikitkina, Angelina I. et al. (2021): Cathepsin D-Managing the Delicate Balance. In *Pharmaceutics* 13 (6). DOI: 10.3390/pharmaceutics13060837.

Mizushima, Noboru (2014): Sugar modification inhibits autophagosome-lysosome fusion. In *Nature cell biology* 16 (12), pp. 1132–1133. DOI: 10.1038/ncb3078.

Mizushima, Noboru; Komatsu, Masaaki (2011): Autophagy: renovation of cells and tissues. In *Cell* 147 (4), pp. 728–741. DOI: 10.1016/j.cell.2011.10.026.

Mizushima, Noboru; Yoshimori, Tamotsu (2007): How to interpret LC3 immunoblotting. In *Autophagy* 3 (6), pp. 542–545. DOI: 10.4161/auto.4600.

Mizushima, Noboru; Yoshimori, Tamotsu; Levine, Beth (2010): Methods in mammalian autophagy research. In *Cell* 140 (3), pp. 313–326. DOI: 10.1016/j.cell.2010.01.028.

Molineaux, Susan M. (2012): Molecular pathways: targeting proteasomal protein degradation in cancer. In *Clinical cancer research : an official journal of the American Association for Cancer Research* 18 (1), pp. 15–20. DOI: 10.1158/1078-0432.CCR-11-0853.

Morris, B. J. (1978): Activation of human inactive ("pro-") renin by cathepsin D and pepsin. In *The Journal of clinical endocrinology and metabolism* 46 (1), pp. 153–157. DOI: 10.1210/jcem-46-1-153.

Morrone, Carmela; Smirnova, Natalia F.; Jeridi, Aicha; Kneidinger, Nikolaus; Hollauer, Christine; Schupp, Jonas Christian et al. (2021): Cathepsin B promotes collagen biosynthesis, which drives bronchiolitis obliterans syndrome. In *The European respiratory journal* 57 (5). DOI: 10.1183/13993003.01416-2020.

Müller, Thorsten; Meyer, Helmut E.; Egensperger, Rupert; Marcus, Katrin (2008): The amyloid precursor protein intracellular domain (AICD) as modulator of gene expression, apoptosis, and cytoskeletal dynamics-relevance for Alzheimer's

disease. In *Progress in neurobiology* 85 (4), pp. 393–406. DOI: 10.1016/j.pneurobio.2008.05.002.

Müller-Esterl, W. (2018): Biochemie. Berlin, Heidelberg: Springer Berlin Heidelberg.

Murcha, Monika W.; Wang, Yan; Whelan, James (2012): A molecular link between mitochondrial preprotein transporters and respiratory chain complexes. In *Plant signaling & behavior* 7 (12), pp. 1594–1597. DOI: 10.4161/psb.22250.

Muzio, Luca; Viotti, Alice; Martino, Gianvito (2021): Microglia in Neuroinflammation and Neurodegeneration: From Understanding to Therapy. In *Frontiers in neuroscience* 15, p. 742065. DOI: 10.3389/fnins.2021.742065.

Myerowitz, Rachel; Puertollano, Rosa; Raben, Nina (2021): Impaired autophagy: The collateral damage of lysosomal storage disorders. In *EBioMedicine* 63, p. 103166. DOI: 10.1016/j.ebiom.2020.103166.

Nakagawa, T.; Roth, W.; Wong, P.; Nelson, A.; Farr, A.; Deussing, J. et al. (1998): Cathepsin L: critical role in Ii degradation and CD4 T cell selection in the thymus. In *Science (New York, N.Y.)* 280 (5362), pp. 450–453. DOI: 10.1126/science.280.5362.450.

Nhan, Hoang S.; Chiang, Karen; Koo, Edward H. (2015): The multifaceted nature of amyloid precursor protein and its proteolytic fragments: friends and foes. In *Acta neuropathologica* 129 (1), pp. 1–19. DOI: 10.1007/s00401-014-1347-2.

Oakley, Holly; Cole, Sarah L.; Logan, Sreemathi; Maus, Erika; Shao, Pei; Craft, Jeffery et al. (2006): Intraneuronal beta-amyloid aggregates, neurodegeneration, and neuron loss in transgenic mice with five familial Alzheimer's disease mutations. Potential factors in amyloid plaque formation. In *The Journal of neuroscience : the official journal of the Society for Neuroscience* 26 (40), pp. 10129–10140. DOI: 10.1523/JNEUROSCI.1202-06.2006.

Oberstein, Timo Jan; Utz, Janine; Spitzer, Philipp; Klafki, Hans Wolfgang; Wiltfang, Jens; Lewczuk, Piotr et al. (2020): The Role of Cathepsin B in the Degradation of Aβ and in the Production of Aβ Peptides Starting With Ala2 in Cultured Astrocytes. In *Frontiers in molecular neuroscience* 13, p. 615740. DOI: 10.3389/fnmol.2020.615740.

Ohkuma, S.; Poole, B. (1978): Fluorescence probe measurement of the intralysosomal pH in living cells and the perturbation of pH by various agents. In *Proceedings of the National Academy of Sciences of the United States of America* 75 (7), pp. 3327–3331. DOI: 10.1073/pnas.75.7.3327.

Papassotiropoulos, Andreas; Lewis, Huw D.; Bagli, Metin; Jessen, Frank; Ptok, Ursula; Schulte, Andrea et al. (2002): Cerebrospinal fluid levels of beta-amyloid(42) in patients with Alzheimer's disease are related to the exon 2 polymorphism of the cathepsin D gene. In *Neuroreport* 13 (10), pp. 1291–1294. DOI: 10.1097/00001756-200207190-00015.

Parodi-Rullán, Rebecca; Ghiso, Jorge; Cabrera, Erwin; Rostagno, Agueda; Fossati, Silvia (2020): Alzheimer's amyloid β heterogeneous species differentially affect brain endothelial cell viability, blood-brain barrier integrity, and angiogenesis. In *Aging cell* 19 (11), e13258. DOI: 10.1111/acel.13258.

Patel, Seema; Homaei, Ahmad; El-Seedi, Hesham R.; Akhtar, Nadeem (2018): Cathepsins: Proteases that are vital for survival but can also be fatal. In *Biomedicine & pharmacotherapy = Biomedecine & pharmacotherapie* 105, pp. 526–532. DOI: 10.1016/j.biopha.2018.05.148.

Pei, Junping; Wang, Guan; Feng, Lu; Zhang, Jifa; Jiang, Tingting; Sun, Qiu; Ouyang, Liang (2021): Targeting Lysosomal Degradation Pathways: New Strategies and Techniques for Drug Discovery. In *Journal of medicinal chemistry* 64 (7), pp. 3493–3507. DOI: 10.1021/acs.jmedchem.0c01689.

Pimenta, D. C.; Oliveira, A.; Juliano, M. A.; Juliano, L. (2001): Substrate specificity of human cathepsin D using internally quenched fluorescent peptides derived from reactive site loop of kallistatin. In *Biochimica et biophysica acta* 1544 (1-2), pp. 113–122. DOI: 10.1016/s0167-4838(00)00209-0.

Platt, Frances M.; d'Azzo, Alessandra; Davidson, Beverly L.; Neufeld, Elizabeth F.; Tifft, Cynthia J. (2018): Lysosomal storage diseases. In *Nature reviews. Disease primers* 4 (1), p. 27. DOI: 10.1038/s41572-018-0025-4.

Poole, Brian; Ohkuma, Shoji; Warburton, Michael (1978): SOME ASPECTS OF THE INTRACELLULAR BREAKDOWN OF EXOGENOUS AND ENDOGENOUS PROTEINS. In : Protein Turnover and Lysosome Function: Elsevier, pp. 43–58.

References

Poreba, Marcin; Groborz, Katarzyna; Vizovisek, Matej; Maruggi, Marco; Turk, Dusan; Turk, Boris et al. (2019): Fluorescent probes towards selective cathepsin B detection and visualization in cancer cells and patient samples. In *Chemical science* 10 (36), pp. 8461–8477. DOI: 10.1039/c9sc00997c.

Poreba, Marcin; Rut, Wioletta; Vizovisek, Matej; Groborz, Katarzyna; Kasperkiewicz, Paulina; Finlay, Darren et al. (2018): Selective imaging of cathepsin L in breast cancer by fluorescent activity-based probes. In *Chemical science* 9 (8), pp. 2113–2129. DOI: 10.1039/c7sc04303a.

Prieto Huarcaya, Susy; Drobny, Alice; Marques, André R. A.; Di Spiezio, Alessandro; Dobert, Jan Philipp; Balta, Denise et al. (2022): Recombinant pro-CTSD (cathepsin D) enhances SNCA/α-Synuclein degradation in α-Synucleinopathy models. In *Autophagy* 18 (5), pp. 1127–1151. DOI: 10.1080/15548627.2022.2045534.

Puzer, Luciano; Cotrin, Simone S.; Alves, Marcio F. M.; Egborge, Tobore; Araújo, Mariana S.; Juliano, Maria Aparecida et al. (2004): Comparative substrate specificity analysis of recombinant human cathepsin V and cathepsin L. In *Archives of biochemistry and biophysics* 430 (2), pp. 274–283. DOI: 10.1016/j.abb.2004.07.006.

Raju, T. S. (2019): Co□ and Post-Translational Modifications of Therapeutic Antibodies and Proteins: Wiley.

Rappsilber, Juri; Ishihama, Yasushi; Mann, Matthias (2003): Stop and go extraction tips for matrix-assisted laser desorption/ionization, nanoelectrospray, and LC/MS sample pretreatment in proteomics. In *Analytical chemistry* 75 (3), pp. 663–670. DOI: 10.1021/ac026117i.

Ratko et al. (2013): Enzyme-Replacement Therapies for Lysosomal Storage Diseases. FDA-approved prescribing information for enzyme-replacement therapy products for lysosomal storage diseases. In *Effective Health Care program* (Technical Brief Number 12). Available online at https://www.ncbi.nlm.nih.gov/books/NBK117223/table/findings.t1/.

Ravid, Tommer; Hochstrasser, Mark (2008): Diversity of degradation signals in the ubiquitin-proteasome system. In *Nature reviews. Molecular cell biology* 9 (9), pp. 679–690. DOI: 10.1038/nrm2468.

Rogers, Lindsay D.; Overall, Christopher M. (2013): Proteolytic post-translational modification of proteins: proteomic tools and methodology. In *Molecular & cellular proteomics : MCP* 12 (12), pp. 3532–3542. DOI: 10.1074/mcp.M113.031310.

Roth, W.; Deussing, J.; Botchkarev, V. A.; Pauly-Evers, M.; Saftig, P.; Hafner, A. et al. (2000): Cathepsin L deficiency as molecular defect of furless: hyperproliferation of keratinocytes and pertubation of hair follicle cycling. In *FASEB journal : official publication of the Federation of American Societies for Experimental Biology* 14 (13), pp. 2075–2086. DOI: 10.1096/fj.99-0970com.

Rudnik, Sönke; Damme, Markus (2021): The lysosomal membrane-export of metabolites and beyond. In *The FEBS journal* 288 (14), pp. 4168–4182. DOI: 10.1111/febs.15602.

Sadik, G.; Kaji, H.; Takeda, K.; Yamagata, F.; Kameoka, Y.; Hashimoto, K. et al. (1999): In vitro processing of amyloid precursor protein by cathepsin D. In *The international journal of biochemistry & cell biology* 31 (11), pp. 1327–1337. DOI: 10.1016/S1357-2725(99)00053-9.

Sadleir, Katherine R.; Eimer, William A.; Cole, Sarah L.; Vassar, Robert (2015): Aβ reduction in BACE1 heterozygous null 5XFAD mice is associated with transgenic APP level. In *Molecular neurodegeneration* 10, p. 1. DOI: 10.1186/1750-1326-10-1.

Saftig, P.; Hetman, M.; Schmahl, W.; Weber, K.; Heine, L.; Mossmann, H. et al. (1995): Mice deficient for the lysosomal proteinase cathepsin D exhibit progressive atrophy of the intestinal mucosa and profound destruction of lymphoid cells. In *The EMBO journal* 14 (15), pp. 3599–3608. DOI: 10.1002/j.1460-2075.1995.tb00029.x.

Saftig, Paul; Klumperman, Judith (2009): Lysosome biogenesis and lysosomal membrane proteins. Trafficking meets function. In *Nature reviews. Molecular cell biology* 10 (9), pp. 623–635. DOI: 10.1038/nrm2745.

Sahani, Mayurbhai Himatbhai; Itakura, Eisuke; Mizushima, Noboru (2014): Expression of the autophagy substrate SQSTM1/p62 is restored during prolonged starvation depending on transcriptional upregulation and autophagy-derived amino acids. In *Autophagy* 10 (3), pp. 431–441. DOI: 10.4161/auto.27344.

Sakamoto, K. M.; Kim, K. B.; Kumagai, A.; Mercurio, F.; Crews, C. M.; Deshaies, R. J. (2001): Protacs: chimeric molecules that target proteins to the Skp1-Cullin-F box complex for ubiquitination and degradation. In *Proceedings of the National Academy of Sciences of the United States of America* 98 (15), pp. 8554–8559. DOI: 10.1073/pnas.141230798.

Schechter, Israel; Ziv, Etty (2008): Kinetic properties of cathepsin D and BACE 1 indicate the need to search for additional beta-secretase candidate(s). In *Biological chemistry* 389 (3), pp. 313–320. DOI: 10.1515/BC.2008.025.

Schechter, Israel; Ziv, Etty (2011): Cathepsins S, B and L with aminopeptidases display β-secretase activity associated with the pathogenesis of Alzheimer's disease. In *Biological chemistry* 392 (6), pp. 555–569. DOI: 10.1515/bc.2011.054.

Schläfli, Anna M.; Adams, Olivia; Galván, José A.; Gugger, Mathias; Savic, Spasenija; Bubendorf, Lukas et al. (2016): Prognostic value of the autophagy markers LC3 and p62/SQSTM1 in early-stage non-small cell lung cancer. In *Oncotarget* 7 (26), pp. 39544–39555. DOI: 10.18632/oncotarget.9647.

Schleyer, Kelton A.; Cui, Lina (2021): Molecular probes for selective detection of cysteine cathepsins. In *Organic & biomolecular chemistry* 19 (28), pp. 6182–6205. DOI: 10.1039/d1ob00225b.

Schmitz, Janina; Gilberg, Erik; Löser, Reik; Bajorath, Jürgen; Bartz, Ulrike; Gütschow, Michael (2019): Cathepsin B. Active site mapping with peptidic substrates and inhibitors. In *Bioorganic & medicinal chemistry* 27 (1), pp. 1–15. DOI: 10.1016/j.bmc.2018.10.017.

Schmued, Larry; Raymick, James; Tolleson, William; Sarkar, Sumit; Zhang, Yi-Hong; Bell-Cohn, Ashlee (2012): Introducing Amylo-Glo, a novel fluorescent amyloid specific histochemical tracer especially suited for multiple labeling and large scale quantification studies. In *Journal of neuroscience methods* 209 (1), pp. 120–126. DOI: 10.1016/j.jneumeth.2012.05.019.

Schoenheimer, R (1943): The Dynamic State of Body Constituents. In *Physiological Zoology* 16 (1), p. 134. DOI: 10.1086/physzool.16.1.30151679.

Schulz, Angela; Kohlschütter, Alfried; Mink, Jonathan; Simonati, Alessandro; Williams, Ruth (2013): NCL diseases - clinical perspectives. In *Biochimica et biophysica acta* 1832 (11), pp. 1801–1806. DOI: 10.1016/j.bbadis.2013.04.008.

Schwagerl, A. L.; Mohan, P. S.; Cataldo, A. M.; Vonsattel, J. P.; Kowall, N. W.; Nixon, R. A. (1995): Elevated levels of the endosomal-lysosomal proteinase cathepsin D in cerebrospinal fluid in Alzheimer disease. In *Journal of neurochemistry* 64 (1), pp. 443–446. DOI: 10.1046/j.1471-4159.1995.64010443.x.

Seeman, Philip; Seeman, Neil (2011): Alzheimer's disease: β-amyloid plaque formation in human brain. In *Synapse (New York, N.Y.)* 65 (12), pp. 1289–1297. DOI: 10.1002/syn.20957.

Selkoe, Dennis J.; Hardy, John (2016): The amyloid hypothesis of Alzheimer's disease at 25 years. In *EMBO molecular medicine* 8 (6), pp. 595–608. DOI: 10.15252/emmm.201606210.

Semeniak, Daniela; Faber, Kristina; Öftering, Patricia; Manukjan, Georgi; Schulze, Harald (2019): Impact of Itga2-Gp6-double collagen receptor deficient mice for bone marrow megakaryocytes and platelets. In *PloS one* 14 (8), e0216839. DOI: 10.1371/journal.pone.0216839.

Settembre, Carmine; Fraldi, Alessandro; Medina, Diego L.; Ballabio, Andrea (2013): Signals from the lysosome. A control centre for cellular clearance and energy metabolism. In *Nature reviews. Molecular cell biology* 14 (5), pp. 283–296. DOI: 10.1038/nrm3565.

Sharda, Nidhi; Ahlschwede, Kristen M.; Curran, Geoffry L.; Lowe, Val J.; Kandimalla, Karunya K. (2021): Distinct Uptake Kinetics of Alzheimer Disease Amyloid-β 40 and 42 at the Blood-Brain Barrier Endothelium. In *The Journal of pharmacology and experimental therapeutics* 376 (3), pp. 482–490. DOI: 10.1124/jpet.120.000086.

Shibata, M.; Yamada, S.; Kumar, S. R.; Calero, M.; Bading, J.; Frangione, B. et al. (2000): Clearance of Alzheimer's amyloid-ss(1-40) peptide from brain by LDL receptor-related protein-1 at the blood-brain barrier. In *The Journal of clinical investigation* 106 (12), pp. 1489–1499. DOI: 10.1172/JCI10498.

Shir, Dror; Graff-Radford, Jonathan; Hofrenning, Ekaterina I.; Lesnick, Timothy G.; Przybelski, Scott A.; Lowe, Val J. et al. (2022): Association of plasma glial fibrillary acidic protein (GFAP) with neuroimaging of Alzheimer's disease and vascular pathology. In *Alzheimer's & dementia (Amsterdam, Netherlands)* 14 (1), e12291. DOI: 10.1002/dad2.12291.

Sigismund, Sara; Lanzetti, Letizia; Scita, Giorgio; Di Fiore, Pier Paolo (2021): Endocytosis in the context-dependent regulation of individual and collective cell properties. In *Nature reviews. Molecular cell biology* 22 (9), pp. 625–643. DOI: 10.1038/s41580-021-00375-5.

Singh, Jasjot; Kaade, Edgar; Muntel, Jan; Bruderer, Roland; Reiter, Lukas; Thelen, Melanie; Winter, Dominic (2020): Systematic Comparison of Strategies for the Enrichment of Lysosomes by Data Independent Acquisition. In *Journal of proteome research* 19 (1), pp. 371–381. DOI: 10.1021/acs.jproteome.9b00580.

Spies, Petra E.; Verbeek, Marcel M.; van Groen, Thomas; Claassen, Jurgen A. H. R. (2012): Reviewing reasons for the decreased CSF Abeta42 concentration in Alzheimer disease. In *Frontiers in bioscience (Landmark edition)* 17 (6), pp. 2024–2034. DOI: 10.2741/4035.

Stahl, Sonja; Reinders, Yvonne; Asan, Esther; Mothes, Walther; Conzelmann, Ernst; Sickmann, Albert; Felbor, Ute (2007): Proteomic analysis of cathepsin B- and L-deficient mouse brain lysosomes. In *Biochimica et biophysica acta* 1774 (10), pp. 1237–1246. DOI: 10.1016/j.bbapap.2007.07.004.

Steinfeld, Robert; Reinhardt, Konstanze; Schreiber, Kathrin; Hillebrand, Merle; Kraetzner, Ralph; Bruck, Wolfgang et al. (2006): Cathepsin D deficiency is associated with a human neurodegenerative disorder. In *American journal of human genetics* 78 (6), pp. 988–998. DOI: 10.1086/504159.

Stoka, Veronika; Turk, Vito; Turk, Boris (2016): Lysosomal cathepsins and their regulation in aging and neurodegeneration. In *Ageing research reviews* 32, pp. 22–37. DOI: 10.1016/j.arr.2016.04.010.

Storck, Steffen E.; Meister, Sabrina; Nahrath, Julius; Meißner, Julius N.; Schubert, Nils; Di Spiezio, Alessandro et al. (2016): Endothelial LRP1 transports amyloid-β(1-42) across the blood-brain barrier. In *The Journal of clinical investigation* 126 (1), pp. 123–136. DOI: 10.1172/JCI81108.

Suire, Caitlin N.; Abdul-Hay, Samer O.; Sahara, Tomoko; Kang, Dongcheul; Brizuela, Monica K.; Saftig, Paul et al. (2020): Cathepsin D regulates cerebral Aβ42/40 ratios via differential degradation of Aβ42 and Aβ40. In *Alzheimer's research & therapy* 12 (1), p. 80. DOI: 10.1186/s13195-020-00649-8.

Sun, Angela (2018): Lysosomal storage disease overview. In *Annals of translational medicine* 6 (24), p. 476. DOI: 10.21037/atm.2018.11.39.

Sun, Huiying; Lou, Xiaomin; Shan, Qiang; Zhang, Ju; Zhu, Xu; Zhang, Jia et al. (2013): Proteolytic characteristics of cathepsin D related to the recognition and cleavage of its target proteins. In *PloS one* 8 (6), e65733. DOI: 10.1371/journal.pone.0065733.

Suzuki, Chigure; Yamaguchi, Junji; Sanada, Takahito; Oliva Trejo, Juan Alejandro; Kakuta, Souichirou; Shibata, Masahiro et al. (2022): Lack of Cathepsin D in the central nervous system results in microglia and astrocyte activation and the accumulation of proteinopathy-related proteins. In *Scientific reports* 12 (1), p. 11662. DOI: 10.1038/s41598-022-15805-3.

Tanaka, Keiji (2009): The proteasome: overview of structure and functions. In *Proceedings of the Japan Academy. Series B, Physical and biological sciences* 85 (1), pp. 12–36. DOI: 10.2183/pjab/85.12.

Tanida, Isei; Minematsu-Ikeguchi, Naoko; Ueno, Takashi; Kominami, Eiki (2005): Lysosomal turnover, but not a cellular level, of endogenous LC3 is a marker for autophagy. In *Autophagy* 1 (2), pp. 84–91. DOI: 10.4161/auto.1.2.1697.

Tanzi, R.; Moir, R.; Wagner, S. (2004): Clearance of Alzheimer's Aβ PeptideThe Many Roads to Perdition. In *Neuron* 43 (5), pp. 605–608. DOI: 10.1016/S0896-6273(04)00533-1.

Tanzi, Rudolph E. (2012): The genetics of Alzheimer disease. In *Cold Spring Harbor perspectives in medicine* 2 (10). DOI: 10.1101/cshperspect.a006296.

Teunissen, Charlotte E.; Chiu, Ming-Jang; Yang, Che-Chuan; Yang, Shieh-Yueh; Scheltens, Philip; Zetterberg, Henrik; Blennow, Kaj (2018): Plasma Amyloid-β (Aβ42) Correlates with Cerebrospinal Fluid Aβ42 in Alzheimer's Disease. In *Journal of Alzheimer's disease : JAD* 62 (4), pp. 1857–1863. DOI: 10.3233/JAD-170784.

Thinakaran, Gopal; Koo, Edward H. (2008): Amyloid precursor protein trafficking, processing, and function. In *The Journal of biological chemistry* 283 (44), pp. 29615–29619. DOI: 10.1074/jbc.R800019200.

Tholen, Stefan; Biniossek, Martin L.; Gansz, Martina; Gomez-Auli, Alejandro; Bengsch, Fee; Noel, Agnes et al. (2013): Deletion of cysteine cathepsins B or L yields differential impacts on murine skin proteome and degradome. In *Molecular & cellular proteomics : MCP* 12 (3), pp. 611–625. DOI: 10.1074/mcp.M112.017962.

Thottacherry, Joseph Jose; Sathe, Mugdha; Prabhakara, Chaitra; Mayor, Satyajit (2019): Spoiled for Choice: Diverse Endocytic Pathways Function at the Cell Surface. In *Annual review of cell and developmental biology* 35, pp. 55–84. DOI: 10.1146/annurev-cellbio-100617-062710.

Torres, Manuel; Jimenez, Sebastian; Sanchez-Varo, Raquel; Navarro, Victoria; Trujillo-Estrada, Laura; Sanchez-Mejias, Elisabeth et al. (2012): Defective lysosomal proteolysis and axonal transport are early pathogenic events that worsen with age leading to increased APP metabolism and synaptic Abeta in transgenic APP/PS1 hippocampus. In *Molecular neurodegeneration* 7, p. 59. DOI: 10.1186/1750-1326-7-59.

Towatari, T.; Katunuma, N. (1983): Selective cleavage of peptide bonds by cathepsins L and B from rat liver. In *Journal of biochemistry* 93 (4), pp. 1119–1128. DOI: 10.1093/oxfordjournals.jbchem.a134237.

Trivedi, Purvi C.; Bartlett, Jordan J.; Pulinilkunnil, Thomas (2020): Lysosomal Biology and Function. Modern View of Cellular Debris Bin. In *Cells* 9 (5). DOI: 10.3390/cells9051131.

Turk, B.; Dolenc, I.; Lenarcic, B.; Krizaj, I.; Turk, V.; Bieth, J. G.; Björk, I. (1999): Acidic pH as a physiological regulator of human cathepsin L activity. In *European journal of biochemistry* 259 (3), pp. 926–932. DOI: 10.1046/j.1432-1327.1999.00145.x.

Turk, B.; Dolenc, I.; Turk, V.; Bieth, J. G. (1993): Kinetics of the pH-induced inactivation of human cathepsin L. In *Biochemistry* 32 (1), pp. 375–380. DOI: 10.1021/bi00052a046.

Turk, Vito; Stoka, Veronika; Vasiljeva, Olga; Renko, Miha; Sun, Tao; Turk, Boris; Turk, Dušan (2012): Cysteine cathepsins. From structure, function and regulation to new frontiers. In *Biochimica et biophysica acta* 1824 (1), pp. 68–88. DOI: 10.1016/j.bbapap.2011.10.002.

Tusher, V. G.; Tibshirani, R.; Chu, G. (2001): Significance analysis of microarrays applied to the ionizing radiation response. In *Proceedings of the National Academy of Sciences of the United States of America* 98 (9), pp. 5116–5121. DOI: 10.1073/pnas.091062498.

Tyanova, Stefka; Temu, Tikira; Sinitcyn, Pavel; Carlson, Arthur; Hein, Marco Y.; Geiger, Tamar et al. (2016): The Perseus computational platform for comprehensive analysis of (prote)omics data. In *Nature methods* 13 (9), pp. 731–740. DOI: 10.1038/nmeth.3901.

Tyynelä, J.; Sohar, I.; Sleat, D. E.; Gin, R. M.; Donnelly, R. J.; Baumann, M. et al. (2000): A mutation in the ovine cathepsin D gene causes a congenital lysosomal storage disease with profound neurodegeneration. In *The EMBO journal* 19 (12), pp. 2786–2792. DOI: 10.1093/emboj/19.12.2786.

Uhlén, Mathias; Fagerberg, Linn; Hallström, Björn M.; Lindskog, Cecilia; Oksvold, Per; Mardinoglu, Adil et al. (2015): Proteomics. Tissue-based map of the human proteome. In *Science (New York, N.Y.)* 347 (6220), p. 1260419. DOI: 10.1126/science.1260419.

Uribe-Querol, Eileen; Rosales, Carlos (2020): Phagocytosis: Our Current Understanding of a Universal Biological Process. In *Frontiers in immunology* 11, p. 1066. DOI: 10.3389/fimmu.2020.01066.

Vasiljeva, Olga; Reinheckel, Thomas; Peters, Christoph; Turk, Dusan; Turk, Vito; Turk, Boris (2007): Emerging roles of cysteine cathepsins in disease and their potential as drug targets. In *Current pharmaceutical design* 13 (4), pp. 387–403. DOI: 10.2174/138161207780162962.

Vassar, R.; Bennett, B. D.; Babu-Khan, S.; Kahn, S.; Mendiaz, E. A.; Denis, P. et al. (1999): Beta-secretase cleavage of Alzheimer's amyloid precursor protein by the transmembrane aspartic protease BACE. In *Science (New York, N.Y.)* 286 (5440), pp. 735–741. DOI: 10.1126/science.286.5440.735.

Verdoes, Martijn; Oresic Bender, Kristina; Segal, Ehud; van der Linden, Wouter A.; Syed, Salahuddin; Withana, Nimali P. et al. (2013): Improved quenched fluorescent probe for imaging of cysteine cathepsin activity. In *Journal of the American Chemical Society* 135 (39), pp. 14726–14730. DOI: 10.1021/ja4056068.

Vernon, Philip J.; Tang, Daolin (2013): Eat-me: autophagy, phagocytosis, and reactive oxygen species signaling. In *Antioxidants & redox signaling* 18 (6), pp. 677–691. DOI: 10.1089/ars.2012.4810.

Vesa, Jouni; Chin, Mark H.; Oelgeschläger, Kathrin; Isosomppi, Juha; DellAngelica, Esteban C.; Jalanko, Anu; Peltonen, Leena (2002): Neuronal ceroid lipofuscinoses are connected at molecular level: interaction of CLN5 protein with CLN2 and CLN3. In *Molecular biology of the cell* 13 (7), pp. 2410–2420. DOI: 10.1091/mbc.e02-01-0031.

Vidoni, Chiara; Follo, Carlo; Savino, Miriam; Melone, Mariarosa A. B.; Isidoro, Ciro (2016): The Role of Cathepsin D in the Pathogenesis of Human Neurodegenerative Disorders. In *Medicinal research reviews* 36 (5), pp. 845–870. DOI: 10.1002/med.21394.

Voet, D.; Voet, J. G. (op. 2011): Biochemistry. 4th ed. Hoboken, NJ: John Wiley & Sons.

Wang, Dong; Chen, Fanglian; Han, Zhaoli; Yin, Zhenyu; Ge, Xintong; Lei, Ping (2021): Relationship Between Amyloid-β Deposition and Blood-Brain Barrier Dysfunction in Alzheimer's Disease. In *Frontiers in cellular neuroscience* 15, p. 695479. DOI: 10.3389/fncel.2021.695479.

Wang, Haizhi; Sang, Nianli; Zhang, Can; Raghupathi, Ramesh; Tanzi, Rudolph E.; Saunders, Aleister (2015): Cathepsin L Mediates the Degradation of Novel APP C-Terminal Fragments. In *Biochemistry* 54 (18), pp. 2806–2816. DOI: 10.1021/acs.biochem.5b00329.

Wang, Xin; Zhou, Xuan; Li, Gongying; Zhang, Yun; Wu, Yili; Song, Weihong (2017): Modifications and Trafficking of APP in the Pathogenesis of Alzheimer's Disease. In *Frontiers in molecular neuroscience* 10, p. 294. DOI: 10.3389/fnmol.2017.00294.

Weller, Jason; Budson, Andrew (2018): Current understanding of Alzheimer's disease diagnosis and treatment. In *F1000Research* 7. DOI: 10.12688/f1000research.14506.1).

Whitton, Bradleigh; Okamoto, Haruko; Packham, Graham; Crabb, Simon J. (2018): Vacuolar ATPase as a potential therapeutic target and mediator of treatment

resistance in cancer. In *Cancer medicine* 7 (8), pp. 3800–3811. DOI: 10.1002/cam4.1594.

Whyte, Lauren S.; Hassiotis, Sofia; Hattersley, Kathryn J.; Hemsley, Kim M.; Hopwood, John J.; Lau, Adeline A.; Sargeant, Timothy J. (2020): Lysosomal Dysregulation in the Murine AppNL-G-F/NL-G-F Model of Alzheimer's Disease. In *Neuroscience* 429, pp. 143–155. DOI: 10.1016/j.neuroscience.2019.12.042.

Wilke, Sonja; Krausze, Joern; Büssow, Konrad (2012): Crystal structure of the conserved domain of the DC lysosomal associated membrane protein: implications for the lysosomal glycocalyx. In *BMC biology* 10, p. 62. DOI: 10.1186/1741-7007-10-62.

Willem, Michael; Tahirovic, Sabina; Busche, Marc Aurel; Ovsepian, Saak V.; Chafai, Magda; Kootar, Scherazad et al. (2015): η-Secretase processing of APP inhibits neuronal activity in the hippocampus. In *Nature* 526 (7573), pp. 443–447. DOI: 10.1038/nature14864.

Wiltfang, J.; Esselmann, H.; Cupers, P.; Neumann, M.; Kretzschmar, H.; Beyermann, M. et al. (2001): Elevation of beta-amyloid peptide 2-42 in sporadic and familial Alzheimer's disease and its generation in PS1 knockout cells. In *The Journal of biological chemistry* 276 (46), pp. 42645–42657. DOI: 10.1074/jbc.M102790200.

Wiśniewski, Jacek R.; Zougman, Alexandre; Mann, Matthias (2009): Combination of FASP and StageTip-based fractionation allows in-depth analysis of the hippocampal membrane proteome. In *Journal of proteome research* 8 (12), pp. 5674–5678. DOI: 10.1021/pr900748n.

Wolf, Dieter H.; Menssen, Ruth (2018): Mechanisms of cell regulation - proteolysis, the big surprise. In *FEBS letters* 592 (15), pp. 2515–2524. DOI: 10.1002/1873-3468.13109.

Wong, C. W.; Quaranta, V.; Glenner, G. G. (1985): Neuritic plaques and cerebrovascular amyloid in Alzheimer disease are antigenically related. In *Proceedings of the National Academy of Sciences of the United States of America* 82 (24), pp. 8729–8732. DOI: 10.1073/pnas.82.24.8729.

Wyant, Gregory A.; Abu-Remaileh, Monther; Wolfson, Rachel L.; Chen, Walter W.; Freinkman, Elizaveta; Danai, Laura V. et al. (2017): mTORC1 Activator

SLC38A9 Is Required to Efflux Essential Amino Acids from Lysosomes and Use Protein as a Nutrient. In *Cell* 171 (3), 642-654.e12. DOI: 10.1016/j.cell.2017.09.046.

Wyczalkowska-Tomasik, Aleksandra; Bartlomiejczyk, Irena; Wirkowska, Agnieszka; Koperski, Lukasz; Gornicka, Barbara; Paczek, Leszek (2015): The Blocking on the Cathepsin B and Fibronectin Accumulation in Kidney Glomeruli of Diabetic Rats. In *International journal of endocrinology* 2015, p. 812825. DOI: 10.1155/2015/812825.

Xu, Haoxing; Ren, Dejian (2015): Lysosomal physiology. In *Annual review of physiology* 77, pp. 57–80. DOI: 10.1146/annurev-physiol-021014-071649.

Yadati, Tulasi; Houben, Tom; Bitorina, Albert; Shiri-Sverdlov, Ronit (2020): The Ins and Outs of Cathepsins. Physiological Function and Role in Disease Management. In *Cells* 9 (7). DOI: 10.3390/cells9071679.

Yim, Willa Wen-You; Mizushima, Noboru (2020): Lysosome biology in autophagy. In *Cell discovery* 6, p. 6. DOI: 10.1038/s41421-020-0141-7.

Yoon, Michael C.; Hook, Vivian; O'Donoghue, Anthony J. (2022): Cathepsin B Dipeptidyl Carboxypeptidase and Endopeptidase Activities Demonstrated across a Broad pH Range. In *Biochemistry* 61 (17), pp. 1904–1914. DOI: 10.1021/acs.biochem.2c00358.

Zavodszky, Eszter; Vicinanza, Mariella; Rubinsztein, David C. (2013): Biology and trafficking of ATG9 and ATG16L1, two proteins that regulate autophagosome formation. In *FEBS letters* 587 (13), pp. 1988–1996. DOI: 10.1016/j.febslet.2013.04.025.

Zengerle, Michael; Chan, Kwok-Ho; Ciulli, Alessio (2015): Selective Small Molecule Induced Degradation of the BET Bromodomain Protein BRD4. In *ACS chemical biology* 10 (8), pp. 1770–1777. DOI: 10.1021/acschembio.5b00216.

Zhang, Xiaojie; Song, Weihong (2013): The role of APP and BACE1 trafficking in APP processing and amyloid-β generation. In *Alzheimer's research & therapy* 5 (5), p. 46. DOI: 10.1186/alzrt211.

Zhao, Lin; Zhao, Jia; Zhong, Kunhong; Tong, Aiping; Da Jia (2022): Targeted protein degradation: mechanisms, strategies and application. In *Signal transduction and targeted therapy* 7 (1), p. 113. DOI: 10.1038/s41392-022-00966-4.

Zheng, Xin; Chu, Fei; Mirkin, Bernard L.; Sudha, Thangirala; Mousa, Shaker A.; Rebbaa, Abdelhadi (2008): Role of the proteolytic hierarchy between cathepsin L, cathepsin D and caspase-3 in regulation of cellular susceptibility to apoptosis and autophagy. In *Biochimica et biophysica acta* 1783 (12), pp. 2294–2300. DOI: 10.1016/j.bbamcr.2008.07.027.

Zlokovic, Berislav V. (2005): Neurovascular mechanisms of Alzheimer's neurodegeneration. In *Trends in neurosciences* 28 (4), pp. 202–208. DOI: 10.1016/j.tins.2005.02.001.

Zlokovic, Berislav V. (2011): Neurovascular pathways to neurodegeneration in Alzheimer's disease and other disorders. In *Nature reviews. Neuroscience* 12 (12), pp. 723–738. DOI: 10.1038/nrn3114.

# 10 Appendix

## 10.1 Supplement Figure

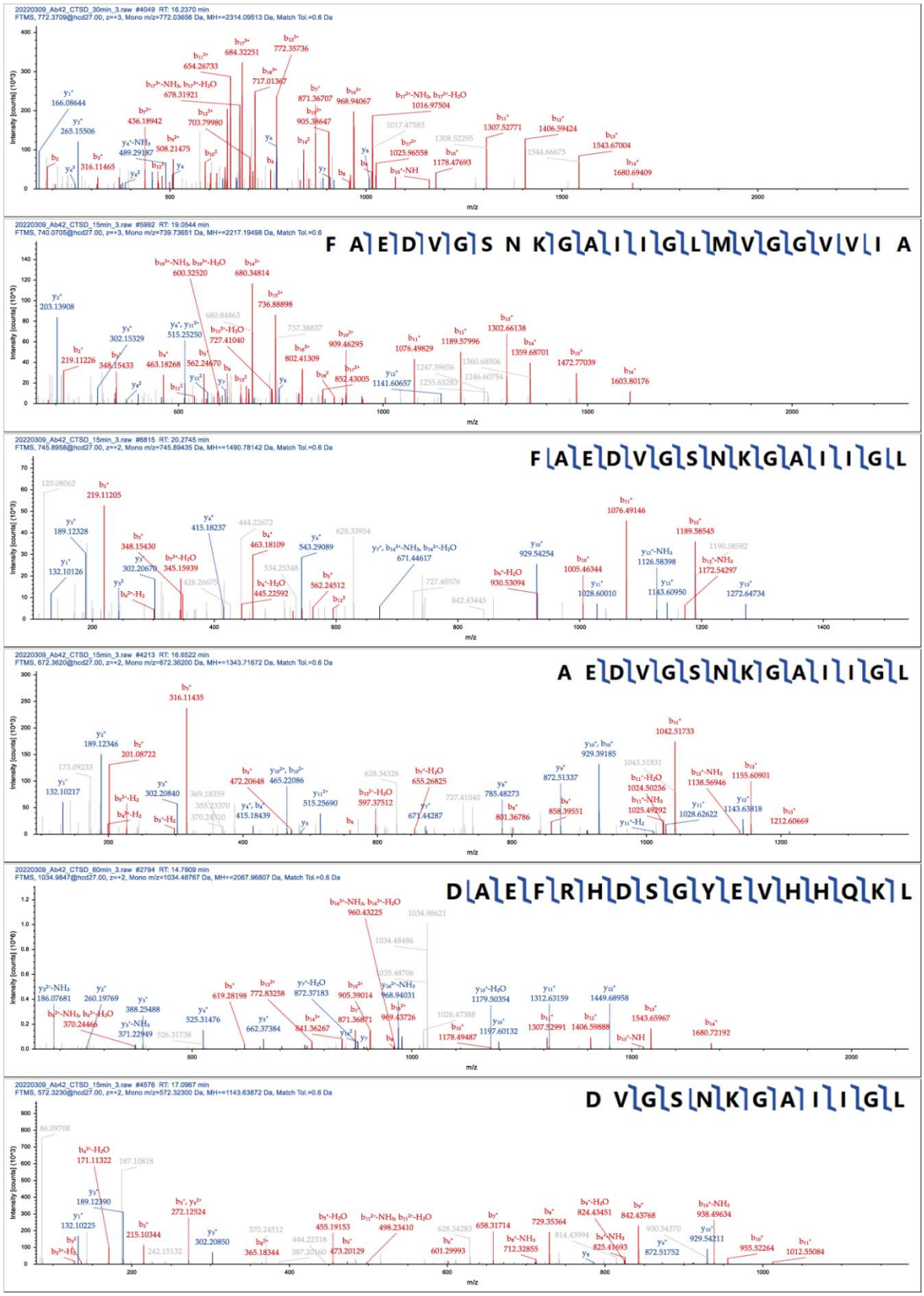


**Figure 52: Selected LC/MS spectra of Aβ1-42-derived peptides formed by proteolysis by rh-CTSD**

## 10.2 List of Abbreviations

| | |
|---|---|
| AA, aa | Amino acid |
| AD | Alzheimer’s disease |
| AICD | APP intracellular domain |
| AMC | 7-Amino-4-Methylcoumarin |
| ANOVA | analysis of variance |
| APF-1 | ATP-dependent proteolysis factor |
| APP | Amyloid Precursor Protein |
| APPswe | APP swedish |
| APS | Ammonium persulfate |
| Aβ | Amyloid-β |
| BafA1 | Bafilomycin A1 |
| BBB | blood-brain barrier |
| bp | base pair |
| BSA | Bovine Serum Albumin |
| CLN | Neuronal Ceroid Lipofuscinosis |
| CNS | central nervous system |
| CRISPR | Clustered Regularly Interspaced Short Palindromic Repeats |
| CSF | cerebrospinal fluid |
| CTF | C-terminal fragment |
| CTS | cathepsin |
| DABCO | 1,4-diazabicyclo[2.2.2]octane |
| DAPI | 4′,6-diamidino-2-phenylindole |
| DEA | diethanolamine |
| DMEM | Dulbecco’s modified eagle medium |
| DMSO | dimethyl sulfoxide |
| DNA | deoxyribonucleic acid |
| dNTP | nucleoside triphosphate |
| DUB | ubiquitin ligases and de-ubiquitinating enzyme |
| *E.coli* | *Eschericha coli* |
| EBSS | Earle’s Balanced Salt Solution |
| ECL | electrochemiluminescence |
| EDTA | ethylenediaminetetraacetic acid |
| ELISA | enzyme-linked immunosorbent assay |
| ER | endoplasmic reticulum |
| ERT | enzyme replacement therapy |
| ESCRT | Andosomal Sorting Complex Required for Transport |
| FA | formic acid |
| fl | full length |
| fw | forward |
| GA | glutaraldehyde |
| GAPDH | glyceraldehyde 3-phosphate dehydrogenase |
| GBA | glucocerebrosidase |
| GFAP | glial fibrillary acidic protein |
| GFP | green fluorescent protein |
| GLA | α-Galactosidase |
| GUSB | β-glucuronidase |
| h | hour |
| hAPP | human Amyloid Precursor Protein |
| HEK | human embryonic kidney |

| | |
|---|---|
| HeLa | Henrietta Lacks |
| HEXA/B | Hexosaminidase A/B |
| HRP | horseradish peroxidase |
| Iba1 | Ionized Calcium-binding Adapter Molecule 1 |
| ICE | Interference of CRISPR Edits |
| ICV | intracerebroventricular |
| ISF | interstitial fluid |
| ITGA2 | Integrin alpha 2 |
| IVC | individually ventilated cage |
| kDA | kilo Dalton |
| KEGG | Kyoto Encyclopedia of Genes and Genomes |
| KO | knockout |
| LAMP | Lysosomal Associated Membrane Proteins |
| LB | lysogeny broth |
| LC-MS | Liquid chromatography–mass spectrometry |
| LDL-R | Low-Density Lipoprotein Receptor |
| LGMN/AEP | Legumain |
| LIMP | Lysosomal Integral Membrane Protein |
| LRP1 | Low Density Lipoprotein Receptor-related Protein 1 |
| LSD | Lysosomal Storage Disease |
| LSM | laser scanning microscopy |
| MAP1LC3B/LC3 | Microtubule-associated Proteins 1A/1B light chain 3B |
| MAP2 | Microtubule-associated Protein 2 |
| MCOLN1 | mucolipin-1 |
| MES | 2-(*N*-morpholino) ethane sulfonic acid |
| min | minute |
| MPR | Mannose-6-phosphate Receptor |
| NHEJ | non-homologous end joining |
| NPC | Niemann-Pick C1 protein |
| P/S | Penicillin/Streptomycin |
| P1/P20/P22 | postnatal day 1/20/22 |
| PB | phosphate saline |
| PBS | phosphate buffered saline |
| PCR | polymerase chain reaction |
| PD | Parkinson’s disease |
| PE | phosphatidylethanolamine |
| PepA | Pepstatin A |
| PFA | paraformaldehyde |
| PI3K | phosphoinositide 3-kinases |
| PLD3 | Phospholipase D3 |
| PSEN | Presenilin |
| PTM | post-translational modification |
| qABP | quenched activity-based-probe |
| RFP | red fluorescent protein |
| rh | recombinant human |
| RIPA | radioimmunoprecipitation assay buffer |
| RNA | ribonucleic acid |
| rpm | revolutions per minute |
| RT | room temperature |
| rv | reverse |
| s | seconds |

| | |
|---|---|
| SDS | sodium dodecyl sulfate |
| SDS-PAGE | sodium dodecyl sulfate–polyacrylamide gel electrophoresis |
| SEM | standard error of the mean |
| sgRNA | single guide RNA |
| SNARE | Soluble NSF Attachment Protein Receptor |
| SQSTM/p62 | Sequestosome 1 |
| SRP | signal recognition particle |
| TAE | Tris-acetate ethylenediaminetetraacetic acid |
| TBS | Tris-buffered saline |
| TEM | transmission electron microscopy |
| TEMED | tetramethyl ethylenediamine |
| TGN | trans-golgi network |
| TMB | tetra methyl benzidine |
| TPP1 | Tripeptidyl-peptidase 1 |
| ULK1 | Unc-51 like Autophagy Activating Kinase |
| UPS | Ubiquitin-proteasome system |
| v-ATPase | Vacuolar- adenylpyrophosphatase |
| WT | wildtype |

## 10.3 List of Figures

Figure 1: Schematic overview of endocytosis, phagocytosis and autophagy. ..... 5

Figure 2: Macroautophagy pathway. ..... 8

Figure 3: Maturation process of Cathepsin B, Cathepsin D and Cathepsin L. ..... 10

Figure 4: Major cleavage events on the Amyloid precursor protein (APP)..... 18

Figure 5: Schematic overview of the CRISPR gene editing strategy. ..... 32

Figure 6: Active Cysteine-type cathepsins can bind and cleave the pan-reactive cysteine quenched activity-based-probe (qABP) BMV-109. ..... 34

Figure 7: Scheme for protein transfer from SDS-gel to a nitrocellulose membrane used for western blotting. ..... 38

Figure 8: Normalized transcript expression values of cathepsins in HeLa and SH-SY5Y cells. ..... 50

Figure 9: Cell-type specific expression of Cathepsin B, D, L and Z in HeLa and SH-SY5Y cells. ..... 51

Figure 10: Schematic mechanism of fluorescent cysteine-protease activity-based probe BMV 109 assay and its application in HeLa and SH-SY5Y WT cells using different lysosomal protease inhibitors..... 52

Figure 11: CTSD-activity in HeLa and SH-SY5Y WT cells. ..... 53

Figure 12: Analysis of the SH-SY5Y CTSB mixed clone. ..... 54

Figure 13: Protein sequences of edited CTS-deficient SH-SY5Y cell lines..... 55

Figure 14: Immunoblot analysis and activity determination using the cysteine-protease activity-based probe BMV-109 of SH-SY5Y CTS-deficient cell lines. ..... 56

Figure 15: CTSBDL-deficiency in SH-SY5Y leads to enlarged lysosomes. ..... 58

Figure 17: Enlarged lysosomes of CTSBDL-deficient SH-SY5Y cells are filled with electron-dense storage material. ..... 60

Figure 18: Lipofuscin accumulates within lysosomes of the SH-SY5Y CTSD- and CTSBDL-deficient cells. ..... 61

Figure 19: LC3 accumulates in SH-SY5Y CTSBDL-deficient lysosomes. ..... 63

Figure 20: The autophagosomal marker LC3-II is increased in SH-SY5Y CTSBDL-deficient cells. ..... 64

Figure 22: Schematic overview to monitor the autophagic flux using the tandem mRFP EGFP LC3 reporter construct. ..... 67

Figure 23: Fusion of autophagosomes with lysosomes is unaffected in the SH-SY5Y CTSBDL-deficient cells. ..... 68

Figure 24: SH-SY5Y CTSBDL-deficient cells accumulate a 50 kDa BSA fragment.. 71

Figure 25: Proteomic analysis of SH-SY5Y WT and two CTSBDL-deficient cell lines reveals dysregulation of several proteins..... 72

Figure 26: Lysosomal pathway analysis of SH-SY5Y CTSBDL-deficient cells. ..... 73

Figure 27: Accumulation of APP N- and C-terminal fragments in SH-SY5Y CTSBDL-deficient cells. ..... 74

Figure 28: The dysregulation of certain proteins in the SH-SY5Y CTSBDL-deficient cells can partially be rescued after re-transfection of CTSs. ..... 76

Figure 29: Rhpro-CTSD gets self-activated at acidic pH. ..... 77

Figure 30: In vitro digestion of human Aβ1-42 by rhCTSD. ..... 79

Figure 31: Principal of intracerebroventricular injections of rhpro-CTSD and beneficial effects on body weight gain in CTSD KO mice. ..... 80

Figure 32: Rhpro-CTSD ICV-injected to CTSD KO mice is taken up and matured by neurons and microglia. ..... 81

Figure 33: Rhpro-CTSD treatment of CTSD KO mice does not alter their APP metabolism. ..... 83

Figure 34: Aβ species in CTSD-deficient mice treated with rhpro-CTSD are not altered. ..... 84

Figure 35: CTSD activity assay of HEK APPswe cell lysates and supernatant. ..... 86

Figure 36: Inhibition of CTSD increases intracellular Aβ1-42 in HEK APPswe cells. 87

Figure 37: Rhpro-CTSD application to cells has no effect on soluble APP fragments. ..... 88

Figure 38: Analyzing APP and Aβ in 5xFAD mice of different ages..... 90

Figure 39: Injection schedule for 5xFAD mice with rhpro-CTSD..... 90

Figure 40: ICV injection of rhpro-CTSD of 5xFAD mice does not alter APP or Aβ metabolites after one month. ..... 91

Figure 41: Aβ1-40 and Aβ1-42 expressopn is upregulated in the CSF of rhpro-CTSD-treated 5xFAD mice. ..... 92

Figure 42: ICV injection of rhpro-CTSD of 5xFAD mice does not alter APP or Aβ metabolites after two months. ..... 93

Figure 43: Aβ1-40 and Aβ1-42 levels are upregulated in the brains of rhpro-CTSD-treated 5xFAD mice. ..... 94

Figure 44: Intracranial injection of rhpro-CTSD of 5xFAD mice does not alter APP or Aβ metabolites after three months of age. ..... 95

Figure 45: Rhpro-CTSD dosing to 5xFAD mice at early age does not affect the levels of Aβ species after three months of age. ..... 96

Figure 46: ICV injection of rhpro-CTSD of 5xFAD mice does not lead to a benefit in relation to clearing Aβ. ..... 97

Figure 47: No beneficial effect of rhpro-CTSD treatment in 5xFAD mice on microgliosis. ..... 99

Figure 48: There is no beneficial effect of rhpro-CTSD treatment in 5xFAD on astrogliosis..... 100

Figure 49: Impacts of a deficiency of CTSB, CTSD and CTSL in SH-SY5Y cells on the autophagic pathway. ..... 107

Figure 50: How could intracranially injected CTSD cleave APP and Aβ?..... 116

Figure 51: The influence of rhpro-CTSD on Amyloid-β clearance in the brain..... 119

Figure 52: Selected MS/MS spectra of Aβ1-42-derived peptides formed by proteolysis by rh-CTSD..... 158

## 10.4 List of Tables

Table 1: Favorable amino acids for P4-P1' positions of CTSB and CTSL (Turk et al. 2012; Poreba et al. 2018; Poreba et al. 2019) ..... 11

Table 2: Favorable amino acids for P3-P1' positions of CTSD (Pimenta et al. 2001; Sun et al. 2013) ..... 12

Table 3: List of primary antibodies. Dilution factors are presented for either immunofluorescence stainings (IF) or immunoblots (WB) ..... 24

Table 4: List of secondary antibodies used for immunoblots (coupled to horseradish peroxidase - HRP) or immunofluorescence stainings (coupled to Alexa fluor dyes). 24

Table 5: List of primers to genotype CRISPR/Cas9-modified cells (indicated with 'g'), 5xFAD and CTSD-deficient mice. ..... 25

Table 6: List of single guide RNAs used to modify cells by CRISPR/Cas9 ..... 25

Table 7: List of cell lines. ..... 26

Table 8: List of mouse strains and their mutations. ..... 26

Table 9: List of plasmids used for transfection. ..... 27

Table 10: List of buffers and aqueous solutions. ..... 28

Table 11: PCR pipetting scheme and cycling program. ..... 30

Table 12: Preparation of cell, sgRNA and Cas9 mixture for CRISPR/Cas9-mediated genome editing ..... 33

Table 13: Content of different percentage of SDS-gels ..... 37

Table 14: Genotyping PCR pipetting scheme for CTSD-deficient mice and the PCR program for both premixes 1 and 2 ..... 46

Table 15: Genotyping PCR pipetting scheme for 5xFAD mice and the PCR program ..... 46

# 11 Declaration

I hereby declare that apart from guidance from my supervisor, Prof. Dr. Paul Saftig, the content and design of this thesis is my own work. Contribution of other persons to generated data depicted in this thesis is explicitly indicated. Information derived from scientific publications is properly credited. I furthermore confirm the following:

- This thesis (partially or complete) has not been submitted elsewhere as a part of an examination procedure to obtain a doctoral degree.
- Parts of this thesis have been published in scientific journal articles (indicated in 12).
- This thesis was created according to the Rules of Good Scientific Practice of the German Research Foundation.
- No academic degree has been withdrawn.

Kiel, May 2023

_____

Lisa Gallwitz

# 12 Publications and scientific participations

**Publications containing data or images depicted in this thesis:**

**Gallwitz, L.**, Schmidt, L., Marques, A. R., Tholey, A., Cassidy, L., Ulku, I., Multhaup, G., Di Spiezio, A. & Saftig, P. (2022). Cathepsin D: Analysis of its potential role as an amyloid beta degrading protease. *Neurobiology of Disease*, *175*, 105919.

**Publications containing data not depicted in this dissertation:**

Di Spiezio, A., Marques, A. R., Schmidt, L., Thießen, N., **Gallwitz, L.**, Fogh, J., Bartsch, U. & Saftig, P. (2021). Analysis of cathepsin B and cathepsin L treatment to clear toxic lysosomal protein aggregates in neuronal ceroid lipofuscinosis. *Biochimica et Biophysica Acta (BBA)-Molecular Basis of Disease*, *1867*(10), 166205.

Prieto Huarcaya, S., Drobny, A., Marques, A. R., Di Spiezio, A., Dobert, J. P., Balta, D., Werner, C., Rizo, T., **Gallwitz, L.**, Bub, S., Stojkovska, A., Belur, N.R., Fogh, J., Mazulli, J.R., Xiang, W., Fulzele, A., Dejung, M., Sauer, M., Winner, B., Rose-John, S., Arnold, A., Saftig, P. & Zunke, F. (2022). Recombinant pro-CTSD (cathepsin D) enhances SNCA/α-Synuclein degradation in α-Synucleinopathy models. *Autophagy*, *18*(5), 1127-1151.

**Scientific participations:**

| | |
|---|---|
| 10/2022 | The 10th International Symposium on Autophagy (ISA2022), Sapporo, Japan |
| | Oral presentation and poster |
| | Travel Award Winner |
| 09/2022 | 3rd International Symposium of the CRC877 “Protease World in Health & Disease”, Kiel, Germany |
| | Poster presentation |
| 02/2022 | 39th Winter School on Proteinase and Inhibitors (online) |
| | Oral presentation |
| | Best Speaker Award among the session “Caspases and lysosomal proteases” |

# 13 Acknowledgements

First of all, I would express my sincere gratitude to my supervisor Prof. Dr. Paul Saftig for providing me the opportunity to work on my PhD thesis within his research group. I am grateful for his guidance, encouragement and support throughout the duration of this project.

Also, I would like to thank Prof. Dr. Eric Beitz for reviewing this thesis.

Furthermore, I am grateful to Prof. Dr. Markus Damme and Dr. Florian Bleibaum for their collaboration, engaging scientific discussions and their support during our project. Their contributions and the vibrant exchange of information have significantly enriched my research journey.

I would also like to thank our collaborators: Prof. Dr. Michaela Schweizer from UKE Hamburg for providing her electron microscopy expertise, Prof. Dr. Andreas Tholey from CAU Kiel for the mass spectrometry data, Prof. Dr. Stefan Lichtenthaler from DZNE Munich for providing the proteome data, Dr. Irem Ulku and Prof. Dr. Gerhard Multhaup from McGill University Montreal for their MSD analysis.

Being part of the SFB877 through which I could meet lots of students and scientists was a great experience that I would not want to have missed. With the opportunities to attend several progress reports, retreats, summer schools and also an international conference in Japan I could develop presentation skills in a scientific environment and broaden my scientific interests.

I am grateful to have been a member of ‘AG Bello’ together with Dr. Alessandro Di Spiezio, Lina Schmidt and Einstein. Ale, you always encouraged and motivated me during the past four years. I really miss your songs in the lab. You’ve taught me a lot while working together and I hope we can have pizza, pasta and cake again together. Lina – thank you for laughers, coffee breaks and lots of emotional support. And, Einstein, you were the best office sausage dog!

Getting through my dissertation would not have been possible without my co-workers including past members of the AG Saftig who created the perfect working environment for me. I am glad we were such a nice group and could enjoy funny lunch breaks, beer tastings and several evenings after work. By name, in no particular order: Katharina,

Acknowledgements

Lina, Maja, María, Lisa and Lisa, Brudi Pranji and Brudi Stine, Ceddi, our hero SEB, Sönke, Valli, Saskia, Mara, FloC, Simonas, David, Freddi, Jascha, Patrick, Marie, Anne, Ale, Marlies, Florian, Sophie, Nadja. I had a wonderful time with all of you. Special thanks go to María and Mara for the “Corona Zoom Meetings” and wine tastings. I also would like to appreciate the Pen and Paper group. Thanks for all the adventures and creative days and nights. And, I would also like to recognize my current and former office buddies from room 121: Lina (again!), Marie, Maja, Katharina, my personal barista Stine and Simonas.

Und zuletzt möchte ich mich noch bei meinen Eltern und Freunden bedanken. Meinen Eltern möchte ich danken, weil ich ohne euch nicht an dem Punkt wäre, an dem ich aktuell bin. Und auch ein großes Dankeschön an all meine Freunde, die mich immer unterstützt, motiviert und aufgebaut haben.